THE ROLE OF THE HYPOXIA-INDUCIBLE PATHWAY IN METABOLISM AND CARDIOPULMONARY PHYSIOLOGY

A Thesis submitted for the degree of Doctor of Philosophy

UNIVERSITY OF OXFORD

Mary E. Slingo

University College

Trinity Term 2013

For Dad

ACKNOWLEDGEMENTS

It has been a privilege to study under the supervision of Professors Peter Robbins and Kieran Clarke. I am immensely grateful for their support and for providing me with the opportunity to study at the University of Oxford. I would also like to thank Dr Keith Dorrington for his guidance and mentorship at University College, and for providing me with the particularly enjoyable opportunity of working with him in the hospital.

The research for the ventilatory chapter of this thesis was conducted in collaboration with Drs Keith Buckler and Phil Turner. I am extremely grateful for their guidance and support, and their generosity in providing me with additional laboratory space and equipment. I would also like to thank Drs Helen Christian, Tammie Bishop and Peader O'Donohue for their help and advice.

I was very fortunate in receiving the mentorship and supervision of Dr Mark Cole on my arrival in Oxford. His guidance, assistance and good humour were key to the success of the research for the cardiac metabolism chapter of this thesis. Drs Lisa Heather, Amira Abd-Jamil, Mike Dodd, Carolyn Carr, Damian Tyler and Rhys Evans all provided considerable technical and intellectual expertise, for which I am very grateful. I would also like to thank Vicky Ball, Emma Carter, Latt Mansor, Renata Gomes, Sheena Lee and Lucia Giles for their assistance, all the other members of the Cardiac Metabolism Research Group, and finally Xinzhu Wang and Dr Julian Griffin in Cambridge.

The Robbins hypoxia group at Oxford is an ever-expanding collection of talented scientists and clinicians. It has been a pleasure to work with my colleagues and friends Tom Smith, Nick Talbot, Matthew Frise, Vincent Cheng, David O'Neill, Quentin Croft, Nayia Petousi, Federico Formenti, Nikki Bart, Kate Curtis, Annabel Nickol, David O'Connor, and Samira Lakhal-Littleton.

The research for this thesis would not have been possible without the support and expertise of the animal staff, including Denise Jelfs, James Ward and Caroline Barnwell.

I would like to express my sincere thanks to the Wellcome Trust for providing me with a Clinical Research Training Fellowship and the funding for this project. I am also very grateful to University College for the War Memorial Scholarship.

I thank Mr Mervyn Griffiths at Southampton General Hospital for his mentorship and support upon hearing my decision to leave paediatric surgery. I am also enormously grateful to my close friends for their kindness and support.

Finally, I would like to thank my Mum and my sister Anna, for everything.

ABSTRACT

Mary E. Slingo
University College

D. Phil. Thesis
Trinity Term, 2013

THE ROLE OF THE HYPOXIA-INDUCIBLE PATHWAY IN METABOLISM AND CARDIOPULMONARY PHYSIOLOGY

The research in this thesis investigated the role of the hypoxia-inducible factor (HIF) family of transcription factors in metabolism and cardiopulmonary physiology. Specifically, the effects of HIF on ventilatory control, carotid body morphology, and cardiac metabolism and function were studied using a murine model of a genetic disorder of oxygen sensing known as Chuvash polycythaemia.

HIF coordinates oxygen-regulated gene expression throughout all organ systems, thereby orchestrating cellular, tissue and systemic responses to hypoxia. HIF is primarily regulated by oxygen-dependent prolyl hydroxylase-domain enzymes (PHDs) that initiate its degradation via the von Hippel-Lindau protein (VHL). In Chuvash polycythaemia, a homozygous VHL mutation in humans causes generalised stabilisation of HIF in euoxia, resulting in profound changes in cardiopulmonary physiology, exercise and metabolism. The Chuvash mouse model provides an opportunity to further characterise the role of HIF in different organ systems.

Chapter 2 of this thesis introduces the murine model, demonstrating an increase in haemoglobin and haematocrit in the Chuvash mice as well as a marked reduction in body weight.

Chapter 3 describes the ventilatory and carotid body study. Chuvash mice were shown to have elevated baseline ventilation in euoxia and marked ventilatory sensitivity to hypoxia. These findings were accompanied by changes within the carotid body, including hyperplasia, hypertrophy and altered ultrastructure of the oxygen-sensing type I cells.

Chapter 4 of this thesis describes the study into cardiac metabolism, energetics and function. Chuvash hearts were found to have increased glycolytic flux and lactate production (the latter both *in* and *ex vivo*), with altered myocardial energetics. Despite this, left ventricular function remained normal, although *in vivo* cine MRI revealed clear evidence of pulmonary hypertension and right ventricular hypertrophy.

Overall, this thesis provides evidence that the PHD-VHL-HIF axis plays a major role in calibrating the hypoxic response in the principal organ systems responsible for oxygen uptake, delivery and utilisation.

ABBREVIATIONS USED IN THIS THESIS

ACC	Acetyl-CoA carboxylase
AHVR	Acute hypoxic ventilatory response
ALDA	Aldolase A
ANOVA	Univariate analysis of variance
ARNT	Aryl hydrocarbon receptor nuclear translocator
bHLH	Basis helix-loop-helix
COX	Cytochrome c oxidase
CP	Chuvash polycythaemia
CPT	Carnitine palmitoyl transferase
DCV	Dense-cored vesicle
DNP	Dynamic nuclear polarisation
EDP	End-diastolic pressure
Eno	Enolase
Epo	Erythropoietin
ER	Endoplasmic reticulum
ET-1	Endothelin 1
FABP	Fatty acid binding protein
FACS	Fatty acyl-CoA synthase
FAT	Fatty acid transporter
FIH	Factor inhibiting HIF
GCMS	Gas chromatography mass spectrometry
GLUT	Glucose transporter
HIF	Hypoxia-inducible factor
HK	Hexokinase
HPLC	High pressure liquid chromatography
HR	Heart rate
HRE	Hypoxia response element
HVD	Hypoxic ventilatory decline
IPGTT	Intra-peritoneal glucose tolerance test
ISCU	Iron-sulphur cluster assembly proteins
KH	Krebs-Henseleit
LCMS	Liquid chromatography mass spectrometry
LDHA	Lactate dehydrogenase A
LV	Left ventricle
LVDP	Left ventricular developed pressure
M/L/VLCAD	Medium/long-chain/very long-chain acyl-CoA dehydrogenase
MR S/I	Magnetic resonance spectroscopy/imaging
NEFA	Non-esterified fatty acid
NMR	Nuclear magnetic resonance
NO	Nitric oxide
$PACO_2/O_2$	Alveolar partial pressure of carbon dioxide/oxygen
$PaCO_2/O_2$	Arterial partial pressure of carbon dioxide/oxygen
PCr	Phosphocreatine
PDH	Pyruvate dehydrogenase
PDK	PDK kinase
PFK	Phosphofructokinase
PGK	Phosphoglycerate kinase

PHD	Prolyl hydroxylase domain enzyme
PKM	Pyruvate kinase muscle
PPAR	Peroxisome proliferator-activated receptor
ROS	Reactive oxygen species
RPP	Rate pressure product
RV	Right ventricle
SCG	Superior cervical ganglion
SERCA	Sarcoplasmic endoplasmic reticulum Ca2+ ATPase
SIRT	Sirtuin
TAG	Triacyl glycerol
TH	Tyrosine hydroxylase
UCP	Uncoupling protein
VAH	Ventilatory acclimatisation to hypoxia
VDH	Ventilatory decline from hypoxia
VEGF	Vascular endothelial growth factor

TABLE OF CONTENTS

CHAPTER 1

General Introduction

1.1 HYPOXIA-INDUCIBLE FACTORS: MASTER REGULATORS OF OXYGEN HOMEOSTASIS

All animal life requires molecular oxygen as the terminal electron acceptor in aerobic energy production, and changes in the composition of the atmosphere are associated with key events in evolution (Taylor and McElwain 2010). Consequently, animals have evolved sophisticated mechanisms to detect and react to changes in oxygen availability. In all animal taxa studied to date, this sensing mechanism comprises oxygen-dependent post-translational modification of a conserved transcription factor termed hypoxia-inducible factor (HIF). The core components of the HIF pathway were established in a common metazoan ancestor and it has been shown that the simplest animal, *Trichoplax adhaerens*, possesses a regulatory oxygen-sensing HIF system (Loenarz *et al.* 2011). The pathway has subsequently undergone modification and refinement in descendant lineages, but the conservation of the HIF system throughout evolution underlines its fundamental role in oxygen homeostasis.

1.1.1 The discovery of HIF-1

Mammalian erythrocyte production and, hence, tissue oxygen delivery is regulated by the hormone erythropoietin (Epo). A substantial body of evidence demonstrated that Epo levels were determined by the rate of Epo gene transcription, and that this rate was directly influenced by oxygen availability. Epo mRNA levels were increased markedly in liver and kidney tissue of rodents exposed to hypoxia (Schuster *et al.* 1987; Schuster *et al.* 1989; Eckardt *et al.* 1992). This increase was subsequently demonstrated in Hep3B human hepatoma cells, indicating that the same cell type is able to sense and respond to hypoxia (Goldberg *et al.* 1987; Goldberg *et al.* 1988).

Nuclear extracts from hypoxic Hep3B cells enabled a higher level of Epo mRNA production *in vitro* compared to extracts from euoxic cells (Costa-Giomi *et al.* 1990).

Subsequent investigation of the 3'-flanking region of the human and mouse Epo genes revealed the presence of a hypoxia response element (HRE) which caused transactivation of a reporter gene under hypoxic conditions (Beck *et al.* 1991; Pugh *et al.* 1991; Semenza *et al.* 1991). An electrophoretic mobility-shift assay (EMSA) was performed using an oligonucleotide probe comprising part of the human Epo gene HRE, and identified a nuclear factor that was present only in hypoxic cells (Semenza and Wang 1992). This was designated HIF-1. Mutation of the EMSA probe disrupted binding of HIF-1 and eliminated hypoxia-induced transcription by the HRE (Semenza and Wang 1992). Subsequently, this experimental approach has been used to characterise additional hypoxia-inducible genes involved in diverse aspects of cellular and integrative physiology.

1.1.2 HIF structure

DNA affinity chromatography was used to purify HIF-1 protein (which comprises two subunits, α and β) from HeLa cells (Wang and Semenza 1995). Subsequent cDNA sequence analysis demonstrated that, whilst HIF-1β was in fact identical to the aryl hydrocarbon receptor (AHR) nuclear translocator (ARNT), HIF-1α was the unique and defining subunit (Wang *et al.* 1995). The NH_2-terminal half of both HIF-1α and HIF-1β consists of bHLH (basic helix-loop-helix) and PAS (Per-ARNT-Sim homology) domains (see Figure 1.1), through which the two subunits heterodimerise and bind DNA (Jiang *et al.* 1996a). The COOH-terminal half of HIF-1α contains two transactivation domains (TADs), separated by an inhibitory domain (ID, Figure 1.1). Hypoxia-inducible transcription of a reporter gene can be mediated by the entire

COOH-terminal half, TAD-N, or TAD-C domains (Jiang *et al.* 1997; Pugh *et al.* 1997). HIF-1α is encoded by the *HIF1A* gene and it has now been demonstrated that multiple HIF-1α isoforms are generated as a result of alternative splicing and promoter utilisation. All of these shorter isoforms differ at the COOH terminus and have been shown to have altered biological properties (Gothie *et al.* 2000; Chun *et al.* 2001; Chun *et al.* 2002; Chun *et al.* 2003; Lee *et al.* 2004), but the role of these variants in physiological responses to hypoxia is not well known.

Figure 1.1: Structure of HIF subunits

Domain structure of HIF subunits (adapted from (Prabhakar and Semenza 2012). Basic helix-loop-helix (bHLH); Per-Arnt-Sim homology domains (PAS); oxygen-dependent degradation domain (ODDD); NH_2-transactivation domain (TAD-N); inhibitory domain (ID); COOH-TAD (TAD-C).

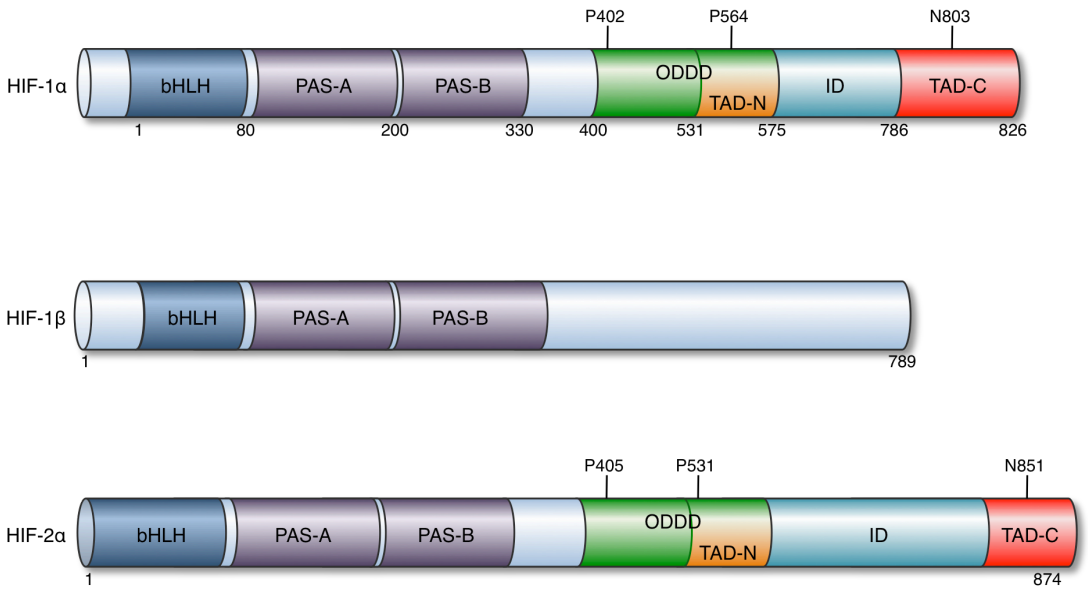

Database searches for nucleotide sequences similar to those of HIF-1α cDNA identified a protein previously known as endothelial PAS domain protein 1 (EPAS1) (Tian *et al.* 1997) – this has now been renamed as HIF-2α. HIF-1α and HIF-2α are the products of different genes, yet they share considerable amino acid identity (see Figure 1.1). This identity is highest in the NH2-terminal half of the protein (bHLH

and PAS domains) (Tian *et al.* 1997). HIF-2α is thus able to dimerise with HIF-1β and the resulting transcription factor can activate the expression of a reporter gene containing an HRE.

Further database searches also identified another protein, originally designated IPAS and now called HIF-3α (Makino *et al.* 2001; Makino *et al.* 2002). Multiple isoforms exist, some of which may dimerise with HIF-1β whilst others appear to bind to HIF-1α (Maynard *et al.* 2003), both resulting in inhibition of HIF-1 transcriptional activity. As *HIF3A* gene expression is induced by HIF-1 in hypoxic cells, it is possible that this provides a negative feedback mechanism (Makino *et al.* 2007).

HIF-1α is expressed in all mammalian tissues and cell types analyzed (Wenger *et al.* 1996; Wiener *et al.* 1996; Yu *et al.* 1998), whilst HIF-2α expression is more restricted (Ema *et al.* 1997; Flamme *et al.* 1997; Tian *et al.* 1997). Exposure of rats to hypoxia induced HIF-2α expression in distinct cell populations in brain, heart, intestine, kidney, liver and pancreas (Wiesener *et al.* 2003). Furthermore, whilst HIF-1α is present in all metazoans, HIF-2α appears to have arisen during vertebrate evolution (Epstein *et al.* 2001; Jiang *et al.* 2001). Some known HIF target genes, such as *EPO, GLUT1, VEGF* and *EGLN3*, can be activated by either HIF-1 or HIF-2. Others are activated only by HIF-1 (for example, *BNIP3, CAR9, LDHA, PGK1*) (Hu *et al.* 2003; Sowter *et al.* 2003; Raval *et al.* 2005; Elvidge *et al.* 2006) or HIF-2 (such as those encoding stem cell markers NANOG, OCT4/POU5F1, and SOX2) (Forristal *et al.* 2010).

1.1.3 The effect of hypoxia on HIF

Exposure of HeLa cells to hypoxia results in a dramatic increase in HIF-1α protein levels at O_2 concentrations below 6%, with half-maximal induction at approximately

1.5% and maximal induction at 0.5%. Reoxygenation to 20% O_2 causes rapid decay of HIF-1α with a half life of less than 5 minutes (Wang and Semenza 1995; Jiang *et al.* 1996b). HIF-1α levels have been shown to be the limiting factor for HIF-1 dependent gene transcription (Jiang *et al.* 1996a; Semenza *et al.* 1996). The short-half life of HIF-1α under euoxic conditions is due to rapid ubiquitination and proteasomal degradation (Salceda and Caro 1997; Huang *et al.* 1998; Kallio *et al.* 1999). HIF-1α residues 400 – 600 were required for this effect and hence this region was termed the oxygen-dependent degradation domain (ODDD) (Huang *et al.* 1998). The processes underlying the rapid degradation of HIF-α in euoxia are now well understood, and the roles of specific residues within the ODDD have been better defined.

HIF-α protein stability is regulated by prolyl hydroxylation

In well-oxygenated cells, HIF-α subunits are bound by the von Hippel-Lindau protein (VHL), which recruits an E3-ubiquitin protein ligase and mediates ubiquitination of HIF-α, marking it for proteasomal degradation (Maxwell *et al.* 1999; Kamura *et al.* 2000) (see Figure 1.1 and Figure 1.2). Binding of VHL is conditional upon prior hydroxylation of proline-564 (in human HIF-1α) (Ivan *et al.* 2001; Jaakkola *et al.* 2001) by prolyl-4-hydroxylase domain proteins (PHDs 1, 2 and 3) (Bruick and McKnight 2001; Epstein *et al.* 2001; Ivan *et al.* 2002). The PHDs are members of a superfamily of dioxygenases that contain Fe^{2+} in their catalytic centre and utilise O_2 and α–ketoglutarate as substrates, resulting in the production of HIF-1α-HydroxyPro564, PHD-Fe^{3+}, succinate, and CO_2. Ascorbate is required for the reduction of Fe^{3+} to Fe^{2+} for a subsequent catalytic cycle. HIF-1α is also hydroxylated at proline 402 (Masson *et al.* 2001), which requires prior hydroxylation of Pro564 (Chan *et al.* 2005). Both of these prolyl hydroxylation sites allow hydrogen bonds to form with VHL (Hon *et al.* 2002; Min *et al.* 2002), increasing the affinity of HIF-α

peptides for VHL almost three-fold (Schofield and Ratcliffe 2004); analogous proline residues are hydroxylated in HIF-2α (Masson *et al.* 2001) (see Figure 1.1).

Figure 1.2: Regulation of HIF-α

In euoxia, proline hydroxylation of HIF-α by PHDs allows binding of VHL. VHL recruits an E3-Ubiquitin protein ligase consisting of Elongin 2 and 3, Cullin 2, and RBX1 that is capable of functioning with E1-Ub-activating and E2-Ub-conjugating enzymes to mediate ubiquitination of HIF-α, targeting it for proteasomal degradation. Asparaginyl hydroxylation by FIH prevents recruitment of the transcriptional coactivators p300 and CBP. In hypoxia, HIF-α hydroxylation is limited, it escapes degradation and translocates to the nucleus where it dimerises with HIF-β and activates gene transcription via hypoxia response elements (HREs). p300/CBP recruitment may be modified by sirtuin 1, and Cited 2 and 4.

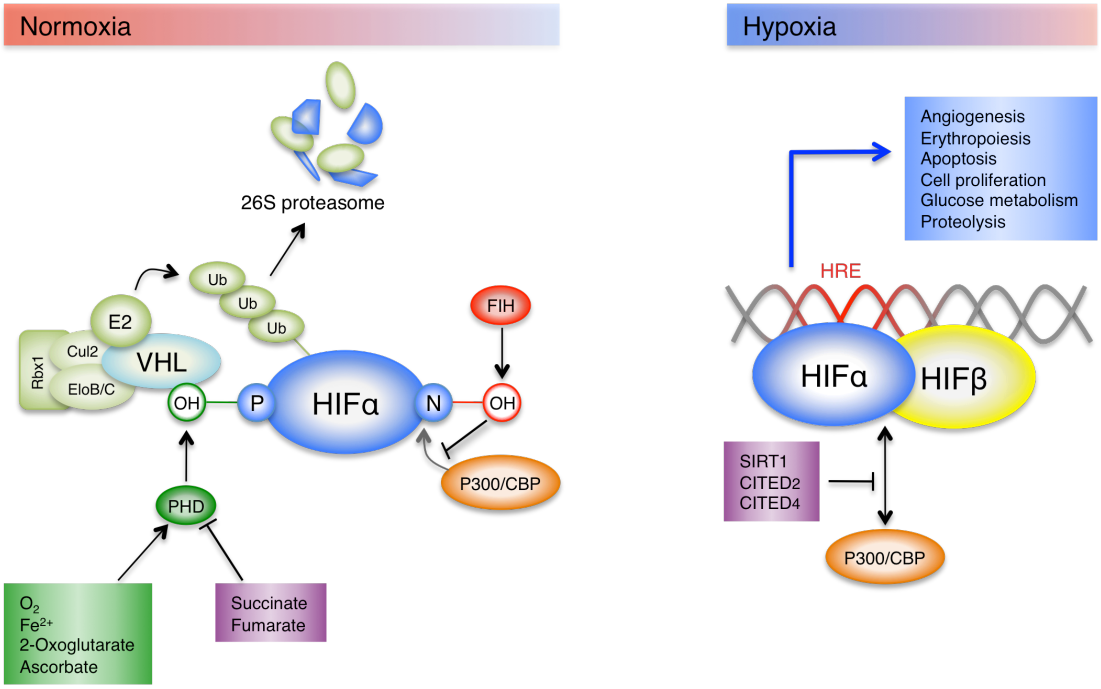

HIF-α protein function is regulated by asparaginyl hydroxylation

Hydroxylation of Asn-803, in the TAD-C (Figure 1.1), prevents the binding of the transcriptional coactivators p300 and CBP (Lando *et al.* 2002b) (see Figure 1.2). This asparaginyl hydroxylation is catalyzed by FIH (factor inhibiting HIF) (Lando *et al.* 2002a) which also utilises O_2 and 2-oxoglutarate and contains Fe^{2+} in its catalytic centre (Dann *et al.* 2002; McNeill *et al.* 2002; Lee *et al.* 2003). Asparaginyl hydroxylation therefore provides a second oxygen-dependent mechanism by which

HIF-α peptides that escape the PHD/VHL degradation pathway are prevented from activating transcription through the p300 coactivator.

Control of HIF hydroxylase activity

Emerging data indicate that the HIF hydroxylases are sensitive to moderate hypoxia, and that their activity may be affected by other factors, providing flexibility in the physiological responses to hypoxia.

Oxygen

The HIF hydroxylases have an absolute requirement for O_2. Assays of HIF hydroxylation *in vitro*, using cell extracts and recombinant PHD enzymes in graded-hypoxia conditions, have demonstrated a reduction in hydroxylation activity at 10% O_2, with progressive inhibition at lower oxygen tensions (Epstein *et al.* 2001). These studies indicate that the effective K_m of PHD enzymes for O_2 is high in relation to the physiological range of oxygen tension in tissues, and thus supports a sensing function. In contrast, similar studies of FIH indicate that its effective K_m for oxygen is lower and that its catalytic properties towards other co-substrates is also different (Koivunen *et al.* 2004).

Iron

Iron binding by enzymes such as the HIF hydroxylases is relatively labile. As a consequence, both the PHDs and FIH can be readily inhibited by iron chelators. This mechanism explains the stabilisation of HIF-α and the activation of HIF transcriptional activity in cells exposed to the iron chelator desferrioxamine. Fe^{2+} may also be substituted by other metals that are unable to participate in catalysis, such as Co^{2+}, Cu^{2+}, Zn^{2+} and Mn^{2+}, thus explaining the known hypoxia-mimetic effect of cobaltous ions.

Metabolic intermediates

A potential interface between the HIF hydroxylases and energy metabolism exists, since the Krebs cycle intermediates 2-oxoglutarate and succinate are required as co-substrate and product, respectively. Indeed, in addition to requiring 2-oxoglutarate, the HIF hydroxylases have been reported to be inhibited, to varying degrees, by citrate, isocitrate, succinate, fumarate, malate, oxaloacetate, and pyruvate (Dalgard *et al.* 2004; Isaacs *et al.* 2005; Selak *et al.* 2005; Hewitson *et al.* 2007; Koivunen *et al.* 2007). However, the most consistent effects have been observed with fumarate and succinate, which have been shown to inhibit all three PHDs competitively (Koivunen *et al.* 2007). FIH, in contrast, appears to be more sensitive to citrate and oxaloacetate (Hewitson *et al.* 2007; Koivunen *et al.* 2007). Thus, changes in the relative levels of metabolites may provide a link between metabolism and modulation of the HIF pathway. The clearest evidence that this may indeed be the case comes from the study of patients who are heterozygous for germline mutations in either fumarate hydratase or succinate dehydrogenase. Somatic inactivation of the second allele in susceptible cells results in marked accumulation of fumarate or succinate, with HIF-α activation that can be corrected by exogenous 2-oxoglutarate (in cell culture) (Isaacs *et al.* 2005; Pollard *et al.* 2005; Selak *et al.* 2005; MacKenzie *et al.* 2007).

Reactive oxygen species (ROS)

There is growing evidence that genetic and pharmacological interventions that enhance or reduce ROS generation result in enhanced or reduced, respectively, accumulation of hydroxylated HIF-α (Brunelle *et al.* 2005; Guzy *et al.* 2005; Mansfield *et al.* 2005). Controversy regarding the source(s) and mechanism(s) of ROS generation exists, but possible explanations for the altered hydroxylated HIF-α

levels include direct inhibition of the PHDs, or effects of ROS on levels of Fe^{2+}, ascorbate, or Krebs cycle intermediates.

Nitric oxide (NO)

NO is an *in vitro* inhibitor of the 2-oxoglutarate-dependent dioxygenases, since it is able to compete with O_2 for the binding of iron at the reactive site (Zhang *et al.* 2002). However, the role of NO *in vivo* is less clearly defined.

Multiple HIF hydroxylase isoforms

Higher metazoans contain three paralogous *PHD* genes. All three PHD enzymes are widely expressed (Lieb *et al.* 2002), but there are tissue-specific variations in their relative abundance. PHD2 appears to be the main player, contributing to the majority of HIF prolyl hydroxylase activity in euoxic cells, and thus setting euoxic HIF-1α levels (Berra *et al.* 2003; Minamishima *et al.* 2008; Takeda *et al.* 2008). The central role of PHD2 is emphasised by the fact that inactivation of *PHD2* severely disrupts murine development and results in embryonic lethality, whilst $PHD1^{-/-}$ and $PHD3^{-/-}$ mice are viable (Takeda *et al.* 2006).

1.1.4 Mechanisms by which HIFs mediate biological effects

Heterodimerisation of HIF-α and HIF-β underlies the majority of HIF-mediated responses to hypoxia, although it is now known that HIF-1α can also regulate gene expression without binding to DNA at all (by binding to and altering the function of other transcription factors, for example).

HIF-1 and HIF-2 bind to the conserved sequence 5'-(A/G)CGTG-3' within HREs of target genes in order to activate their transcription (Wang *et al.* 1995). The combination of microarray gene chip, RNA interference, and whole-genome chromatin immunoprecipitation (ChIP) technology has allowed the identification of

hundreds of direct HIF target genes in any given cell type. Intriguingly, whilst microarray assays have shown that the levels of hundreds of mRNAs are decreased in response to hypoxia, and that this reduction is HIF-dependent, ChIP assays have demonstrated that HIF does not bind directly to any of these hypoxia-repressed genes (in contrast to those which are upregulated) (Mole *et al.* 2009). Several possible mechanisms exist whereby HIF can indirectly repress gene transcription in hypoxia (Prabhakar and Semenza 2012). First, HIF may activate the transcription of a transcriptional repressor. Second, HIF may bind to and transactivate a target gene encoding one or more micro-RNAs which can subsequently bind to, and promote the degradation of, their target mRNAs. Third, a small number of genes appear to be directly repressed by the binding of HIF-1 to a "reverse-HRE".

Multiple feedback loops exist in which HIF gene targets themselves may modulate HIF activity. For example, *PHD2* is itself a HIF target gene (D'Angelo *et al.* 2003; Henze *et al.* 2010), providing a simple negative feedback mechanism whereby increased HIF protein levels bring about an increase in enzymes involved in their degradation. The molecular mechanism by which proteins encoded by HIF target genes may bring about feedback also varies. For example, rather than direct binding, a protein may interfere with HIF-1α function, as is the case of CITED2, which competes with HIF-1α for binding to the co-activator CBP (see Figure 1.2) (Freedman *et al.* 2003). Negative feedback is not necessarily provided by a protein product – HIF-1α antisense mRNA is also produced under hypoxic conditions and may downregulate the levels of HIF-1α protein (Thrash-Bingham and Tartof 1999). Feed-forward mechanisms also exist. For example, *SIRT1* transcription in hypoxic cells is activated by HIF-1 and HIF-2. Sirtuin1 (SIRT1) is then able to bind HIF-2α, catalyze deacetylation of one or more lysine residues and thus stimulate its transactivation

domain function, resulting in further *SIRT1* transcription (see Figure 1.2) (Dioum *et al.* 2009; Chen *et al.* 2011).

Figure 1.3: Transcriptional targets of HIF

Direct HIF transcriptional targets are involved in diverse cellular and physiological processes. Adapted from (Schofield and Ratcliffe 2004).

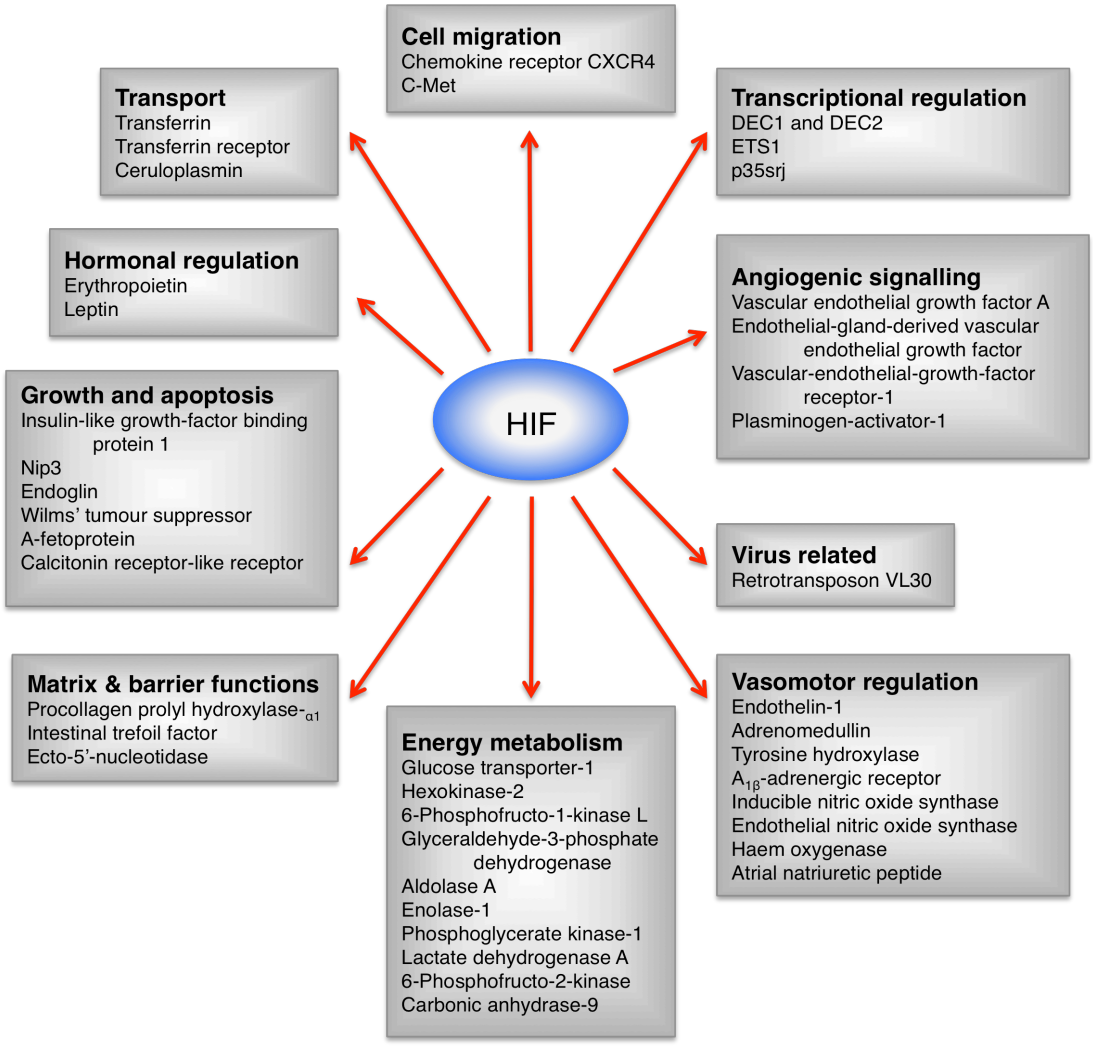

The large number of these feedback loops, both positive and negative, emphasise the critical importance of regulating oxygen delivery and utilisation. These feedback mechanisms are often specific to certain cell types, thus providing customised physiological responses to hypoxia. Furthermore, these feedback loops are mediated by a wide variety of molecular mechanisms. This therefore provides a means for integration of various physiological stimuli such as oxygen, metabolites, ROS, cytokines, and growth factors. Thus, HIF-signaling is a complex, integrative process with a high degree of flexibility.

1.1.5 Transcriptional targets of HIF

Direct transcriptional targets of HIF are involved in diverse cellular and integrative physiological processes such as energy metabolism, cell growth and hormonal regulation (see Figure 1.3). The individual responses of a given cell type or tissue to hypoxia add further complexity to the diversity of the HIF pathway. It is therefore unsurprising that genetic disorders of the PHD-VHL-HIF axis have diverse effects on cellular and integrative physiology.

1.2 MUTATIONS WITHIN THE HIF PATHWAY – CHUVASH POLYCYTHAEMIA

Familial or congenital polycythaemias are an uncommon group of inherited disorders that may be primary (in which erythroid progenitors are over-sensitive to Epo) or secondary (due to abnormally elevated circulating Epo levels). Most of the disorders described in the literature occur sporadically. However, in the Chuvash Autonomous Republic of European Russia an endemic form of familial polycythaemia was identified in the 1970s and brought to the attention of the wider scientific community (Sergeyeva *et al.* 1997). CP patients develop polycythaemia, varicose veins and haemangiomas, and have an increased risk of mortality from cerebrovascular events and peripheral thrombosis (Gordeuk 2004).

1.2.1 Mechanism underlying Chuvash polycythaemia

The wider awareness of CP and the elucidation of the PHD-VHL-HIF axis occurred contemporaneously, allowing the mutation underlying CP to be mapped and the molecular mechanisms underlying the polycythaemia to be described. Linkage to the *EPO, EPOR* (Epo receptor) and *HIF1A* genes had already been excluded (Ang *et al.* 2002a), and subsequent research localised the CP locus to chromosome 3p25, specifically to the region encoding VHL. Sequence analysis showed a 598-C → T transition in *VHL* that resulted in an Arg → Trp substitution at amino acid residue 200. All CP patients were homozygous with respect to the T allele (Ang *et al.* 2002b). Subsequent to this original identification, the Chuvash mutation has been found in other diverse ethnic groups, including a novel cluster on the island of Ischia (Pastore *et al.* 2003a; Pastore *et al.* 2003b; Percy *et al.* 2003; Bento *et al.* 2005; Cario *et al.*

2005; Perrotta *et al.* 2006). Haplotype analysis of Chuvash patients and controls indicated that the VHL 598-C → T mutation was spread from a single founder 14,000 to 62,000 years ago (Liu 2004).

An *in vitro* ubiquitination assay using EBV-transformed lymphoblasts showed that HIF-1α was ubiquitinated at a lower rate in CP cells. A subsequent *in vitro* capture assay showed that the interaction between VHL and HIF-1α (and also HIF-2α) was lower in CP than in wild type cells (Ang *et al.* 2002b). The CP *VHL* mutation therefore diminishes VHL's ability to bind hydroxylated HIF-α, resulting in impaired HIF-α degradation and pathological activation of HIF target genes, such as *EPO (Ang et al. 2002b)*.

CP has features of both primary and secondary polycythaemia (Ang *et al.* 2002b). Whilst the secondary polycythaemia, due to increased circulating Epo, can be readily explained by the chronic activation of the HIF pathway, the explanation for the increased sensitivity of erthyroid progenitors to Epo has only recently been identified (Russell *et al.* 2011). In brief, normal VHL is required for the ubiquitin-mediated degradation of pJAK2, a protein involved in the activation of erythroid progenitors (via the JAK2-STAT5 pathway). The CP mutation in VHL impairs the ubiquitination, and subsequent degradation, of both HIF-α and pJAK2, thus causing secondary and primary polycythaemia, respectively.

1.2.2 The Chuvash mutation affects metabolism and cardiopulmonary physiology

Chuvash patients present with polycythaemia (with associated fatigue, headaches and plethora), often before the age of 20 (Sergeyeva *et al.* 1997). They are at increased risk of early mortality, particularly from cerebrovascular events and peripheral

thrombosis (Sergeyeva *et al.* 1997; Gordeuk 2004). Interestingly, more recent studies have identified further profound effects of the Chuvash mutation on both metabolism and cardiopulmonary physiology.

Cardiopulmonary physiology

A comprehensive study of both ventilatory and pulmonary vascular responses to hypoxia, in Chuvash patients compared to matched controls, found several striking abnormalities (Smith *et al.* 2006). Many of these have been shown to be recapitulated in the recently-engineered mouse model that forms the basis of this thesis (Hickey *et al.* 2007; Hickey *et al.* 2010). These findings will be summarised in this chapter, and discussed in more detail in the relevant subsequent chapters.

Ventilation

Arterial blood analysis in Chuvash patients revealed a lowered air-breathing partial pressure of CO_2 (Pco_2), indicating an altered set point for respiratory control in the direction of elevated pulmonary ventilation. This was consistent with the tendency towards higher ventilation measured during isocapnic euoxia. Furthermore, exposure of Chuvash patients to mild (70 mm Hg) and moderate (50 mm Hg) isocapnic hypoxia resulted in marked increases in ventilation, well above those observed in normal subjects (Smith *et al.* 2006). The reduced Pco_2 set point for ventilation and an abnormally high acute hypoxic ventilatory sensitivity are striking, as together these features are characteristic of individuals acclimatised to chronic hypoxia. Arterial blood analysis in the Chuvash mouse similarly demonstrated the presence of a chronic respiratory alkalosis with metabolic compensation, consistent with the increased ventilation in euoxia that was also measured (Hickey *et al.* 2010). These findings are consistent with the notion that the VHL-HIF system is involved in ventilatory

acclimatisation to hypoxia, as well as establishing an important role for VHL in regulating respiratory control.

Pulmonary vasculature

Chuvash patients have been found to have a degree of pulmonary arterial hypertension (Smith *et al.* 2006; Sable *et al.* 2011). This has also been demonstrated in the mouse model, together with pulmonary vascular remodelling and right ventricular hypertrophy (Hickey *et al.* 2010). Strikingly, exposure of Chuvash patients to even mild hypoxia revealed exquisite pulmonary vascular sensitivity, whilst the moderate stimulus provoked peak systolic pulmonary arterial pressures of approximately 70 mm Hg (Smith *et al.* 2006). Similar to the ventilatory phenotype, the increased baseline pulmonary arterial pressure and marked sensitivity of the pulmonary vascular response to hypoxia are both characteristic features of acclimatisation to high altitude. Interestingly, *HIF2a* heterozygosity in the Chuvash mouse prevented the development of pulmonary hypertension, and caused partial protection against the vascular remodelling (Hickey *et al.* 2010).

Metabolism

A recent study of Chuvash patients and matched controls demonstrated striking effects on metabolism (Formenti *et al.* 2010). During an incremental exercise test, Chuvash patients failed to achieve the same work rate as control subjects. They stopped exercising early, and had significantly elevated ventilation and blood lactate levels. Exercise of a small muscle mass revealed early and marked phosphocreatine depletion and acidosis (measured using ^{31}P magnetic resonance spectroscopy). Muscle biopsy specimens from Chuvash patients showed elevated transcript levels for pyruvate dehydrogenase kinases 1, 2 and 4, phosphofructokinase, and muscle pyruvate kinase.

Comparison of a large number (88) of Chuvash patients with control subjects from Chuvashia revealed significantly reduced random blood glucose and glycosylated haemoglobin A1c levels (indicating chronic hypoglycaemia) (McClain *et al.* 2012). Chuvash mice also had lower fasting glucose levels and reduced glucose excursions in response to a glucose tolerance test. Furthermore, analysis of Chuvash mouse liver demonstrated decreased transcript levels of both glucose-6-phosphatase (involved in gluconeogenesis) and GLUT-2 (a glucose transporter), whilst analysis of skeletal muscle showed increased transcript levels of GLUT-1 and pyruvate dehydrogenase kinases 1 and 4 (McClain *et al.* 2012). These results suggested that both decreased liver gluconeogenesis and increased skeletal muscle glucose uptake and usage contributed to the decreased serum glucose levels.

Taken together, these studies indicate that the Chuvash mutation, whilst resulting in only a moderate increase in HIF-α levels, has profound effects on integrative physiology and metabolism.

1.3 OTHER MUTATIONS IN THE HIF PATHWAY

1.3.1 Mutations in *VHL*

Prior to the discovery of its role in oxygen sensing, VHL protein was primarily known as a tumour suppressor. Over 100 years ago, a hereditary cancer syndrome was described by Eugene von Hippel and Arvind Lindau in which patients developed a variety of tumours, including haemangioblastomas, clear cell renal carcinoma, phaeochromocytoma, and cystadenomas (Kaelin 2007). The VHL gene was successfully isolated in 1993 (Latif *et al.* 1993) and essentially all patients with a clinical diagnosis of VHL disease have been shown to be germline heterozygotes at the VHL locus, with one wild-type and one defective VHL allele (Stolle *et al.* 1998). Somatic inactivation of the remaining wild-type allele in a susceptible cell results in the development of pathological changes. VHL disease is thus transmitted clinically in an autosomal dominant manner, although it is in fact due to recessive mutations.

The CP mutation results in modest dysregulation of VHL in all cells from conception, with consequent systemic disruption of oxygen sensing. In contrast, the mutations associated with classic VHL disease cause markedly defective VHL function in only a subset of cells. Unless as part of a paraneoplastic syndrome (polycythaemia due to an Epo-secreting tumour, for example), patients with classic VHL disease do not tend to develop systemic pathology, nor do they demonstrate any of the altered physiology of oxygen sensing that is seen in the Chuvash patients (Formenti *et al.* 2011).

1.3.2 Mutations in *HIFa*

Several gain-of-function HIF-2α mutations exist in humans, and mouse models have been used to investigate the impact of loss-of-function mutations in both HIF-1α and HIF-2α.

Human diseases – gain-of-function mutations in HIF-2α

Several studies have described gain-of function mutations within *HIF2A* resulting in erythrocytosis (Gale *et al.* 2008; Martini *et al.* 2008; Percy *et al.* 2008a; Percy *et al.* 2008b; van Wijk *et al.* 2010); one of these studies also confirmed the presence of pulmonary hypertension (Gale *et al.* 2008). Subsequently, it was shown that patients with gain-of-function *HIF2A* mutations, similar to CP patients, have increased cardiac output and heart rate, and increased pulmonary vascular sensitivity to hypoxia (Formenti *et al.* 2011). However, other aspects of the CP phenotype (such as increased ventilatory sensitivity to hypoxia, reduced exercise capacity and elevated blood lactate levels) were not present. Similar findings were demonstrated in the mouse model (Tan *et al.* 2013). More recently, several studies have demonstrated the presence of polycythaemia and paragangliomas in patients with novel *HIF2A* mutations (Lorenzo *et al.* 2012; Zhuang *et al.* 2012; Yang *et al.* 2013).

Mouse studies – loss-of-function mutations

Homozygous deficiency of HIF-2α in mice is often embryonically lethal and surviving mice exhibit severe multiple organ pathology (Scortegagna *et al.* 2003). Heterozygous null mice exhibit hypertension, breathing instability and exaggerated carotid body response to hypoxia (Peng *et al.* 2011b), as well as impaired responses to chronic hypoxia such as impaired pulmonary vascular remodelling, erythropoiesis and

retinal neovascularisation (Brusselmans *et al.* 2003; Scortegagna *et al.* 2005; Dioum *et al.* 2008).

Complete loss of HIF-1α also results in embryonic lethality (Iyer *et al.* 1998). Heterozygous null mice develop normally, but when exposed to chronic hypoxia they exhibit delayed development of polycythaemia, pulmonary hypertension, pulmonary vascular remodelling and right ventricular hypertrophy (Yu *et al.* 1999). The mice also exhibit blunted cardio-respiratory and carotid body responses to both chronic and intermittent hypoxia (Kline *et al.* 2002; Peng *et al.* 2006), as well as altered metabolic responses to intermittent hypoxia (Li *et al.* 2006).

1.3.3 Mutations in the prolyl and asparaginyl hydroxylases

A variety of loss-of-function mutations in *PHD2* in patients with polycythaemia have been described (Percy *et al.* 2006; Percy *et al.* 2007; Ladroue *et al.* 2008; Albiero *et al.* 2012; Ladroue *et al.* 2012). Complete loss of *PHD2* in mice results in embryonic lethality (Takeda *et al.* 2006) whilst conditional somatic inactivation causes polycythaemia and congestive heart failure (Minamishima *et al.* 2008). Complete loss of the other prolyl hydroxylases is not embryonic lethal (Takeda *et al.* 2006), but adult mice deficient for *PHD1* develop altered basal metabolism (Aragonés *et al.* 2008) whilst those deficient for *PHD3* exhibit abnormal sympathoadrenal development and systemic hypotension (Bishop *et al.* 2008).

Intriguingly, mice deficient for *FIH* do not develop changes in classical aspects of HIF function, such as angiogenesis, erythropoiesis and development (Zhang *et al.* 2010). However, they have elevated baseline ventilation and hypoxic ventilatory sensitivity (with respiratory alkalosis), elevated metabolic rate, reduced body mass, and improved glucose and lipid homeostasis.

1.4 SUMMARY AND THESIS AIMS

There is a rapidly expanding body of evidence demonstrating that mutations within the PHD-VHL-HIF axis, in both patients and animal models, result in profound effects on integrative metabolism and cardiopulmonary physiology. The Chuvash mouse model provides a powerful opportunity to investigate these abnormalities in more detail and to increase our understanding of the effects of long-term activation of the HIF pathway.

The purpose of this thesis is to characterise the ventilatory and cardiac phenotypes of the mouse model of Chuvash polycythaemia. A systematic approach has been taken in this thesis to achieve these aims. First, Chapter 2 introduces the model and demonstrates that the Chuvash mouse develops polycythaemia. Chapter 3 focuses on the ventilatory phenotype of the Chuvash mouse, demonstrating the increased baseline ventilation and hypoxic ventilatory sensitivity that is also observed in the patients. Possible underlying mechanisms for this phenomenon are explored by analysis of carotid body morphology and Type I cell ultrastructure. A comprehensive study into the metabolic phenotype of the Chuvash heart is covered in Chapter 4. This includes a systematic study of substrate flux and utilisation, with consequent effects on cardiac energetics and function. Metabolomic and transcriptomic analysis complement these physiological studies. Finally, Chapter 5 draws together the final conclusions and proposals for future work.

CHAPTER 2

Introducing the Chuvash mouse model

2.1 INTRODUCTION

The CP mouse model was first reported in 2007 (Hickey *et al.* 2007). To generate the Chuvash Vhl $^{-/-}$ mice, a targeting vector was initially constructed (see Figure 2.1).

Figure 2.1: Generation of Vhl -/- mice

Representation of targeting construct used to introduce the R200W mutation in murine embryonic stem (ES) cells by homologous recombination. TK (HSV thymidine kinase – absence of TK confers resistance to ganciclovir); Neo^R (neomycin resistance); Wt (wild type). Adapted from (Hickey *et al.* 2007).

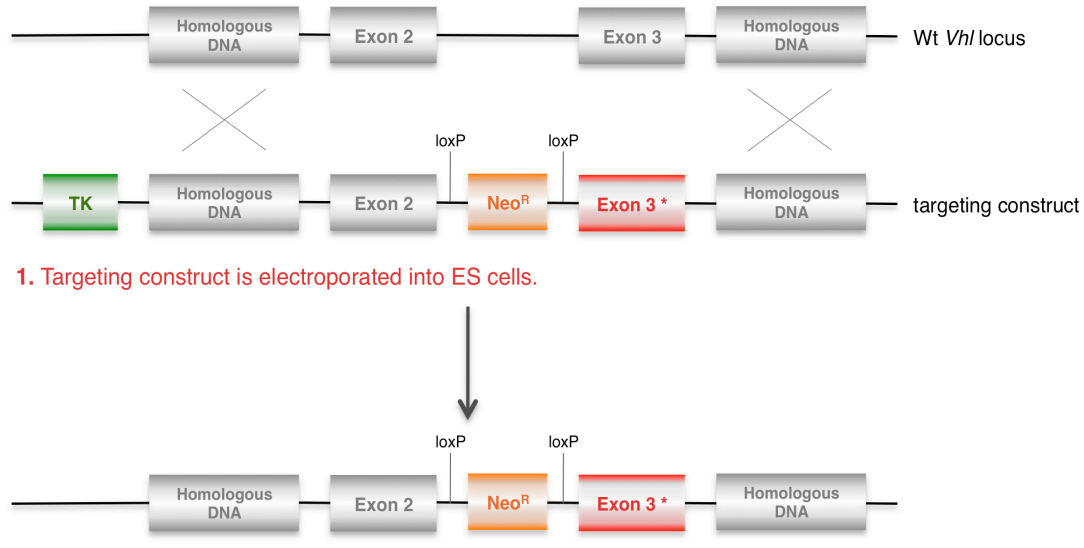

Briefly, a DNA fragment containing exons 2 and 3 of mouse *Vhl* was digested to separate the two exons. Exon 2 was then subcloned into a targeting vector, between a HSV-TK gene and floxed Neo^R cassette. Site-directed mutagenesis of exon 3 was performed and this mutated exon was directionally cloned adjacent to the Neo^R cassette. The completed construct also included 3 kb of homology upstream of exon 2, and 4 kb of homology downstream of exon 3, to enable homologous

recombination. The targeting construct was then electroporated into embryonic stem (ES) cells. Doubly ganciclovir- and neomycin-resistant ES clones were subsequently injected into murine blastocysts and transferred to pseudopregnant females. Heterozygous Vhl $^{-/+}$ mice were bred to transgenic Cre mice and subsequently to C57BL/6 mice to completely delete the Neo^R cassette.

The Chuvash mouse has been shown to be a faithful recapitulation of the human disease, with increased polycythaemia, ventilation and pulmonary hypertension (Hickey *et al.* 2007; Hickey *et al.* 2010). For the purpose of this thesis, Chuvash mouse breeding pairs (Vhl $^{-/-}$ and Vhl $^{+/+}$) were initially provided by Celeste Simon, University of Pennsylvania, US.

2.2 METHODS

2.2.1 Animal housing and breeding

All studies in this thesis conformed to the Home Office Guidance on the Operation of the Animals (Scientific Procedures) Act of 1986 and to University of Oxford institutional guidelines. Mice were housed in a 12/12 hour light/dark cycle at the University of Oxford. Normal chow and water were available *ad libitum*. Heterozygous Vhl $^{-/+}$ breeding pairs were used. Chuvash Vhl $^{-/-}$ and littermate wild type controls were used wherever possible.

2.2.2 Genotyping

Genomic DNA was extracted from mouse earclips using the Maxwell 16 Research System (Promega, UK). Mice were genotyped by PCR using primers that differentiated between the mutant and wild type alleles – primer 1: 5'-tgt gcc atc cct caa tgt cga tgg aca gc-3'; primer 2: 5'- cag aaa gtg gct ctg tag tct tga cct tg (Hickey *et al.* 2007). PCR was performed on a MJ-PTC-200 Thermal Cycler (MJ Research) using the optimised reaction mix and temperature protocol (adapted from (Hickey *et al.* 2007)) in Table 2.1.

The PCR products were subsequently separated by gel electrophoresis using a 2% agarose gel (Topvision Agarose, Fermentas UK) in 0.5% TBE (Ultrapure TBE, Invitrogen, UK) containing SYBR Safe DNA gel stain (Invitrogen, UK) and visualised using an ultraviolet lamp.

Table 2.1: PCR reagents and protocol for genotyping

Reagent (supplier)	Volume in μl (for 25 μl reaction)	Temperature protocol
Nuclease-free water (Qiagen, UK)	17.5	Step 1: 15 minutes at 95 °C Step 2: 1 minute at 94 °C Step 3: 1 minute at 58 °C Step 4: 1 minute at 72 °C Step 5: Repeat steps (2 to 4) 34 times Step 6: 10 minutes at 72 °C Step 7: Hold at 4 °C
10x PCR Buffer (Qiagen, UK)	2.5	
10 mM PCR Nucleotide Mix (Roche, UK)	0.5	
Hotstar Taq Polymerase (5 U/μl, Qiagen, UK)	0.5	
10 μM Primer 1 (Eurofins MWG Operon)	1	
10 μM Primer 2 (Eurofins MWG Operon)	1	
Genomic DNA	2	

2.2.3 Measurement of haemoglobin, haematocrit and body mass

Haemoglobin, haematocrit and body mass were measured in the majority of mice undergoing a terminal anaesthetic for studies described later in this thesis.

Mice were anaesthetised with 0.1 – 0.3 ml of intraperitoneal sodium pentobarbital (200 mg in 1 ml, Merial, UK). After loss of the withdrawal reflex, mice were weighed using electronic scales. The chest cavity was opened using scissors and brief dissection performed to visualise the heart, if necessary. The heart was excised for subsequent studies (see Chapter 4). Blood in the chest cavity was immediately collected in a microcuvette (10 μl) for haemoglobin quantification using a HemoCue Hb 201+ (HemoCue, UK). Further blood (up to 100 μl) was then rapidly collected in a heparin-coated glass Clinitube capillary tube (Micrometer, UK) which was sealed with clay (Micrometer, UK) and subsequently centrifuged at 10,000 RPM for 10 minutes in a Haematokrit 210 centrifuge (Hettich, Germany). Blood clearly separated into three layers – plasma (top), a thin layer of white blood cells and platelets

(middle) and red blood cells (bottom) – allowing measurement of haematocrit using a micro-haematocrit reader (Hawksley, UK).

2.2.4 Statistical analysis

Chuvash were compared to wild type mice. Deviation from the Hardy-Weinberg equilibrium was assessed using Pearson's Chi-squared test. All other comparisons between Chuvash and wild type were analysed using un-paired T tests. Significance was taken as $p < 0.05$. Statistical analysis was performed using SPSS Statistics 19 (IBM). Results are presented as mean ± standard error unless otherwise indicated.

2.3 RESULTS

2.3.1 Animal breeding and genotyping

Over the course of this thesis 829 experimental mice were bred and genotyped (see Figure 2.2).

Figure 2.2: Genotyping

Representative image of the DNA electrophoresis used for genotyping. Upper band is Hom (Chuvash, Vhl $^{-/-}$), lower band WT (wild type), and two bands Het (heterozygous, Vhl $^{-/+}$). Blank is PCR reagents with 2 μl nuclease-free water to replace DNA.

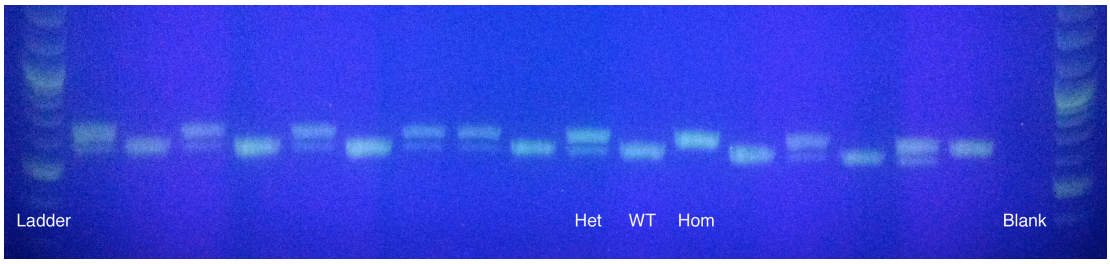

Table 2.2: Deviation from Hardy-Weinberg equilibrium

'Observed' indicates the number of mice of each genotype born from Het-Het matings. 'Expected' indicates what would be predicted from the Hardy-Weinberg principle – 25% of offspring would be either homozygous or wild type, and the remaining 50% would be heterozygous.

Genotype	Homozygous Vhl $^{-/-}$	Heterozygous Vhl $^{-/+}$	Wild type Vhl $^{+/+}$
Observed	88	497	244
Expected	207	415	207

Chuvash mice were born at well below the expected frequency that would be predicted by the Hardy-Weinberg principle ($p < 0.001$, see Table 2.2). Unless young (less than 4 months old) breeding pairs were used, litters frequently contained no Chuvash mice at all. Pups appeared to be dying *in utero*, rather than postnatally.

2.3.2 Body mass

Chuvash mice were significantly underweight compared to controls (see Table 2.3 and Figure 2.3). This was true for both male and female mice, although the effect of genotype was more marked in the male mice.

Figure 2.3: Body mass

White bars represent wild type; black bars represent Chuvash. * ($p < 0.05$); ** ($p < 0.02$); *** ($p < 0.01$); **** ($p < 0.001$).

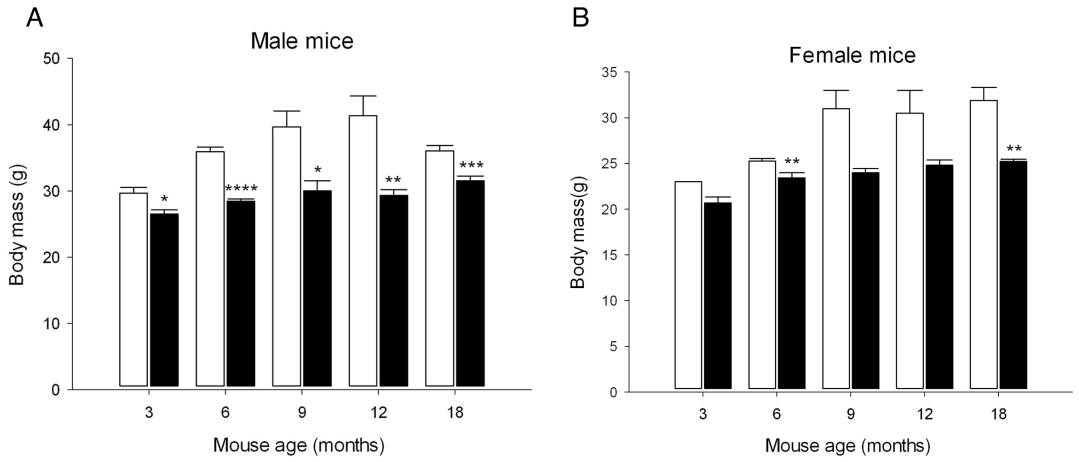

Table 2.3: Body mass

Summary of body mass data and the number of mice studies in each group. Age is in months.

	Male mice			Female mice		
Age	Wild type (n)	Chuvash (n)	*p* value	Wild type (n)	Chuvash (n)	*p* value
3	29.7 ± 0.9 (3)	26.5 ± 0.6 (4)	**0.031**	23.0 (1)	20.7 ± 0.7 (3)	--
6	35.9 ± 0.7 (12)	28.4 ± 0.4 (12)	**< 0.001**	25.3 ± 0.3 (4)	23.4 ± 0.5 (8)	**0.016**
9	39.7 ± 2.4 (3)	30.0 ± 1.5 (3)	**0.027**	31.0 ± 2.0 (2)	24.0 ± 0.4 (5)	0.163
12	41.3 ± 3.0 (3)	29.3 ± 0.9 (3)	**0.018**	30.5 ± 2.5 (2)	24.8 ± 0.6 (5)	0.249
18	36.1 ± 0.8 (3)	31.5 ± 0.7 (6)	**0.007**	31.9 ± 1.5 (4)	25.2 ± 0.2 (3)	**0.018**

2.3.3 Haemoglobin and haematocrit

Chuvash mice developed polycythaemia (see Figure 2.4; Table 2.4).

Figure 2.4: Haemoglobin and haematocrit

White represents wild type; black represents Chuvash. There was a strong correlation between haemoglobin and haematocrit (Pearson r = 0.89, $p < 0.0001$). *** ($p < 0.01$); **** ($p < 0.001$).

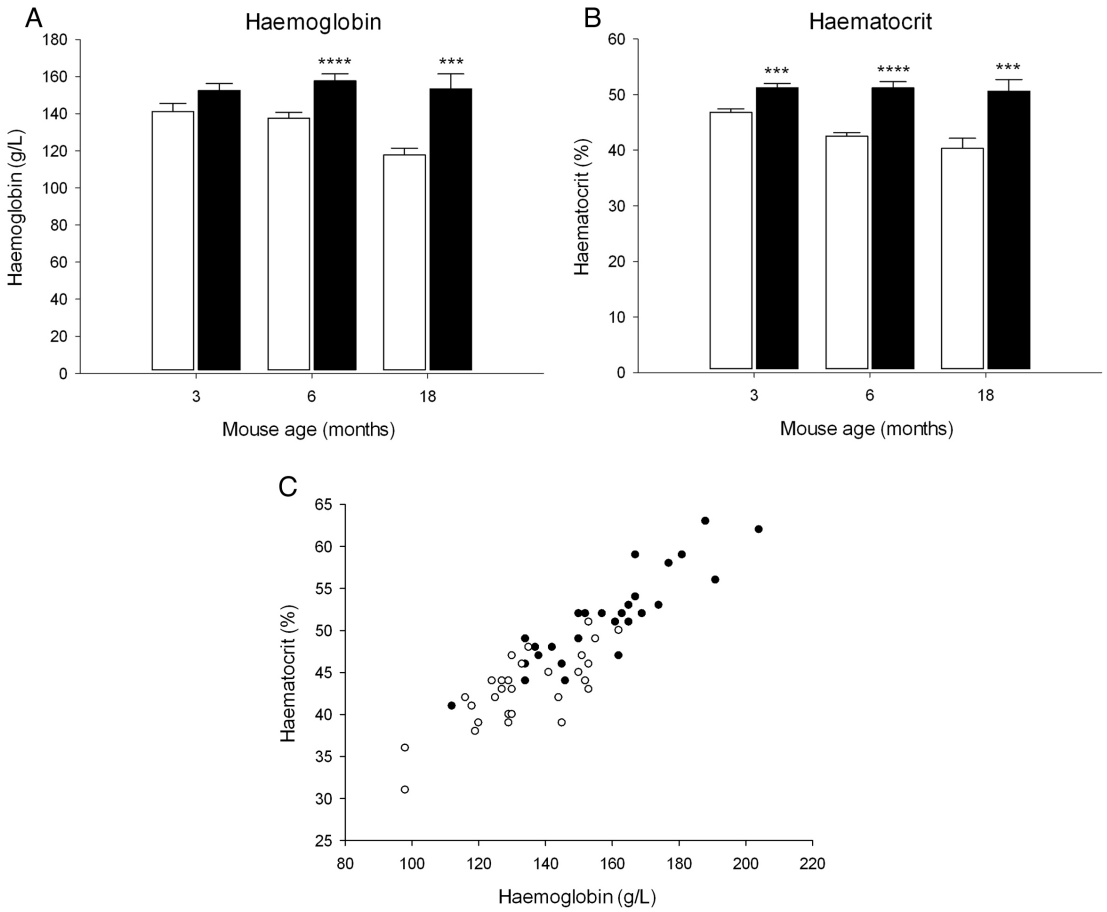

Table 2.4: Haemoglobin and haematocrit

Summary of haematology data and the number of mice used in each group. Age is in months.

	Haemoglobin (g/L)			Haematocrit (%)		
Age	Wild type (n)	Chuvash (n)	*p* value	Wild type (n)	Chuvash (n)	*p* value
3	141 ± 4 (6)	152 ± 4 (7)	0.073	46.8 ± 0.6 (6)	51.3 ± 0.8 (4)	**0.002**
6	138 ± 3 (16)	158 ± 4 (13)	**< 0.001**	42.5 ± 0.6 (13)	51.2 ± 1.1 (13)	**< 0.001**
18	118 ± 4 (10)	153 ± 8 (14)	**0.001**	40.3 ± 1.8 (9)	50.6 ± 2.1 (13)	**0.003**

2.4 DISCUSSION

2.4.1 Effect of the Chuvash Vhl $^{-/-}$ mutation on embryogenesis

The first notable effect of the Chuvash mutation was on mouse breeding. Chuvash mice were born at significantly lower frequency than would be predicted – only 11% (rather than 25%) of the offspring from het-het matings carried the Chuvash mutation. Young (less than 4 months old) breeding pairs were required to ensure that litters contained at least one Chuvash mouse, as it was observed that older breeding pairs produced litters that contained no Chuvash mice at all. The Chuvash mice appeared to by dying *in utero* as pups, once born, generally survived well.

It therefore appears that the Chuvash mutation has detrimental effects on embryogenesis. Whilst the reduced frequency of Chuvash mice (18%) was also noted previously (Hickey *et al.* 2007), the authors stated that there was no significant difference between the observed and predicted birth rates. This is surprising, as a simple Chi^2 analysis of the data published shows a significant difference (X^2=5.9; $p < 0.05$).

Murine models designed to inactivate the key players of the HIF pathway (HIF 1α, HIF 2α, PHD1/2/3, and VHL), resulting in either markedly increased or decreased HIF levels, have all now been engineered and shown to have profound effects on embryogenesis and placentation. HIF 1α $^{-/-}$ embryos initially comprise 25% of those *in utero*, but all of these die by embryonic day 11 (E11) from neural tube defects, cardiovascular malformations and cephalic abnormalities (Iyer *et al.* 1998). Similarly, HIF 2α $^{-/-}$ embryos comprise 25% of the total, but half of these die *in utero* from cardiac failure (Compernolle *et al.* 2002). Those that survive to term die a few hours postnatally from severe respiratory distress syndrome. Mice homozygous for a *HIF*

2α gain-of-function mutation are also born at reduced frequency (13% rather than 25%) (Tan *et al.* 2013). PHD 2 $^{-/-}$ embryos develop normally until E12.5, comprising 25% of the total, but from E13.5 die from severe placental and cardiac defects (Takeda *et al.* 2006). In contrast, PHD 1 $^{-/-}$ and PHD 3 $^{-/-}$ mice survive normally (Takeda *et al.* 2006). Complete knockout of Vhl (Vhl $^{-/-}$) results in normal embryonic development initially, followed by placental dysgenesis and lethality at E10.5-12.5, whilst Vhl $^{-/+}$ mice develop normally (Gnarra *et al.* 1997).

Taken together, these studies demonstrate clearly the central role of the PHD-VHL-HIF axis in embryogenesis and placentation. It is therefore unsurprising that the Chuvash mutation similarly results in detrimental effects during development. Without characterising the lost Chuvash embryos themselves, it is difficult to identify with certainty the underlying defect. However, the central role of HIF in placentation and organ development make these two areas likely candidates. This thesis does not develop this hypothesis further, but it would make an interesting future project.

2.4.2 Abnormal mass of the Chuvash mice

The Chuvash mice, both male and female, were significantly underweight compared to controls. Interestingly, previous large-scale studies of Chuvash patients also demonstrated significant reductions in body mass and/or body mass index (BMI) (Gordeuk 2004; Yoon *et al.* 2010; McClain *et al.* 2012). Prior to this thesis, no comment had been made on the body mass of the Chuvash mouse (Hickey *et al.* 2007; Hickey *et al.* 2010; McClain *et al.* 2012). Body mass was shown to be unchanged in HIF 1α $^{-/+}$ (Yu *et al.* 1999; Kline *et al.* 2002), HIF 2α $^{-/+}$ (Brusselmans *et al.* 2003), and HIF 2α gain-of-function mice (Tan *et al.* 2013), and was not commented upon in other studies of PHD 1/2/3 null mice (Takeda *et al.* 2006;

Aragonés *et al.* 2008; Bishop *et al.* 2008). However, FIH null mice have reduced body mass and elevated metabolic rate, and are resistant to high-fat diet-induced mass gain and hepatic steatosis (Zhang *et al.* 2010).

The mechanism(s) underlying the reduction in body mass in both Chuvash patients and mice is likely to be multifactorial. The Chuvash mutation is known to result in polycythaemia, pulmonary hypertension, hypoglycaemia, pulmonary fibrosis and increased organ size. The presence of multiple pathologies and disease processes is therefore a possible explanation. An alternative consideration is the elevated metabolic rate seen in the FIH null mice (Zhang *et al.* 2010). Whilst several studies have documented marked metabolic abnormalities in both Chuvash patients and mice (Formenti *et al.* 2010; McClain *et al.* 2012), no measurements of metabolic rate or respiratory exchange ratio have yet been made. Whilst the lowered body mass in the Chuvash mouse was taken into account during this thesis (for example, during measurements of heart mass and of ventilation), no further investigation was performed to identify the underlying cause(s).

2.4.3 Confirmation of the model - Chuvash mice develop polycythaemia

The Chuvash mice developed elevated haemoglobin and haematocrit from as early as 3 months of age. The degree of polycythaemia documented in this thesis is very similar to that shown in a previous study on the Chuvash mouse (Hickey *et al.* 2007). The use of the HemoCue for measurement of haemoglobin proved to be very successful. Difficulties in blood sampling in mice include venous access and blood volume. The HemoCue requires only 10 μl of blood, giving a result within 2 minutes, and is therefore perfectly suited to murine haemoglobin measurement. Furthermore, there was a significant correlation between haemoglobin and haematocrit

measurements. The presence of polycythaemia was therefore a useful surrogate measure to confirm that the Chuvash mice for this thesis did indeed recapitulate the human phenotype.

2.5 CONCLUSIONS

This opening experimental chapter aimed to introduce and confirm the Chuvash polycythaemia mouse model. In keeping with previous studies, the mice developed moderate polycythaemia from 3 months of age. In addition, it has also been shown that both male and female Chuvash mice were underweight compared to wild type controls, and that they were born at a markedly lower frequency than would be predicted. The latter finding is of considerable importance for the subsequent chapters of this thesis. A particular limiting factor with regards to experimental design was the number of Chuvash mice available; the studies were conducted carefully so that maximum information could be gathered from a small number of experimental animals. Nevertheless, a comprehensive analysis of the ventilatory and cardiac metabolic phenotype of the Chuvash mouse has been conducted and will be presented in subsequent chapters.

CHAPTER 3

Ventilation study

3.1 ABSTRACT

The hypoxia-inducible factor (HIF) family of transcription factors coordinates diverse cellular and systemic responses to hypoxia. Chuvash polycythaemia is an autosomal recessive disorder in humans in which there is impaired oxygen-dependent degradation of HIF, resulting in long-term systemic elevation of HIF levels at normal oxygen tensions. Chuvash patients demonstrate the characteristic features of ventilatory acclimatisation to hypoxia, namely an elevated baseline ventilation and enhanced acute hypoxic ventilatory response. The study in this thesis investigated the ventilatory and carotid body phenotype of a mouse model of Chuvash polycythaemia, using whole-body plethysmography, immunohistochemistry, and electron microscopy. In keeping with studies in humans, Chuvash mice had elevated ventilation in euoxia and a significantly exaggerated acute hypoxic ventilatory response when exposed to 10% oxygen, with or without the addition of 3% carbon dioxide. Carotid body immunohistochemistry demonstrated marked hyperplasia of the oxygen-sensing Type I cells, and the cells themselves appeared enlarged with more prominent nuclei. This hypertrophy was confirmed by electron microscopy, which also revealed that the Type I cells contained an increased number of mitochondria, enlarged dense-cored vesicles, and markedly expanded rough endoplasmic reticulum. The morphological and ultrastructural changes seen in the Chuvash mouse carotid body are strikingly similar to those observed in animals exposed to chronic hypoxia. This study demonstrates that the HIF pathway plays a major role, not only in regulating both euoxic ventilatory control and the sensitivity of the response to hypoxia, but also in determining the morphology of the carotid body.

3.2 INTRODUCTION

Lowland sojourners to high altitude experience considerable physiological changes due to environmental hypoxia. Of all these changes, the increase in ventilation is the one most profoundly experienced – Reinhold Messner, upon summitting Everest without supplemental oxygen in 1978, eloquently stated "I have nothing more to do than breathe…. I am nothing more than a single, narrow, gasping lung floating over the mists and summits".

The landmark 1911 Oxford-Yale expedition to Pike's Peak, Colorado, confirmed a previous observation that the alveolar partial pressure of carbon dioxide (P_ACO_2) falls linearly with altitude, whilst also demonstrating that that of oxygen (P_AO_2) rises as a result of hyperventilation (Douglas *et al.* 1913). The increase in ventilation upon exposure to hypoxia is initially very rapid, peaking within minutes and then declining towards pre-hypoxic levels over the following minutes to hours. If hypoxia continues, the process of ventilatory acclimatisation to hypoxia follows, which comprises both a progressive increase in ventilation together with increased sensitivity to further hypoxic stimuli (Douglas *et al.* 1913; Sato *et al.* 1992; Howard and Robbins 1995b; Howard and Robbins 1995a).

The mechanisms underlying ventilatory responses to hypoxia are not fully understood. Here, the successive phases of the response and their hypothesised mechanisms are discussed. The study of genetic disorders of oxygen sensing is beginning to shed new light on this area and will be placed in context prior to presenting the results from the Chuvash mouse.

3.2.1 Acute hypoxic ventilatory response

The acute hypoxic ventilatory response (AHVR) describes the rapid increase in ventilation that occurs immediately upon exposure to hypoxia and which peaks within minutes. This increase in ventilation varies considerably from individual to individual and does not tend to begin until the P_AO_2 falls to approximately 50 mm Hg, after which ventilation increases progressively with falling P_AO_2 (Lenfant and Sullivan 1971; Dempsey and Forster 1982; Powell *et al.* 1998). Although P_AO_2 is considered to be the primary chemosensory stimulus, the relationship between it and ventilation is hyperbolic, whilst that of arterial haemoglobin saturation and ventilation is approximately linear (West *et al.* 2007).

The carotid body mediates AHVR

The carotid bodies, located bilaterally in the carotid artery bifurcations in the neck, have the highest blood flow (to metabolism) in the body. As well as playing a pivotal role in oxygen sensing, carotid bodies are also sensitive to a variety of stimuli such as hypercapnia, acidosis, hyperkalaemia and hypoglycaemia (Teppema and Dahan 2010). The peripheral chemoreceptors, specifically those in the carotid body (in humans), mediate the AHVR. Removal of the carotid bodies results in loss of the AHVR in animals (Bisgard and Vogel 1971) and humans (Lugliani *et al.* 1971; Wasserman *et al.* 1975; Honda *et al.* 1979), as does surgical denervation (Timmers *et al.* 2003).

The glomus (Type I) cells within the carotid body have many similarities with sensory neurons and are thought to be the main oxygen sensors. These cells are in close proximity to nerve endings of sensory neurons which have cell bodies in the petrosal ganglia and peripheral axons running with the carotid sinus nerve (a branch of the

glossopharyngeal nerve). The central axons of these sensory neurons enter the brainstem and terminate in subnuclei of the nucleus tractus solitarius that have multiple connections with the brainstem respiratory centre (Teppema and Dahan 2010).

Whilst controversy remains over the signal-transduction cascade in the carotid body, a general consensus has been reached regarding some aspects of the Type I cell response to hypoxia. In brief, a decrease in oxygen tension within the cells is detected by as yet unknown primary oxygen sensors that rapidly communicate with potassium channels in the cell membrane, leading to their closure (Wyatt and Peers 1995). This results in membrane depolarisation, influx of calcium ions via voltage-dependent Ca^{2+} channels (Benot and Lopez-Barneo 1990), and subsequent release of neurotransmitters into the synaptic cleft (Urena *et al.* 1994; Pardal *et al.* 2000). These excitatory neurotransmitters include acetylcholine (Eyzaguirre and Zapata 1968) and ATP (Zhang *et al.* 2000), ultimately resulting in an increase in afferent discharge in the carotid sinus nerve and, hence, in the respiratory centres of the brainstem. Many neurotransmitters have been implicated in the central control of ventilation within these centres, including adenosine, serotonin, dopamine, substance-P, amino acids (glutamate, γ-aminobutyric acid (GABA), taurine, glycine) and acetylcholine (Burton and Kazemi 2000). It should be noted that the carotid body itself is also under neural control and that the chemoreceptor gain can be both decreased (by carotid sinus nerve efferents) and increased (by excitation of the carotid body's sympathetic nerve supply).

The role of HIFs in the carotid body and the AHVR

Type I cells of the rat and mouse carotid bodies express both HIF-1α and HIF-2α (Kline *et al.* 2002; Roux *et al.* 2005; Lam *et al.* 2008) and there is increasing evidence that HIFs play an important role in oxygen sensing by the carotid body.

Whole-body plethysmography has been used to measure AHVR in response to 12% O_2 in *Hif-1α*$^{+/-}$ mice and wild type controls (Kline *et al.* 2002). Interestingly, whilst there was no difference in AHVR between the two groups, a Dejours test indicated diminished carotid body function. During this test, the magnitude of the transient ventilatory decline that occurs in response to a brief hyperoxic exposure is used as an index of carotid body sensitivity (Dejours 1962). Demonstration of markedly impaired AHVR in *Hif-1α*$^{+/-}$ mice following vagotomy revealed an increased reliance on O_2 sensing by chemoreceptors other than the carotid body, corroborating the results of the Dejours test. Furthermore, carotid sinus nerve activity in response to acute hypoxia in carotid bodies removed from *Hif-1α*$^{+/-}$ mice was almost completely absent. Despite this, carotid body and Type I cell morphology themselves were normal. The authors concluded that partial HIF-1α deficiency in mice causes impaired oxygen sensing and/or signal transduction in the carotid body, resulting in increased reliance upon non-carotid body chemoreceptors for O_2 sensing and maintenance of AHVR.

In contrast, both AHVR and hypoxia-induced carotid sinus nerve recordings from *Hif-2α*$^{+/-}$ mice have been shown to be markedly increased, despite normal carotid body morphology (Peng *et al.* 2011b). Reduced expression of antioxidant enzymes in the carotid body, together with restoration of ventilatory and carotid body responses to hypoxia with antioxidant treatment, led to the hypothesis that the heightened hypoxic sensitivity in *Hif-2α*$^{+/-}$ mice may be due to oxidative stress. More recent work

has suggested that redox balance, determined by mutual antagonism between HIF 1α and HIF 2α, determines the set point for hypoxic sensing by the carotid body (Yuan *et al.* 2013).

Mice lacking FIH have elevated baseline ventilation in euoxia with consequent hypocapnia and respiratory alkalosis, although data on carotid body morphology and function are lacking (Zhang *et al.* 2010). Similarly, Chuvash patients also exhibit augmented ventilatory responses to acute hypoxia (Smith *et al.* 2006). In contrast, patients heterozygous for a HIF 2α gain-of-function mutation have a degree of elevated ventilation relative to metabolism (indicated by arterial and end-tidal hypocapnia) but do not exhibit any increase in ventilatory sensitivity to hypoxia (Formenti *et al.* 2011). This finding has been confirmed in a recently-engineered mouse model (Tan *et al.* 2013).

3.2.2 Hypoxic ventilatory decline

Hypoxic ventilatory decline (HVD) describes the decrease in ventilation that occurs if the duration of hypoxia exceeds several minutes. Ventilation falls over the following minutes-to-hours towards (but not reaching) the pre-hypoxic level (Weil and Zwillich 1976; Khamnei and Robbins 1990). HVD is not simply due to the respiratory alkalosis that results from the initial increase in ventilation, since it has also been demonstrated during isocapnic hypoxia (Khamnei and Robbins 1990). The cause and site of action of HVD remain unknown, although it seems to represent a decline in hypoxic chemosensitivity rather than a change in ventilatory drive (Robbins 1995).

3.2.3 Ventilatory acclimatisation to hypoxia

When hypoxia is sustained for at least several hours the characteristic features of ventilatory acclimatisation to hypoxia (VAH) occur, namely a progressive increase in

baseline ventilation and augmented ventilatory response to subsequent acute hypoxia (Douglas *et al.* 1913; Rahn and Otis 1949; Sato *et al.* 1992; Howard and Robbins 1995b; Howard and Robbins 1995a). VAH occurs in response to both isocapnic and poikilocapnic hypoxia, and the time course varies across species.

The carotid body is essential for VAH

A large body of evidence suggests that carotid body stimulation and the ensuing chemosensory reflex are critical for evoking VAH. Carotid body denervation in animals renders them incapable of acclimatising normally (Forster *et al.* 1981; Lahiri *et al.* 1981; Smith *et al.* 1986). In a series of experiments in goats, employing perfusion of the carotid body independent from the systemic circulation, it was demonstrated that, in the presence of systemic euoxia, several hours of isolated carotid body hypoxia were able to produce VAH (Busch *et al.* 1985). Conversely, acclimatisation did not occur when systemic hypoxia was applied in the presence of isolated carotid body euoxia (Weizhen *et al.* 1992).

Chronic hypoxia leads to hypersensitivity of the carotid body to acute hypoxia (Bisgard 2000). Exposure to chronic hypoxia results in an increase in the size and number of Type I cells, the diameter of their cytoplasmic dense-cored vesicles (DCV) and the quantity of their mitochondria and rough endoplasmic reticulum (ER) (Moller *et al.* 1974; Laidler and Kay 1975; Laidler and Kay 1978; Pequignot *et al.* 1984; Kameda *et al.* 1998; Wang and Bisgard 2002; Pardal *et al.* 2007; Wang *et al.* 2008). Various mechanisms may account for the chronic hypoxia-induced hypersensitivity of the carotid body. Alterations in ion channel proteins, heme and/or redox-sensitive proteins, neurotransmitters, and in the recruitment of additional excitatory neuromodulator(s) have all been described (Prabhakar and Jacono 2005).

HIF and the carotid body response to chronic hypoxia

Many HIF target genes are implicated in chronic hypoxia-induced changes in carotid body morphology and physiology of the chemoreflex pathway, and there is growing support for the concept that these may drive VAH. For example, vascular endothelial growth factor (VEGF, a well-established HIF target) has been implicated in the morphological changes of the carotid body (Jyung *et al.* 2000). The expression of endothelin-1 (ET-1) is markedly increased in Type I cells during chronic hypoxia (Chen *et al.* 2002). Chronic hypoxia-induced sensitisation of the hypoxic response and changes in carotid body morphology are blocked by ET_A receptor antagonists (Chen *et al.* 2002; Chen *et al.* 2007), whilst mice with heterozygous loss of the gene encoding pre-pro-ET-1 have a blunted HVR (Kuwaki *et al.* 1996).

Genetic disorders of oxygen sensing also provide useful insights. Whilst wild type mice develop the characteristic features of VAH in response to hypobaric hypoxia, *Hif-1α*$^{+/-}$ mice display a remarkable absence of ventilatory acclimatisation (Kline *et al.* 2002). Chuvash patients display the characteristic features of VAH, with elevated baseline ventilation (and consequent respiratory alkalosis) and increased hypoxic ventilatory sensitivity (Smith *et al.* 2006).

3.2.4 Ventilatory de-acclimatisation to hypoxia

After prolonged exposure to hypoxia, ventilation and AHVR remain elevated even upon restoration of euoxia. If euoxia persists, they progressively normalise over a time course similar to that of the increases seen during VAH. This ventilatory de-acclimatisation to hypoxia (VDH) has been demonstrated immediately following several weeks at simulated high altitude (Schoene *et al.* 1990) and is present when volunteers are studied within an hour following 8 hours of isocapnic hypoxia in the

laboratory (Clar *et al.* 2001). The mechanisms underlying VDH are presumed to be the same as those that are responsible for VAH.

3.2.5 Ventilatory phenotype of Chuvash Polycythaemia in humans and mice

Patients with CP have elevated baseline ventilation (with consequent respiratory alkalosis) and an abnormally high AHVR (Smith *et al.* 2006). In other words, they demonstrate the characteristic features of individuals acclimatised to hypoxia. In keeping with the human disease, the mouse model of CP demonstrated elevated ventilation in euoxia, but the increase in AHVR appeared to be absent which led the authors to conclude that the model did not recapitulate this aspect of the human disorder (Hickey *et al.* 2010). However, a concern with this study is that the authors measured averaged ventilation over 10 minutes of 12% oxygen, and thus the associated hypocapnia and HVD may well have masked the true phenotype. The purpose of the study in this thesis was to use a form of hypoxia and data analysis in which the confounding effects of hypocapnia and HVD have been minimised.

3.3 SUMMARY AND STUDY AIMS

There is growing evidence to support the notion that carotid body changes, mediated by HIF, drive ventilatory acclimatisation to hypoxia. The purpose of this study was to investigate the ventilatory and carotid body phenotype in the Chuvash mouse in more detail by linking physiological responses, morphological and ultrastructural changes together. Whole-body plethysmography allowed measurement of ventilatory responses to hypoxia and hypoxia/hypercapnia. Immunohistochemistry of the carotid body enabled gross morphological changes to be assessed, whilst transmission electron microscopy provided further insights into Type I cell ultrastructure.

3.4 METHODS

Mice were bred and housed according to the methods described in 2.2.1. The age, sex and number of mice used in each study will be specified in the relevant results sections.

3.4.1 Measurement of AHVR – whole body plethysmography

Whole body plethysmography describes the technique in which a mouse is placed within a specially-designed closed chamber and the pressure inside this container is measured. As the mouse breathes, cyclic variations in chamber pressure occur during inspiration and expiration. The reason for this is that as the mouse breathes in, the inhaled air is heated and humidified, thus causing the thoracic cavity to expand slightly more than the absolute volume breathed in. These pressure changes are used to measure respiratory frequency and tidal volume (Epstein and Epstein 1978). Whole body plethsymography is a widely-used technique for the measurement of AHVR in mice and other animals (Bates and Irvin 2003).

Plethysmography apparatus

Four parallel plethysmograph chambers were used (Buxco Europe Ltd, UK), allowing measurements to be made in four mice simultaneously. Each chamber had an approximate volume of 600 ml^3 and mice rapidly became adjusted to their new temporary surroundings. A pressure transducer enabled measurement of the chamber pressure and this signal was connected via pre-amplifier modules to a standard laptop computer, on which proprietary software was used to collect and analyse ventilatory data. Respiratory rate and tidal volume (corrected to body mass) were measured, and minute ventilation calculated as the product of these.

Gas was supplied to the chamber from one of three gas cylinders of certified oxygen content – one of 21 % O_2/balance N_2 (euoxia), one of 10 % O_2/balance N_2 (hypoxia), and one of 10 % O_2/3 % CO_2/balance N_2 (hypoxia/hypercapnia) (BOC, Manchester, UK). Gas was delivered from these cylinders via a three-way tap that allowed switching of the gas supply from euoxia to hypoxia or hypoxia/hypercapnia according to the experimental protocol. Gas was subsequently delivered to a set of four flow regulators that controlled the gas flow to each individual plethysmograph chamber.

Figure 3.1: The plethysmography apparatus

Whole body plethysmography was used to measure AHVR in awake mice. Multiple chambers could be used simultaneously (A). 8 chambers are illustrated here, but for the studies in this thesis only 4 chambers were used at any one time. Each plethysmograph had a separate gas supply and outlet, as well as a pressure transducer for the measurement of ventilation (B).

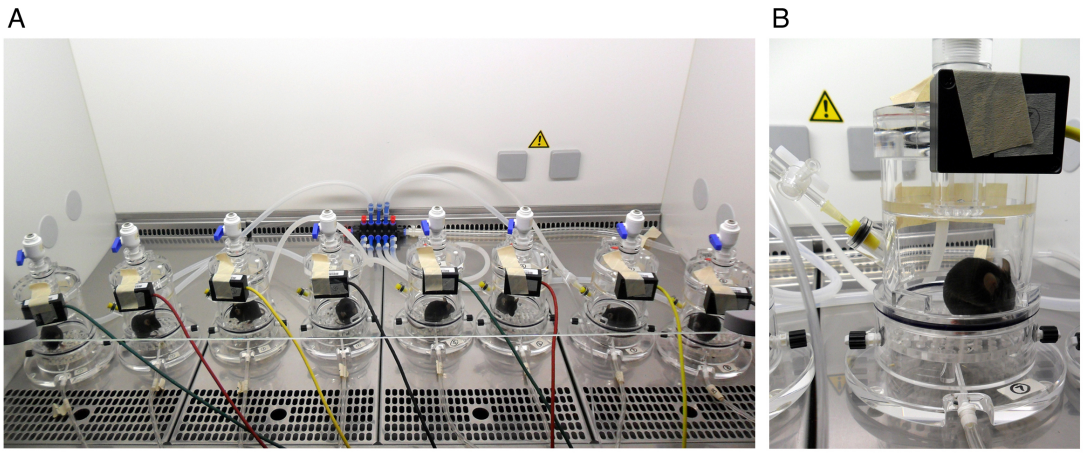

Acute hypoxic challenge protocol

The plethysmography apparatus was located in a room adjacent to the normal animal housing, thus minimising disruption to the mice. The full experimental protocol was performed on all mice during one morning, and repeated the following morning, thus generating two full data-sets. Each mouse was weighed and then placed within its plethysmograph chamber. Before commencement of ventilatory measurements, mice were allowed to breathe room air within the chamber for at least 30 minutes. Baseline

ventilation measurements during euoxia (room air) were then made over a 5-minute period, after which mice were exposed to a 5-minute hypoxic stimulus before returning to room air for a further 5 minutes.

Addition of 3% CO_2 to the hypoxic stimulus

The hypocapnic attenuation of AHVR in humans can partly be prevented by clamping of the end-tidal CO_2 level (Howard and Robbins 1995a; Smith *et al.* 2006). Since this procedure is not possible in mice, this study sought to offset the hypocapnia of increased ventilation by the addition of a low concentration of CO_2 to the hypoxic stimulus. The choice of 3% CO_2 was based upon, first, published data demonstrating that its addition prevents a major rise in arterial pH or fall in PCO_2 when mice are exposed to 7% oxygen (Ishiguro *et al.* 2006) and, second, that it has been shown previously that CP patients do not have an increased hypercapnic ventilatory sensitivity (Smith *et al.* 2008).

Data and statistical analysis

For each mouse the two data-sets (from each morning of recording) were averaged. The ventilatory responses of the wild type and Chuvash mice were then plotted against time, as illustrated in Figure 3.2. For quantitation, baseline euoxic respiratory rate, tidal volume and minute ventilation were determined during the 90 seconds prior to the onset of hypoxia. Corresponding values for the hypoxic stimuli were determined during the first 60 seconds of stable hypoxia (i.e. excluding the first 30 seconds of hypoxia). The AHVR was defined as the difference between hypoxic and euoxic minute ventilation. This approach is illustrated in Figure 3.2. Results are mean ± standard error unless otherwise indicated and un-paired T tests were used to compare Chuvash and wild type.

Figure 3.2: Quantification of the ventilatory responses measured using plethysmography

Each plot illustrates the minute ventilation in response to five minutes of hypoxia (black bar, A) or hypoxia/hypercapnia (open bar, B). Wild type are represented by open circles; Chuvash by closed circles. The value for baseline (euoxic) ventilation was determined by taking the average (for each genotype) of the last 90 seconds in the first period of euoxia (illustrated in red). Corresponding values for the hypoxic stimuli were determined during the first 60 seconds of stable hypoxia (thus excluding the first 30 seconds of hypoxia). The AHVR was defined as the difference (in grey, B) between hypoxic and euoxic minute ventilation.

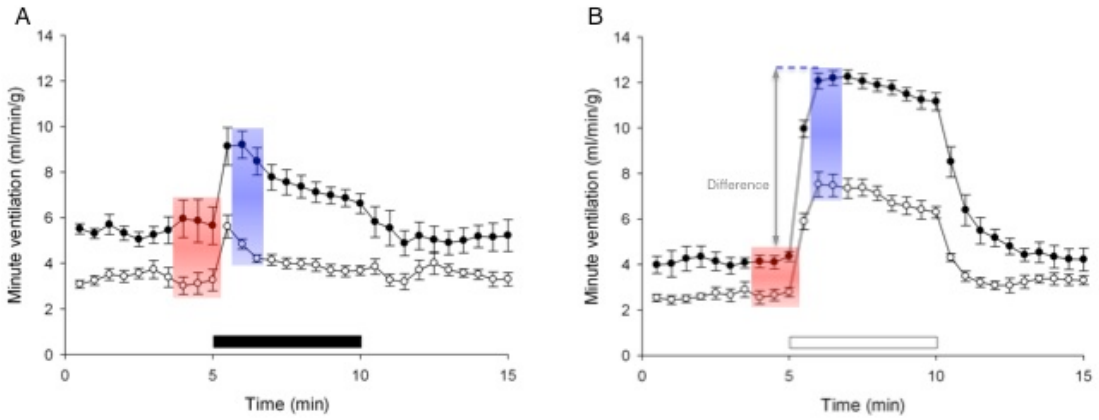

3.4.2 Immunohistochemistry of the carotid body

Carotid bifurcation dissection and fixation

Carotid bifurcations were harvested from mice that had been killed by overdose of inhaled anesthetic (halothane); they were then fixed in 4% paraformaldehyde overnight then transferred to 70% ethanol. Bifurcations were subsequently processed, wax-embedded and sectioned to 4 μm thickness.

Staining protocol

Slides were de-waxed in xylene, washed with decreasing concentrations of ethanol and then with phosphate buffered saline (PBS). Antigen retrieval was performed by immersing the slides in sodium citrate buffer (10 mM sodium citrate acid, 0.05% Tween, pH 6.0) in a water bath set at 97 °C for 30 minutes. The slides were allowed to cool in the buffer for 30 minutes before washing in PBS.

Sections were blocked with 5% goat serum (Sigma, UK) for one hour at room temperature. The primary antibody to tyrosine hydroxylase (TH) (Ab112 rabbit polyclonal to TH, Abcam Biochemicals UK; 1:750 dilution in 5% goat serum) was applied overnight at 4 °C. After washing the slides in PBS, the secondary antibody (Ab6717 goat polyclonal antibody to rabbit IgG with fluorescein isothiocyanate (FITC), Abcam; 1:500 dilution in 5% goat serum) was applied for two hours at room temperature. After washing in PBS, the sections were mounted in Prolong Gold Antifade Reagent with DAPI (Invitrogen, UK), glass coverslides applied and sealed with clear nail varnish.

Imaging protocol

Slides were imaged using a Nikon TE200 microscope fitted with a 75 W xenon arc lamp (Cairn, UK) and a Qimaging Retiga Fast 1394 digital camera. A 485 nm excitation filter was used for FITC; 340 nm for DAPI; 535 nm emission filter for both. Images were acquired using AndorIQ imaging software (Andor) on a desktop computer and subsequently analysed using ImageJ (NIH Image, Bethesda, MD). Micrometer images were also acquired for quantification.

Quantification

Every single 4 μm-thick section through the carotid bifurcation was viewed at low- and high-power. Type I cells were easy to identify due to their distinctive bright staining, location, and their tendency to form clusters. Any section containing Type I cells was photographed for both TH and DAPI staining at low- and high-power and these images were subsequently analysed using ImageJ (see Figure 3.3).

The ‘magic wand’ tool was used to highlight only TH-positive tissue (i.e. Type I cells, including nuclei) to quantify its area in each slice. The total area from all slices for

each carotid body, multiplied by 4 μm, gave the total volume of Type I cells. The cells in each section were counted; to avoid 'double counting', only those with clearly defined nuclei were chosen. The total volume of TH-positive tissue for each carotid body, divided by cell count, gave a measure of individual Type I cell size. Finally, the area of individual Type I cell nuclei in multiple sections was measured by highlighting the most clearly defined nuclei using the 'magic wand' tool (approximately 100 nuclei per mouse were measured). These techniques are summarised in Figure 3.3.

Results are mean ± standard error unless otherwise indicated and un-paired T tests were used to compare Chuvash and wild type.

Figure 3.3: Carotid bifurcation dissection and immunohistochemistry quantification

(A) Typical mouse carotid bifurcation, pinned out after dissection, prior to fixation. (B) The 'magic wand' tool in ImageJ was used to highlight only the TH-positive (i.e. Type I) cells and none of the intervening spaces (pink lines), thus enabling accurate measurement of the volume of TH-positive tissue in the carotid body. (C) Similarly, the area of individual Type I cell nuclei could be measured (white spaces).

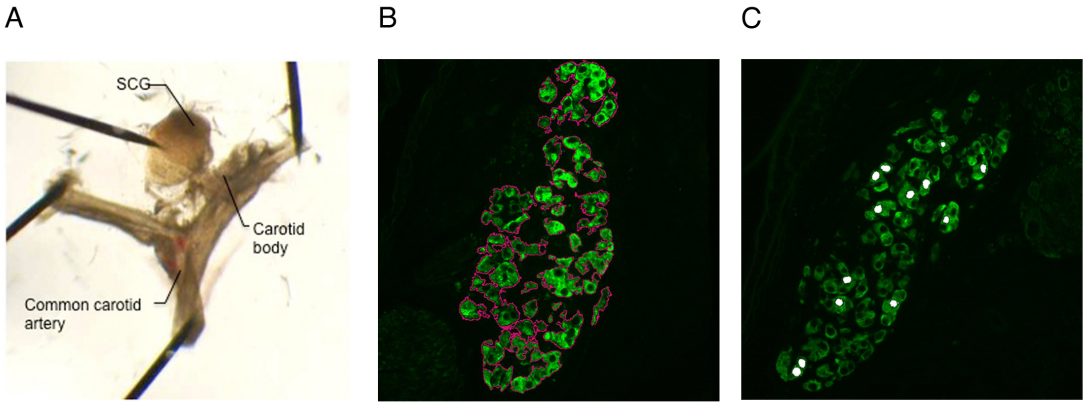

3.4.3 Type I cell electron microscopy

Carotid bifurcation dissection and fixation

Carotid bifurcations were removed as before and immersion-fixed in 3% paraformaldehyde/0.05% glutaraldehyde in phosphate buffer (pH 7.2) for 2 hours at room temperature and stored overnight at 4 °C in a ten-fold dilution of the fixative. The next day bifurcations were contrasted with uranyl acetate (2% (w/v) in distilled water), dehydrated in ethanol and embedded in LR Gold resin (Agar Scientific, UK). This study was performed in collaboration with Dr Helen Christian.

Staining protocol

Semi-thin sections were initially prepared to identify the carotid body and subsequently ultra-thin sections (50-80 nm) were cut using a Reichart-Jung ultracut microtome and mounted on nickel grids (Agar Scientific, UK). For identification of Type I cells, sections were immunogold-labelled for TH by incubation for 2 hours at room temperature with TH antibody (Abcam Biochemicals, UK) followed by a 1 hour incubation with a 15 nm protein A immunogold-conjugate (1:60; British Biocell, UK). All antibodies were diluted in 0.1 M PBS (containing 0.1% egg albumin). Specificity of antibody labelling was confirmed in negative control sections in which the primary antibody was replaced with non-immune serum. Sections were counterstained with lead citrate and uranyl acetate and examined on a JOEL 1010 transmission electron microscope (JOEL Inc., USA).

Quantification and analysis of Type I cell ultrastructure

For analysis of cell morphology six micrographs of TH-positive cells per animal were taken at a magnification of x4000 and scanned into Adobe Photoshop (Adobe, USA, Version 5.5) and analysed using Axiovison (Zeiss, UK, Version 4.5) image analysis

software. The analyst (Dr Helen Christian) was blind to the sample code. The following parameters were calculated: nuclear and total cell areas; mitochondria number and DCV granule diameter. Expansion of the rough ER was assessed visually and graded on a scale of 0-4 (0, no expansion; 4 the most expansion). The ER estimates do not provide absolute measurements but do provide a basis for comparison.

Results are mean ± standard error unless otherwise indicated and un-paired T tests were used to compare Chuvash and wild type.

3.5 RESULTS

3.5.1 Measurement of AHVR in response to 10% O_2

Figure 3.4 illustrates the ventilatory responses (frequency, tidal volume, and minute ventilation) of the wild type and Chuvash mice in response to five minutes of 10% inspired O_2. These results are also summarised in Table 3.1. The Chuvash mice had an elevated baseline ventilation of 5.8 ml/min/g, which was 1.9 fold greater than that of the wild type mice (3.1 ml/min/g; $p < 0.02$). Exposure to 10% O_2 provoked an increase in ventilation of 3.0 ml/min/g in the Chuvash mice, which was 2.2 fold greater than the 1.4 ml/min/g increase seen in the wild type mice ($p < 0.05$). However, as seen clearly in Figure 3.4, ventilation decreased rapidly after the first minute of hypoxia because the initial hyperventilation would have lowered the $PaCO_2$, and therefore the respiratory drive. Thus, the measurement of ventilatory sensitivity to hypoxia would have been an underestimation. The addition of 3% CO_2 to the gas mixture (Section 3.5.2) would be hypothesised to prevent this.

Table 3.1: Summary of plethysmography data measuring AHVR in response to 10% O_2
Six male wild type and six male Chuvash mice, aged 4 - 6 months, were used.

Parameter		Wild type	Chuvash	*p* value
Frequency (breaths/min)	Euoxia	297 ± 38	370 ± 31	0.172
	Hypoxia	309 ± 11	407 ± 9	**< 0.001**
	Difference	11 ± 30	37 ± 29	0.548
Tidal volume (µl/g)	Euoxia	11.0 ± 0.6	16.3 ± 1.4	**0.006**
	Hypoxia	15.1 ± 0.6	22.2 ± 1.3	**0.001**
	Difference	4.1 ± 0.2	6.0 ± 0.7	**0.035**
Minute ventilation (ml/min/g)	Euoxia	3.1 ± 0.4	5.8 ± 0.8	**0.017**
	Hypoxia	4.5 ± 0.2	8.8 ± 0.6	**< 0.001**
	Difference	1.4 ± 0.3	3.0 ± 0.7	**0.045**

Figure 3.4: Measurement of AHVR in response to 10% O_2

Wild type are shown in white (circles or bars); Chuvash in black. Black bar represents five minutes of 10% O_2. Bar charts illustrate the mean value for each parameter in euoxia and hypoxia, and the difference (AHVR) between them. * ($p < 0.05$); ** ($p < 0.02$); *** ($p < 0.01$); **** ($p < 0.001$).

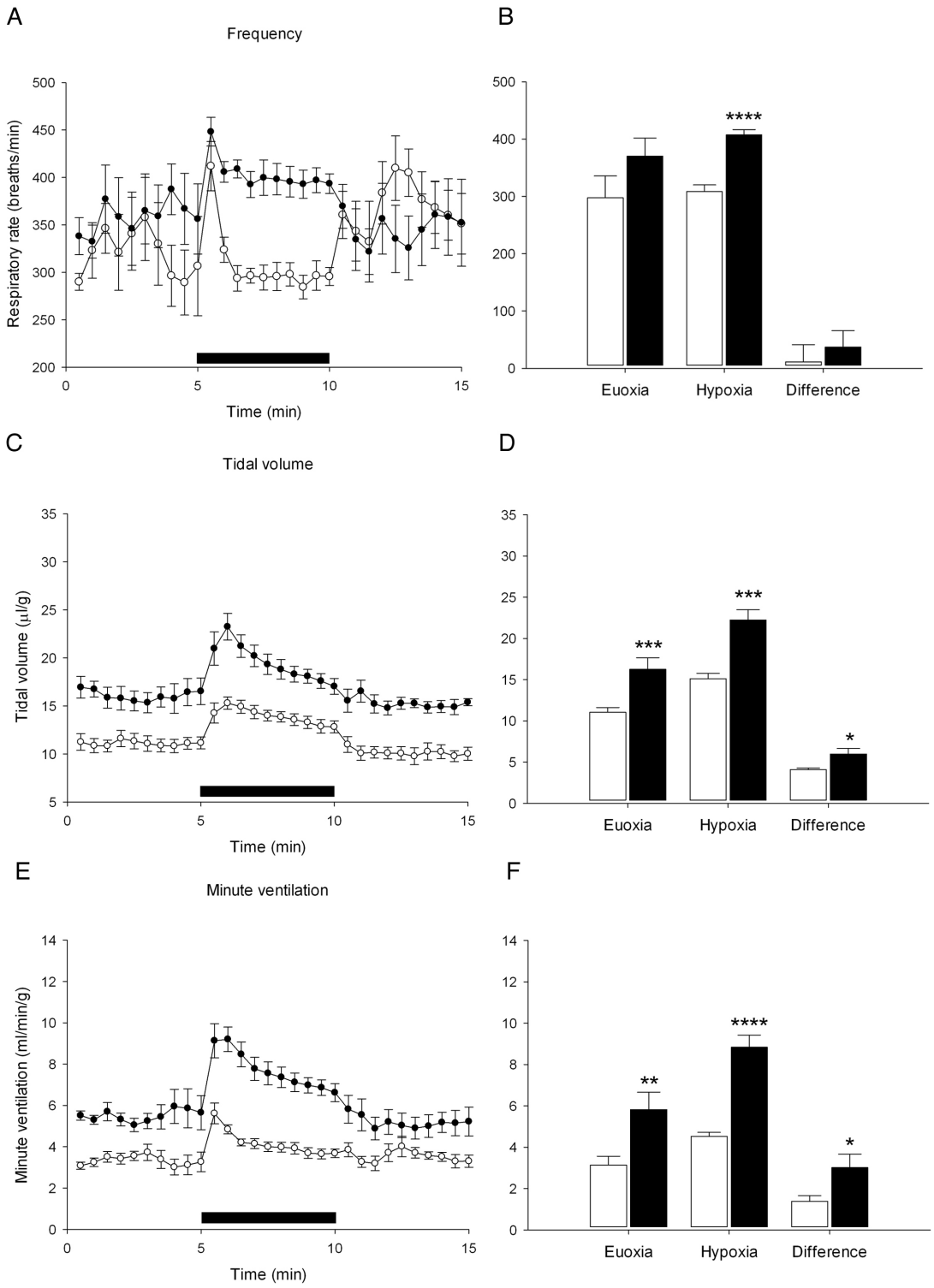

3.5.2 Measurement of AHVR in response to 10% O_2 with 3% CO_2

The addition of 3% CO_2 to the hypoxic stimulus prevented the marked decline in ventilation seen in 3.5.1. Table 3.2 and Figure 3.5 summarise these results. Again, the Chuvash mice had an elevated baseline ventilation in euoxia which was 1.6 fold greater than that of the wild type mice ($p < 0.001$). Exposure to 10% O_2 with 3% CO_2 provoked a marked and sustained increase in ventilation of 7.9 ml/min/g in the Chuvash mice, which was 1.6 fold greater than the 4.8 ml/min/g increase seen in the wild type mice ($p < 0.01$). Figure 3.6 shows representative plethysmography traces of wild type and Chuvash mice in both euoxia and hypoxia.

Table 3.2: Summary of measurement of AHVR in response to 10% O_2 with 3% CO_2
The same six male wild type and six male Chuvash mice were used.

Parameter		Wild type	Chuvash	*p* value
Frequency (breaths/min)	Euoxia	286 ± 32	290 ± 12	0.936
	Hypoxia	363 ± 7	386 ± 5	**0.023**
	Difference	76 ± 31	96 ± 11	0.546
Tidal volume (µl/g)	Euoxia	9.9 ± 0.6	15.1 ± 0.8	**< 0.001**
	Hypoxia	20.9 ± 1.3	31.8 ± 1.2	**< 0.001**
	Difference	11.0 ± 0.8	16.6 ± 0.7	**0.001**
Minute ventilation (ml/min/g)	Euoxia	2.7 ± 0.2	4.2 ± 0.2	**0.001**
	Hypoxia	7.5 ± 0.5	12.1 ± 0.3	**< 0.001**
	Difference	4.8 ± 0.5	7.9 ± 0.3	**0.001**

Figure 3.5: Measurement of AHVR in response to 10% O_2 with 3% CO_2

Wild type are shown in white (circles or bars); Chuvash in black. White bar represents five minutes of 10% O_2 with 3% CO_2. Bar charts illustrate the mean value in euoxia and hypoxia, and the difference (AHVR) between them. * ($p < 0.05$); ** ($p < 0.02$); *** ($p < 0.01$); **** ($p < 0.001$).

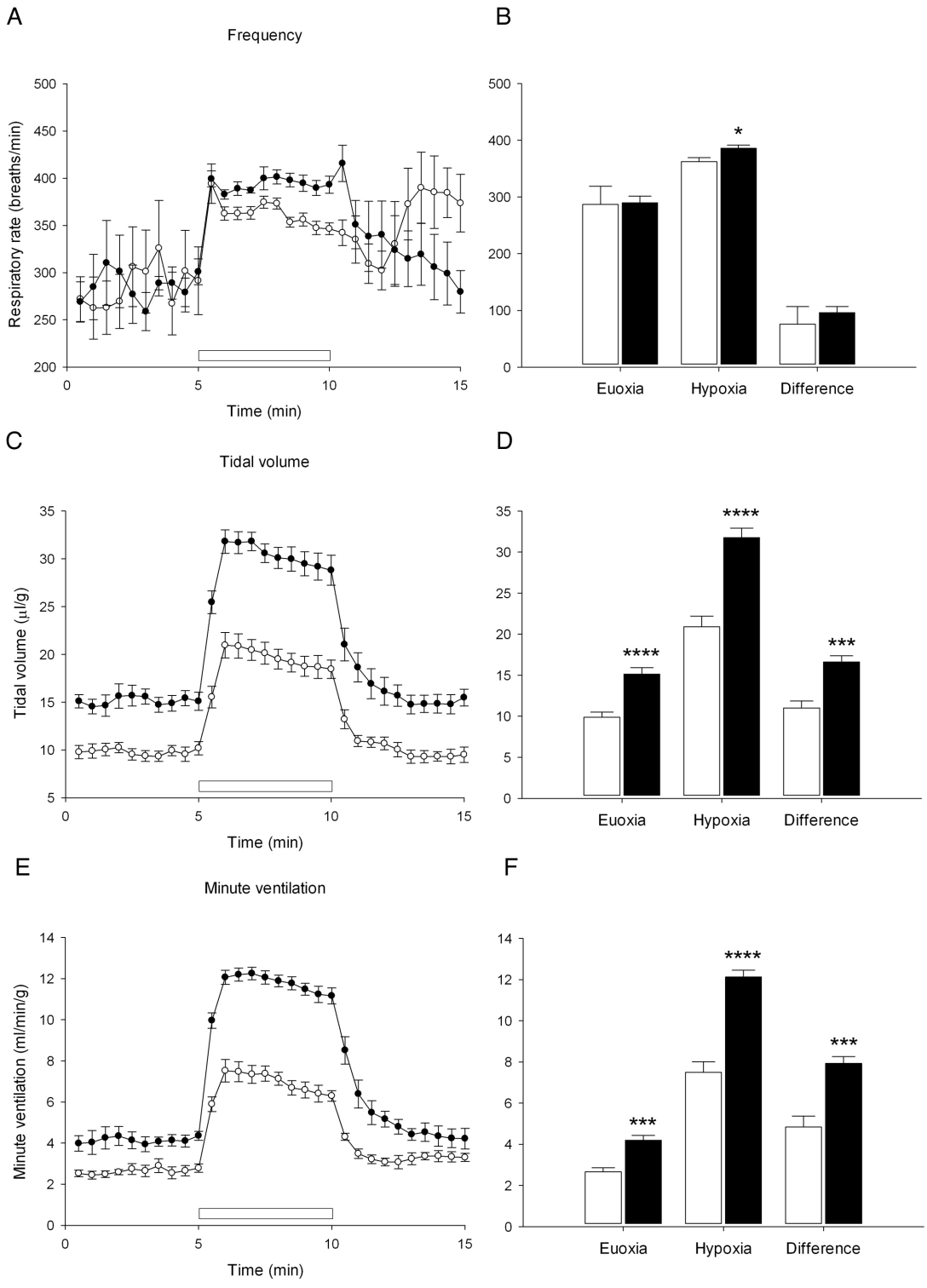

Figure 3.6: Representative plethysmography traces in euoxia and hypoxia

Representative plethysmography traces of wild type and Chuvash mice in both euoxia and hypoxia (10% O_2 with 3% CO_2). Three-second euoxic traces were taken from the final 30 s prior to the hypoxic stimulus; three-second hypoxic traces were taken after 30 s of the hypoxic stimulus had elapsed. Tracings represent the measured 'box flow' of the plethysmograph, which is used to calculate physiological flow. a.u. (arbitrary units). Note the increased ventilation of the Chuvash mouse in both euoxia and hypoxia, despite a reduced body mass.

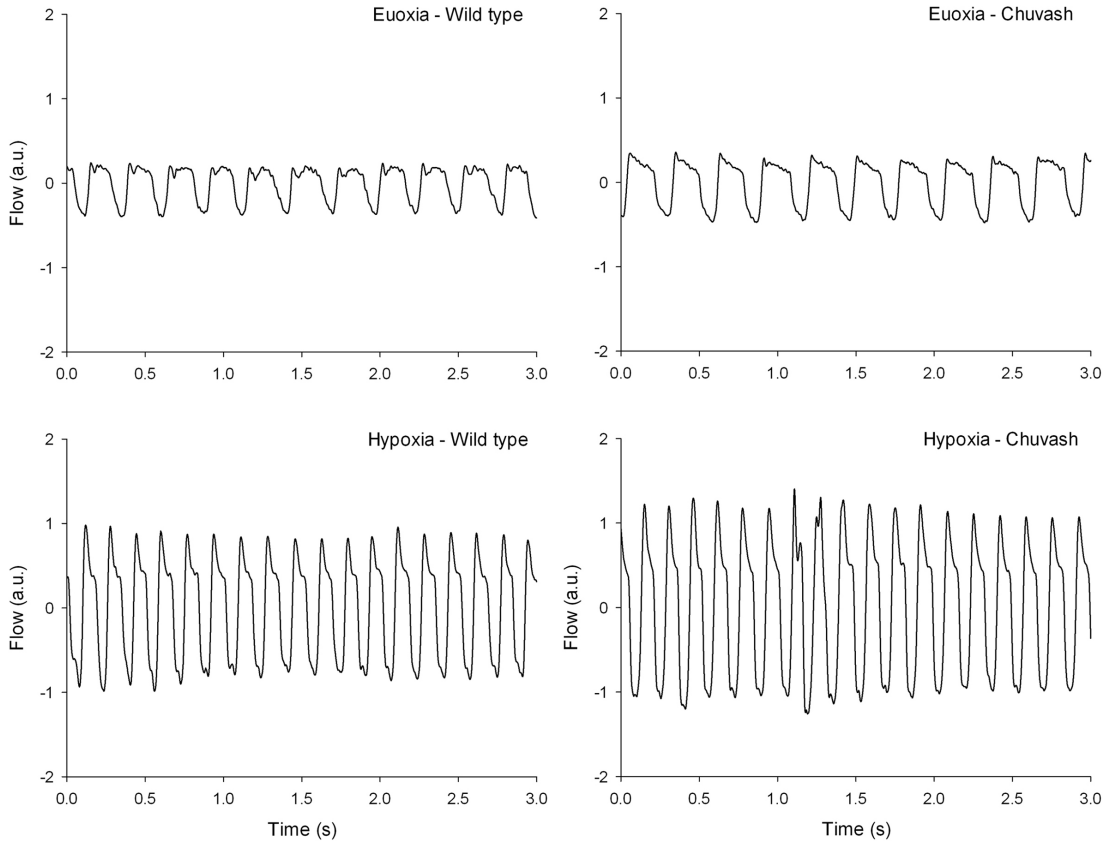

3.5.3 Effect of body mass normalisation on AHVR

Tidal volume and minute ventilation are routinely corrected to body mass. However, in small mammals such as the mouse, hypoxia-induced reductions in metabolism and oxygen consumption (V_{O_2}) can produce confounding effects upon the measurement of the hypoxic ventilatory response. Resting metabolism is an important determinant of the hypoxic drop in V_{O_2}, such that smaller animals (with higher metabolic rates) tend to demonstrate greater reductions (Frappell *et al.* 1992). Since mammalian basal metabolic rate has been shown to be proportional to body mass$^{2/3}$ (White and Seymour 2003), alternative ventilatory normalisation was performed (Table 3.3 and Table 3.4). Correction of the ventilatory data to body mass$^{2/3}$ had little effect upon the striking differences between the Chuvash and wild type mice. Furthermore, the enhanced AHVR in the Chuvash mice remained statistically significant even if no normalisation was performed.

Table 3.3: AHVR in response to 10% O_2 (alternative normalisation)

Tidal volume and minute ventilation, in euoxia and in response to 10% O_2, either normalised to body surface area (body mass$^{2/3}$) or expressed without normalisation.

Parameter (normalised to body surface area)		Wild type	Chuvash	*p* value
Tidal volume (µl/g$^{2/3}$)	Euoxia	36.9 ± 1.3	49.3 ± 4.0	**0.025**
	Hypoxia	49.5 ± 2.2	67.1 ± 4.3	**0.004**
	Difference	12.6 ± 1.6	17.8 ± 1.7	**0.046**
Minute ventilation (ml/minute/g$^{2/3}$)	Euoxia	10.5 ± 1.3	17.7 ± 2.5	**0.028**
	Hypoxia	17.5 ± 1.0	27.8 ± 2.0	**0.001**
	Difference	7.0 ± 0.4	10.2 ± 1.5	0.074
Parameter (no normalisation)		**Wild type**	**Chuvash**	***p* value**
Tidal volume (µl)	Euoxia	418 ± 10.0	456 ± 33	0.313
	Hypoxia	574 ± 19	624 ± 23	0.129
	Difference	156 ± 12	168 ± 18	0.592
Minute ventilation (ml/minute)	Euoxia	119 ± 15	163 ± 21	0.115
	Hypoxia	173 ± 8	248 ± 12	**< 0.001**
	Difference	54 ± 11	85 ± 18	0.173

Table 3.4: AHVR in response to 10% O_2 with 3% CO_2 (alternative normalisation)

Tidal volume and minute ventilation, in euoxia and in response to 10% O_2 with 3% CO_2, either normalised to body surface area (body mass$^{2/3}$) or expressed without normalisation.

Parameter (normalised to body surface area)		Wild type	Chuvash	*p* value
Tidal volume (µl/g$^{2/3}$)	Euoxia	33.1 ± 1.6	46.0 ± 2.3	**0.001**
	Hypoxia	69.5 ± 2.8	96.7 ± 3.1	**< 0.001**
	Difference	36.3 ± 2.1	50.6 ± 2.1	**0.001**
Minute ventilation (ml/minute/g$^{2/3}$)	Euoxia	9.0 ± 0.8	12.8 ± 0.7	**0.004**
	Hypoxia	24.9 ± 1.1	37.0 ± 0.9	**< 0.001**
	Difference	15.9 ± 1.5	24.3 ± 1.0	**0.001**
Parameter (no normalisation)		**Wild type**	**Chuvash**	***p* value**
Tidal volume (µl)	Euoxia	375 ± 16	427 ± 21	0.082
	Hypoxia	790 ± 23	896 ± 32	**0.023**
	Difference	415 ± 16	469 ± 22	0.074
Minute ventilation (ml/minute)	Euoxia	103 ± 12	118 ± 6	0.287
	Hypoxia	283 ± 7	342 ± 10	**0.001**
	Difference	180 ± 12	224 ± 11	**0.022**

3.5.4 Carotid body immunohistochemistry

Figure 3.8 and Figure 3.9 show representative low- and high-power images of wild type and Chuvash carotid body sections. Figure 3.7 shows typical images with the relevant anatomy labelled. The full immunohistochemistry results are summarised in Table 3.5 and Figure 3.10. The Chuvash mice showed clear evidence of hypertrophy and hyperplasia of the Type I cells. The number of cells was increased 2.7 fold in the Chuvash carotid body, compared to wild type ($p < 0.0001$). Individual Type I cells were 1.6 fold greater in size ($p < 0.01$) with 1.3 fold larger nuclei ($p < 0.05$).

Table 3.5: Summary of carotid body immunohistochemistry

Three male wild type and Chuvash mice were used, aged 4 – 6 months.

Parameter	Wild type	Chuvash	*p* value
Cell count (number)	973 ± 27	2662 ± 112	**< 0.001**
Volume of TH-positive tissue (μm^3 x 10^6)	0.71 ± 0.06	3.1 ± 0.3	**0.001**
Type I cell volume (μm^3)	727 ± 41	1159 ± 62	**0.004**
Type I cell nuclei area (μm^2)	22.0 ± 0.8	29.6 ± 2.1	**0.027**

Figure 3.7: Representative immunohistochemistry images showing typical anatomy

Typical low-power views of wild type (A) and Chuvash (B) carotid bifurcations. The small Type I cells form clusters around arterial branches. The superior cervical ganglion (SCG) is a useful positive control.

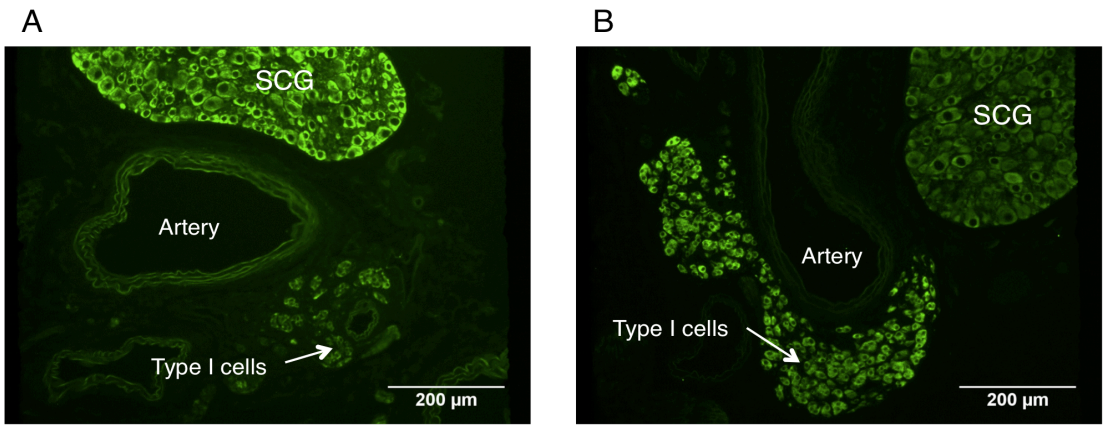

Figure 3.8: Representative low- and high-power images of the wild type carotid body

Typical images from one wild type section are shown at both low-power (A) and high-power (B). TH (stain for tyrosine hydroxylase); DAPI (stain for nuclei); MERGE (an overlay of the two previous images).

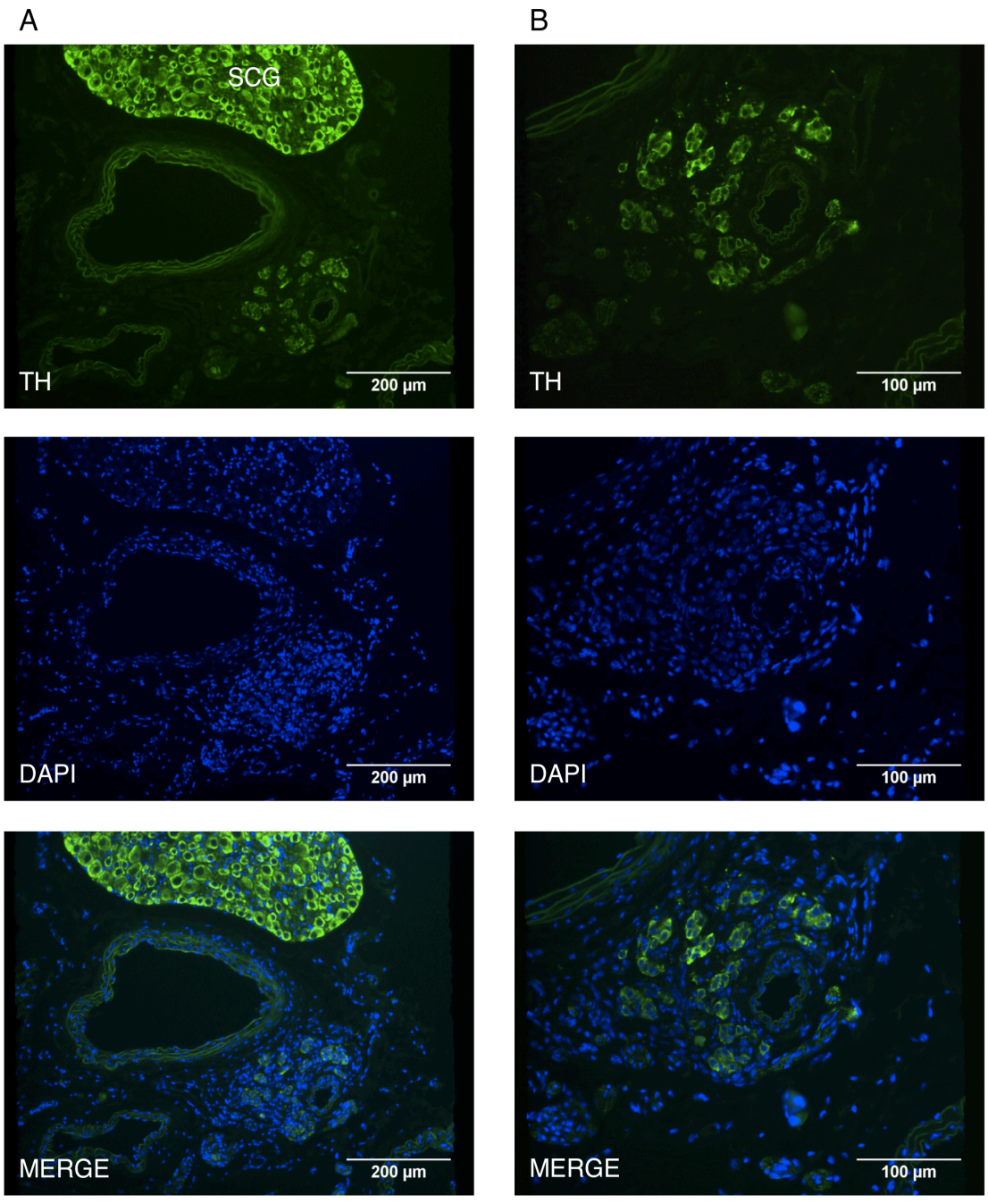

Figure 3.9: Representative low- and high-power images of the Chuvash carotid body

Typical images from one Chuvash section are shown at both low-power (A) and high-power (B). TH (stain for tyrosine hydroxylase); DAPI (stain for nuclei); MERGE (overlay of the two previous images).

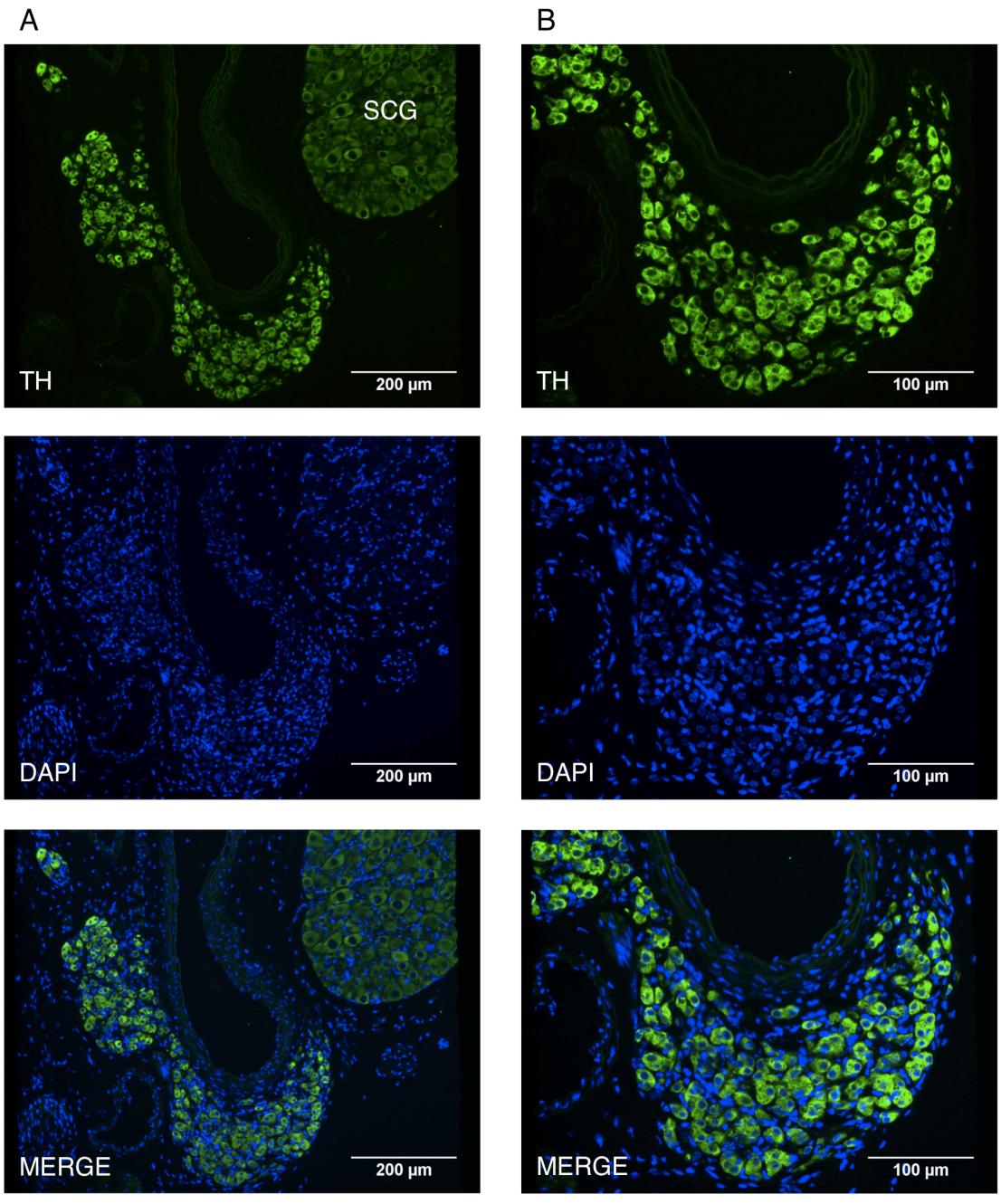

Figure 3.10: Summary of the carotid body immunohistochemistry analysis

Wild type are shown in white; Chuvash in black. * ($p < 0.05$); *** ($p < 0.01$); **** ($p < 0.001$). TH (tyrosine hydroxylase, a marker for Type I cells).

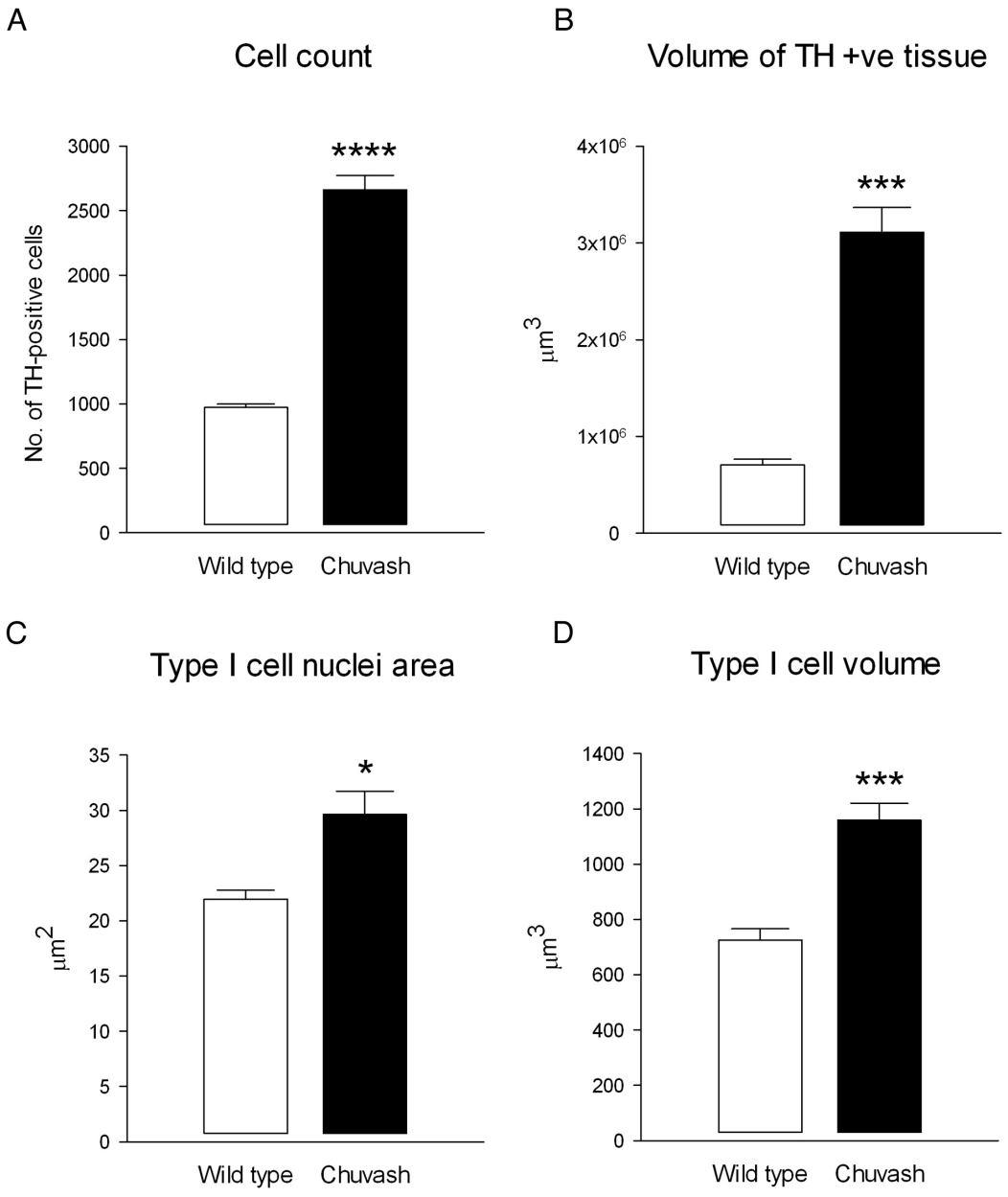

3.5.5 Type I cell electron microscopy

The increased cell and nuclear size of the Type I cells evident from the immunohistochemistry was confirmed by electron microscopy. Furthermore, Type I cells contained an increased number of mitochondria, enlarged dense-cored vesicles, and markedly expanded rough endoplasmic reticulum. Figure 3.11 shows a representative electron micrograph of a Chuvash Type I cell and the electron microscopy findings are summarised in Table 3.6 and Figure 3.12.

Figure 3.11: Representative electron micrograph of a Chuvash Type I cell

Representative electron micrograph of Chuvash Type I cell. Nucleolus (1); nucleus (2); peri-vascular space (3); dilated, abundant rough endoplasmic reticulum (ER) (4); dense-cored vesicles (DCV) (5); mitochondrion (6). Scale bar = 1 µm.

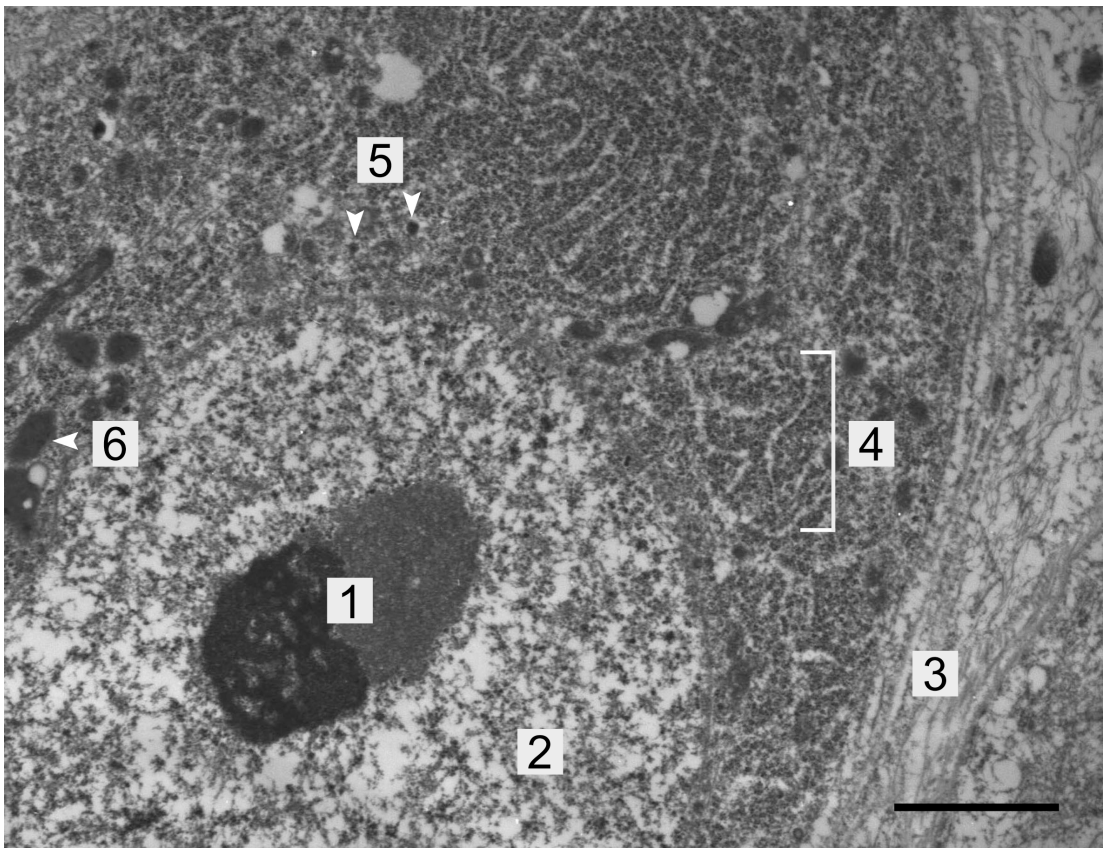

Table 3.6: Summary of Type I cell electron microscopy

Three male wild type and Chuvash mice were used. ER (endoplasmic reticulum); DCV (dense-cored vesicle).

Parameter	Wild type	Chuvash	*p* value
Cell area (μm^2)	66.8 ± 1.7	87.8 ± 2.6	**0.003**
Nucleus area (μm^2)	18.4 ± 0.4	21.4 ± 0.3	**0.003**
Number of mitochondria per μm^2	0.93 ± 0.03	1.23 ± 0.03	**0.001**
Rough ER expansion (arbitrary units)	1.2 ± 0.2	2.1 ± 0.1	**0.009**
DCV diameter (nm)	64.4 ± 1.7	74.7 ± 1.1	**0.006**

Figure 3.12: Summary of the Type I cell electron microscopy analysis

Wild type are shown in white; Chuvash in black. *** ($p < 0.01$).

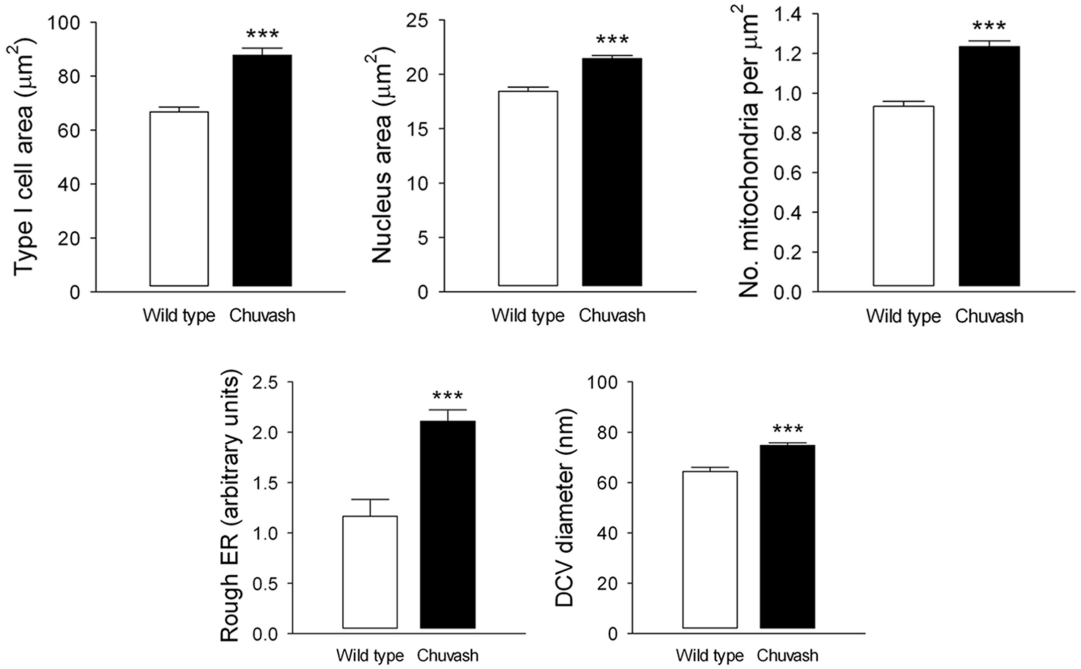

3.5.6 Summary of key findings

Table 3.7 summarises the major findings from this chapter.

Table 3.7: Summary of key findings

The key findings from the main experiments performed in this chapter, grouped by topic.

Parameter	Wild type	Chuvash	*p*
Minute ventilation (10% oxygen stimulus, ml/min/g)			
Euoxia	3.1 ± 0.4	5.8 ± 0.8	**0.017**
Hypoxia	4.5 ± 0.2	8.8 ± 0.6	**< 0.001**
Difference	1.4 ± 0.3	3.0 ± 0.7	**0.045**
Minute ventilation (10% oxygen 3% carbon dioxide, ml/min/g)			
Euoxia	2.7 ± 0.2	4.2 ± 0.2	**0.001**
Hypoxia	7.5 ± 0.5	12.1 ± 0.3	**< 0.001**
Difference	4.8 ± 0.5	7.9 ± 0.3	**0.001**
Carotid body immunohistochemistry			
Cell count (number)	973 ± 27	2662 ± 112	**< 0.001**
Volume of TH-positive tissue (μm^3 x 10^6)	0.71 ± 0.06	3.1 ± 0.3	**0.001**
Type I cell volume (μm^3)	727 ± 41	1159 ± 62	**0.004**
Type I cell nuclei area (μm^2)	22.0 ± 0.8	29.6 ± 2.1	**0.027**
Type I cell electron microscopy			
Cell area (μm^2)	66.8 ± 1.7	87.8 ± 2.6	**0.003**
Nucleus area (μm^2)	18.4 ± 0.4	21.4 ± 0.3	**0.003**
Number of mitochondria per μm^2	0.93 ± 0.03	1.23 ± 0.03	**0.001**
Rough ER expansion (arbitrary units)	1.2 ± 0.2	2.1 ± 0.1	**0.009**
DCV diameter (nm)	64.4 ± 1.7	74.7 ± 1.1	**0.006**

3.6 DISCUSSION

3.6.1 Ventilatory findings

Elevated ventilation and enhanced AHVR in the Chuvash mice

Previous studies have demonstrated that both Chuvash patients and mice have an elevated baseline ventilation in euoxia, with a consequent respiratory alkalosis (Smith *et al.* 2006; Hickey *et al.* 2010). This finding has been confirmed in the ventilatory studies performed in this thesis. Similarly, the second characteristic feature of VAH, namely an elevated ventilatory sensitivity to hypoxia, was also demonstrated in the present study. This increased sensitivity was seen most markedly when 10% O_2 with 3% CO_2 was used as the stimulus. Both wild type and Chuvash mice demonstrated the characteristic features of HVD during a five minute exposure to 10% O_2 (although Chuvash ventilation remained elevated compared to the wild type mice). The addition of CO_2 (to mimic the isocapnic studies performed in humans) prevented this decline in ventilation and allowed the ventilatory phenotype of the Chuvash mouse to be seen more clearly.

Interestingly, whilst both features of VAH were demonstrated in Chuvash patients (Smith *et al.* 2006), a study of the same mouse model used for this thesis failed to show the expected increase in hypoxic ventilatory sensitivity (Hickey *et al.* 2010). The authors concluded that the R200W mutation in mice did not appear to affect respiratory sensitivity to hypoxia. The results from this thesis contradict that finding, for which there are several reasons.

First, the hypoxic stimulus used previously was slightly less severe (12% versus 10% O_2) which may have been a contributory factor. More importantly, this stimulus was

poikilocapnic and the duration of exposure was ten minutes (versus 5 minutes in the study for this thesis). The hypoxic ventilatory decline seen in the present study would undoubtedly have occurred. Since the entire ten minute hypoxia period in the Hickey study was averaged to give a value for hypoxic minute ventilation, it is unsurprising that the authors saw no evidence for increased respiratory sensitivity. Indeed, if the data points from the entire five minute hypoxic exposure in the present study (10% O_2 only) are averaged, no significant difference in AHVR is found (1.9 ± 0.7 ml/min/g for Chuvash versus 1.0 ± 0.3 ml/min/g, $p = 0.29$).

The study in this thesis has several advantages and therefore presents the novel finding of increased hypoxic ventilatory sensitivity in the Chuvash mouse. First, by plotting the changes in minute ventilation as a time course (rather than an averaged value from the entire exposure) one is able to visualise clearly the different components of the ventilatory response to hypoxia and hence take appropriate averages of the data points when performing statistical analysis. Second, the addition of 3% CO_2 to the hypoxic stimulus enabled a more stable stimulation of ventilation to occur (similar to techniques used to perform isocapnic hypoxic studies in humans).

This study therefore demonstrates that the Chuvash mutation in mice results in features that are characteristic of ventilatory acclimatisation to hypoxia, namely an elevated baseline ventilation and enhanced AHVR. However, humans exposed to very long-term hypoxia (e.g. through a life-time's residency at high altitude) ventilate less than individuals acclimatised to high altitude and have a blunted, rather than enhanced, AHVR (Chiodi 1957; Severinghaus *et al.* 1966; Milledge and Lahiri 1967; Weil *et al.* 1971). As such, it is somewhat surprising that the Chuvash patients and mice, in whom there is life-long up-regulation of HIF, more closely resemble individuals recently acclimatised to high altitude, rather than those exposed to life-

long hypoxia. This suggests that the changes in ventilatory control that occur in response to very long-term hypoxia are not solely dependent upon HIF.

Further interpretation of data for frequency and tidal volume

Differences in minute ventilation, rather than in ventilatory frequency or tidal volume, have been focused on during this study, since minute ventilation is the variable of primary physiological importance. Nevertheless, marked abnormalities of either individual parameter may be of relevance to the pattern of breathing (frequency) or to lung development (and hence lung volume). Indeed, *Hif-2α*$^{+/-}$ mice exhibit instability of breathing, with periods of hyperventilation followed by hypoventilation (Peng *et al.* 2011b). However, whilst no such abnormalities were observed in this study, consistent with previous reports (Hickey *et al.* 2010), it is interesting to note that during five minutes of 10% O_2 the Chuvash mice were able to maintain a high respiratory rate throughout the hypoxic stimulus, whilst that of the wild type mice rapidly decreased towards pre-hypoxic levels.

Validity of data from plethysmography

Whole-body plethysmography in awake, un-restrained mice is not without technical limitations. For example, the recording of ventilatory frequency is particularly susceptible to interference from mouse movements, sniffing and grooming. This is reflected in the variability of the data recorded during euoxia. However, during hypoxia the mice tended to sit very still and refrain from additional movements; this is reflected in the much clearer recordings obtained during this five minute period.

Whole-body plethysmography also makes the assumption that expired gas returns to ambient temperature and humidity in the chamber prior to the next inspiration. Since this may not always be the case, there is potential for underestimation of tidal

volumes. As a consequence, care must be taken in comparing values for minute ventilation across different studies, as reflected in the wide range of published values in euoxia from less than 1 ml/min/gram (Hickey *et al.* 2010) to greater than 5 ml/min/gram (Boudinot *et al.* 2004). However, if conditions are kept relatively constant the magnitude of any such error should be similar during euoxia and hypoxia across experimental groups, permitting relevant comparisons within a single study such as that presented in this thesis.

Finally, it has been shown previously that hypoxia results in hypothermia and a depressed thermogenic response to cold (Wood 1991). A decrease in core body temperature in this study could have influenced both oxygen consumption (and hence ventilation) as well as the algorithms used by the plethysmography software to scale the measured flow and volumes to physiological values. It was not technically possible in this study to measure core body temperature during the plethysmography experiments. However, there are several reasons why a reduction in temperature should not have occurred. First, whilst core body temperature does fall in mice exposed to hypoxia, this decrease only becomes significant when the hypoxic stimulus is below 10% oxygen (studies of core temperature and hypoxia often use 5-7% oxygen to elicit marked changes) (Gordon and Fogelson 1991; Wood 1991). Second, the time-course of this decrease is longer than the five minutes of hypoxia employed in this study (Gordon and Fogelson 1991). Therefore it is unlikely that a reduction in body temperature would have occurred during a five minute stimulus of 10% oxygen.

Validity of the addition of 3% CO_2 to the hypoxic stimulus

Clamping of the end-tidal CO_2 partly prevents the hypocapnic attenuation of AHVR in humans (Howard and Robbins 1995a). To mimic this technique in mice, 3% CO_2

was added to the hypoxic stimulus in order to offset the hypocapnia of increased ventilation. The choice of 3% CO_2 was based upon published data demonstrating that its addition prevents a major rise in arterial pH or fall in PCO_2 when mice are exposed to 7% O_2 (Ishiguro *et al.* 2006). Furthermore, it has been shown previously that Chuvash patients do not have an increased hypercapnic ventilatory sensitivity (Smith *et al.* 2008). Measurement of the ventilatory response to 3% CO_2 alone in the Chuvash mouse would have been of interest and is a potential weakness of this study. However, this does not detract from the clear finding of increased hypoxic sensitivity, since this was also present when only 10% O_2 was used as the stimulus.

Complicating metabolic factors

In small mammals such as the mouse, hypoxia-induced reductions in metabolism and oxygen consumption (V_{O_2}) can produce confounding effects upon the measurement of the hypoxic ventilatory response. Resting metabolism is an important determinant of the hypoxic drop in V_{O_2}, such that smaller animals (with higher metabolic rates) tend to demonstrate greater reductions (Frappell *et al.* 1992). Whilst the metabolic rate of the Chuvash mouse is unknown, the markedly lower body mass demonstrated in Section 2.3.2 and the presence of a hypermetabolic state in the FIH null mice raise the possibility of an abnormal hypoxic hypometabolic response in the Chuvash mouse that could theoretically influence the AHVR. Ideally, studies of hypoxia and ventilation in mice would include measurements of V_{O_2}, V_{CO_2} and body temperature. This study would have benefitted from their inclusion, as well as the formal measurement of metabolic rate and respiratory exchange ratio (RER). However, normalisation of the ventilatory data to body mass$^{2/3}$ (White and Seymour 2003) had very little effect upon the striking differences seen between the Chuvash and wild type mice. Furthermore, the enhanced AHVR of the Chuvash mice in response to

10% O_2 with 3% CO_2 remained statistically significant even if no normalisation to body mass was performed.

Final methodological considerations

Whilst the number of animal studies investigating the impact of gender on the AHVR is small, they all point towards a greater carotid body response to hypoxia in female animals (Tatsumi *et al.* 1991; Mortola and Saiki 1996; Joseph *et al.* 2000). The ventilatory study for this thesis was designed to avoid the confounding influence of gender and thus only male mice were used throughout this chapter. If mice numbers had allowed, it would have been interesting to run identical parallel experiments in female mice.

Finally, both ventilation and metabolism will vary throughout the day. To avoid this confounding influence, the plethysmography experiments were only performed in the morning and two technical replicates, on separate days, were used. Furthermore, since four plethysmography chambers could be used in parallel, both Chuvash and wild type mice could be studied simultaneously. This approach would have minimised any effect of circadian rhythms on the ventilatory data.

Conclusions

This study demonstrates that the Chuvash mutation in mice results in features that are characteristic of ventilatory acclimatisation to hypoxia, namely an elevated baseline ventilation and enhanced AHVR. These findings are consistent with those seen in patients with Chuvash polycythaemia (Smith *et al.* 2006). Subsequent sections of this chapter will investigate the possible mechanisms underlying these ventilatory changes.

3.6.2 Carotid body immunohistochemistry findings

Hypertrophy and hyperplasia of Type I cells in the Chuvash mice

This study demonstrates, for the first time, striking changes within the carotid body of the Chuvash mice. An augmented carotid body sensitivity due to morphological, neurochemical, and membrane-electrophysiological adaptations is hypothesised to underlie the increased HVR seen in chronic hypoxia. It is certainly plausible that the marked hypertrophy and hyperplasia of the Type I cells of the carotid body that are seen in the Chuvash mice may be driving, in part, the ventilatory changes. The demonstration of similar findings in mice with heterozygous deficiency of *PHD2* adds weight to this argument (Bishop *et al.* 2013). In contrast, despite abnormalities in ventilation and carotid sinus nerve activity, neither *Hif-1α*$^{+/-}$ nor *Hif-2α*$^{+/-}$ mice demonstrate any changes in Type I cell size or number (Kline *et al.* 2002; Peng *et al.* 2006). However, it is important to note that these two models represent under-expression, rather than over-expression of HIF-α. It is possible that the relatively low number of Type I cells in the wild type mouse carotid body (approximately 1000, based upon the study in this thesis) may represent a 'critical' number. Since both *Hif-1α*$^{-/-}$ and *Hif-2α*$^{-/-}$ mice die *in utero*, it is difficult to draw further conclusions.

It is therefore striking that the relatively modest Chuvash mutation results in such marked changes in carotid body morphology and that they mimic very closely the adaptations seen in response to chronic hypoxia. Whilst it is tempting to ascribe the elevated ventilation described to these morphological changes, there are many other aspects of the oxygen sensing pathway that remain to be interrogated. The carotid body morphological, neurochemical and membrane-electrophysiological changes that

occur in chronic hypoxia do so in parallel, so that their separate contributions to the increased carotid body gain are hard to assess.

Validity of the immunohistochemistry analysis

The analysis of the carotid body immunohistochemistry performed for this thesis focused on the TH-positive Type I cells rather than on overall carotid body size or on other cell types. However, the general consensus is that the Type I cells are those responsible for oxygen sensing and hence of the most physiological relevance. Had mouse availability allowed, assessment of Type II cell number and morphology would have been of interest. In addition, previous studies have demonstrated success in staining Type I cells for either HIF-1α or HIF-2α (Kline *et al.* 2002; Peng *et al.* 2011b). Investigating whether either, or indeed both, of these proteins demonstrate increased staining in the Chuvash Type I cells would be particularly interesting.

Various methods are employed for quantifying both the size of the carotid body and the number of cells, and they all have limitations. In the wild type carotid body it was particularly clear that the clusters of Type I cells were surrounded by small blood vessels and other cell types. Measuring the size of the entire carotid body would be difficult and error-prone, since there was no obviously demarcated border. Some previous studies have employed H+E staining of the carotid body sections and measured the 'carotid body area' free-hand (Wang *et al.* 2008), which could be an over-estimation of its real size and does not take into account the different cell types. Since the purpose of the quantification in this thesis was to determine the amount of Type I cell tissue present, the 'magic wand' tool was used to highlight only the TH-positive tissue. This technique proved to be extremely easy to perform and was very successful at highlighting and measuring only the TH-positive areas, thus avoiding the intervening spaces between the clusters of Type I cells. Whilst this technique did

not provide an overall measure of carotid body volume, it was very clear that the Chuvash carotid bodies were much larger.

Quantifying the number of cells, both in individual sections and in the whole carotid body, is another procedure in which there is the potential for error. Since all of the sections for each mouse carotid body were used for cell counting, it is possible that certain cells may have been counted more than once. The increased size of the Type I cells within the Chuvash carotid body could also contribute to this potential error since a particular cell would be present in multiple slices. To minimise this problem, a cell was only counted if the nucleus was clearly visible; cells were not counted if the nucleus was unclear or if no nucleus was seen. The typical nuclear diameter of a wild type or Chuvash Type I cell is 4.8 μm or 5.2 μm, respectively (calculated from the mean nuclear area measured using electron microscopy, see Table 3.6). Since each carotid body section was 4 μm thick, it is unlikely that the nucleus would have been clearly visible in more than one section. Therefore, this approach would have minimised the possibility of 'double-counting'. Furthermore, independent proof-of-principle analysis of several wild type and Chuvash carotid bodies, prior to the immunohistochemistry studies in this thesis, demonstrated very similar numbers of Type I cells (Dr Tammie Bishop, personal communication).

Staining for tyrosine hydroxylase is routinely used to identify Type I cells. The presence of the superior cervical ganglion (whose cells also contain TH) provided a useful 'positive control' in slices in which no carotid body was present. Additional carotid bifurcation sections were processed in which either the primary or secondary antibodies were omitted, to ensure specificity of the immunohistochemistry technique for the Type I cells and SCG. Thus, non-specific binding of the antibodies would not have affected the results in this study.

Source(s) of the increased number of Type I cells

Whilst hyperplasia of the Type I cells has long been recognised as an important component of the hypoxia-induced carotid body hypertrophy, the molecular and cellular mechanisms underlying this process have remained poorly understood. However, recent studies have begun to shed some light on both the source of the increased number of Type I cells and on the signaling pathways driving this change.

Several studies provide evidence that sustained hypoxia results in Type I cell mitosis (Dhillon *et al.* 1984; Bee *et al.* 1986). More recently, this finding was confirmed by a study which exposed rats to 1 – 7 days' hypoxia and measured the incorporation of bromodeoxyuridine (BrdU, a uridine analogue that is stably incorporated into cells undergoing DNA synthesis) into Type I cells (Wang *et al.* 2008). Carotid body mitogenesis has also been shown to be activated by basic fibroblast growth factor (bFGF) induced by hypoxia in Type I cells, and that bFGF promotes cell survival (Nurse and Vollmer 1997; Paciga and Nurse 2001). Endothelin-1 (ET-1), a well-established HIF target gene (Minchenko and Caro 2000), is expressed within Type I cells and its levels increase following exposure to hypoxia (Chen *et al.* 2002). Furthermore, exogenous ET-1 results in increased BrdU uptake in cultured Type I cells in euoxia, a finding that is abolished if an ET-1 receptor antagonist is also applied (Paciga *et al.* 1999). This finding has been confirmed using an *in vivo* model, in which the hypoxia-induced Type I cell hyperplasia and increased mitotic markers were blunted by concomitant administration of bosentan (an ET-1 receptor antagonist) (Chen *et al.* 2007).

A recent study has shed light on the source of the new Type I cells, proposing that the carotid body Type II cells do not simply serve a supportive glia-type function, but in fact have a role as neural stem cells acting as progenitors of Type I cells during

periods of sustained hypoxia (Pardal *et al.* 2007). Exposure of both young and old mice to hypoxia resulted in an approximate doubling of Type I cell number, in association with an increase in replicating DNA. This increase in cell number was reversible upon return to euoxia, by which time almost half of the carotid body comprised retained, newly-formed cells. Furthermore, cell fate-mapping studies demonstrated that the new Type I cells had originated from the glia-like sustentacular Type II cells. More remarkably, these newly-formed cells possessed the same complex chemosensory properties as mature Type I cells.

The close relationships between the small blood vessels, Type II and Type I cells within the carotid body are of major importance in the detection of and response to hypoxaemia. This structural arrangement is now also proposed to be critical for the crosstalk between the vascular tissue and carotid body progenitors during hypoxia, particularly since VEGF and ET-1 (established vascular HIF target genes) have been shown to play important roles in Type I cell mitosis and carotid body neovascularisation (Pardal *et al.* 2007). It is therefore possible that "the carotid body constitutes a vascular niche for adult neurogenesis where autocrine and paracrine interactions during hypoxia trigger stem cell activation and differentiation" (Pardal *et al.* 2007).

Conclusions

It is a compelling concept that HIF may be the upstream 'driving force' of carotid body neurogenesis in response to hypoxia. Whilst the study presented in this thesis did not utilise BrdU as a marker of increased mitosis, this would certainly be of interest. Measurement of potential HIF target genes within the Chuvash Type I cells, such as VEGF and ET-1, using quantitative PCR or immunohistochemical techniques would also yield valuable mechanistic insights. Considerable work is needed to tease

out the different cellular and molecular mechanisms underlying the Type I cell hyperplasia seen in response to hypoxia. However, the Chuvash mouse model would provide an exciting opportunity to take this investigation further.

3.6.3 Type I cell electron microscopy findings

Confirmation of Type I cell hypertrophy

The immunohistochemistry described in the previous section provides evidence for increased Type I cell size and nuclear area. This finding was confirmed by performing scanning electron microscopy of ultra-thin carotid body sections and examining individual Type I cells. Despite the relatively imprecise measurement technique used to quantify nuclear area in the immunohistochemistry study, the values obtained are very similar to those found using electron microscopy of individual cells.

Type I cell hypertrophy has been shown to be a characteristic feature of the carotid body response to sustained hypoxia (Laidler and Kay 1975; Laidler and Kay 1978; Pequignot *et al.* 1984). Interestingly, it has also been demonstrated in rats exposed to 6 weeks of cobalt administration (Di Giulio *et al.* 1991). Cobalt has long been known to result in polycythaemia (Goldwasser *et al.* 1958), a finding readily explained by its ability to inhibit the interaction between HIF-α and VHL (Yuan *et al.* 2003). The discovery that the Chuvash mice also exhibit Type I cell hypertrophy adds weight to the hypothesis that HIF may play a role in the morphological changes seen within the carotid body in response to chronic hypoxia.

Altered Type I cell ultrastructure

In addition to demonstrating increased Type I cell size and nuclear area, the electron microscopy study also revealed alterations to the quantity of key intracellular organelles. Chuvash Type I cells contained more mitochondria, markedly expanded

rough endoplasmic reticulum, and enlarged dense-cored vesicles. Again, these are characteristic findings that are seen in response to chronic hypoxia (Moller *et al.* 1974; Laidler and Kay 1978; Pequignot *et al.* 1984; Kameda *et al.* 1998).

It is generally acknowledged that neurosecretion is fundamental to the carotid body chemosensory excitation by hypoxia and that the Type I cells contain a large number of putative neurotransmitters and neuromodulators (Kumar and Prabhakar 2012). Catecholamines, particularly dopamine, are stored within the characteristic dense-cored vesicles within the Type I cells (Kumar and Prabhakar 2012). Chronic hypoxia leads to augmentation of the sensory response to hypoxia and affects the component neurotransmitters/modulators (Bisgard 2000; Prabhakar and Jacono 2005). One would hypothesise that this increase in Type I cell neurotransmitter content (shown by the dense-cored vesicle size and/or number) would be accompanied by a requirement for more mitochondria and rough endoplasmic reticulum in order to support the elevated biosynthesis. These changes have been shown to occur in Type I cells in response to chronic hypoxia; the same finding in the Chuvash mouse has now been demonstrated in this thesis.

Possible limitations of this study

There are several possible limitations to the electron microscopy study performed for this thesis. First, only 6 Type I cells per mouse (3 mice per genotype) were examined. It is possible that this small sample size may not be entirely representative of the carotid body as a whole. Second, the identification of intracellular structures and organelles is not always straightforward and requires practice and experience. Therefore, Dr Helen Christian (HC) performed the electron micrograph analysis to minimise this possible source of error. The identification of the dense-cored vesicles and the grading of the rough ER expansion are subjective and could theoretically be

subject to bias; the analyst (HC) was therefore blinded to the genotype of each mouse. Finally, the structure of the carotid body is often difficult to identify. Semi-thin sections were first used to identify the correct area within the carotid bifurcation. The ultra-thin sections were then immunogold-labelled for TH to identify the Type I cells. Whilst the cells of the SCG would also have been labelled using this technique, it is highly unlikely that they would have been analysed in error since they are entirely different in appearance. Furthermore, the measurements of Type I cell nuclear area using immunohistochemistry and electron microscopy were comparable; the nuclei of SCG cells are considerably larger.

Final considerations

This study only examined the ultrastructure of the Type I cells. Whilst the general consensus is that they are the primary oxygen sensors, it would be interesting to examine the other cells types within the carotid body. Finally, the resin required for the immunogold staining resulted in some distortion of the mitochondria so that their ultrastructure and cristae could not be carefully examined. Studies of further carotid bifurcations, using an alternative resin, would be of interest.

Conclusions

The study in this thesis is the first to use electron microscopy to examine the ultrastructure of Type I cells in a genetic disorder of oxygen sensing. Despite the limited number of mice available, striking changes were seen. The increase in cell size, nuclear area, mitochondrial number, dense-cored vesicle diameter and rough ER expansion are all characteristic of the changes seen within Type I cells in response to chronic hypoxia. Furthermore, these changes are logical in the context of increased carotid body chemosensory activity.

3.7 CONCLUSIONS

The work in this chapter presents the novel finding that the Chuvash mice, like the patients, display the characteristic features of ventilatory acclimatisation to hypoxia, namely an elevated baseline ventilation and augmented AHVR. Furthermore, the Chuvash mutation results in marked morphological and ultrastructural changes in the Type I cells of the carotid body. In other words, the elevated ventilation and increased hypoxic sensitivity are accompanied by changes within the carotid body that could lead to enhanced chemosensory activity.

Possible future work on the Type I cell and carotid body responses to acute hypoxia

Whilst the morphological and ultrastructural changes within the Type I cells would be hypothesised to increase their chemosensory activity, this remains to be tested. Exposure of isolated Type I cells to acute hypoxia results in a measurable and quantifiable increase in intracellular calcium. It would be of particular interest to know whether the response of individual Chuvash cells to hypoxia is augmented; this study is already underway. Measurement of carotid sinus nerve activity in response to hypoxia would also be of value, although this study is not currently planned.

Several studies have demonstrated success in performing immunohistochemistry for HIF-1α and HIF-2α within the carotid body. Other studies have performed quantitative real-time PCR on mouse carotid bodies in order to investigate alterations in gene expression. Both techniques are challenging, but it would be particularly worthwhile to optimise and perform them on the Chuvash carotid bodies and/or Type I cells.

HIF-1α versus HIF-2α

Mice with heterozygous deletion of *HIF-1α* (with associated increased HIF-2α levels in the carotid body) have a normal AHVR and carotid body morphology, but manifest markedly impaired ventilatory responses to either sustained or intermittent chronic hypoxia (Kline *et al.* 2002; Peng *et al.* 2006; Yuan *et al.* 2013). In contrast, heterozygous null *HIF-2α* mice also have normal carotid body structure (yet with increased HIF-1α levels), but exhibit irregular breathing patterns and increased ventilatory sensitivity to hypoxia (Peng *et al.* 2011b; Yuan *et al.* 2013). It has been proposed that it is the relative balance, rather than absolute levels, of the HIF-α isoforms within the carotid body that establishes the set point for hypoxic sensing and that HIF-2α may serve an inhibitory role (Yuan *et al.* 2013). In keeping with this, both patients and mice with HIF-2α gain-of-function mutations do not exhibit increased ventilatory sensitivity to hypoxia (Formenti *et al.* 2011; Tan *et al.* 2013). However, the *VHL* Chuvash mutation in mice and humans results in increased expresssion of both HIF-1-specific and HIF-2-preferential target genes (Ang *et al.* 2002b; Hickey *et al.* 2007; Formenti *et al.* 2010; Hickey *et al.* 2010; McClain *et al.* 2012); thus the mechanism underlying the ventilatory and carotid body phenotypes is likely to be complex. This point is emphasised by the finding that mice with heterozygous deficiency of *PHD2*, with consequent increased euoxic levels of HIF-1α and HIF-2α (Mazzone *et al.* 2009), also exhibit carotid body hyperplasia and augmented hypoxic ventilatory sensitivity (Bishop *et al.* 2013).

HIF-2α (but not HIF-1α) heterozygosity in the Chuvash mouse genetically suppressed both the polycythaemic and pulmonary hypertensive phenotypes (Hickey *et al.* 2010). However, no comment was made upon whether the ventilatory phenotype was similarly affected. Taken with the studies on patients and mice with HIF-2α gain-of-

function mutations (Formenti *et al.* 2011; Tan *et al.* 2013), these findings suggest that HIF-2α, rather than HIF-1α, may play the major physiological role in the regulation of pulmonary blood pressure and red blood cell production. It would be of particular interest to repeat the studies described in this thesis upon Chuvash mice that are heterozygous for either HIF-1α or HIF-2α; one would hypothesise that HIF-1α heterozygosity might genetically reverse the ventilatory and carotid body phenotypes.

Final considerations

The Chuvash mice have been shown to exhibit some degree of lung disease, with evidence of haemorrhage, oedema, macrophage infiltration and pulmonary fibrosis (Hickey *et al.* 2010). It is plausible that chronic hypoxaemia, from impaired pulmonary gas exchange, could be driving the ventilatory and carotid body changes described in this chapter. However, this is unlikely since the Chuvash mice have normal arterial PO_2 and haemoglobin oxygen saturation when measured in room air (Hickey *et al.* 2010). The haemoglobin oxygen saturation was shown to decrease to a greater extent in the Chuvash mice upon exposure to acute hypoxia (18% and 12% O_2) which could in theory cause disproportionately elevated ventilation and, hence, mimic an increase in AHVR (Hickey *et al.* 2010). However, two arguments against this explanation are, first, that the authors failed to demonstrate an increased AHVR and, second, that the haemoglobin oxygen saturation measurements were made under anaesthesia. The ability to make these measurements during the awake-plethysmography experiments would be of value, but this is not currently technically feasible.

The Chuvash mice were clearly very different to wild type in terms of their ventilatory and carotid body phenotypes, despite demonstrating only a moderate increase in haemoglobin and haematocrit. The latter is unlikely to have been a

confounding influence, since other animal studies have demonstrated that the hypoxic ventilatory response is either inhibited (Bisgard *et al.* 1969) or unchanged (Eisele *et al.* 1969) acutely by polycythaemia. The Chuvash patients and mice demonstrate features of both primary and secondary polycythaemia, with elevated levels of circulating erythropoietin (Epo) (Ang *et al.* 2002b; Hickey *et al.* 2007). Recent studies have suggested that the latter may play a role in hypoxic ventilatory responses, since transgenic mice over-expressing Epo in the brain and/or peripheral tissues have abnormal ventilatory responses to hypoxia (Soliz *et al.* 2005; Soliz *et al.* 2007). However, this would not explain the marked changes seen within the carotid body in the Chuvash mice and it remains to be seen whether Epo plays an important role in the control of ventilation in humans.

Summary

In conclusion, the findings in this chapter provide evidence that chronic upregulation of the VHL-HIF pathway results in marked ventilatory and carotid body changes that are strikingly similar to those seen in response to sustained hypoxia. However, there remain many unanswered questions regarding the underlying mechanism(s) and further work is warranted.

CHAPTER 4

Cardiac metabolism study

4.1 ABSTRACT

In order to maintain contractile function, the heart produces ATP from a variety of fuel sources and adjusts the flux through metabolic pathways according to the current physiological or pathological state. In response to chronic hypoxia, or in heart failure, there is a switch in cardiac metabolism towards an increased reliance upon glucose, rather than fatty acids, with accompanying alterations in myocardial energetics. It is hypothesised that activation of the HIF pathway may underlie these changes. The mouse model of Chuvash polycythaemia, in which there is long-term systemic HIF stabilisation, provides a unique opportunity to investigate this hypothesis. The study in this thesis demonstrated that Langendorff-perfused hearts from Chuvash mice exhibited increased glycolytic flux and net lactate efflux. Furthermore, using the novel technique of hyperpolarised $^{13}C_1$ pyruvate MR spectroscopy, it was shown that there was also increased label incorporation into lactate *in vivo*. This shift in substrate utilisation towards increased reliance upon glucose was accompanied by alterations in myocardial energetics, as shown by more marked depletion of phosphocreatine (relative to ATP, measured using ^{31}P MR spectroscopy) when the workload of the perfused heart was increased by an isoprenaline infusion. However, despite these changes in myocardial substrate utilisation and energetics, left ventricular mass and function, when measured over the course of 12 months using cine MRI, were unaffected. Interestingly, gene expression analyses failed to demonstrate alterations in key metabolic genes that are known to be affected by HIF and/or hypoxia. Nevertheless, this does not detract from the finding in this study that the PHD-VHL-HIF axis in the heart plays an important role in controlling both myocardial substrate utilisation and cardiac energetics.

4.2 INTRODUCTION

The purpose of the work in this chapter is to provide an overview of cardiac metabolism in health and (briefly) heart failure, to describe the effects of hypoxia and HIF on the heart, and finally to present the comprehensive analysis of cardiac function and metabolism in the Chuvash mouse.

4.2.1 Cardiac energy metabolism

The heart consumes more energy than any other organ - in order to maintain contractile function it produces and consumes vast quantities of ATP. Myocardial metabolism and its regulation are complex, yet are flexible depending on the prevailing physiological and pathological environment (see Figure 4.1 for an overview of cardiac metabolism and key points of regulation).

Under normal conditions, the vast majority of ATP in the heart is produced from oxidative phosphorylation in the mitochondrion (Stanley *et al.* 2005). Approximately 60-70% of this ATP is used for myocardial contraction, whilst the remainder is required for the sarcoplasmic reticulum Ca^{2+}-ATPase and other ion pumps (Gibbs 1978; Suga 1990).

The heart is able to metabolise a variety of fuel substrates, including fatty acids, glucose, pyruvate and lactate (Wisneski *et al.* 1987; Taegtmeyer 2002). The common metabolic product of these substrates is acetyl-CoA which enters the Krebs Cycle, resulting in the generation of NADH + H^+ and $FADH_2$ (Figure 4.1). These reducing equivalents donate electrons that are passed along the electron transport chain from complexes I (II, in the case of $FADH_2$) to IV within the inner mitochondrial membrane. The electrons are finally donated to molecular oxygen, with the

production of water, at complex IV. This electron transport drives proton pumps in complexes I, III and IV which transport positively charged protons out of the mitochondrial matrix, thus generating an electrochemical potential across the membrane. It is this potential difference that provides the energy for the ATP synthesis when the protons return to the matrix through the F_1F_O ATP synthetase (Salway 2004).

Instead of being used immediately for myocardial work, at the point of production, the high-energy bond in ATP is transferred to form phosphocreatine (PCr) and ADP (catalysed by creatine kinase). Due to its smaller size, PCr is then able to diffuse out of the mitochondria into the myofibrils. Myofibrillar creatine kinase releases the high-energy bond from PCr, thus re-forming ATP (Figure 4.1). An important function of the creatine kinase system is therefore to act as a high energy buffer – during periods of high demand, PCr is depleted in order to maintain constant levels of ATP for contractile work. However, the increased level of free intracellular ADP will inhibit many important enzymatic processes and therefore contractile dysfunction can occur even if ATP levels are normal. The ratio of PCr to ATP is a sensitive indicator of the energetic status of the heart (Neubauer 2007).

In the healthy heart, the rate of production of ATP is tightly linked to its rate of hydrolysis. The rates of flux through metabolic pathways linked to the generation of ATP are determined by the requirement of external power for myocardial contraction and by the rate of ATP hydrolysis (Stanley *et al.* 2005). In the well-perfused heart, 60-90% of acetyl-CoA is provided by the β-oxidation of fatty acids, with the remainder coming from the oxidation of pyruvate (which is provided in roughly equal quantities from glycolysis and lactate oxidation) (Wisneski *et al.* 1985a; Wisneski *et al.* 1985b; Gertz *et al.* 1988; Wisneski *et al.* 1990; Stanley *et al.* 1997). It should be

noted that fatty acid (e.g. palmitate) yields more ATP per carbon atom that glucose, but that glucose metabolism is more oxygen efficient (yielding 11% more ATP per oxygen atom consumed) (Salway 2004).

Carbohydrate metabolism

Substrate for glycolysis is provided by exogenous glucose and from glycogen stores. Glucose uptake into the cardiomyocyte is determined by the concentration gradient across the sarcolemma and also by the quantity of glucose transporters (GLUTs). GLUT-1 is constitutively present in the sarcolemma and is responsible for basal glucose uptake, whilst GLUT-4 is the predominant regulator. Insulin stimulation, increased work demand, and ischaemia result in the translocation of GLUT-4 from intracellular vesicles to the sarcolemma, thus increasing glucose uptake into the cardiomyocyte (Stanley *et al.* 1997; Young *et al.* 1997; Young *et al.* 2000). Once inside the cell, glucose is converted by hexokinase to glucose-6-phosphate (G-6-P), thus trapping it within the cytoplasm. Glycogen provides an additional source of G-6-P, although the glycogen pool within the heart is relatively small (Stanley *et al.* 2005).

An important irreversible step in glycolysis (and thus a key regulatory point) is the conversion of fructose-6-phosphate to fructose-1,6-bisphosphate by phosphofructokinase 1 (PFK-1). This enzyme is inhibited by ATP and activated by ADP, AMP and Pi – in other words, flux through glycolysis is accelerated when the phosphorylation potential falls. Citrate is also an allosteric inhibitor of PFK-1, thus linking changes in mitochondrial oxidative metabolism (from increased fatty acid utilisation, for example) to glycolysis (Garland *et al.* 1963; Newsholme and Randle 1964; Randle *et al.* 1968; Randle *et al.* 1970).

Figure 4.1: Cardiac metabolism

Schematic depiction of myocardial metabolism and major points of regulation (see main text for details and discussion). GLUT (glucose transporters); HK (hexokinase); Glu/Fru-6-P (Glucose- or Fructose-6-phosphate); PFK (phosphofructokinase); PDH (pyruvate dehydrogenase); PDK (PDH kinase); ANT (adenine nucleotide transporter); Cr (creatine); PCr (phosphocreatine); CK (creatine kinase – mitochondrial or myofibrillar); LCFA (long-chain fatty acids); FAT (fatty acid transporter); FABPpm (fatty acid binding protein); LCFAcycl-CoA (long chain fatty acyl Co-A); CPT (carnitine palmitoyl transferase; β-ox (β oxidation); ACL (ATP citrate lyase); ACC (acetyl-CoA carboxylase); FAS (fatty acid synthase).

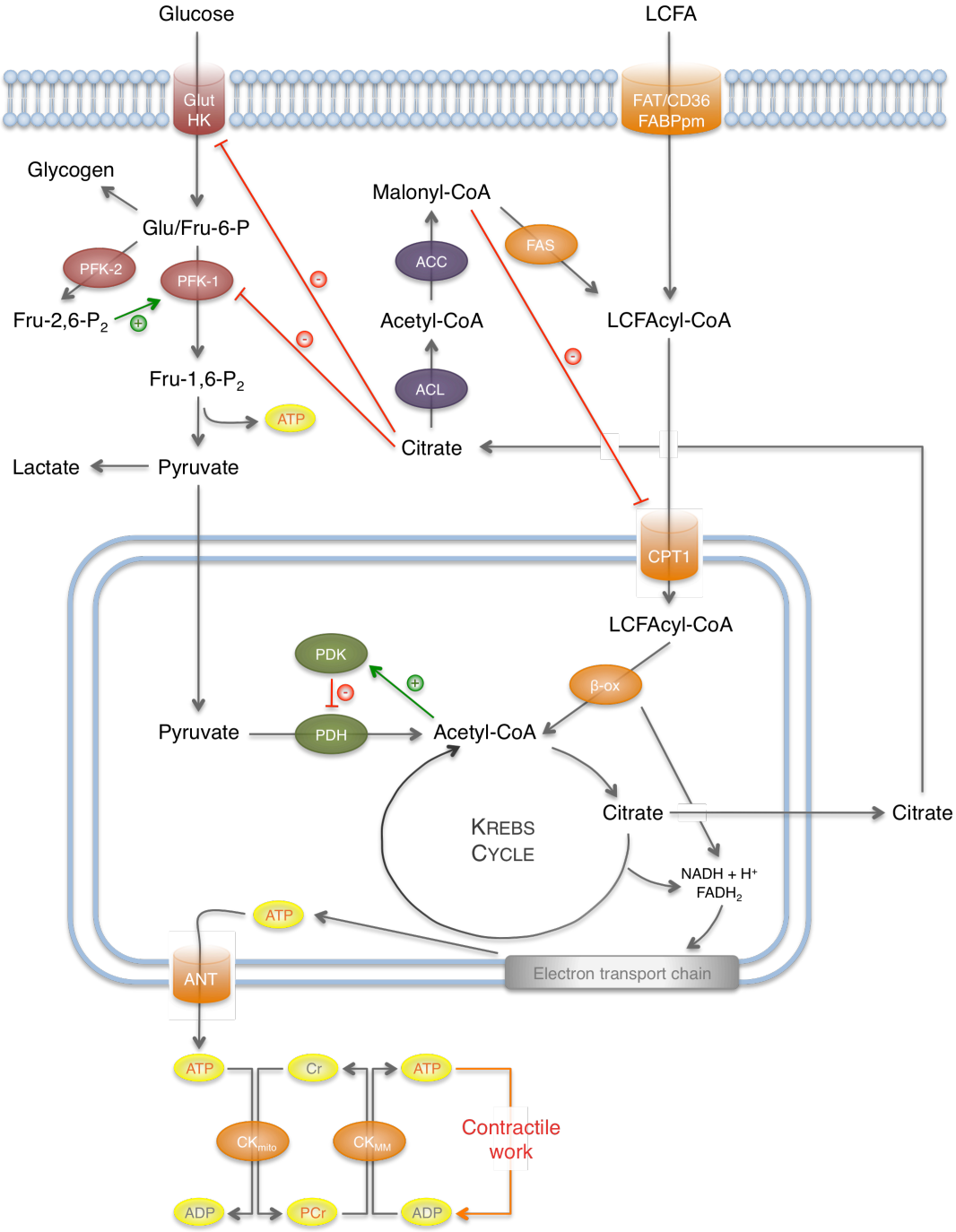

Anaerobic glycolysis results in the production of two molecules of pyruvate and the net yield of two molecules of ATP (Salway 2004). The pyruvate generated then has three main fates: conversion to lactate, decarboxylation to acetyl-CoA, or carboxylation to oxaloacetate or malate. The decarboxylation of pyruvate to acetyl-CoA, through pyruvate dehydrogenase (PDH), is a key irreversible control point in carbohydrate oxidation (Randle 1986). PDH is inactivated by specific kinases (PDKs, of which PDK-4 is the predominant isoform in the heart) which themselves are inhibited both by pyruvate and by decreases in the acetyl-CoA/free CoA and $NADH/NAD^+$ ratios (Wieland *et al.* 1971; Whitehouse *et al.* 1974; Kerbey *et al.* 1976; Randle 1986). The expression of PDK-4 is increased in diabetes and starvation, and also by an increase in the transcription factor peroxisome proliferator-activated receptor alpha (PPARα), the ligand of which is fatty acids (Bowker-Kinley *et al.* 1998; Harris *et al.* 2001; Wu *et al.* 2001). This therefore provides another mechanism for reciprocal feedback between fatty acid and carbohydrate oxidation.

The pyruvate formed during glycolysis can also be converted to lactate in the cytosol. Under normal conditions, the heart is a net consumer of lactate even when cardiac power is near-maximal. Net production of lactate only occurs when there is accelerated glycolysis with concomitant impaired pyruvate oxidation (in poorly-controlled diabetes or ischaemia, for example) (Stanley *et al.* 2005).

Fatty acid metabolism

In contrast to glucose, fatty acid uptake into the cardiomyocyte is determined by the plasma concentration of non-esterified fatty acids (Bing *et al.* 1954; Wisneski *et al.* 1987; Lopaschuk *et al.* 1994a). The circulating levels of free fatty acids can vary considerably during the day, and are significantly elevated by periods of metabolic stress such as starvation, ischaemia and diabetes (Lopaschuk *et al.* 1994b). In the

plasma, fatty acids are transported attached to albumin (the predominant source for myocardial fatty acid oxidation), or bound in triglyceride (Stanley *et al.* 2005). Transport across the sarcolemma is either by passive diffusion or, predominantly, by protein-mediated transport involving a fatty acid transporter (FAT, commonly CD36) or a plasma membrane fatty acid binding protein ($FABP_{pm}$) (van der Vusse *et al.* 2000; Glatz *et al.* 2001; Schaffer 2002).

Once inside the sarcoplasm, the non-esterified fatty acids bind to FABP and are activated by esterification to fatty acyl-CoA by fatty acyl-CoA synthase (FACS) (Stanley *et al.* 2005). The long-chain fatty acyl-CoA can either enter the myocardial triglyceride pool (10-30%) or be converted to long-chain fatty acylcarnitine by carnitine palmitoyl transferase-1 (CPT-1; 70-90%) in the space between the inner and outer mitochondrial membranes. Carnitine acyltransferase then transports this long-chain acylcarnitine across the inner membrane (in exchange for free carnitine) so that it can be re-converted to long-chain fatty acyl-CoA by CPT-2 in the mitochondrial matrix (Stanley *et al.* 2005).

CPT-1 is the key regulator of mitochondrial fatty acid uptake in the heart (Lopaschuk *et al.* 1994a; Kerner and Hoppel 2000). Its activity is strongly inhibited by cytosolic malonyl-CoA, which is itself derived from cytosolic citrate via acetyl-CoA (see Figure 4.1) (Stanley *et al.* 2005). Thus, a rise in malonyl-CoA levels results in decreased fatty acid uptake and β-oxidation, providing another link between glucose and fatty acid oxidation.

Once inside the mitochondria, long-chain fatty acyl-CoA undergoes β-oxidation, during which two-carbon acetyl-CoA units are repeatedly cleaved off and enter the

Krebs Cycle. NADH and $FADH_2$ are generated in the process, which feed into the electron transport chain (Salway 2004).

Reciprocal regulation of carbohydrate and fatty acid metabolism

In 1963, Philip Randle and colleagues described a 'glucose-fatty acid cycle' in which the utilisation of one substrate for metabolism inhibited the use of another directly and without hormonal mediation (see Figure 4.1) (Randle *et al.* 1963). The main regulator of the rate of glucose oxidation in the heart is in fact the rate of fatty acid oxidation. High rates of fatty acid oxidation mediate short-term inhibitory effects along the glycolytic pathway; the inhibition is graded and is most severe at the level of PDH. Fatty acid oxidation increases the mitochondrial acetyl-CoA/free CoA and $NADH/NAD^+$ ratios, thus activating PDK and resulting in phosphorylation and inhibition of PDH. Citrate accumulation in the cytosol also inhibits PFK. Glucose uptake is also inhibited by an, as yet, unknown mechanism. Thus, increased rates of fatty acid oxidation allow 'glucose sparing' by inhibiting glucose oxidation at multiple levels (Hue and Taegtmeyer 2009).

Conversely, glucose oxidation is able to inhibit fatty acid oxidation. Increased levels of cytosolic malonyl-CoA (generated from acetyl-CoA, itself derived from cytosolic citrate, via ACC) strongly inhibit CPT-1 and thus fatty acid entry into the mitochondrion (Figure 4.1) (Hue and Taegtmeyer 2009).

4.2.2 Control of the expression of metabolic genes in the heart

The substrate preference by the heart at a given metabolic, haemodynamic and inotropic state (in other words, the cardiac metabolic phenotype) is primarily dependent upon the content of the proteins that enable flux through the metabolic pathways and the structure of the key cellular organelles such as mitochondria

(Stanley *et al.* 2005). Considerable interest has focused on understanding the mechanisms controlling the expression of metabolic genes in the heart, particularly with reference to changes seen in heart failure, and their impact on the cardiac metabolic phenotype. However, it is important to bear in mind that, at rest, the heart operates at roughly 15-25% of its maximal oxidative capacity and flux through metabolic pathways can be rapidly turned on or off by the allosteric modifications, metabolite concentrations and enzyme localisations described earlier. Therefore, the expression or maximal activity of a key regulatory metabolic protein can be greatly reduced or increased without necessarily affecting ATP production or flux through relevant pathways (Fell and Sauro 1990; Fell 1998; Stanley *et al.* 2005). The study of gene expression therefore should be combined with measurements of actual metabolic flux.

PPARα

Ligand-activated transcription factors, named peroxisome proliferator-activated receptor (PPARs), play an important role in the regulation of myocardial fatty acid oxidation (Berger and Moller 2002; Huss and Kelly 2004). The best-characterised of these, PPARα, is activated by long-chain fatty acids, resulting in heterodimerisation with retinoid X receptors and subsequent binding to specific response elements within the promoter regions of many genes encoding metabolic enzymes (see Table 4.1). Thus, fatty acids, acting via PPARs, are able to 'prime' the myocytes for increased fatty acid oxidation.

HIF

HIF-1 is present in all metazoan species, even in the simple roundworm *C. elegans* which has no specialised oxygen delivery systems. A primordial function of HIF-1 is

to find the optimal balance between oxidative and glycolytic metabolism for a given local oxygen concentration. Many genes for the key regulatory enzymes and transporters in glucose metabolism are direct HIF targets (see Table 4.1), underlying the fundamental importance of linking oxygen sensing to metabolism.

Table 4.1: Control of the expression of metabolic genes

The expression of many key metabolic genes is increased by the transcription factors PPARα (predominantly fatty acid oxidation) and HIF (predominantly glucose oxidation).

PPARα	Metabolic pathway	Genes
	Fatty acid transport & utilisation	FATP, FAT/CD36, FABP, ACS (Motojima *et al.* 1998; van der Lee *et al.* 2000; van Bilsen *et al.* 2002)
	Fatty acid mitochondrial uptake	M-CPT-1 (Brandt *et al.* 1998; Djouadi *et al.* 1999)
	β-oxidation	MCAD, LCAD, VLCAD (Gulick *et al.* 1994; van der Lee *et al.* 2000)
	Mitochondrial uncoupling	UCP3 (Young *et al.* 2001; Murray *et al.* 2004)
	Glucose oxidation	PDK-4 (Harris *et al.* 2001; Huang *et al.* 2002)
HIF	**Metabolic pathway**	**Genes**
	Glucose uptake	GLUT-1 (Iyer *et al.* 1998)
	Glycolysis	HK-1, HK-2, ALDA, PGK-1, Eno-1, PKM (Firth *et al.* 1994; Semenza *et al.* 1996; Iyer *et al.* 1998; Seagroves *et al.* 2001)
	Production of lactate	LDHA (Semenza *et al.* 1996)
	Entry of pyruvate to Krebs Cycle	PDK-1 (Kim *et al.* 2006; Papandreou *et al.* 2006)
	Electron transport chain efficiency	COX-4 subunits (Fukuda *et al.* 2007)
	Mitochondrial autophagy	BNIP-3 (Zhang *et al.* 2008)
	Iron-sulphur cluster proteins	microRNA miR-210 (Chan *et al.* 2009)

HIF is able to influence the fate of pyruvate by activating the transcription of the genes encoding LDHA and PDK-1, resulting in a shift from oxidative to glycolytic metabolism. To compensate for the markedly reduced efficiency of ATP production via glycolysis, HIF also activates the transcription of genes encoding glucose transporters and glycolytic enzymes, thus increasing flux through the pathway. By activating the transcription of the microRNA miR-210, which inhibits the expression of iron-sulphur cluster assembly proteins ISCU-1/2, HIF is also able to affect the

Krebs Cycle and electron transport chain, since ISCU are required for both aconitase and complex I. The performance of the electron transport chain is further modulated, as HIF orchestrates a subunit switch from COX4-1 to COX4-2 in complex IV, thus fine-tuning the activity of cytochrome *c* oxidase under hypoxic conditions. HIF is also able to influence mitochondrial number by transcriptional activation of the gene encoding BNIP-3, a mitochondrial protein that competes with Beclin-1 for binding to Bcl2, thereby freeing Beclin-1 to trigger selective mitochondrial autophagy.

4.2.3 Cardiac metabolism in heart failure

There is growing evidence to support the notion that alterations in substrate utilisation seen in heart failure may contribute to contractile dysfunction. The concept that the failing heart is energy depleted is not new – in 1939 it was first demonstrated that there was a significantly reduced creatine content in the failing myocardium (Neubauer 2007). Today, much more is known about the energetics of the failing heart, revealing a hugely complex and multi-factorial story. The focus of this thesis is not on the metabolism of heart failure, but a brief overview will allow the changes seen in the hypoxic and Chuvash hearts to be placed into context.

As the heart fails, changes occur in all three components of cardiac energy metabolism: substrate utilisation, oxidative phosphorylation, and high-energy phosphate metabolism. The multi-factorial nature of both heart failure and the experimental design of many studies mean that there are often conflicting findings. However, the general consensus is that fatty acid oxidation is unchanged or slightly increased in early heart failure, but is markedly reduced when heart failure is advanced. Conversely, many studies indicate that glucose oxidation is increased in early heart failure (Neubauer 2007). A marked reduction in the ratio of PCr to ATP (a

sensitive indicator of myocardial energetics) is a well-established feature in heart failure. PCr:ATP ratios correlate with New York Heart Association classes and with indices of systolic and diastolic function, and have been shown to be predictive of mortality (Neubauer *et al.* 1992; Neubauer *et al.* 1995; Neubauer *et al.* 1997; Lamb *et al.* 1999).

The expression of PPARα, as well as some downstream targets (e.g. MCAD), is decreased in proportion to the decrease in fatty acid utilisation demonstrated in cardiac hypertrophy in both animal models and patients (Sack *et al.* 1996; Barger *et al.* 2000; Karbowska *et al.* 2003). It is thought, therefore, that this downregulation in PPARα is the driving force in the switch from fatty acid to glucose oxidation (Neubauer 2007). More recently, it has been hypothesised that myocardial hypoxia in heart failure, with consequent activation of the HIF pathway, may also play a role in altering cardiac energetics.

4.2.4 Cardiac metabolism in chronic hypoxia

There are surprisingly few studies linking the effects of chronic hypoxia on myocardial gene expression, substrate utilisation and energetics.

Metabolic gene and protein expression

Two studies have measured the temporal changes in metabolic genes over two weeks of moderate hypobaric hypoxia (11% O_2), analysing the right and left ventricles separately (Sharma 2003; Adrogue *et al.* 2005). They demonstrated dynamic changes in gene expression, with a reduction in PDK-4 but no alteration in the transcript levels of GLUT-1 or GLUT-4. In contrast, a separate study did show increased expression of GLUT-1 (and unaltered GLUT-4) for a similar hypoxic exposure (Sivitz *et al.* 1992). Following one week of hypoxia, PPARα expression, and its downstream targets

MCAD and CPT-1, was shown to be decreased (Sharma 2003). This is in agreement with a separate study that utilised alternative models of hypoxia (cobalt chloride treatment and isovolaemic haemodilution) and demonstrated a reduction in PPARα, PDK-4 and CPT-1 expression (Razeghi 2001). More recent doctoral work in Oxford has shown many whole-heart changes in gene expression and protein levels in mice exposed to two weeks of 11% O_2 (Abd-Jamil 2012). The expression of PPARα, and the downstream genes PDK-4, MCAD (mRNA and protein) and UCP-3 (protein) were reduced. Whilst the expression of PDK-1 was increased, there were no changes in the transcript levels of GLUT-1 or GLUT-4.

Myocardial substrate uptake and utilisation

Cardiac glucose uptake is increased in rats exposed to hypobaric hypoxia (Hurford *et al.* 1990) and high-altitude natives such as Himalayan Sherpa and Andean Quechua display enhanced myocardial glucose uptake (Holden *et al.* 1995). More recently, it has been demonstrated that exposure of mice to 11% O_2 for two weeks results in significantly increased myocardial glycolytic flux and net lactate efflux, with reduced rates of fatty acid oxidation (Abd-Jamil 2012). This result is particularly interesting as the observed alterations in substrate utilisation corroborate the findings at the molecular level.

Myocardial energetics

Lower PCr:ATP ratios were observed in Sherpa hearts (Hochachka *et al.* 1996), in lowlanders exposed to 20 hours of normobaric hypoxia (Holloway *et al.* 2011), and in trekkers travelling to Everest base camp at 5300 m (Holloway *et al.* 2010). Similarly, myocardial PCr:ATP ratios were reduced in mice exposed to 11% O_2 for two weeks (Abd-Jamil 2012).

Taken together, these studies demonstrate that chronic hypoxia results in changes in the expression of key metabolic genes, a switch towards glucose utilisation rather than the use of fatty acids, and alterations in cardiac energetics. However, the role of HIF in these metabolic changes is less clear.

4.2.5 Hypoxia-inducible factor and cardiac metabolism

Over the past decade, various systemic and cardiac-specific under- or over-expression models of HIF have been created. However, all of these are 'non-physiological', in the sense that they do not represent a human disorder of modest, systemic HIF-pathway activation. The Chuvash mouse therefore provides a unique opportunity to explore more 'physiological' cardiac effects of increased HIF levels. Nevertheless, these other studies do provide interesting insights into the importance of HIF in cardiac function and metabolism.

Most studies investigating the importance of HIF in the heart have created cardiac-specific models, employing tactics to either over-express HIF-1α itself or impair HIF degradation using altered levels of PHDs or VHL. Mice with cardiomyocyte-specific loss of VHL have markedly elevated HIF levels in the heart and develop severe progressive heart failure and early death (Lei *et al.* 2008). The hearts demonstrate increased lipid accumulation and elevated expression of LDHA, GLUT-1, PGK (phosphoglycerate kinase) and Bnip3. In contrast, cardiac-specific reduction in the level of PHD2 (with resulting elevated expression of PGK-1, GLUT-1 and PDK-1) causes no cardiomyopathy and, indeed, results in cardioprotection from ischaemia-reperfusion injury (Hyvarinen *et al.* 2010). However, combined cardiac-specific loss of PHD2 and PHD3 together (with elevated expression of Bnip3 and PGK-1, and decreased expression of PPARα) causes severe cardiomyopathy with myocyte

accumulation of lipid and glycogen (Moslehi *et al.* 2010). Conditional somatic inactivation of PHD2 (since germline loss is embryonic lethal) results in increased cardiac expression of Bnip-3 and PGK and the development of cardiomyopathy (Minamishima *et al.* 2008).

Inducible cardiac-specific overexpression of a mutated, oxygen-stable, form of HIF-1α resulted in increased transcript levels of PGK-2, hexokinase-2 and aldolase-A, decreased levels of SERCA (sarcoplasmic endoplasmic reticulum Ca^{2+} ATPase) and progressively impaired cardiac function (Bekeredjian *et al.* 2010). Mice with constitutive cardiac-specific overexpression of HIF-1α were protected against diabetes-induced cardiac injury by restoring expression of GLUT-1 and hexokinase-2 (Xue *et al.* 2010). However, long-term constitutive overexpression of HIF-1α in the heart results in increased glucose uptake, altered calcium handling with decreased expression of SERCA-2a, and the development of cardiomyopathy (Holscher *et al.* 2012). Interestingly, cardiac-specific loss of HIF-1α also resulted in impaired cardiac contractility, high-energy phosphate content and lactate production (Huang *et al.* 2004).

Taken together, these studies clearly illustrate the importance of HIF in cardiac function and metabolism. The Chuvash mouse model provides a unique opportunity to study the effect of 'physiological' systemic HIF stabilisation on the heart for the first time.

4.3 SUMMARY AND STUDY AIMS

Cardiac metabolism and function are enormously complex and there is a growing body of evidence demonstrating that altered cardiac energetics can affect contractile function. The expression of many key metabolic genes is increased by HIF and it is becoming increasingly clear that either systemic hypoxia or manipulations of the PHD-VHL-HIF axis result in altered cardiac metabolism and function.

Chuvash polycythaemia provides a unique opportunity to investigate the effects of chronic, systemic HIF stabilisation on the heart in a 'physiological' model. The main hypothesis is that chronic elevation of HIF levels in the heart will alter the expression of genes involved in glucose and fatty acid metabolism, and that these alterations will result in an increased reliance on glucose utilisation. This increased reliance on a less ATP-efficient substrate may subsequently affect cardiac energetics and function.

A systematic approach was used to address these questions. First, *in vivo* cardiac function was assessed repeatedly over the course of a year, using cine MRI. Cardiac substrate utilisation (glycolysis, lactate efflux, palmitate oxidation, and pyruvate metabolism) was measured using both radiolabelled isolated-perfused heart techniques and *in vivo* real-time ^{13}C magnetic resonance spectroscopy (MRS). Cardiac energetics were assessed using the isolated-perfused heart and ^{31}P MRS. Transcriptome (microarray) and metabolome analysis of heart tissue were also performed.

4.4 METHODS

Mice were bred and housed according to the methods described in 2.2.1. The age, sex and number of mice used in each study will be specified in the relevant results sections.

4.4.1 Plasma chemistry analysis and glucose tolerance test

Following excision of the heart, blood was immediately collected from the chest cavity. The blood was centrifuged at 4 °C and the plasma subsequently frozen in liquid nitrogen. All plasma analysis was performed on an ABX Pentra 400 clinical chemistry analyser (Horiba ABX S.A.S, UK). All tests were purchased from Horiba, with the exception of the NEFA and D-3-hydroxybutyrate assays which were purchased from Randox Laboratories, Co. Antrim.

An intraperitoneal glucose tolerance test (IPGTT) was carried out to study the response of the Chuvash mice to a glucose load. Following a 15 – 16 hour overnight fast, conscious mice were weighed and their tails anaesthetised with lidocaine EMLA topical cream (Astrazeneca). Twenty minutes after application of the cream, a baseline glucose measurement for each mouse was obtained using blood collected via tail vein puncture. Mice were then injected intraperitoneally with a glucose load of 2 g/kg body mass. Blood samples were obtained 30, 60 and 120 minutes after the glucose injection. Blood glucose concentrations were determined using a Freestyle Lite handheld glucose meter (Abbott).

4.4.2 Langendorff perfused heart

The *ex vivo* Langendorff perfused heart set-up was used to perform the radiolabelled substrate utilisation and ^{31}P MR spectroscopy studies.

Buffer preparation

Krebs-Henseleit (KH) buffer was prepared as per Table 4.2. Due to the hydrophobic nature of fatty acids, 0.4 mM palmitate was pre-bound to 1.5 % fatty acid-free bovine serum albumin (Sigma UK; and Apollo Scientific, UK) in warmed KH. This mixture was placed in dialysis tubing and allowed to equilibrate overnight in KH. To avoid the problem of calcium chelation by albumin, calcium concentration of the albumin-palmitate solution was checked immediately prior to use using an ABL 700 Series blood gas analyser (Radiometer, UK) and corrected to 1.8 – 1.9 mM if necessary.

Immediately before use, KH was supplemented with 1.2 mM KH_2PO_4 and 1.8 mM pyruvate; the albumin-palmitate solution was supplemented with 1.2 mM KH_2PO_4 only. The KH_2PO_4 was used for the ^{31}P MRS study and for consistency was included in all perfusion experiments.

Table 4.2: Krebs-Henseleit buffer

Component	Concentration
Sodium chloride	118 mM
Potassium chloride	3.7 mM
Magnesium sulphate (heptahydrate)	1.2 mM
Calcium chloride (dihydrate)	1.97 mM
EDTA disodium salt	0.5 mM
Sodium hydrogen carbonate	25 mM
Glucose	11 mM

Ex vivo Langendorff perfused heart set-up

Mice were anaesthetised with 0.1 – 0.3 ml of intraperitoneal sodium pentobarbital (200 mg in 1 ml, Merial, UK). After loss of the withdrawal reflex, mice were weighed using electronic scales. The chest cavity was opened using scissors and brief dissection performed to visualise the heart, if necessary. The heart was excised and

arrested in ice-cold KH buffer, quickly trimmed of extraneous tissue, weighed, and then cannulated via the aorta.

Figure 4.2: The perfusion apparatus and a perfused heart *in situ*

These representative photographs of the perfusion apparatus for the radiolabelled studies show a perfused heart *in situ*. The aorta is cannulated with a 21 G needle (cut short) and a water-filled balloon is inserted into the left ventricle. The coin shown is a UK five pence piece.

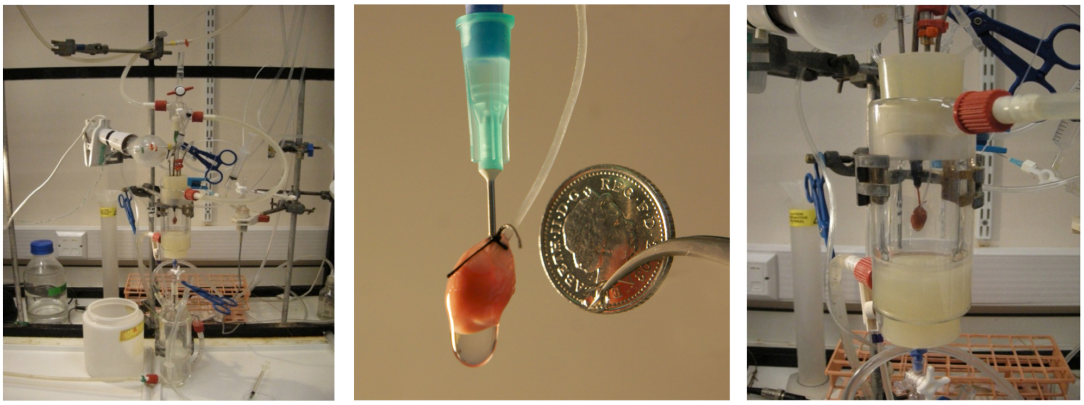

Hearts were perfused in Langendorff mode, initially with KH (oxygenated with 95% O_2 and 5% CO_2) warmed to 37°C at a constant perfusion pressure of 80 mm Hg. The left atrium was opened and a small fluid-filled PVC balloon, connected via fluid-filled polyethylene tubing to a pressure transducer, was inserted into the LV and its volume adjusted to produce an end-diastolic pressure (EDP) of 4 – 8 mm Hg. The signal acquired from the pressure transducer was passed via a bridge amplifier to a PowerLab data acquisition system (ADInstruments, UK) and allowed measurement of the pressure waveform, LV developed pressure (LVDP; systolic pressure on the waveform minus EDP) and heart rate (see Figure 4.3). Rate pressure product (RPP) was calculated as the product of LVDP and heart rate.

Once the balloon was in place and a suitable pressure tracing was being recorded, the perfusate was switched from KH to the palmitate buffer (still oxygenated, warmed, and at a perfusion pressure of 80 mm Hg). The heart was then placed within a water-

jacketed glass chamber so that it was perfused with re-circulating buffer. Figure 4.4 illustrates the re-circulating Langendorff perfusion set-up and Figure 4.2 shows pictures of a perfused heart *in situ* as well as the apparatus used for the radiolabelled studies.

Figure 4.3: Typical LV pressure tracings

LV pressure was measured using a calibrated PVC balloon within the ventricle. Heart rate was calculated by setting trigger points within the ascending portion of the pressure wave. LV developed pressure (LVDP) was calculated as the difference between the systolic and end-diastolic pressures.

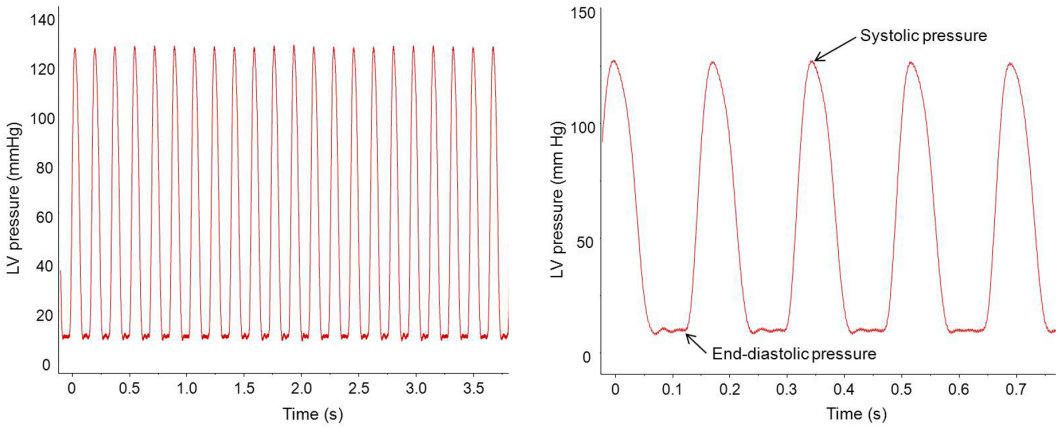

Figure 4.4: Diagram of the Langendorff perfusion set-up

See main text for full details. The glass lung was situated to provide a perfusion pressure of 80 mm Hg. Overflow from the lung (not shown) was re-circulated to the lower reservoir. Perfusate was warmed in the water-jacketed chambers and by a heater situated adjacent to the inlet cannula in the aorta. A fluid-filled PVC balloon in the LV allowed heart rate and LV developed pressure measurement.

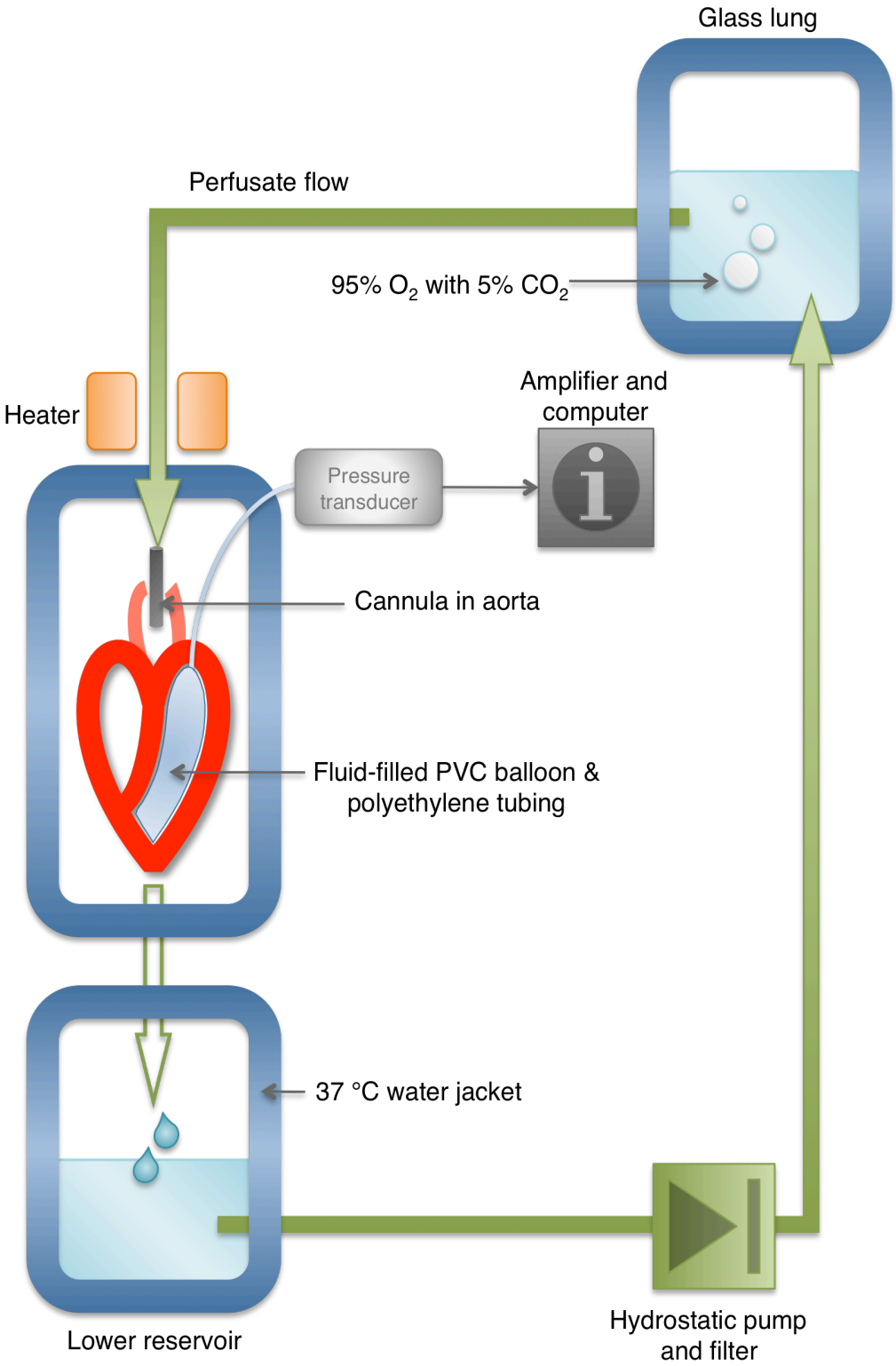

4.4.3 Measurement of glycolytic flux

Hearts were perfused with 100 ml of re-circulating KH buffer containing 11 mM glucose, 1.2 mM KH_2PO_4, 0.4 mM palmitate bound to 1.5% fatty acid-free bovine serum albumin and 50 μCi of D[5-^{3}H]-glucose (Amersham, UK). Following a ten minute stabilisation period, 1 ml aliquots (in duplicate) of the re-circulating buffer were collected every five minutes, for 35 minutes. At the end of the protocol the perfusate was switched back to KH and the heart subsequently freeze-clamped for subsequent analysis.

The 1 ml aliquots were used to determine the glycolytic rate (Lopaschuk and Barr 1997). First, the ^3H_2O was separated from the [^{3}H]-glucose using glass pipettes containing Dowex® 1-X4 anion exchange resin (Sigma, UK). 0.2 ml of perfusate from each aliquot, including the duplicates, was added to the column, enabling elution of the ^3H_2O into scintillation vials. Ecolite® scintillant was then added to the vials and the samples subjected to standard isotope counting procedures, yielding a value of 'counts per minute' (cpm) for each time point. The 'specific activity' of the original 100 ml of re-circulating buffer was determined by adding 0.2 ml of the first aliquot directly to a scintillation vial.

For each aliquot sample, the amount of ^3H_2O present (and thus [^{3}H]-glucose consumed, in μmol) was calculated using the following equation:

$$\text{Amount of } [^3\text{H}]\text{-glucose consumed} = \frac{[\text{sample cpm} - \text{cpm of time-zero sample}] \times 5 \times \text{buffer volume}}{[\text{specific activity} - \text{cpm of time-zero sample}] \times 5 \times \text{glucose concentration}}$$

Buffer volume was in ml; glucose concentration was 11 mM; the factor of 5 is used to scale the 0.2 ml used to 1 ml.

These values were then plotted against time (in minutes), with the slope of the linear regression line giving the rate of glycolysis in μmol/minute/heart.

4.4.4 Measurement of lactate efflux

The assay for lactate is based upon the reaction catalysed by lactate dehydrogenase:

Lactate + NAD → pyruvate + hydrazine (converted into pyruvate hydrazone) + NADH

Since NADH absorbs light at a wavelength of 340 nm, whilst NAD does not, absorbance (as measured using a spectrophotometer) will increase as the reaction proceeds, depending upon the starting concentration of lactate (if all else is kept equal). The assay buffer for all reactions (100 ml, pH 9.5) comprised 0.2 M Tris base, 10 mM EDTA, 5 ml hydrazine hydrate, and 10 ml of 1% NAD solution.

First, a standard curve was constructed by taking 1 ml of the assay buffer and adding a further 1 ml of lactate of 10 different concentrations (from 0 – 100 μM). Initial readings of absorbance at 340 nm gave baseline values, after which 10 μl of lactate dehydrogenase were added. Absorbance was re-read after a reaction period of 20 minutes had elapsed. Plotting starting lactate concentration against the increase in absorbance from baseline gave the equation of the linear regression line. The protocol was repeated with the buffer samples and the increase in absorbance used to calculate the lactate concentration in each aliquot.

These values were then plotted against time (in minutes), with the slope of the linear regression line giving the rate of net lactate efflux in μmol/minute/heart.

4.4.5 Measurement of palmitate oxidation rates

Hearts were perfused with 100 ml of re-circulating KH buffer containing 11 mM glucose, 1.2 mM KH_2PO_4, 0.4 mM palmitate bound to 1.5% fatty acid-free bovine

serum albumin and 50 μCi of [9,10-^{3}H]-palmitate (Amersham, UK). Following a ten minute stabilisation period, 1.2 ml aliquots of the re-circulating buffer were collected every five minutes, for 40 minutes. At the end of the protocol the perfusate was switched back to KH for eight minutes and the heart subsequently freeze-clamped for subsequent analysis.

The 1.2 ml aliquots were used to determine the rate of palmitate oxidation (Lopaschuk and Barr 1997). First, the $^{3}H_2O$ was separated from the [^{3}H]-palmitate by treating 0.5 ml of the buffer samples with 1.88 ml of a mixture of chloroform and methanol (ratio of 1:2, volume), adding 0.625 ml of chloroform and 0.625 ml of a 2 M KCl:0.4 M HCl solution, mixing, and then allowing the mixture to stand. The top aqueous phase was collected with a Pasteur pipette and subsequently treated with 1 ml each of chloroform and methanol, and 0.9 ml of the KCl:HCl solution. Following mixing and allowing the layers to form, two 0.5 ml samples of the top layer were removed and added to separate scintillation vials containing Ecolite® scintillant. The same standard isotope counting procedure was then used. The 'specific activity' of the original 100 ml of re-circulating buffer was determined by adding 0.5 ml of the first aliquot directly to a scintillation vial.

For each aliquot sample, the amount of $^{3}H_2O$ present (and thus [^{3}H]-palmitate consumed, in μmol) was calculated using the following equation:

$$\text{Amount of } [^{3}\text{H}]\text{-palmitate consumed} = \frac{[\text{sample cpm} - \text{cpm of time-zero sample}] \times 2 \times 8.556 \times \text{buffer volume}}{[\text{specific activity} - \text{cpm of time-zero sample}] \times 2 \times \text{palmitate concentration}}$$

Buffer volume was in ml; palmitate concentration was 0.4 mM; the factor of 2 is used to scale the 0.5 ml used to 1 ml; the factor of 8.556 is the dilution factor taking into account the different reagents added to the buffer sample.

These values were then plotted against time (in minutes), with the slope of the linear regression line giving the rate of palmitate oxidation in μmol/minute/heart.

4.4.6 Measurement of high-energy phosphate metabolism

Mouse hearts were perfused in Langendorff mode as described above (KH with 11 mM glucose, 0.4 mM palmitate, 1.2 mM KH_2PO_4). Hearts were inserted into an 11.7 Tesla vertical bore magnet (Magnex Scientific, UK) using a Bruker Advance console (Bruker Medical, Ettlingen, Germany) with a 10 mm I.D probe containing concentric ^{1}H and ^{31}P sensitive coils. The heart was centralised in these coils using acquisition of a brief ^{1}H image.

Fully relaxed ^{31}P spectra were then acquired using pulse-and-collect sequence at a repetition time of 10s and a flip angle of 90°. Two ^{31}P spectra of 64 averages (32 each per spectrum) were acquired during perfusion with palmitate buffer under standard conditions. Approximate doubling of the RPP was then achieved by an infusion of the positively inotropic and chronotropic non-selective beta-adrenergic agonist isoprenaline (concentration received by the heart 2 – 5 nM). Further spectra (minimum of 2; 64 averages) were then acquired. At the end of the experiment the hearts were freeze-clamped for subsequent analysis. Spectra were analysed using the jMRUI software to give values for PCr and γATP abundance, and the ratio of these two. Spectra for each perfusion condition (standard, or isoprenaline) were averaged to give a final value of PCr:ATP.

4.4.7 Measuring *in vivo* $^{13}C_1$ pyruvate metabolism in real-time

The advent of dynamic nuclear polarisation (DNP) has enabled the inherently low sensitivity of ^{13}C MRS to be increased 10,000-fold (Ardenkjaer-Larsen *et al.* 2003). Hyperpolarised compounds can be infused *in vivo* and their metabolism followed in

real-time (Schroeder *et al.* 2008). Recently, hyperpolarised $^{13}C_1$ pyruvate MRS has been demonstrated successfully in mice (Dodd *et al.* 2013), opening up many exciting new experimental prospects.

Mice were studied in the early absorptive (fed) state, between 7 and 11 am. Anaesthesia was induced with 2.5 – 3% isoflurane in medical oxygen (100%) and maintained using 2 % isoflurane through a nose cone. ECG and respiration were monitored throughout and air heating was provided to maintain body temperature. A 32 G cannula was inserted into a tail vein for intravenous infusion of hyperpolarised solutions. The mouse was then placed into a purpose-built cradle and a ^{13}C radiofrequency (RF) coil positioned over the chest, enabling localisation of the signal from the heart (Dodd *et al.* 2013). Mice were positioned in a 7 T horizontal bore MR scanner interfaced to a direct-drive console (Varian Inc, Yarnton, UK). Using a 72 mm ^{1}H volume transmit/receive RF coil (Rapid Biomedical, Rimpar Germany), a 3-plane FLASH localiser image was obtained to confirm the location of the heart at the magnet isocentre. A fiducial marker containing water, positioned on top of the ^{13}C RF coil, was used to ensure the correct position of the coil over the heart. Using the ^{1}H volume coil, an ECG-gated shim was used to reduce the proton linewidth to ~150 Hz.

Approximately 40 mg of $^{13}C_1$ pyruvic acid doped with 15 mmol/L trityl radical (OXO63, Oxford Instruments, Abingdon, UK) and 3 µl Dotarem (1:50 dilution) (Guerbet, Birmingham, UK), was hyperpolarised in a polariser (General Electric Prototype Polarizer, GE Healthcare, Amersham, UK), with 45 min of microwave irradiation, as previously described (Ardenkjaer-Larsen *et al.* 2003). The sample was subsequently dissolved in a pressurised and heated alkaline solution, containing 60 mmol/L sodium hydroxide and 247 mmol/L EDTA dipotassium salt (Sigma-Aldrich),

to yield a solution of 80 mM hyperpolarised sodium $^{13}C_1$ pyruvate with a polarisation of ~30 %, at physiological temperature and pH (Ardenkjaer-Larsen *et al.* 2003).

Following dissolution, 0.15 ml of hyperpolarised pyruvate was injected over 10 s into the anaesthetised mouse (dose of 0.48 mmol/kg), followed by a 0.05 ml flush of heparinised saline to clear the delivery line. Sixty individual ECG-gated ^{13}C MR pulse-acquire cardiac spectra were acquired over 1 min following injection. All cardiac ^{13}C spectra were analysed using the AMARES algorithm in the jMRUI software package. The peak areas of $^{13}C_1$ pyruvate, $^{13}C_1$ lactate, $^{13}C_1$ alanine and $^{13}C_1$ bicarbonate at each time point were quantified and used as input data for a kinetic model which was based on (Zierhut *et al.* 2010; Atherton *et al.* 2011). Significant differences between mean values were determined by one-way analysis of variance (ANOVA) followed by Bonferroni's multiple comparison post-hoc test. Differences between groups were considered significant if $p < 0.05$.

4.4.8 Assay of PDH activity

The activities of both the active and total fractions of PDH (PDH_a and PDH_t respectively) were determined spectrophotometrically (Seymour and Chatham 1997). Briefly, the active fraction of PDH was extracted under conditions where both PDH phosphatase and PDH kinase were inhibited, using a buffer containing 25 mM HEPES, 25 mM KH_2PO_4, 25 mM KF, 1 mM dichloroacetate, 3 mM EDTA (K salt), 1 mM ADP, 1 mM dithiothreitol, 0.05 mM leupeptin, and 1% Triton X-100, adjusted to pH 7.0. KH_2PO_4 and KF were included to inhibit PDH phosphatase, whilst ADP and dichloroacetate served to inhibit PDK. In addition, EDTA and leupeptin were included to inhibit non-specific phosphatases and proteinases, respectively, and Triton X-100 was added to permeabilise the mitochondrial membrane. The total activity of

PDH was extracted under conditions where PDH phosphatase was stimulated and PDK inhibited, using a buffer containing 75 mM HEPES, 5 mM dichloroacetate, 5 mM $MgCl_2$, 1 mM ADP, 1 mM dithiothreitol, 0.05 mM leupeptin, and 1% Triton X-100, adjusted to pH 7.0.

Frozen cardiac tissue was powdered and 50 mg was homogenised in 250 µl of the appropriated extraction buffer using a Polytron for 30 seconds. The homogenate was then rapidly frozen in liquid nitrogen, thawed and homogenised again; this procedure was repeated 3 times. The sample was centrifuged at 4 °C for 7 minutes at maximum speed and the resulting supernatant removed, stored on ice and enzyme activity assayed immediately.

PDH activity was assayed by measuring the production of NADH spectrophotometrically (340 nm) in a 30 °C assay buffer containing 50 mM HEPES, 1 mM $MgCl_2$, 0.08 mM EGTA, 1 mM dithiothreitol, 4 µM rotenone, 1.67 mM NAD, 0.1 mM Co-enzyme A, 0.2 mM thiamine pyrophosphate, 16.7 mM lactate and 2 U lactate dehydrogenase. The assay mixture was incubated at 30 °C for at least 5 minutes prior to the addition of the tissue sample. 50 µl of either the PDH_a or PDH_t extract were added to the assay and the reaction followed for 2 minutes; each sample was run in triplicate. The period of NADH production from 10 – 40 seconds was used to determine the PDH activity in units of µmol/min/g wet weight tissue.

4.4.9 Cardiac metabolomics

Mice were anaesthetised initially with 5% isoflurane in medical oxygen (100%); anaesthesia was maintained via a nose cone with 1-2% isoflurane in oxygen. When adequate analgesia was attained the chest cavity was opened and careful dissection was performed to visualise the heart. The apex of the heart was grasped with forceps

and the ventricles quickly cut free, leaving the atria and other tissues in situ. The ventricular muscle was quickly dabbed on gauze to remove the majority of the blood and then snap frozen in liquid nitrogen within a few seconds. Approximately half of the frozen tissue was crushed to a fine powder in liquid nitrogen and used for the metabolomics study; the remainder was used for the micro-array study.

Metabolite extraction

Metabolites were extracted from the crushed heart tissue using a methanol-chloroform extraction method (Le Belle *et al.* 2002; Atherton *et al.* 2006). Tissue was added to 600 µl chloroform-methanol (2:1; v/v) and the samples were homogenised using a TissueLyser (Qiagen, UK) for 5 minutes at 20 Hz, and then sonicated for 15 minutes. Water and chloroform (200 µl each) were added to the samples, which were then centrifuged at 13,000 RPM for 7 minutes. The resulting aqueous and organic phases were separated from the protein pellets. The extraction procedure was repeated on the remaining protein pellets to form a double extract. Both organic and aqueous phases were collected and dried under nitrogen. The dried samples were stored at -20 °C until further analysis. The tissue processing and metabolite extraction stages were performed in collaboration with Xinzhu Wang, in Cambridge. She performed the subsequent specialist data analysis.

Proton nuclear magnetic resonance (NMR) spectroscopy

Dried aqueous extracts were dissolved in 600 µl D_2O containing 0.25 mM sodium-3-(tri-methylsilyl)-2,2,3,3-tetradeuteriopropionate (TSP) (Cambridge Isotope Laboratories Inc., Andover, USA). The samples were analysed by a Bruker AVANCE II+ spectrometer at a frequency of 500.13 MHz (Bruker, Germany) using a 5 mm triple axis inverted (TXI) Automatic Tuning and Matching (ATMA) probe. A one-

dimensional solvent suppression pulse sequence based on the nuclear Overhauser effect spectroscopy (NOESY) pulse sequence was used to suppress the water signal with pre-saturation applied during the mixing time and relaxation delay. 128 transients were collected for each sample into 64k data points over a spectral width of 8000 Hz at 300 K. Peaks were quantified using Chonomx NMR suite library (version 5.1; Chenomx, Alberta, Canada).

Derivatisation of aqueous metabolites and GCMS

A quarter of the aqueous fraction was used for the derivatisation. 30 µl of methoxyamine hydrochloride (20 mg per ml in pyridine) was added to the dried aqueous extracts. The samples were vortexed and left for 17 hours at room temperature. Samples were then silylated with 30 µl of N-methyl-N-trimethylsilytrifluoracetamide (MSTFA) for 1 hour at room temperature. The samples were then diluted in a ratio of 1:10 with hexane before GCMS analysis. The derivatised samples were injected into a Zebron™ 30 m x 0.25 mm ID column with a 0.25 µm arylene bonded 5% phenyl-95% dimethypolysiloxane stationary phase (Phenomenx Inc., Torrance, USA) in a TRACE GC unit (Thermo Scientific, UK). The column temperature was held at 70 °C for 2 minutes, increased by 10 °C/minute to 130 °C and then by 5 °C/minute up to 230 °C, followed by 20 °C/minute to 310 °C, and then held for 5 minutes. The GC was interfaced with either a DSC II mass spectrometer or a FID detector (Thermo Scientific, UK). Mass spectra were recorded between 50 – 650 m/z with a scan speed of 3 scans/s (transfer line temperature, and ion source = 250 °C). All GCMS chromatograms were processed using Xcalibur (version 2.0, Thermo Scientific). The peaks were integrated manually and normalised to total spectral area. The peaks were assigned based upon mass fragmentation patterns matched to the National Institute of Standards and Technology library.

Targeted LCMS

The aqueous heart tissue extract was dissolved in 300 µl of 70:30 acetonitrile:water containing 20 µM universally ^{13}C and ^{15}N labelled glutamate. The resulting solution was vortexed then sonicated for 15 mins followed by centrifugation at 15000 RPM with a bench top centrifuge to pellet any remaining undissolved material. The supernatant was transferred with an automatic pipette into a 300 µl vial and capped ready for analysis. Samples were analysed using a 5500 QTRAP mass spectrometer (AB Sciex) coupled to an Acquity UPLC system from Waters (Milford, MA, USA). The strong mobile phase (A) was 10 mM ammonium acetate with 0.05% ammonium hydroxide and the weak mobile phase was acetonitrile (B). The LC column was a BEH amide HILIC column (100 × 2.1 mm, 1.7 µm; Waters Ltd). The following linear gradient was used: 20% A was increased to 60% A over 3.5 minutes with further re-equilibration for 3 min, the total run time was 6.5 min and the flow rate was 0.6 ml/min with an injection volume of 2 µl. The negative and positive ion mode metabolites were separated into two chromatographic runs and measured with unscheduled MRMs using a source temperature of 650 ºC, an ion spray voltage of 5.5 kV (-5.5 kV for negative ion mode) and a dwell time of 10 msec for each analyte. Compound dependent parameters were established using infusion standards prepared in the running buffer. Data were acquired and processed using Quantitation Wizard within Analyst (version 1.6; AB Sciex Ltd).

Data handling

The dataset obtained was first pre-processed, during which the peaks from the NMR- and MS-based measurements were picked to generate a dataset with optimised resolution. The processed dataset was mean-centered and normalised prior to multivariate statistical analysis within the SIMCA-P+ 12.0 software package

(Umetrics, Umea, Sweden). Pareto scaling was used in order to increase the influence of low concentration metabolites without significantly amplifying the influence of baseline noise. After pre-treatment, the dataset was visualised and analysed using pattern recognition tools which enabled visual examination of the dataset. Both the un-supervised pattern recognition tool PCA and the supervised tools PLS and PLS-DA were used within SIMCA-P+. Loading plots were used to display the metabolites responsible for the clustering of the observed differences between the wild type and Chuvash hearts and the contribution of each metabolite to the clustering was ranked using the coefficient plot. The robustness of the multivariate model generated in this way was assessed by R^2 and Q^2 values (Q^2 indicates the predictive power of the model, which is considered to be significant for $Q^2 > 0.4$). Univariate analysis was also carried out using the Student's T-test with the significance level set to $p < 0.05$.

4.4.10 Cine MRI

In vivo recovery cine MRI was used to measure cardiac morphology and function over the course of a 12 month period. Figure 4.5 illustrates the experiment set-up.

Mice were anaesthetised initially with 5% isoflurane in medical oxygen (100%); anaesthesia was maintained via a nose cone with 1-2% isoflurane in oxygen. The mice were positioned in a purpose-built cradle which contained a warming blanket. ECG electrodes were inserted into the forepaws and a respiration loop loosely taped across the chest. The cradle was sealed and lowered into a vertical-bore 11.7 T MR system (Magnex Scientific, UK) with a 40 mm birdcage coil (Rapid Biomedical, Würzburg, Germany) connected to a Bruker console running Paravision 2.1.1 (Bruker, Ettlingen, Germany). A stack of contiguous, 1 mm thick, true short axis

ECG- and respiration-gated cine/FLASH images were acquired to cover the entire heart.

Figure 4.5: *In vivo* cine MRI set-up

Mice were positioned in a purpose-built cradle; anaesthesia was maintained with 1-2% isoflurane in oxygen via a nose cone (A and B). ECG electrodes were inserted into the forepaws and a respiration loop taped across the chest (B). The cradle was sealed and lowered into a vertical-bore MR system (C).

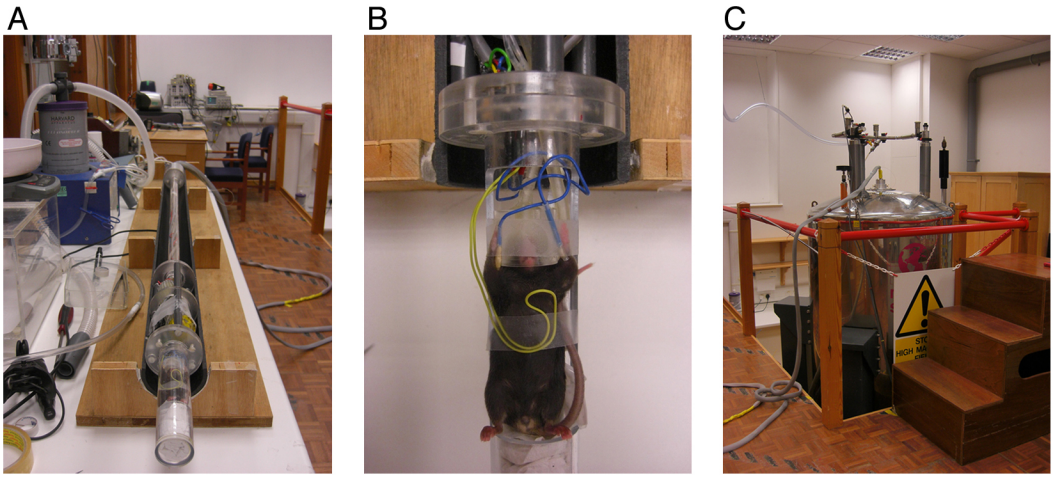

Image data were analysed using the ImageJ program (NIH Image, Bethesda, MD). End-systole (ES) and end-diastole (ED) (corresponding to the minimal and maximal ventricular volumes, respectively) frames for each slice were identified. Left ventricular (LV) endo- and epi-cardial borders were outlined free-hand for ES and ED frames for all slices. Defining the mid-ventricular (MV) slice as the one in which the papillary muscles (PM) were most prominent, right ventricular free wall thickness was measured in three separate locations and an average taken (see Figure 4.6). See Table 4.3 for a summary of the calculations used for cardiac function parameters.

Figure 4.6: Cine MRI image analysis

Epi- and endo-cardial LV outlines were drawn in end-diastole and end-systole (for all slices), enabling calculation of ED and ES luminal and muscle volumes (A). Right ventricular (RV) wall thickness was measured from the ED mid-ventricular slice (defined as slice with most prominent papillary muscles, PM) (A, green). The ratio of actual MV LV area (A_A) to predicted calculated area (A_C) would be close to 1 if the LV was a circle (B). As the LV shape distorts, this ratio falls (C). See main text for full details.

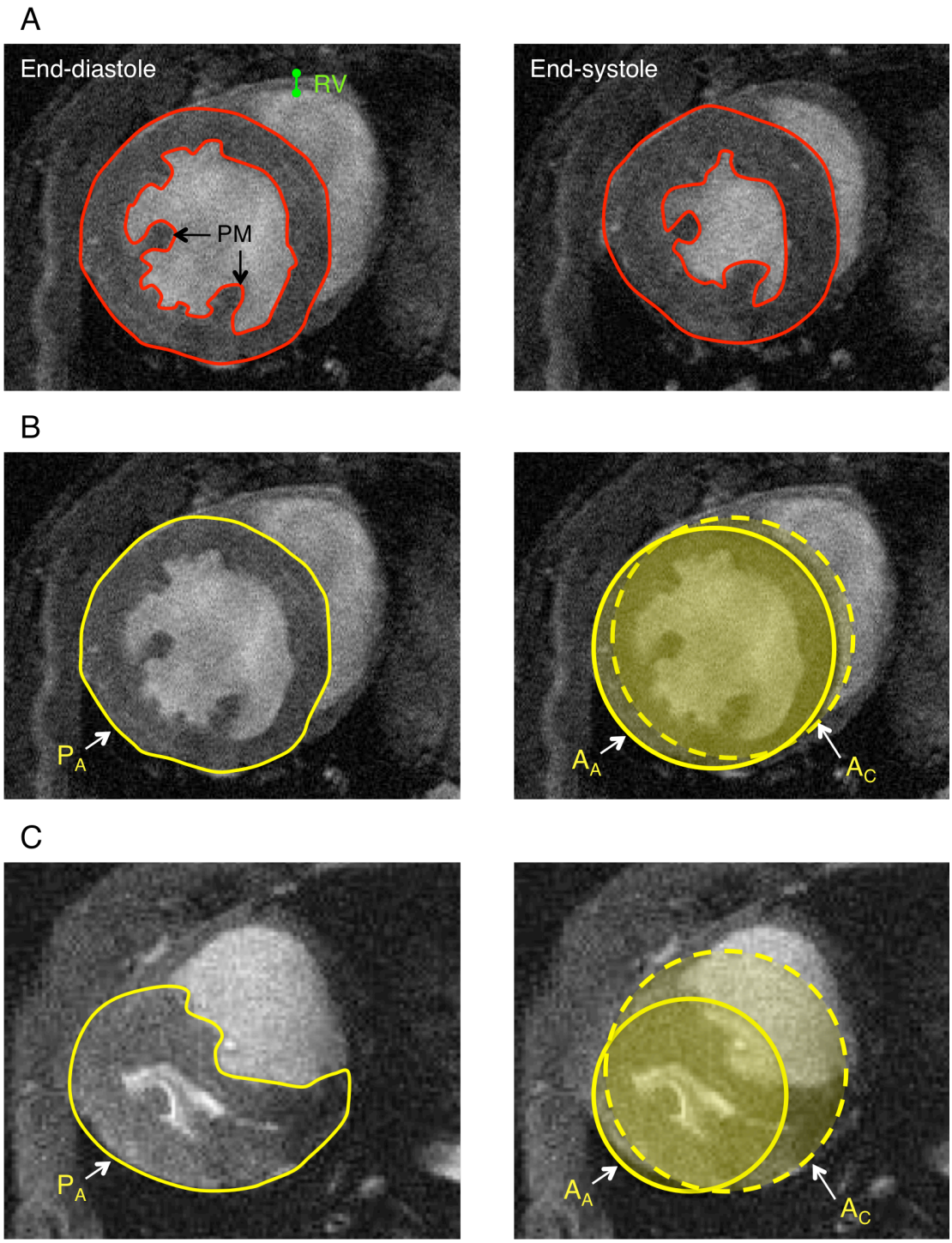

Table 4.3: Calculations used for cardiac morphology and function from cine MRI images

See main text for details regarding septal bowing ratio.

Calculated parameter	Calculation
Stroke volume	End-diastolic volume – End-systolic volume
Ejection fraction	(Stroke volume / EDV) x100
Cardiac index	(Stroke volume x Heart rate) / Body mass
Left ventricular mass	LV volume x Specific gravity of myocardium (1.05 g/cm^3)
Septal bowing ratio	Measured LV Area / Calculated ideal LV area

To quantify septal bowing (the distortion of the LV), a novel method was used. First, the LV epi-cardial border in early-diastole in the MV slice was outlined, giving an actual perimeter (P_A) and area (A_A). If the LV was perfectly circular, then the ratio of A_A to the predicted area calculated from P_A (A_C) would be 1. As the LV becomes increasingly distorted in shape P_A increases, as does A_C, and hence the ratio will fall below 1. This 'septal bowing ratio' thus enables quantification of the distortion of the septum using the LV itself as the comparator.

4.4.11 Gene expression: micro-array

Ventricular tissue (both right and left) was obtained and crushed to a fine powder (in liquid nitrogen) as described in Section 4.4.9. Approximately 20 – 30 mg crushed tissue was used. Total RNA was extracted using the Rneasy Fibrous Kit (Qiagen, UK), including a DNase treatment step to remove DNA, according to the manufacturer's instructions. The RNA integrity was assessed on a BioAnalyzer (Agilent Laboratories, US); all samples had a RNA Integrity Number (RIN) ≥ 7.

Following RNA extraction and quality assessment, the micro-array was performed by Sheena Lee. Labelled sense ssDNA for hybridisation was generated from 200 ng starting RNA with the Ambion WT expression kit (P/N 4411973) and the Affymetrix GeneChip WT Terminal Labeling and Controls Kit (P/N 901525) according to the

manufacturer's instructions. The distribution of fragmented sense ssDNA lengths was measured on the BioAnalyser. The fragmented ssDNA was labeled and hybridised for 17 hours at 45C to the Affymetrix GeneChip Human Mouse 1.0 ST Array (Affymetrix). Chips were processed on an Affymetrix GeneChip Fluidics Station 450 and Scanner 3000. Affymetrix Command Console was used to generate cel files and Affymetrix Expression Console was used for the quality control.

Arrays were RMA normalised in GeneSpring GX 12 and differentially expressed genes were identified using Limma with a Benjamini and Hochberg multiple testing correction of ≤ 0.05. As few genes were detected using this method the data were re-analysed using PLIER normalisation and a Student's t-test with a p-value cut off of ≤ 0.05 and a fold change difference between wild type and Chuvash of ≥ 1.3.

4.4.12 Gene expression: quantitative real-time PCR

Further gene expression studies were conducted using quantitative real-time polymerase chain reaction (PCR). Total RNA was extracted from powdered whole-heart tissue as described in Section 4.4.11. RNA concentration and purity were determined using a NanoDrop Spectrophotometer (NanoDrop Technologies, UK); if RNA quality fell below accepted standards the extraction process was repeated. RNA was stored on ice and complementary single-strand DNA (cDNA) was immediately synthesised from 1 µg RNA using the Applied Biosystems High Capacity cDNA Reverse Transcription Kit (Life Technologies, UK) according to the manufacturer's instructions. cDNA was stored in aliquots (to avoid freeze-thawing) at -80 °C.

Real-time PCR was performed using an ABI Prism 7000 Sequence Detection System (Applied Biosystems, UK) with TaqMan Universal PCR Master Mix and TaqMan Gene Expression Assays (choosing manufacturer-recommended assays; Applied

Biosystems, UK) according to the manufacturer's instructions. Relative quantification of mRNA expression levels was determined using the standard curve method and normalised to beta-actin. An identical method was applied to lung tissue in order to quantify expression of endothelin-1 (ET-1), normalised to 18s ribosomal RNA. This was used as a positive control to confirm the real-time PCR methodology, since a 2.2-fold increase in ET-1 had previously been demonstrated in the Chuvash mouse (Hickey *et al.* 2010).

4.4.13 Statistical analysis

Comparisons between wild type and Chuvash mice were analysed using un-paired T tests unless otherwise stated. Significance was taken as $p < 0.05$. Statistical analysis was performed using SPSS Statistics 19 (IBM). Results are presented as mean ± standard error unless otherwise indicated.

4.5 RESULTS

4.5.1 Plasma metabolites

Non-fasting plasma metabolites were measured in male and female mice aged 6 – 7 months (summarised in Table 4.4 and Figure 4.7). Plasma cholesterol, TAG and NEFA were reduced in the male Chuvash mice. Conversely, plasma cholesterol was increased in the female Chuvash mice. No other significant differences were seen.

Table 4.4: Summary of plasma metabolites (non-fasting)

Non-fasting plasma metabolite concentrations are shown for both male and female mice, aged 6 – 7 months. NEFA (non-esterified fatty acid); TAG (triacyl glycerol).

Parameter		Wild type (n)	Chuvash (n)	*p* value
3-hydroxybutyrate (mM)	Male	0.16 ± 0.04 (5)	0.12 ± 0.03 (4)	0.529
	Female	0.22 ± 0.08 (3)	0.33 ± 0.1 (3)	0.444
Glucose (mM)	Male	14.8 ± 1.3 (4)	13.6 ± 0.4 (4)	0.399
	Female	11.5 ± 0.9 (3)	13.2 ± 1.1 (3)	0.298
Lactate (mM)	Male	15.2 ± 1.2 (5)	13.7 ± 2.1 (4)	0.526
	Female	11.0 ± 0.9 (3)	12.4 ± 1.3 (3)	0.417
NEFA (mM)	Male	0.16 ± 0.01 (5)	0.11 ± 0.02 (4)	**0.05**
	Female	0.14 ± 0.02 (3)	0.17 ± 0.02 (3)	0.342
TAG (mM)	Male	2.7 ± 0.13 (5)	1.5 ± 0.5 (4)	**0.043**
	Female	2.1 ± 0.36 (2)	3.1 ± 0.62 (3)	0.32
Cholesterol (mM)	Male	2.0 ± 0.07 (5)	1.5 ± 0.06 (4)	**0.002**
	Female	1.2 ± 0.09 (3)	1.6 ± 0.09 (3)	**0.03**

4.5.2 Glucose tolerance test

Fasting intra-peritoneal glucose tolerance tests were performed in male and female mice aged 6 months. Chuvash mice demonstrated a tendency towards reduced fasting blood glucose concentrations. The male Chuvash mice had significantly lower glucose excursions (represented by the area under the curve) compared to wild type controls. Table 4.5 and Figure 4.8 summarise these results.

Figure 4.7: Summary of non-fasting plasma metabolites

Non-fasting plasma metabolite concentrations are shown for both male and female mice, aged 6 – 7 months. NEFA (non-esterified fatty acid); TAG (triacyl glycerol). *** ($p < 0.01$); * ($p < 0.05$).

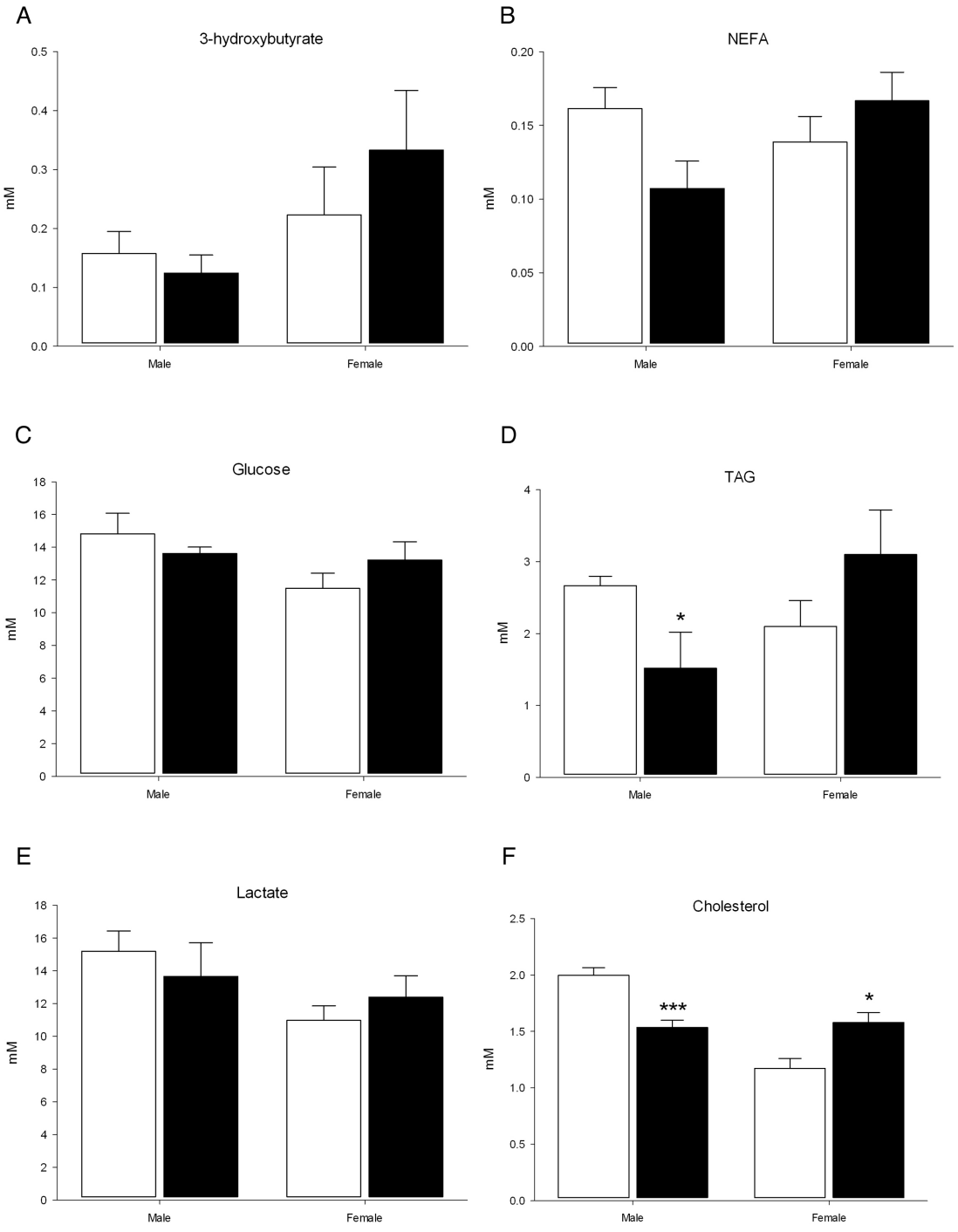

Table 4.5: Summary of the intra-peritoneal glucose tolerance test

IPGTT results, and the number of mice used, are shown for male and female mice, aged 6 months.

Parameter		Wild type	Chuvash	*p* value
Fasting glucose pre-test (mMol/litre)	Male	4.1 ± 0.18 (5)	3.8 ± 0.19 (4)	0.224
	Female	3.9 ± 0.24 (3)	3.2 ± 0.21 (3)	0.08
Area under curve (mMol/litre x120 seconds)	Male	639 ± 27 (5)	539 ± 33 (4)	**0.049**
	Female	563 ± 29 (3)	517 ± 75 (3)	0.597

Figure 4.8: Results from the intra-peritoneal glucose tolerance test

White represents wild type; black represents Chuvash. The glucose tolerance tests for male (A) and female (B) mice are shown. Fasting glucose levels (C) and glucose excursions (area under the curve, D) are also illustrated. * ($p < 0.05$).

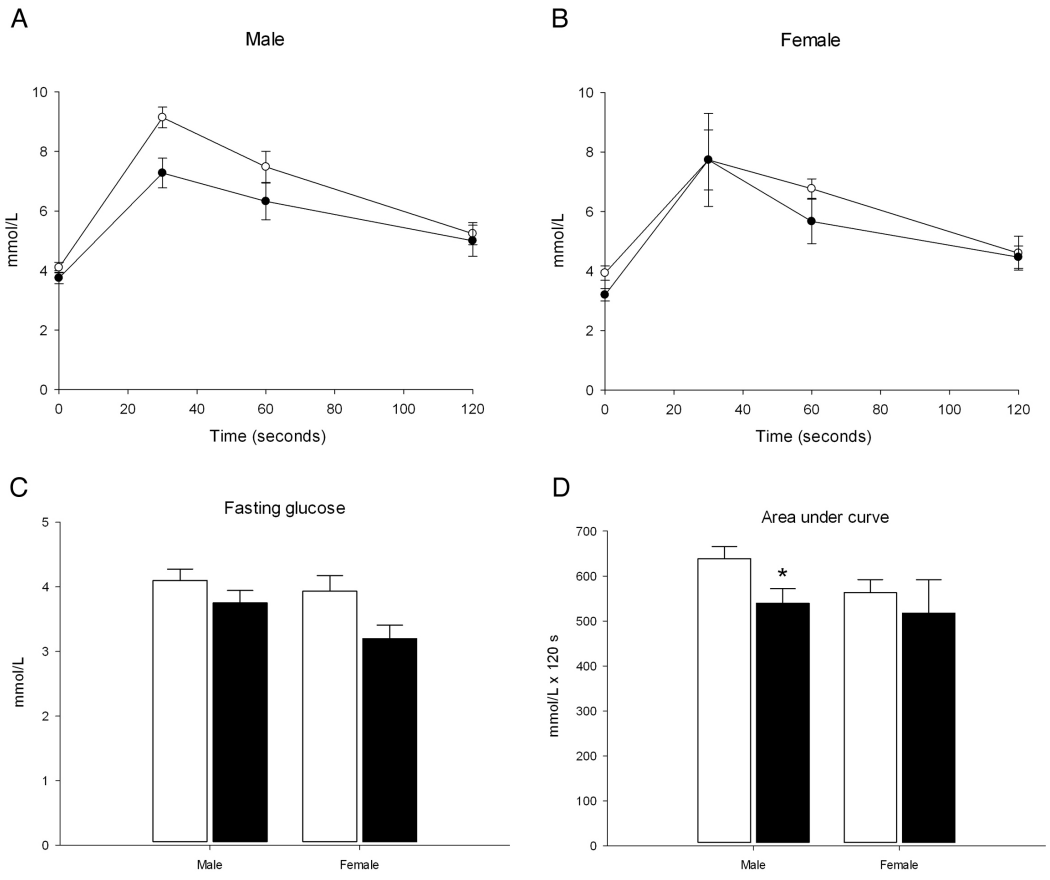

4.5.3 Perfused heart substrate metabolism – glycolytic flux

Glycolytic flux was measured in the perfused heart from mice aged 15 – 17 months. These results are summarised in Figure 4.9 and Table 4.6.

Figure 4.9: Glycolytic flux in the perfused heart

White represents wild type; black represents Chuvash. *** ($p < 0.01$).

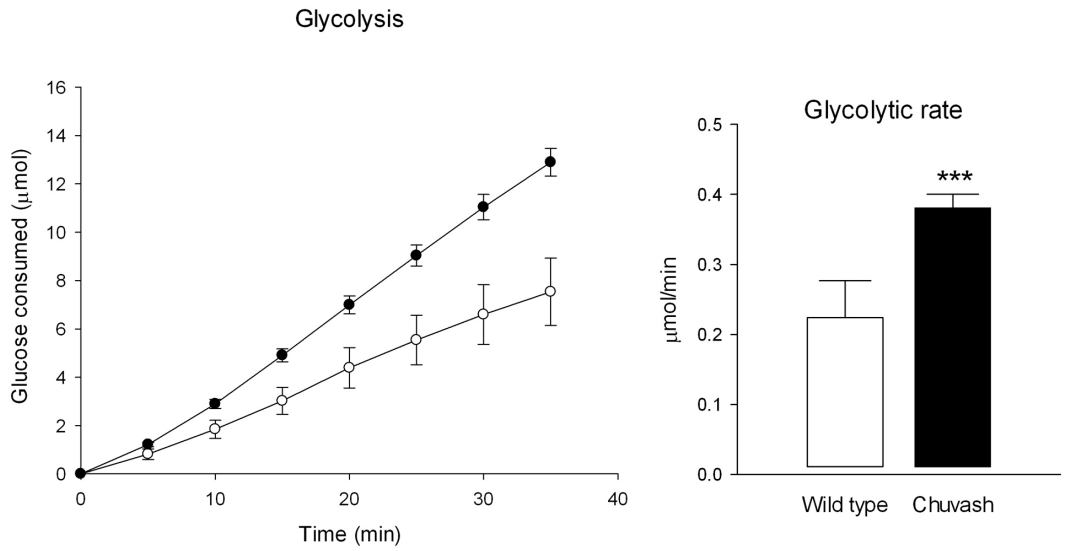

Heart mass, as a percentage of body mass, was significantly greater in the Chuvash mice compared to wild type controls. Glycolytic flux in the perfused heart, measured using [^{3}H]-glucose, was 1.8-fold higher in the Chuvash hearts. Univariate analysis of variance (ANOVA) using genotype as the fixed factor, and heart mass and RPP as co-variates, demonstrated that the presence of the Chuvash mutation was the only significant determining factor upon glycolytic rate ($p = 0.004$ for genotype; $p = 0.095$ for heart weight; $p = 0.147$ for RPP).

Table 4.6: Summary of perfused heart glycolytic rate

Four wild type and seven Chuvash mice, aged 15 – 17 months, were used. Body mass and heart mass (as percentage of body mass) were compared using unpaired T tests. Univariate analysis of variance (ANOVA) was used to determine the significant factor controlling glycolytic rate (see main text for details).

Parameter	Wild type	Chuvash	*p* value
Body mass (grams)	33.8 ± 1.8	29.4 ± 1.6	0.117 (T test)
Heart mass (as % of body mass)	0.86 ± 0.06	1.10 ± 0.03	**0.003** (T test)
Heart mass (grams)	0.29 ± 0.03	0.32 ± 0.02	Only genotype exerted a significant effect on glycolytic rate. ***p* = 0.004**, ANOVA.
Rate pressure product (mm Hg/minute)	34 945 ± 284	32617 ± 3546	
Glycolytic rate (µmol/minute)	0.21 ± 0.05	0.37 ± 0.02	

4.5.4 Perfused heart substrate metabolism – net lactate efflux

Lactate efflux was also determined during the glycolytic rate experiment; the results are summarised in Table 4.7 and Figure 4.10. Net lactate efflux was found to be was 1.5-fold higher in the Chuvash hearts. Univariate analysis of variance (ANOVA) using genotype as the fixed factor, and heart mass and RPP as co-variates, demonstrated that the presence of the Chuvash mutation was the only significant determining factor upon the rate of net lactate efflux ($p = 0.009$ for genotype; $p = 0.121$ for heart weight; $p = 0.123$ for RPP). There was a significant correlation between glycolytic and lactate rates (Pearson $R = 0.935$, $p < 0.0001$).

Table 4.7: Summary of perfused heart lactate efflux (net) rate

The same 4 wild type and 7 Chuvash mice from the glycolytic flux experiment were used. Univariate analysis of variance (ANOVA) was used to determine the significant factor controlling the rate of net lactate efflux (see main text for details).

Parameter	Wild type	Chuvash	*p* value
Heart mass (grams)	0.29 ± 0.03	0.32 ± 0.02	Only genotype exerted a significant effect on lactate efflux. ***p* = 0.009**, ANOVA.
Rate pressure product (mm Hg/minute)	34 945 ± 284	32617 ± 3546	
Rate of net lactate efflux (µmol/minute)	0.022 ± 0.004	0.033 ± 0.002	

Figure 4.10: Net lactate efflux in the perfused heart

White represents wild type; black represents Chuvash. *** ($p < 0.01$).There was a significant correlation between glycolytic and lactate rates and clear separation between wild type and Chuvash hearts (C; Pearson R = 0.935, $p < 0.0001$).

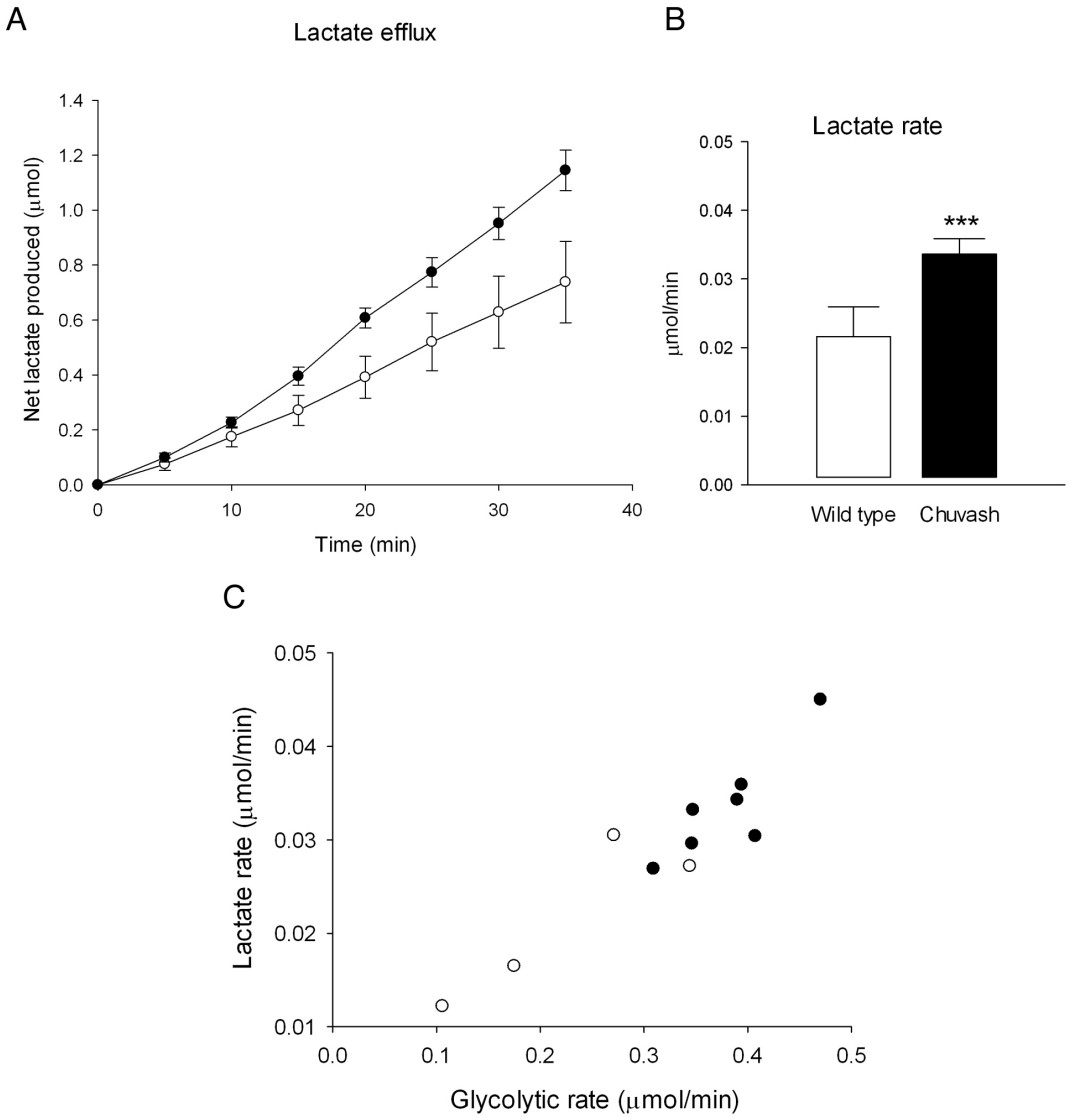

4.5.5 Perfused heart substrate metabolism – palmitate oxidation

A separate group of mice, aged 11 – 17 months, were used for Langendorff perfusion experiments to determine the rate of palmitate oxidation, using [^{3}H]-palmitate. These results are summarised in Figure 4.11 and Table 4.8. As demonstrated previously, heart mass, as a percentage of body mass, was significantly greater in the Chuvash mice compared to wild type controls. Univariate analysis of variance (ANOVA) using genotype as the fixed factor, and heart mass and RPP as co-variates, demonstrated that rate pressure product was the only significant determining factor upon palmitate oxidation rates (p = 0.652 for genotype; p = 0.062 for heart weight; p = 0.001 for RPP).

Figure 4.11: Palmitate oxidation rates in the perfused heart

White represents wild type; black represents Chuvash.

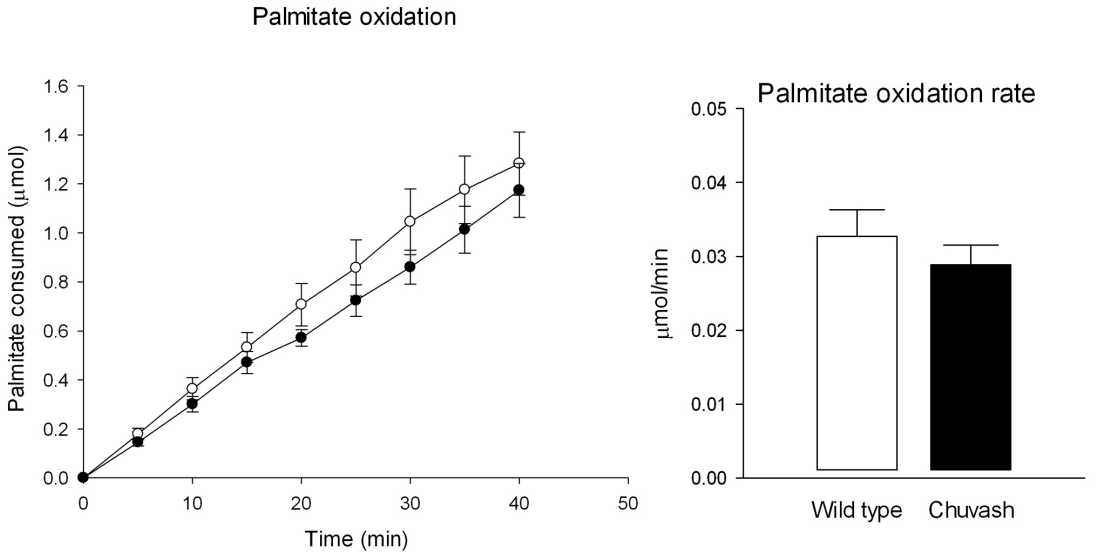

Table 4.8: Summary of perfused heart palmitate metabolism

Five wild type and five Chuvash mice (all female) were used, aged 11 – 17 months. Univariate analysis of variance (ANOVA) was used to determine the significant factor controlling the rate of palmitate oxidation (see main text for details).

Parameter	Wild type	Chuvash	*p* value
Body mass (grams)	27.4 ± 1.5	26.2 ± 2.0	**0.034** (T test)
Heart mass (as % of body mass)	0.85 ± 0.04	1.20 ± 0.10	**0.024** (T test)
Heart mass (grams)	0.23 ± 0.006	0.31 ± 0.026	Only RPP exerted a significant effect on palmitate oxidation. ***p* = 0.001**, ANOVA.
Rate pressure product (mm Hg/minute)	50296 ± 5006	35830 ± 3936	
Rate of palmitate oxidation (µmol/minute)	0.033 ± 0.004	0.029 ± 0.003	

4.5.6 Measuring *in vivo* ^{13}C pyruvate metabolism in real-time

In vivo ^{13}C MR spectroscopy of hyperpolarised $^{13}C_1$ pyruvate was performed in order to measure cardiac metabolism in real-time. These results are summarised in Table 4.9 and Figure 4.12. In keeping with the finding of increased net lactate efflux from the perfused heart, there was a 1.8-fold increase in the rate of $^{13}C_1$ label incorporation from pyruvate to lactate in the Chuvash heart, compared to wild type controls. No significant differences in label incorporation to alanine or bicarbonate were detected.

Table 4.9: Summary of *in vivo* ^{13}C-pyruvate metabolism, measured in real-time

Five wild type and five Chuvash mice (all female) aged 9 – 15 months were used.

Parameter		Wild type	Chuvash	*p* value
Body mass (grams)		32 ± 3	27 ± 3	0.234
Rate of ^{13}C label incorporation x10^{-4} (s^{-1})	Alanine	64.4 ± 16.6	46.2 ± 11.2	0.39
	Lactate	131.1 ± 19.2	239.5 ± 9.0	**0.003**
	Bicarbonate	9.0 ± 1.12	12.8 ± 1.9	0.123

Figure 4.12: *In vivo* ^{13}C-pyruvate metabolism, measured in real-time

White represents wild type; black represents Chuvash. *** ($p < 0.01$). (A) Example summed spectrum of 40 individual spectra from a fed wild type C57Bl/6 mouse (Dodd *et al.* 2013). (B) Example time-course of spectra in a fed wild type C57Bl/6 mouse (Dodd *et al.* 2013).

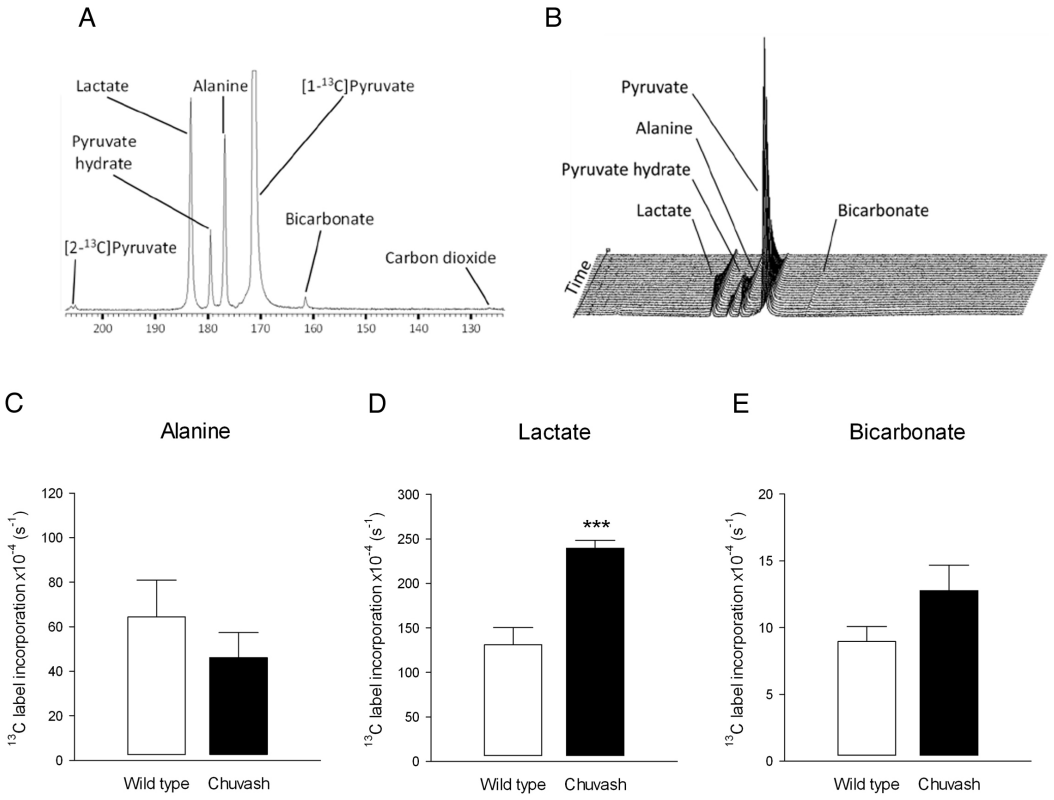

4.5.7 Perfused heart energetics

The Langendorff perfused-heart set-up was also used to investigate cardiac energetics using ^{31}P MR spectroscopy. These results are summarised in Table 4.10 and Figure 4.13. Infusion of isoprenaline resulted in depletion of the phosphocreatine levels, with consequent reduction of the PCr:ATP ratio, which was significantly more marked in the Chuvash hearts compared to wild type controls (PCr:ATP 1.21 ± 0.08 versus 1.56 ± 0.08, $p < 0.02$).

Figure 4.13: Perfused heart energetics

White bars represent wild type; black represent Chuvash. ** ($p < 0.02$). (A) Representative plot of rate pressure product during the course of an experiment. Blue represents normal perfusion conditions; red represents an infusion of 2-5 nM isoprenaline. Note the marked and sustained increase in RPP. Black bars represent each five minute period during which ^{31}P spectra were acquired.

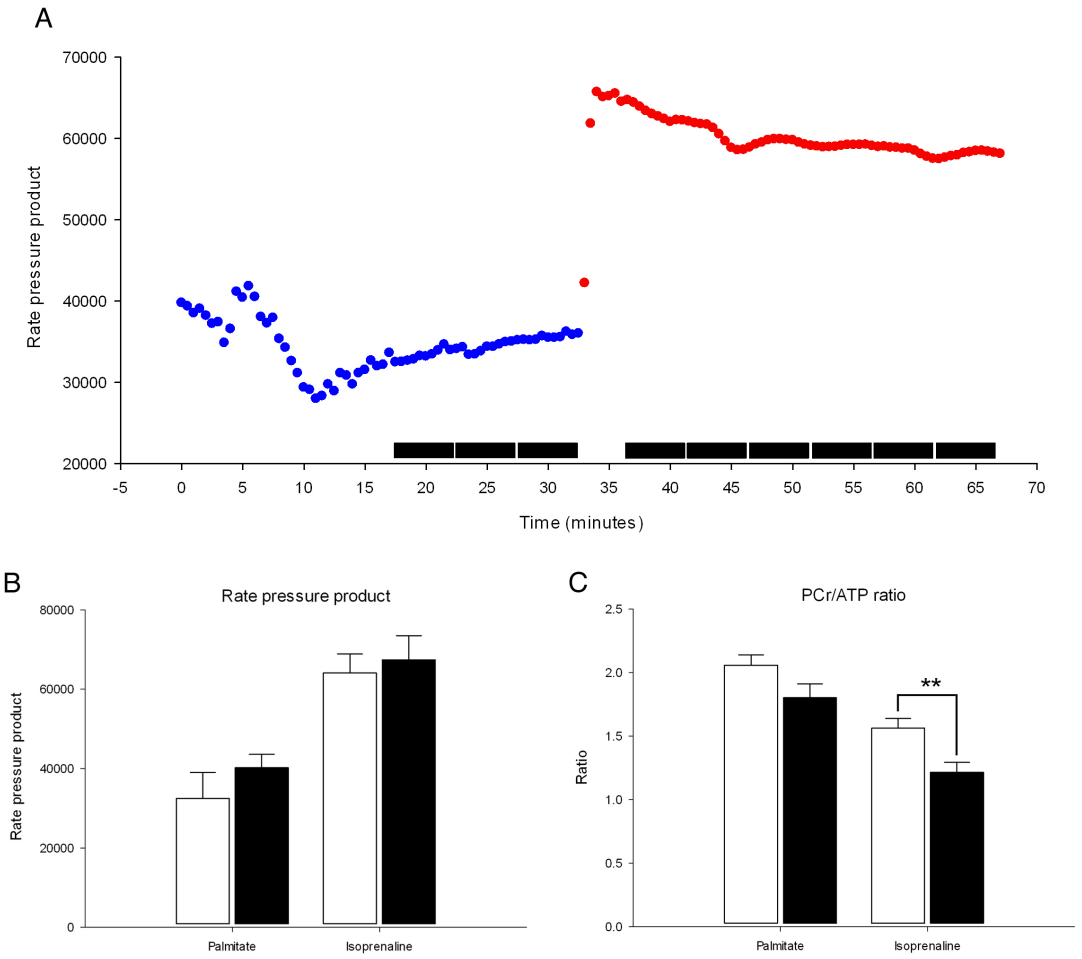

Table 4.10: Summary of perfused heart energetics using ^{31}P MR spectroscopy

Five wild type and five Chuvash mice, aged 6 – 7 months, were used.

Parameter		Wild type	Chuvash	*p* value
Body mass (grams)		30.1 ± 2.1	28.7 ± 1.2	0.602
Heart mass (grams)		0.25 ± 0.03	0.29 ± 0.02	0.293
Heart mass (as % of body mass)		0.82 ± 0.05	1.01 ± 0.06	**0.035**
Rate pressure product	Palmitate	32 489 ± 6533	40 218 ± 3357	0.323
	Isoprenaline	64 095 ± 4779	67 438 ± 6044	0.676
PCr:ATP ratio	Palmitate	2.06 ± 0.08	1.80 ± 0.11	0.097
	Isoprenaline	1.56 ± 0.08	1.21 ± 0.08	**0.014**

4.5.8 Assay of PDH activity

The hearts from the perfusion studies described in Sections 4.5.3 and 4.5.4 were used to assay the activity of both the active and total fractions of PDH. In keeping with the finding that no significantly altered flux of pyruvate to bicarbonate (through PDH) was detected in the Chuvash heart *in vivo* (Section 4.5.6), no significant differences in PDH_a, PDH_t, or the percentage of PDH in the active form were shown. These results are summarised in Figure 4.14 and Table 4.11.

Figure 4.14: Summary of PDH activity assay

Measurement of the activity of the different fractions of PDH, and the percentage of PDH in the active form.

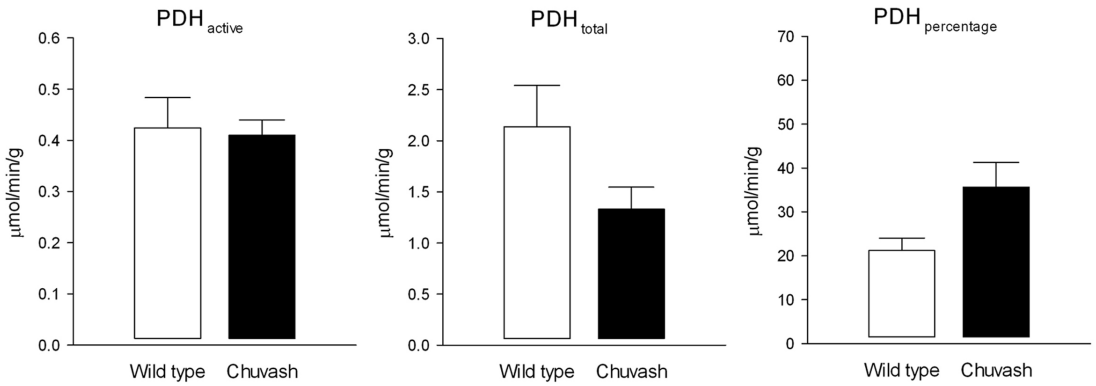

Table 4.11: Summary of PDH activity assay

Values are in µmol/min/g wet weight tissue. Four wild type and seven Chuvash hearts were used.

Parameter	Wild type	Chuvash	*p* value
PDH (active)	0.42 ± 0.06	0.41 ± 0.03	0.812
PDH (total)	2.1 ± 0.4	1.3 ± 0.2	0.084
PDH (percentage)	21.2 ± 2.8	35.6 ± 5.6	0.101

4.5.9 Cardiac metabolomics

Three separate techniques and analyses (NMR, targeted LCMS, and GCMS) were used to optimise the number of metabolites detected.

NMR

No separation of the two groups was demonstrated using this technique (analysed using PLS-DA plots). Whilst differences between wild type and Chuvash were seen in the AMP/ADP/ATP peaks, it was not possible to differentiate between the separate metabolites using this technique and therefore further analysis using targeted LCMS was subsequently performed (see next section). Interestingly, there were no other significant differences in metabolites such as glucose and lactate; the full results are included in Section 7.2, Table 7.1.

Targeted LCMS

Analysis using targeted LCMS showed the best separation between the two groups. O-PLS-DA plots demonstrated separation between the wild type and Chuvash hearts, with Q^2 and R^2 values of 0.514 and 0.627, respectively. The metabolites driving this separation were shown to be succinyl CoA and oxoguanine, which were significantly increased and decreased in the Chuvash hearts, respectively. These results are summarised in Figure 4.15. The full targeted LCMS results can be found in Section 7.2, Table 7.2.

Figure 4.15: Metabolic profiling of ventricular tissue using targeted LCMS

Six wild type and six Chuvash mice, aged 14 – 18 months, were used. Top panel shows the O-PLS-DA score plot showing differentiation of Chuvash and wild type ventricular samples. Chuvash samples in black; wild type in red (values refer to the mouse ID numbers). Q^2 = 0.514, R^2 = 0.627. Succinyl CoA and oxoguanine were shown to be driving the separation in metabolites. ** ($p < 0.02$); * ($p < 0.05$).

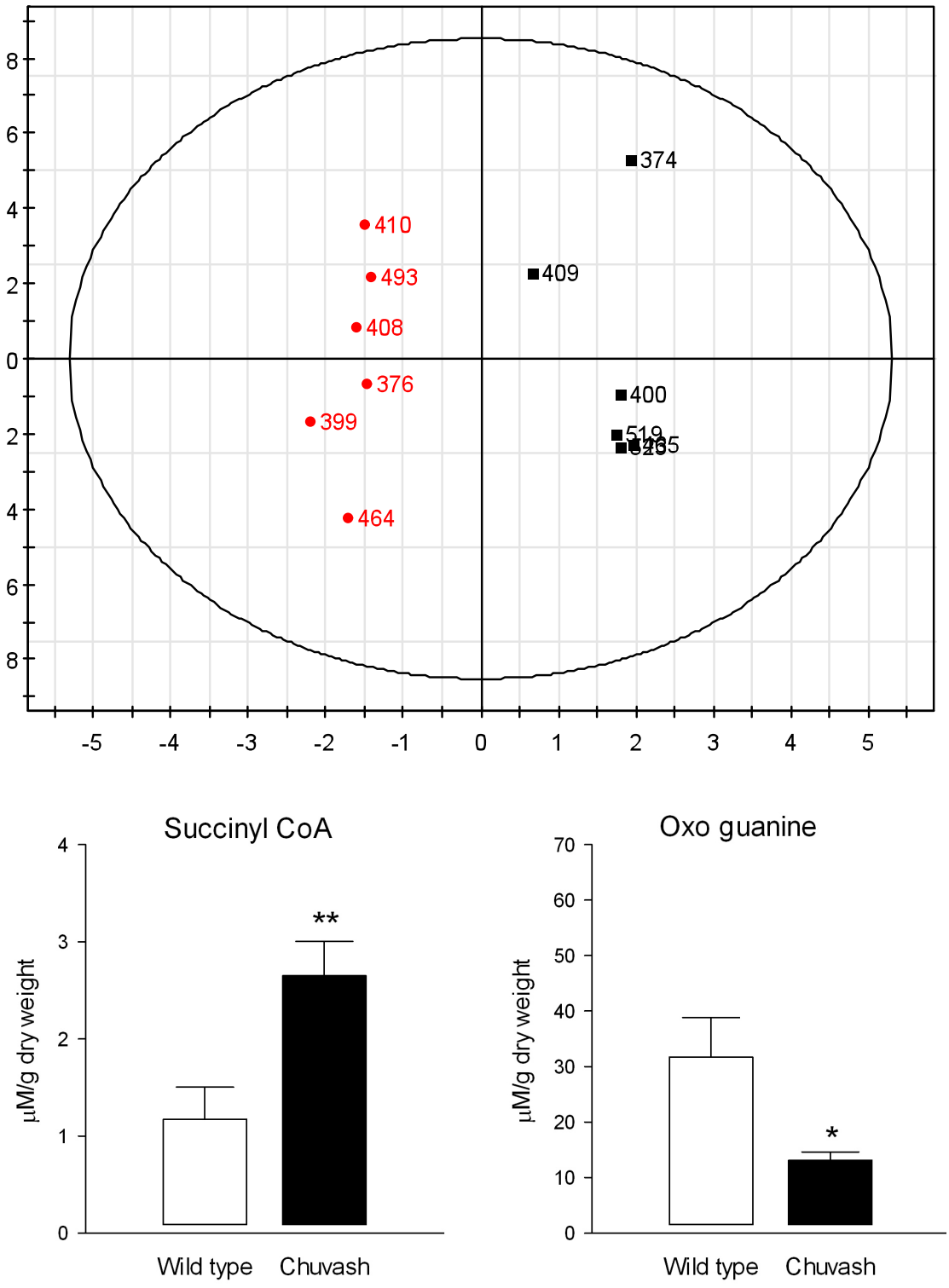

GCMS

Analysis of the results from GCMS showed reasonable separation between the Chuvash and wild type groups, although this was not as robust as that found using targeted LCMS (Q^2 = 0.336). The metabolites shown to be driving this separation were myoinositol, creatinine enol, D-galactopyranoside/galactose and serine. These results are summarised in Figure 4.16 and Figure 4.17. The full results can be found in Section 7.2 and Table 7.3.

Figure 4.16: Metabolic profiling of ventricular tissue using GCMS

O-PLS-DA score plot showing differentiation of Chuvash and wild type ventricular samples following GCMS analysis of aqueous metabolites. Chuvash samples in green; wild type in blue (values refer to the mouse ID numbers). Q^2 = 0.336.

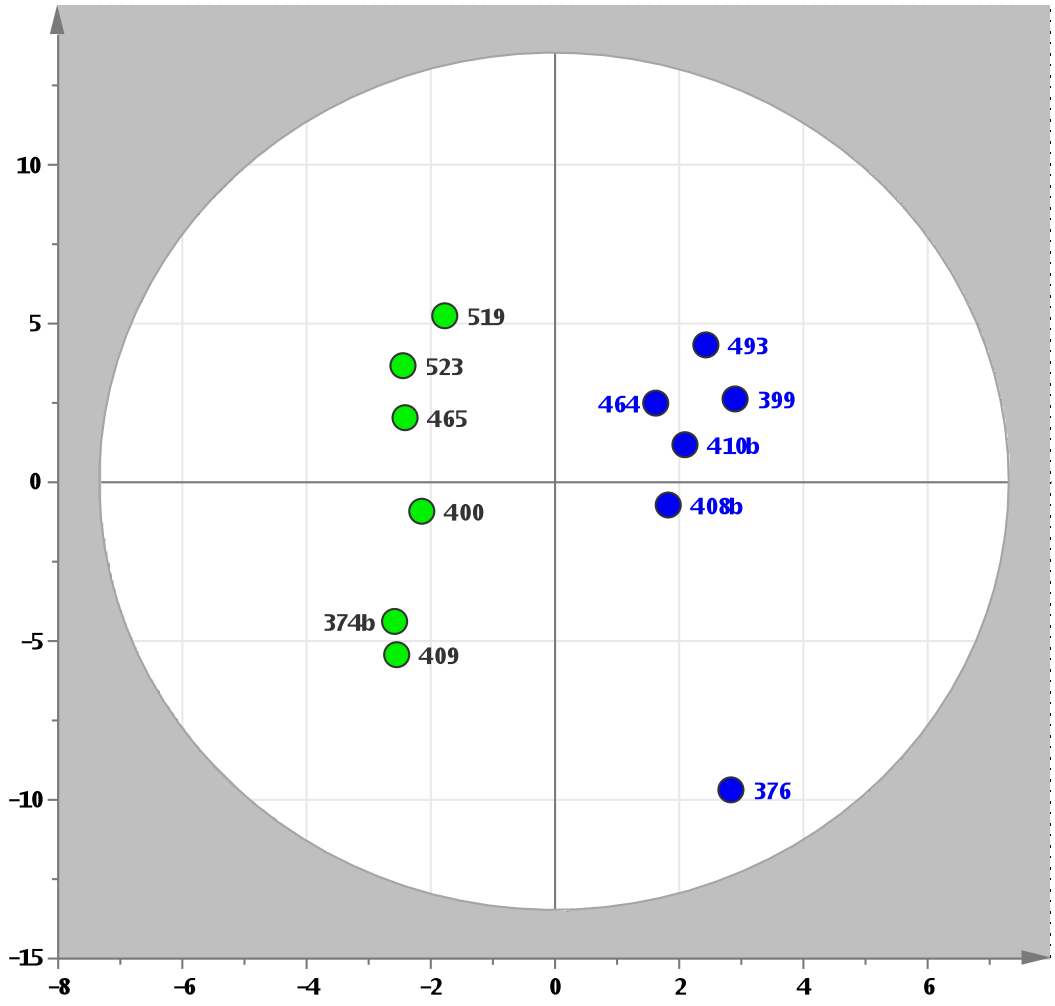

Figure 4.17: Metabolites driving the separation detected using GCMS

*** ($p < 0.01$); ** ($p < 0.02$); * ($p < 0.05$).

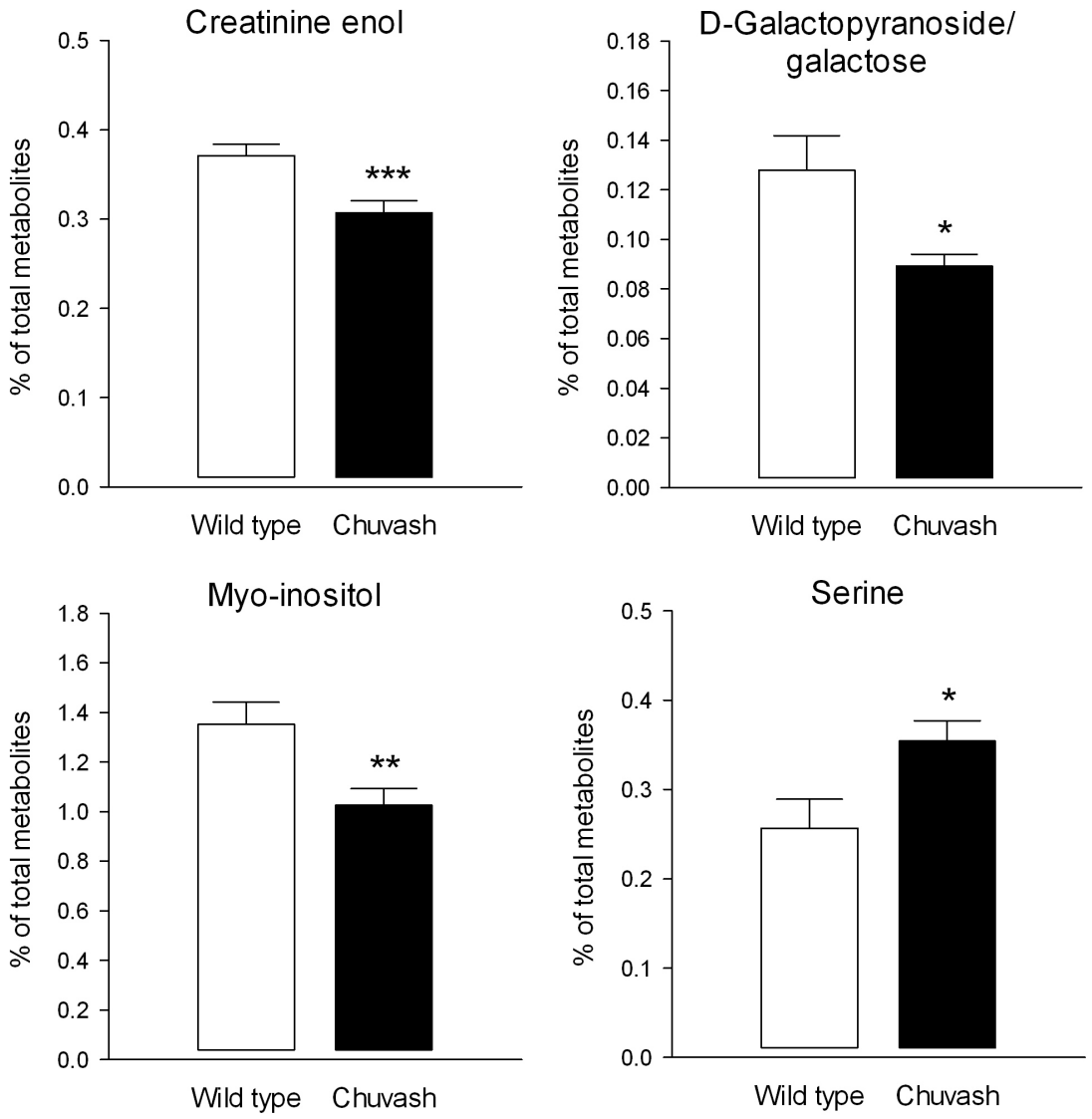

4.5.10 *in vivo* cardiac cine MRI

Chuvash mice and wild type controls were scanned over the course of the year. Figure 4.19 and Table 4.12 summarise the cine MRI results.

There were no differences in LV mass (when corrected to body mass) or cardiac index between the two groups at any time point. LV ejection fraction was significantly higher in the Chuvash mice at both 3 and 6 months of age.

Marked septal bowing, indicative of pulmonary hypertension, was seen in all Chuvash hearts at all time points. This can be clearly visualised in Figure 4.18 and is reflected in the lower septal bowing ratio. Significant thickening of the RV free wall in the Chuvash hearts was also present at all time points.

Figure 4.18: *In vivo* cine MRI images

Representative mid-ventricular two chamber views in early diastole. The wild type hearts have a circular, thick-walled left ventricle (LV) and thinner-walled, crescent-shaped right ventricle (RV) throughout the cardiac cycle. In contrast, the Chuvash hearts have a greatly dilated RV and demonstrate marked septal bowing – bulging of the interventricular septum into the LV chamber, particularly at early diastole.

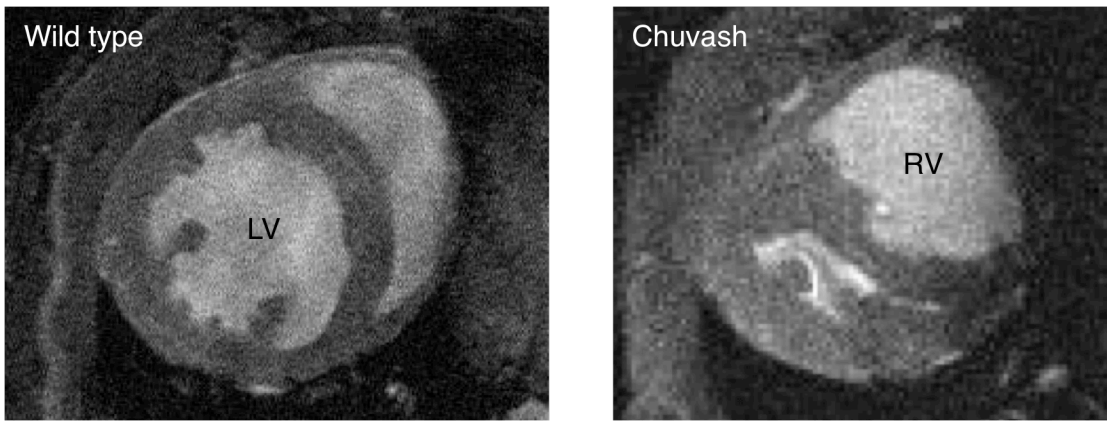

Figure 4.19: Cardiac function measured using *in vivo* cine MRI

White represents wild type; black represents Chuvash.

* ($p < 0.05$); ** ($p < 0.02$); *** ($p < 0.01$); **** ($p < 0.001$)

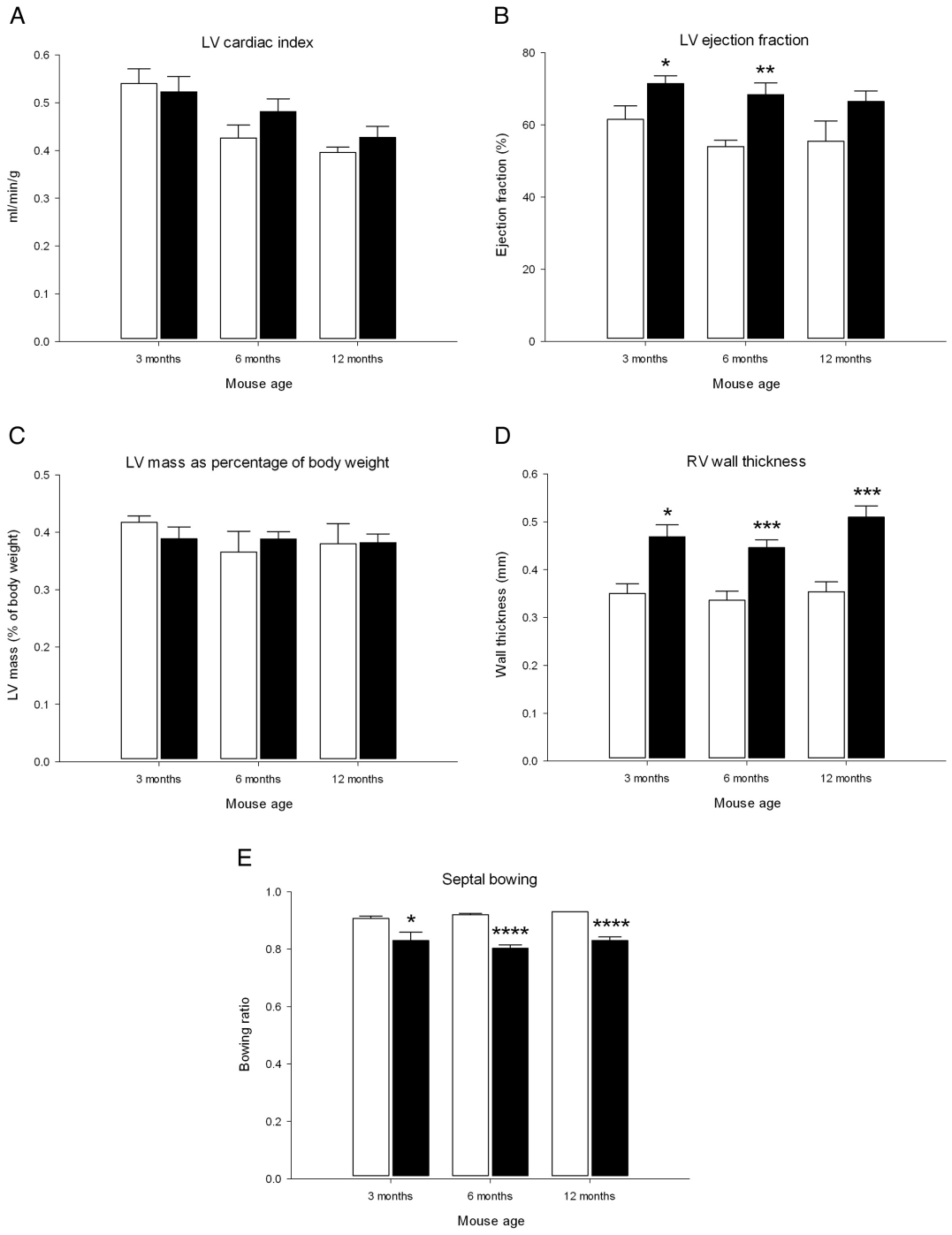

Table 4.12: Summary of cine MRI data

Parameter		Wild type (n)	Chuvash (n)	*p* value
Body mass (grams)	3 months	28 ± 1.8 (4)	24 ± 1.3 (7)	0.093
	6 months	36 ± 1.1 (4)	25 ± 1.2 (9)	**< 0.0001**
	12 months	37 ± 3.2 (5)	27 ± 0.9 (8)	**0.003**
LV ejection fraction (%)	3 months	61.5 ± 3.7 (3)	71.5 ± 2.2 (6)	**0.043**
	6 months	54.0 ± 1.7 (4)	68.4 ± 3.2 (8)	**0.014**
	12 months	55.5 ± 5.6 (5)	66.5 ± 2.9 (8)	0.078
LV mass (as % of body mass)	3 months	0.42 ± 0.01 (3)	0.39 ± 0.02 (6)	0.262
	6 months	0.37 ± 0.04 (5)	0.39 ± 0.01 (7)	0.584
	12 months	0.38 ± 0.04 (5)	0.38 ± 0.02 (8)	0.952
MV RV wall thickness (mm)	3 months	0.35 ± 0.02 (3)	0.47 ± 0.03 (7)	**0.021**
	6 months	0.34 ± 0.02 (5)	0.45 ± 0.02 (8)	**0.001**
	12 months	0.35 ± 0.02 (5)	0.51 ± 0.02 (7)	**0.001**
Septal bowing ratio	3 months	0.91 ± 0.009 (3)	0.83 ± 0.03 (7)	**0.038**
	6 months	0.92 ± 0.004 (5)	0.80 ± 0.01 (7)	**< 0.0001**
	12 months	0.93 ± 0.0 (4)	0.83 ± 0.01 (7)	**< 0.0001**
Heart rate (beats per min)	3 months	420 ± 29 (3)	373 ± 8 (6)	0.069
	6 months	413 ± 10 (5)	398 ± 3 (8)	0.202
	12 months	418 ± 3 (5)	402 ± 7 (8)	0.129
Stroke volume (ml)	3 months	35.1 ± 2.9 (3)	32.2 ± 1.2 (7)	0.282
	6 months	34.5 ± 1.0 (5)	30.8 ± 2.3 (8)	0.24
	12 months	37.1 ± 1.5 (4)	28.1 ± 1.4 (8)	**0.003**
Cardiac output (ml/min)	3 months	14.8 ± 2.0 (3)	12.5 ± 0.8 (7)	0.226
	6 months	14.3 ± 0.5 (5)	12.2 ± 0.9 (8)	0.116
	12 months	14.6 ± 1.2 (5)	11.3 ± 0.7 (8)	**0.025**
LV Cardiac index (ml/min/g)	3 months	0.54 ± 0.03 (3)	0.52 ± 0.03 (7)	0.756
	6 months	0.43 ± 0.03 (5)	0.48 ± 0.03 (8)	0.197
	12 months	0.40 ± 0.01 (5)	0.43 ± 0.02 (8)	0.322

4.5.11 Gene expression: micro-array and quantitative real-time PCR

The gene list identified from the micro-array is summarised in Table 4.13. Only four genes were identified using the most stringent analysis. This is surprising, given the clear changes in cardiac metabolism, particularly since HIF is a transcription factor. Careful database searches (NCBI GEO profiles and datasets) did not reveal any likely roles for the genes identified that would explain the obvious metabolic findings. Less stringent analysis of the micro-array data produced a more extended dataset (which can be found in Section 7.3) but similarly no likely causative genes were identified.

Table 4.13: Summary of micro-array results

RMA normalisation and analysis using Limma. Six male and six female mice, aged 14 – 18 months.

Gene	Fold change	*p* value
α-2-macroglobulin	2.4	0.01
Nebulin	1.7	0.04
Autophagy related 7	- 1.3	0.01
Arachidonate-5-lipoxygenase	-1.7	0.04

To confirm that key regulatory genes within metabolism were not altered in the Chuvash hearts, quantitative real-time PCR was also performed. These results are summarised in Table 4.14. The methodology was confirmed by quantifying lung ET-1 expression – a 2.5-fold increase (1.9 – 3.3) in the Chuvash mouse was shown, in keeping with previous findings (Hickey *et al.* 2010).

Table 4.14: Summary of real-time quantitative PCR results

Nine wild type and seven Chuvash mice, aged 6 – 7 months, were used.

Gene	Fold change	*p* value	Gene	Fold change	*p* value
VEGF	1.0 (0.8 – 1.1)	0.592	PDK 4	0.9 (0.5 – 1.5)	0.576
GLUT 1	1.2 (0.9 – 1.6)	0.202	LDHA	1.1 (0.9 – 1.5)	0.263
GLUT 4	1.0 (0.7 – 1.4)	0.958	PKM2	1.0 (0.8 – 1.3)	0.870
PFKM	0.8 (0.6 – 1.2)	0.291	PPAR α	0.9 (0.6 – 1.2)	0.334
PDK 2	1.1 (0.8 – 1.5)	0.680			

4.5.12 Summary of key findings

Table 4.15 summarises the main findings in this chapter.

Table 4.15: Summary of key findings

The key findings from the main experiments performed in this chapter, grouped by topic.

Parameter	Wild type	Chuvash	*p*
Perfused heart substrate utilisation			
Glycolytic rate (µmol/minute)	0.21 ± 0.05	0.37 ± 0.02	**0.004**
Rate of net lactate efflux (µmol/minute)	0.022 ± 0.004	0.033 ± 0.002	**0.009**
Rate of palmitate oxidation (µmol/minute)	0.033 ± 0.004	0.029 ± 0.003	NS
In vivo metabolism			
Rate of ^{13}C label incorporation into alanine $x10^{-4}$ (s^{-1})	64.4 ± 16.6	46.2 ± 11.2	0.39
Rate of ^{13}C label incorporation into lactate $x10^{-4}$ (s^{-1})	131.1 ± 19.2	239.5 ± 9.0	**0.003**
Rate of ^{13}C label incorporation into bicarbonate $x10^{-4}$ (s^{-1})	9.0 ± 1.12	12.8 ± 1.9	0.123
Perfused heart energetics			
PCr: ATP (palmitate perfusate)	2.06 ± 0.08	1.80 ± 0.11	0.097
PCR: ATP (with isoprenaline infusion)	1.56 ± 0.08	1.21 ± 0.08	**0.014**
Cardiac function (at 12 months)			
Ejection fraction (%)	55.5 ± 5.6	66.5 ± 2.9	0.078
LV cardiac index (ml/min/g)	0.40 ± 0.01	0.43 ± 0.02	0.322
LV mass (as % of body mass)	0.38 ± 0.04	0.38 ± 0.02	0.952
MV RV wall thickness (mm)	0.35 ± 0.02	0.51 ± 0.02	**0.001**
Septal bowing ratio	0.93 ± 0.0	0.83 ± 0.01	**0.001**
Cardiac tissue metabolites			
Succinyl CoA	1.2 ± 0.3	2.7 ± 0.4	**0.012**
Cardiac tissue gene expression (real-time PCR)			
VEGF	1.0 (0.8 – 1.1)		0.592
GLUT 1	1.2 (0.9 – 1.6)		0.202
GLUT 4	1.0 (0.7 – 1.4)		0.958
PFKM	0.8 (0.6 – 1.2)		0.291
PDK 2	1.1 (0.8 – 1.5)		0.680
PDK 4	0.9 (0.5 – 1.5)		0.576
LDHA	1.1 (0.9 – 1.5)		0.263
PKM2	1.0 (0.8 – 1.3)		0.870
PPAR α	0.9 (0.6 – 1.2)		0.334

4.6 DISCUSSION

4.6.1 Plasma metabolites and glucose tolerance

Analysis of random plasma samples, collected when the heart was harvested for the main studies in this thesis, did not reveal particularly striking differences between the wild type and Chuvash mice. Plasma cholesterol, TAG and NEFA levels were reduced in the male Chuvash mice. Conversely, plasma cholesterol was increased in the female Chuvash mice. A recent study collected non-fasting plasma samples from a large number of Chuvash patients (male and female) and matched controls and demonstrated significantly lower cholesterol and higher triglyceride levels (McClain *et al.* 2012). However, these results did not retain significance after correction for other variables. It is difficult to ascribe obvious physiological significance to the findings in this thesis. Certainly, there is no apparent trend towards altered plasma metabolites that would provide an explanation for the markedly increased rates of glycolytic flux and lactate production in the Chuvash heart.

Chronic hypoxia is associated with decreased serum glucose and insulin levels (Lindgarde *et al.* 2004; Baracco *et al.* 2007). The study in this thesis has found that the Chuvash mice demonstrated a tendency towards lowered fasting glucose levels, although this result did not reach statistical significance. However, whilst this thesis was in progress an independent study showed that Chuvash patients have lowered random serum glucose and glycosylated haemoglobin A1c (an indicator of long-term glycaemic control) levels (McClain *et al.* 2012). They were also able to demonstrate both lower fasting serum glucose levels and reduced glucose excursions in response

to an IPGTT in the Chuvash mice (male or female). The study in this thesis (with fewer mice available) has confirmed this finding, albeit only in male mice.

The underlying mechanisms for the altered glucose homeostasis in Chuvash patients and mice have been hypothesised to involve both reduced liver gluconeogenesis and increased skeletal muscle glucose uptake and utilisation (McClain *et al.* 2012). It is plausible that increased glucose uptake in the Chuvash mouse heart may also be a contributory factor, and that this may (at least in part) underlie some of the metabolic changes documented in this thesis.

4.6.2 Perfused heart substrate metabolism

One of the major findings of this thesis is the demonstration that the isolated perfused Chuvash heart had a significantly elevated rate of glycolytic flux and net lactate efflux compared to wild type controls. Furthermore, there was a strong correlation between the rate of glucose consumed and the rate of lactate production. The 1.8-fold increase in glycolysis and 1.5-fold increase in lactate efflux are comparable to values obtained from mice exposed to 11% O_2 for two weeks (2.3-fold and 2.0-fold respectively) (Abd-Jamil 2012). These findings are in keeping with previous genetic studies which have shown that long-term constitutive overexpression of HIF-1α in the heart results in increased glucose uptake (Holscher *et al.* 2012) and that cardiac-specific loss of HIF-1α causes decreased cardiomyocyte lactate concentrations (Huang *et al.* 2004). However, the study in this thesis is the first to measure substrate metabolism in the perfused heart from a model of a human disorder of oxygen sensing.

In 1963, Philip Randle and colleagues described a ‘glucose-fatty acid cycle’ in which the utilisation of one substrate for metabolism inhibited the use of another directly and without hormonal mediation (Randle *et al.* 1963). Perfused hearts from mice exposed

to sustained hypoxia demonstrated a 1.3-fold decrease in the rate of palmitate oxidation, in parallel with the increased glycolytic flux and net lactate efflux (Abd-Jamil 2012). It should be noted, however, that these reciprocal changes may not only reflect the biochemical aspects of the glucose-fatty acid cycle (e.g. increased levels of cytosolic malonyl-CoA inhibiting CPT-1) since it was also demonstrated that the altered substrate utilisation was accompanied by changes in gene expression. Furthermore, the degree of reduction in fatty acid oxidation was modest (1.3-fold, versus a 2.3-fold increase in glycolytic flux) (Abd-Jamil 2012). The study presented in this thesis did not demonstrate reduced palmitate oxidation in the Chuvash heart. However, it is possible that the number of mice available for this experiment was insufficient to reveal what would presumably be a relatively subtle effect.

Validity of the Langendorff perfused-heart experiment

The isolated perfused mammalian heart preparation was first established in 1897 by Oscar Langendorff and it has remained an important tool in cardiovascular research. There are, however, several limitations to consider when using this technique to measure *ex vivo* cardiac metabolism.

First, the perfusate is delivered (at a constant pressure) to the heart via a cannula inserted into the ascending aorta. Retrograde flow into the aorta closes the aortic valve leaflets and thus the perfusate enters the coronary arteries via the ostia. After passing through the coronary circulation and myocardium, the perfusate drains into the right atrium via the coronary sinus. The very small size of the mouse heart means that cannulation of the aorta is a technically challenging procedure; care is taken to avoid damaging the aortic valve and to ensure that the tip of the cannula does not occlude the coronary ostia. The perfusate itself provides resistance against which the heart can contract; the insertion of a water-filled PVC balloon into the left ventricle

provides additional after-load so that the typical developed pressure of the left ventricle exceeds 100 mmHg. However, it should be noted that the Langendorff set-up is not the same as the working-heart model (Neely *et al.* 1967). Since ATP production depends upon the rate of utilisation (Neely and Morgan 1974) it is important that measurement of flux through metabolic pathways is performed under physiological workloads. Whilst the working mouse heart preparation is possible (Belke *et al.* 1999) it is technically demanding. The use of the Langendorff technique, rather than the working heart, is a potential limitation of the study in this thesis. However, it has been demonstrated (using the same perfusion rig as this study) that palmitate oxidation rates in the Langendorff perfused mouse heart are similar to those obtained using the working model (Abd-Jamil 2012).

A second consideration of the *ex vivo* perfused heart experiment is that the substrates provided in the perfusate may not accurately reflect the concentrations *in vivo*. Many studies of perfused heart metabolism omit fatty acids from the perfusate; this would dramatically increase rates of myocardial carbohydrate metabolism. The study in this thesis therefore has the advantage of including 0.4 mM palmitate (bound to albumin) in the perfusate, although it should still be borne in mind that *in vivo* the heart does metabolise other fatty acids, including those not bound to albumin. However, since identical perfusate was used for all Langendorff experiments performed for this thesis, meaningful comparisons between the Chuvash and wild type hearts can still be made.

A final limitation of the perfused heart technique is that the influence of circulating hormones on cardiac metabolism cannot be considered. Until recently, it was not possible to explore real-time cardiac metabolism *in vivo* and compare the findings

with the perfused heart technique. However, the advent of dynamic nuclear polarisation means that this is now feasible.

4.6.3 *In vivo* real-time metabolism

The second major finding of this thesis is the demonstration that there was a significantly greater rate of flux of pyruvate to lactate in the Chuvash heart *in vivo*. This 1.8-fold increase is comparable to the 1.5-fold and 1.8-fold increases in net lactate efflux and glycolysis (respectively) shown in the perfused heart study. This is a striking finding; there are no published reports showing that altered metabolic flux in the perfused mouse heart can also be demonstrated in real-time *in vivo* using hyperpolarised metabolic tracers.

Hyperpolarised MRS has many advantages over other techniques used to measure metabolic flux *ex* and *in vivo.* Since it is non-invasive, it allows multiple studies to be performed in the same animals under different conditions. The ability to measure metabolism *in vivo* is a considerable advantage, since this enables the transient effects of hormones and substrate supply to be taken into account. Other techniques used to measure metabolic flux *in vivo*, such as positron emission tomography with radiolabelled 2-fluoro-2-deoxy-D-glucose, can only study single reactions. In contrast, hyperpolarised MRS evaluates flux through multiple enzyme reactions simultaneously without the need for exposure to radiation. The optimisation of this technique for use in mice, which presents considerable challenges, is a significant development (Dodd *et al.* 2013).

Validity of data from hyperpolarised MRS

A recent study has demonstrated that the rate of flux of pyruvate through PDH, measured *in vivo* using hyperpolarised MRS, correlated significantly with *ex vivo*

assays of PDH activity (Atherton *et al.* 2011). Further validation of hyperpolarised MRS in mice, employing well-established techniques known to manipulate PDH flux, has also been performed (Dodd *et al.* 2013). These, and other studies, have established that hyperpolarised MRS is a valid tool for the measurement of metabolic flux *in vivo*.

A possible drawback to hyperpolarised MRS is that it requires the injection of a high dose of the metabolite of choice (pyruvate, in this instance). The theoretical, calculated, concentration of pyruvate following injection is well above normal physiological levels. However, it has been shown in both animal and human studies that the plasma concentration of pyruvate that is actually obtained is similar to that attained during exercise or high-fat feeding (e.g. 250 μM in rats; 150 μM in humans) (Otonkoski *et al.* 2003; Atherton *et al.* 2011). Nevertheless, it is plausible that if circulating concentrations of pyruvate and its metabolites are dramatically altered during the hyperpolarised experiment, flux through the relevant pathways could be affected by processes such as end-product inhibition. However, a recent study in rats demonstrated that the plasma concentrations of metabolites such as lactate, glucose and β-hydroxybutyrate did not alter during the 60 second MRS protocol (Atherton *et al.* 2011).

A final difficulty with hyperpolarised MRS in mice is the limited volume of pyruvate that can be infused, due to the small animal size. The use of ultra-fine bore tubing and a 32 gauge needle minimised the dead space of the infusion line to 50 μl, enabling a 150 μl injection of pyruvate plus 50 μl saline flush to be given. This total of 200 μl is unlikely to cause any significant haemodynamic effects since the typical blood volume of a 25 g mouse is 1.5 ml. Furthermore, the study in this thesis was designed

so that only female mice were used, in order to avoid the discrepancy in size between, for example, a male wild type and a female Chuvash mouse.

4.6.4 Measurement of PDH activity *ex vivo*

Measurement of the activity of the PDH_{active} and PDH_{total} enzyme fractions was also determined. In keeping with the findings from the hyperpolarised pyruvate experiment (in which no significant change in PDH flux was demonstrated), no significant differences in PDH_a, PDH_t, or the percentage of PDH in the active form were shown. However, it is important to note that the assay of PDH activity was performed on hearts that had undergone the radiolabelled substrate study, and thus had been perfused for approximately one hour with glucose and palmitate. Whilst the perfusate was identical in both the wild type and Chuvash groups, it should be noted that the net lactate efflux was significantly greater in the latter. It is therefore possible that the activity of PDH_a and PDH_t measured from these perfused hearts is not representative of the picture *in vivo*, although the enzyme assay result does tally with the findings from the hyperpolarised study. Had mouse numbers allowed, it would have been of considerable interest to perform the PDH assay on hearts obtained from mice in whom values of PDH flux had also been determined *in vivo*.

4.6.5 The effect of altered substrate utilisation on cardiac energetics

The third major finding in this study is that the changes in myocardial substrate utilisation in the Chuvash mouse were accompanied by altered cardiac energetics under conditions of increased workload. Increasing the rate pressure product with an infusion of isoprenaline resulted in a depletion of phosphocreatine (compared to ATP) that was significantly greater in the Chuvash hearts. This study therefore suggests that the alterations in myocardial substrate utilisation, with an increase in glycolytic flux

and lactate production, result in a situation where, under conditions of increased workload, ATP production becomes limited and the PCr:ATP ratio falls as phosphocreatine is depleted to maintain contractile function.

The findings from this thesis are in agreement with previous studies which demonstrated lower PCr:ATP ratios in Sherpa hearts (Hochachka *et al.* 1996), in lowlanders exposed to 20 hours of normobaric hypoxia (Holloway *et al.* 2011), and in trekkers travelling to Everest base camp at 5300 m (Holloway *et al.* 2010). Furthermore, myocardial PCr:ATP ratios were reduced in mice exposed to 11% O_2 for two weeks and were accompanied by changes in substrate utilisation that were comparable to those seen in the Chuvash hearts (Abd-Jamil 2012). However, using high pressure liquid chromatography (HPLC) the authors were able to show that, despite the reduced PCr:ATP ratio, ATP concentrations and the free energy available from ATP hydrolysis (ΔG_{ATP}) were unchanged. They concluded that, whilst substrate and phosphate metabolism undergo substantial alterations in response to hypoxia, energy provision (and thus contractile function) remains unaltered (Abd-Jamil 2012). Whilst HPLC has not yet been performed on the cardiac tissue obtained from the isoprenaline perfusion experiment in this thesis, it would be of particular interest to do so.

Validity of perfused-heart ^{31}P NMR spectroscopy

The validity of the Langendorff-perfused heart technique has already been discussed in detail in Section 4.6.2. The same limitations apply to the ^{31}P NMR spectroscopy experiment, but there are other technical aspects to consider. ^{31}P NMR spectroscopy is a powerful tool, since it enables measurement of high-energy phosphates within the heart without destruction of the tissue. Hence, serial measurements of the same tissue under different perfusion conditions (e.g. with isoprenaline) can be performed.

However, a limiting factor in NMR spectroscopy can be the magnet field strength; acquisition times will vary accordingly. For the study in this thesis, spectra were acquired every 10 seconds and 32 repetitions were then averaged (resulting in an acquisition time of just over 5 minutes). Rapid changes within myocardial energetics therefore cannot be detected.

Performing Langendorff heart perfusions in a magnet, with the additional complexity of isoprenaline infusion, is technically challenging. As a result, a relatively small number of heart perfusions (5 per genotype) were deemed to be technical successes that would provide robust data. Responses to isoprenaline were variable, and therefore the exact concentration of isoprenaline administered was adjusted (between 2 and 5 nM) so that the primary end-point of an increased rate pressure product was achieved.

The ratio of PCr to ATP is taken as the indicator of cardiac energetic status in humans, since myocardial tissue is generally unavailable for further analysis. Quantification of high-energy metabolites, and the calculation of ΔG_{ATP}, is possible in hearts obtained from animal perfusion experiments by performing HPLC. This would provide confirmation of the cardiac energetic status in the Chuvash hearts, although this would only represent a 'snap-shot' of the final conditions at the end of the perfusion protocol (whilst the spectroscopy enabled repeat measurements). Limited tissue availability meant that this quantification was not performed in the study in this thesis.

4.6.6 Cardiac metabolomics

After finding evidence of altered substrate utilisation and cardiac energetics in the Chuvash hearts, a comprehensive analysis of the aqueous metabolites within the ventricular tissue was performed. Metabolomics represents a newer approach to

cardiac research, attempting to capture the complexity of metabolic networks rather than measuring specific, hypothesis-driven pathways (Griffin *et al.* 2011). It has been shown to be discriminatory for a range of processes including ischaemia, genetic modifications and cardiomyopathy (Griffin *et al.* 2011).

No single analytical tool is able to measure all metabolites within a given tissue, hence a variety of techniques are combined; each has its own advantages and disadvantages. NMR spectroscopy is a low-cost, high-throughput technique which is consistent, but suffers from poor sensitivity. GCMS is able to analyse many more metabolites, at a moderate cost and with good reproducibility, but not all metabolites are suitable for the necessary derivatisation steps. Targeted LCMS overcomes the difficulty of metabolite identification, but is more time consuming and costly (Griffin *et al.* 2011). A combination of all three enabled a thorough analysis of the metabolites in the Chuvash and wild type hearts (ventricles only) to be performed.

An interesting finding from the studies in this thesis was the relative similarity in the metabolome from Chuvash and wild type hearts. This is in keeping with the results from the gene expression and cine MRI studies. In other words, the changes in substrate utilisation and energetics in the Chuvash heart do not appear to have profound effects upon contractile function or the cardiac transcriptome and metabolome. However, the results from the GCMS and LCMS analysis in particular have demonstrated some potentially interesting findings.

Whilst the physiological significance of the changes in myoinositol, creatinine enol and oxoguanine is uncertain, those of galactose, serine and succinyl CoA provide further evidence of altered metabolism in the Chuvash heart. The decrease in galactose, for example, is in keeping with the finding of increased glucose utilisation.

Perhaps the most interesting result is the 2.3-fold increase in succinyl CoA (p = 0.012), detected using targeted LCMS. Succinyl CoA's position at the interface of multiple metabolic pathways means that alterations in its levels can be due to, or have profound effects upon, many different processes that are integral to cardiac metabolism. First, succinyl CoA is an important intermediate in the Krebs cycle, where it is synthesised from α-ketoglutarate and converted to succinate. Second, succinyl CoA is also an end-product of branched-chain amino acid (isoleucine and valine; not leucine) degradation; the resulting acetyl CoA can then be fed back into the Krebs cycle. Third, succinyl CoA may be an end-product of odd-numbered fatty acid beta oxidation. Finally, recent research has identified a novel post-translational modification in the form of lysine succinylation (using succinyl CoA as a co-factor) (Zhang *et al.* 2011), which has been shown to occur on mammalian mitochondrial proteins and can be reversed by Sirt5-mediated desuccinylation *in vivo* (Du *et al.* 2011). The diverse roles of succinyl CoA mean that it is not possible, from the studies in this thesis, to determine either the cause(s) or effect(s) of the increased levels seen in the Chuvash hearts, but it is striking that a metabolite with such a pivotal position in metabolism is so significantly altered.

4.6.7 *In vivo* left ventricular function and evidence of pulmonary hypertension

In order to investigate the effects of altered substrate utilisation and energetics on cardiac function, a comprehensive *in vivo* cine MRI study was undertaken in aging mice. Two key findings were demonstrated. First, there was striking evidence of pulmonary hypertension in the hearts of the Chuvash mice, with marked interventricular septal bowing and thickening of the RV free wall. However, despite clear changes in myocardial substrate utilisation, cardiac energetics, and RV

morphology, no abnormalities in left ventricular mass or contractile function were demonstrated in the Chuvash mice.

Evidence of pulmonary hypertension

A previous study investigating the pulmonary vascular phenotype of the Chuvash mouse demonstrated a 1.5-fold increase in both pulmonary artery pressure and RV wall thickness (measured using histology) (Hickey *et al.* 2010). The study in this thesis confirms the latter finding using non-invasive serial MRI, documenting measurements of wall thickness that were comparable to those obtained using histology.

Whilst the pulmonary hypertension and marked hypoxic pulmonary vascular sensitivity have been well documented using echocardiography in patients with Chuvash polycythaemia, no comment has been made on the impact upon the right ventricle in terms of wall thickness or septal bowing (Bushuev *et al.* 2006; Smith *et al.* 2006; Sable *et al.* 2011). The latter finding was particularly marked in the Chuvash mice and it would seem unlikely for it to be observed but not commented upon in the patient studies. It is possible that the mice display a more severe pulmonary hypertensive phenotype, but measurements of pulmonary artery pressure in both the mice and patients would argue against this as they are broadly comparable (Bushuev *et al.* 2006; Smith *et al.* 2006; Hickey *et al.* 2010). An alternative explanation is that the anaesthesia required for the cine MRI in the mice resulted in hypoxaemia and consequent hypoxic pulmonary vasoconstriction, which would have been much more pronounced in the Chuvash mice due to their known increased sensitivity. Arguments against this are that anaesthesia was maintained in medical oxygen (100%), that the mice were spontaneously breathing throughout, and that the Chuvash mice have been

shown to have normal haemoglobin O_2 saturations during anaesthesia with either 100% or 21% O_2 (Hickey *et al.* 2010).

Measurement of total RV mass (rather than mid-ventricular RV wall thickness) and function by *in vivo* cine MRI in the mouse is at the limit of what is feasible using current technology. Although attempts were made at these measurements during this thesis, the data were deemed to be inaccurate since the RV wall and cavity were often very difficult to delineate in the upper and lower sections. However, there was no clinical evidence of cor pulmonale in the Chuvash mice compared to controls.

Normal left ventricular mass and contractile function

A significant reduction in LV mass (when corrected to body weight) was observed in trekkers travelling to Everest base camp at 5300 m, accompanied by alterations in diastolic function (Holloway *et al.* 2010). Exposure of mice to 11% O_2 for 2 weeks also resulted in a reduction in LV mass (corrected to body weight), but no effects on cardiac index or LV ejection fraction were observed (Abd-Jamil 2012). Long-term constitutive overexpression of HIF-1α in the heart has been shown to result in the development of impaired contractile function (Holscher *et al.* 2012). In contrast, the study in this thesis has shown that the Chuvash mice have normal LV mass and function, even when aged 12 months. These findings are in keeping with previous studies in humans (Bushuev *et al.* 2006; Sable *et al.* 2011). Whilst the LV ejection fraction was found to be significantly increased in the study in this thesis, this could be an artefact from the measurements performed to calculate ejection fraction, since the marked septal bowing in the Chuvash hearts would have reduced the end-systolic volume. However, the possibility remains that this finding is real, and due to the pulmonary hypertension.

4.6.8 Cardiac gene expression

It has been proposed that chronic hypoxia results in long-term cardiac metabolic adaptations, regulated in particular at the transcriptional level (Essop 2007). Indeed, many studies have shown dynamic changes in gene expression in both the right and left ventricles in response to sustained hypoxia (Sivitz *et al.* 1992; Sharma 2003; Adrogue *et al.* 2005; Abd-Jamil 2012). Furthermore, models employing cardiac-specific dysregulation of HIF have similarly demonstrated marked alterations in key regulatory metabolic genes (Lei *et al.* 2008; Minamishima *et al.* 2008; Bekeredjian *et al.* 2010; Hyvarinen *et al.* 2010; Moslehi *et al.* 2010; Xue *et al.* 2010). Both patients and mice with Chuvash polycythaemia have altered gene expression in tissues such as liver, lung and skeletal muscle that are logical in the context of the altered physiology in that organ (Formenti *et al.* 2010; Hickey *et al.* 2010; McClain *et al.* 2012).

It is therefore very surprising that, despite clear alterations in *ex* and *in vivo* myocardial metabolism and energetics, no obvious changes in cardiac gene expression were demonstrated in the Chuvash mice in this thesis. There are several possible explanations for this, but firstly it is important to emphasise that the expression of key regulatory metabolic enzymes can be markedly altered without necessarily affecting flux through the relevant pathway. Hence, studies of gene expression should be combined with measurements of actual metabolic flux. The finding in this thesis of clear changes in substrate utilisation without altered gene expression is of considerable interest.

It is possible that the techniques currently available to study gene expression, such as those used in this thesis, do not possess sufficient sensitivity to detect subtle changes within gene expression. One could argue that if such subtle changes are present, but

difficult to demonstrate, they would be unlikely to influence metabolic flux. However, the system is so complex that it would be challenging to definitively say that this is the case. Genetic models utilising cardiac-specific dysregulation of HIF often show marked changes within gene expression. However, in these instances the down- or up-regulation of HIF can be considerable. In contrast, the Chuvash mutation should result in relatively modest stabilisation of HIF in all tissues from the point of conception. It is therefore a much more subtle model. This point, combined with the fact that the heart is a dynamic organ subjected to a continuous and ever-changing workload, could explain why marked gene expression changes are not necessarily exhibited. Similarly, studies investigating the effect of sustained hypoxia on cardiac gene expression also yield inconsistent results, perhaps reflecting differences in both hypoxia methodology and the choice of heart tissue to analyse (e.g. whole heart, single or both ventricles).

The lack of demonstrable altered gene expression in the Chuvash mouse heart does not detract from the clear physiological finding of altered substrate utilisation and cardiac energetics. Indeed, it is striking that the same findings of increased net lactate efflux in the perfused heart and elevated flux of pyruvate to lactate *in vivo* were seen. This could imply that the changes in metabolic flux are not due to rapidly-reversible allosteric modification of key regulatory enzymes, since the same finding was shown both *in* and *ex vivo*, under very different conditions.

It would be of considerable interest to investigate whether alterations in protein levels, solute transporter locations (e.g. translocation of GLUT-4 to the sarcolemma) or enzyme activities could explain the cardiac metabolic findings. However, whilst the Chuvash mouse model provides exciting opportunities to study the physiological effects of long-term HIF stabilisation, it also presents the significant drawback of

impaired embryogenesis and reduced availability of mice homozygous for the *Vhl* mutation. This, combined with the small size of the mouse heart, has limited the number of studies that are feasible within the scope of this thesis.

Several studies investigating the influence of sustained hypoxia on cardiac gene expression have shown different patterns of dynamic changes between the right and left ventricles (Sharma 2003; Adrogue *et al.* 2005). The authors suggested that this was in part due to the increase in after-load, with subsequent ventricular hypertrophy, experienced only by the right ventricle (Adrogue *et al.* 2005). It is possible that the right ventricular hypertrophy and pulmonary hypertension present in the Chuvash mice, as demonstrated in Section 4.5.10, could lead to a different expression profile compared to the left ventricle. The micro-array data, in Section 4.5.11, were obtained from both ventricles dissected rapidly together, because a portion of this tissue was required for the metabolomics study in Section 4.5.8. Any time taken to dissect the right ventricle separately would have compromised the stability of the metabolites within the tissue. It is possible that the combination of the ventricles in the studies in this thesis is a limitation. However, the majority of studies investigating the effects of hypoxia on cardiac gene expression do so on whole hearts which are often snap-frozen after prolonged perfusion experiments; despite this, clear changes in known HIF target genes have been demonstrated (Abd-Jamil 2012). The possible influence of the right ventricle on the results presented in this thesis will be discussed in further detail in Section 4.7.

4.7 CONCLUSIONS

The studies in this thesis have shown clear changes in myocardial substrate utilisation and energetics that are in keeping with the known effects of HIF stabilisation. These changes have been demonstrated using a variety of different approaches – findings in the perfused heart have been confirmed using *in vivo* techniques, whilst enzyme assays have been used to validate measurements of metabolic flux.

This thesis has also demonstrated that, despite clear alterations in substrate utilisation, it is possible to have normal gene expression patterns in the heart, even in a model of long-term HIF stabilisation. Similarly, altered metabolic flux does not necessarily lead to changes in metabolite levels within the heart. These findings are in keeping with the notion that the altered metabolism within the Chuvash heart is well tolerated and does not have a detrimental effect upon cardiac performance.

Possible impact of altered substrate utilisation

Altered cardiac metabolism and energetics are thought to play an important role in the progression of heart failure (Neubauer 2007). It has been hypothesised that cardiac hypoxia, via HIF, may be one of the mechanisms underlying the changes in substrate utilisation (towards increased reliance upon glucose) and energetics. The finding of a reduced myocardial PCr:ATP ratio, accompanied by impaired diastolic function, in trekkers travelling to Everest base camp added weight to this argument (Holloway *et al.* 2010). However, recent work has shown that whilst myocardial PCr:ATP ratios were reduced in mice exposed to 11% O_2 for two weeks, with changes in substrate utilisation that were similar to those seen in heart failure, the free energy available from ATP hydrolysis (ΔG_{ATP}) was unchanged (Abd-Jamil 2012). This led to the

conclusion that the increased reliance upon glucose utilisation could be viewed as a beneficial adaptation to chronic hypoxia. The findings in this thesis add weight to this argument since, despite similar changes in cardiac metabolism and energetics, contractile function of the perfused heart and cardiac function *in vivo* were maintained in the Chuvash mice. Thus, altered substrate utilisation, with accompanying changes in myocardial energetics, does not inevitably lead to contractile dysfunction and may indeed be a beneficial process.

Influence of the right ventricle

The studies in this thesis have demonstrated clear features of pulmonary hypertension, such as septal bowing and RV hypertrophy, in the Chuvash mice. The latter finding is in keeping with a previous study (Hickey *et al.* 2010). An important question therefore arises as to what influence the RV hypertrophy and/or pulmonary hypertension may have on the metabolic results presented in this thesis.

There is considerable interest in the role that altered metabolism may play in the progression of RV hypertrophy and/or failure due to idiopathic pulmonary arterial hypertension, particularly since the pulmonary artery smooth muscle cells themselves exhibit a metabolic shift towards increased glycolysis (Xu *et al.* 2007). This interest has extended to RV hypertrophy secondary to other forms of pulmonary hypertension (Piao *et al.* 2010). Increased glucose uptake in the RV has been demonstrated in both patients (Oikawa *et al.* 2005) and animal models of pulmonary hypertension (Takeyama *et al.* 1995; Piao *et al.* 2009), together with increased expression of GLUT-1, evidence of augmented glycolysis (Piao *et al.* 2009) and reduced levels of phosphocreatine (Do *et al.* 1997). Intriguingly, many of these metabolic, and accompanying functional, changes can be partially reversed by augmenting PDH flux

(and hence glucose oxidation) by the administration of dichloroacetate (Piao *et al.* 2009).

There are several ways in which the pulmonary hypertension and consequent RV hypertrophy of the Chuvash mice could have influenced the results presented in this thesis. First, one possibility is that the metabolic changes measured come entirely from the RV, rather than from the LV. In other words, the LV is 'normal' and the increased glucose consumption, lactate production and phosphocreatine depletion are occurring solely in the RV and are a consequence of pulmonary hypertension rather than cardiomyocyte HIF stabilisation. There are several arguments against this. First, whilst the RV hypertrophy certainly does increase the ratio of RV:LV within the heart, the left ventricle still comprises the majority of the myocardial tissue. Second, in the Langendorff perfusion set-up it is the LV, not the RV, that is contracting against a significant work-load (in the form of perfusate and the fluid-filled balloon). Whilst the RV certainly does contract, it does so against minimal resistance and therefore its contribution towards glucose consumption and lactate production should be considerably lower compared to the LV. Third, for measurements of PCr and ATP using MR spectroscopy, the perfused heart was positioned at the isocentre of the magnet; the size of the LV means that it would comprise the majority of the signal.

The second possible influence of the RV on the results presented in this thesis is that the pulmonary hypertension and altered RV dynamics (in the form of septal bowing etc) could themselves have affected LV function and metabolism. There is some evidence to suggest that pulmonary hypertension may impair LV diastolic function (Louie *et al.* 1986; Dittrich *et al.* 1989; Stojnic *et al.* 1992) but this has been disputed in a study in which patients with coronary artery disease, hypertension and hypoxaemia were excluded (Jessup *et al.* 1987). Furthermore, the metabolic and

functional changes seen in response to pulmonary hypertension in animal models have been shown to be confined to the RV only, not the LV (Piao *et al.* 2009).

It is therefore unlikely that the profound metabolic changes demonstrated in the Chuvash mouse heart in this thesis are solely due to RV hypertrophy and/or pulmonary hypertension. The fact that very similar metabolic findings are seen in chronic hypoxia and in models of cardiac-specific over-expression of HIF adds weight to this argument (Abd-Jamil 2012; Holscher *et al.* 2012). Nevertheless, teasing out subtle effects of the RV upon the results in this thesis would be of considerable interest, although technically demanding. With regards to the Langendorff perfusion technique and *in vivo* hyperpolarised study, determining the separate influence of the RV is not currently technically feasible. It would certainly be of interest to perform gene expression studies on the right and left ventricles separately since rapid dissection of the heart should not affect mRNA stability. In contrast, performing metabolomic studies on anything other than 'ventricular tissue' in general would be very difficult since metabolites can degrade within seconds. Finally, it would be of particular interest to know whether there is altered glucose uptake within either or both of the ventricles in the Chuvash heart. This could, in theory, be determined using 18-fluorodeoxyglucose positron emission tomography, although this is not currently planned.

Comparisons with the skeletal muscle and exercise phenotype in humans

The Chuvash mutation in humans has been shown to have striking effects on skeletal muscle metabolism and exercise (Formenti *et al.* 2010). Muscle biopsy specimens showed increased transcript levels of key metabolic genes, such as PDK 1, 2 and 4, phosphofructokinase, and muscle pyruvate kinase (increased PDK 1 and 4, and GLUT 1 have also been shown in the Chuvash mice (McClain *et al.* 2012)). One would

predict therefore that Chuvash patients should exhibit an increased capacity for skeletal muscle glycolysis and lactate production. Indeed, during an incremental exercise test, Chuvash patients stopped exercising early (failing to achieve the same work rate as controls) and had significantly elevated blood lactate levels. Furthermore, exercise of a small muscle mass revealed early and marked phosphocreatine depletion and acidosis.

It is interesting that the metabolic phenotypes of skeletal muscle in humans and cardiac muscle in mice with the Chuvash mutation are so similar. In both instances there is increased reliance upon glucose metabolism, with evidence of increased glycolytic flux and lactate production. Furthermore, this alteration in substrate utilisation results in marked depletion of phosphocreatine when the skeletal or cardiac muscle is stressed by exercise or isoprenaline, respectively. However, whilst skeletal muscle function and/or exercise capacity appear to be limited in the Chuvash patients, there was no evidence of impaired cardiac function in the mouse model. The metabolic changes seen are in keeping with the known effects of HIF, and with the altered gene expression seen in both the human and murine skeletal muscle. Taken together, these studies illustrate the profound influence of the HIF system upon metabolism in different organ systems.

Summary

Studies in animals and humans have demonstrated that hypoxia and/or cardiac-specific alterations in HIF levels result in increased myocardial reliance upon glucose metabolism, accompanied by changes in cardiac energetics and function. The findings from this thesis contribute to this significant body of evidence, and support the notion that even a relatively subtle disorder of oxygen sensing can have profound effects upon myocardial metabolism.

CHAPTER 5

Final conclusions

5.1 HIGH-ALTITUDE ADAPTATION – GENETIC VARIATION IN HYPOXIA AND METABOLISM PATHWAYS

Native high altitude populations have been shown to exhibit unique heritable traits that appear to afford protection against life-long hypoxia. For example, natives of the Tibetan plateau have haemoglobin levels that are comparable to those expected at sea level (Beall *et al.* 1998; Moore 2001; Wu *et al.* 2005; Beall 2007). Recently, genome-wide analyses have revealed the first evidence supporting the notion of genetic adaptation to high altitude (Beall *et al.* 2010; Bigham *et al.* 2010; Simonson *et al.* 2010; Yi *et al.* 2010; Peng *et al.* 2011a; Wang *et al.* 2011; Xu *et al.* 2011). Single-nucleotide polymorphisms (SNPs) in the *HIF2A, PHD2* and *PPARA* genes all demonstrate significant associations with the reduced haemoglobin level in Tibetans (see Table 5.1), providing corroborative evidence for adaptive roles of genes that appear to have undergone strong selection (Simonson *et al.* 2012).

Table 5.1: Selection candidate genes

Selection candidate genes that were identified in more than one genome-wide study of high-altitude adaptation or found to be associated with haemoglobin levels in different Tibetan populations. Adapted from (Simonson *et al.* 2012). Studies are numbered 1. (Simonson *et al.* 2010); 2. (Beall *et al.* 2010); 3. (Yi *et al.* 2010); 4. (Bigham *et al.* 2010); 5. (Peng *et al.* 2011a); 6. (Xu *et al.* 2011); 7. (Wang *et al.* 2011).

Gene	Study								
	1	2	3	4	5	6	7	Assoc. with Hb in Tibetans	Target of selection in Tibetans & Andeans
HIF2A	✓	✓	✓	✓	✓	✓	✓	Studies 2 and 3	
PHD2	✓		✓	✓	✓	✓	✓	Study 1	Study 4
PPARA	✓							Study 1	

Although *HIF2A* and *PHD2* are key components of the PHD-VHL-HIF axis, the precise genetic variant(s) and functional role(s) of the identified SNPs remain unknown and are the subject of current research. It is intriguing, however, that one

recent study has revealed a metabolic insight into the mechanisms underlying high-altitude adaptation in Tibetans (Ge *et al.* 2012). This study demonstrated that increased serum lactate levels (suggesting increased glycolysis) and free fatty acid levels (suggesting decreased oxidation) are significantly associated with the putatively advantageous HIF2A and PPARA haplotypes, respectively. Whilst further work is certainly required to elucidate the potential underlying mechanism(s) of these findings, they highlight the complex interplay between hypoxia, metabolism and adaptation. This thesis contributes to the growing body of evidence demonstrating the critical role(s) that the PHD-VHL-HIF axis plays in integrative physiology.

5.2 FUTURE WORK

This thesis contributes to the rapidly-growing body of work showing the diverse influences of the PHD-VHL-HIF axis. However, whilst profound changes have been demonstrated in different organ systems, the mechanism(s) underlying these processes have not been fully determined. The Chuvash mouse provides a unique opportunity to investigate these outstanding questions in more detail. Possible future work has been discussed in the relevant chapters of this thesis, but a summary will be provided here together with additional proposals independent from the presented studies.

5.2.1 Ventilation

Several questions arise from the ventilatory study in this thesis; work investigating some of these is already underway.

Sensitivity of the Chuvash carotid body response to hypoxia

It would be of considerable interest to know both the response of individual type I cells to hypoxia and the response of the carotid body as a whole. This would provide an important link between the observed morphological/ultrastructural changes and the ventilatory responses to hypoxia. Work on the individual type I cell response is already underway.

Expression of HIF and its target genes within the type I cells

Developing the ability to detect HIF and potential target genes within the carotid body cell types would enable some of the mechanisms underlying the morphological changes to be determined.

HIF-1α versus HIF-2α

Considerable interest has been directed towards understanding the relative roles of HIF-1 and HIF-2 in integrative physiology, particularly with regard to the carotid body and ventilatory control. Breeding of Chuvash mice with others heterozygous for either HIF-1 or HIF-2 would be feasible and interesting.

5.2.2 Cardiac metabolism

Determining the effects of pulmonary hypertension and right ventricular hypertrophy on the cardiac phenotypes demonstrated in this thesis would be challenging. However, 18-fluorodeoxyglucose positron emission tomography would provide additional information on the differences between the right and left ventricles. Finally, since treatment with dichloroacetate was shown to prevent the RV metabolic and functional changes in response to established pulmonary hypertension, applying this treatment to the Chuvash mice could be of interest.

5.2.3 Pulmonary hypertension and hypoxic pulmonary vasoconstriction

It is clear from studies in this thesis and elsewhere that the Chuvash mouse model provides an exciting opportunity to study the effect of HIF on the pulmonary vasculature. Whilst the Chuvash mutation certainly results in marked sensitivity of the pulmonary vascular response to hypoxia, the mechanisms underlying this are still unknown. Development of techniques such as isolated lung perfusion and pulmonary artery smooth muscle cell culture would be particularly interesting.

5.2.4 Embryogenesis and placentation

The reduced birth rate of mice homozygous for the Chuvash mutation implies that there may be defects in embryogenesis and/or placentation. It is known that HIF-mediated gene regulation is essential for normal placental development at a stage

when the uterine surface is itself hypoxic (Rodesch *et al.* 1992; Cowden Dahl *et al.* 2005). Furthermore, it has been hypothesised that HIF may play an important role in the pathogenesis of pre-eclampsia (Tal 2012). The study of the PHD-VHL-HIF axis in placentation is a field in which the Chuvash mouse could provide novel insights.

5.3 OVERALL CONCLUSIONS

The conservation of the oxygen-sensing HIF system throughout evolution underlines its fundamental role in oxygen homeostasis. Studies of mutations within the PHD-VHL-HIF axis in humans have revealed the profound influence that this system has upon integrative cardiopulmonary physiology and metabolism. This thesis extends these findings, demonstrating that even a relatively subtle disorder of oxygen sensing in mice is capable of influencing diverse processes. Ventilatory control, sensitivity to hypoxia and carotid body morphology have been shown to be clearly affected by perturbation of the HIF pathway. This thesis has also revealed the novel finding that long-term, modest, systemic HIF stabilisation results in profound changes in cardiac metabolism and energetics.

The Chuvash mutation in humans and mice has now been shown to affect diverse processes encompassing the hypoxic response in the principal organ systems responsible for oxygen uptake, delivery and utilisation. The role of the HIF pathway in systemic and tissue-level physiology is therefore relevant to any clinical scenario featuring hypoxia, as well as to therapeutic strategies aimed at manipulating the PHD-VHL-HIF axis in some way.

Bibliography

Abd-Jamil, A. H. (2012). Role of PPAR alpha in the cardiac metabolic adaptation to chronic hypoxia, University of Oxford. **DPhil**.

Adrogue, J. V., S. Sharma, et al. (2005). "Acclimatization to chronic hypobaric hypoxia is associated with a differential transcriptional profile between the right and left ventricle." *Mol Cell Biochem* 278(1-2): 71-78.

Albiero, E., M. Ruggeri, et al. (2012). "Isolated erythrocytosis: study of 67 patients and identification of three novel germ-line mutations in the prolyl hydroxylase domain protein 2 (PHD2) gene." *Haematologica* 97(1): 123-127.

Ang, S. O., H. Chen, et al. (2002a). "Endemic polycythemia in Russia: mutation in the VHL gene." *Blood Cells Mol Dis* 28(1): 57-62.

Ang, S. O., H. Chen, et al. (2002b). "Disruption of oxygen homeostasis underlies congenital Chuvash polycythemia." *Nature Genetics* 32(4): 614-621.

Aragonés, J., M. Schneider, et al. (2008). "Deficiency or inhibition of oxygen sensor Phd1 induces hypoxia tolerance by reprogramming basal metabolism." *Nature Genetics* 40(2): 170-180.

Ardenkjaer-Larsen, J. H., B. Fridlund, et al. (2003). "Increase in signal-to-noise ratio of > 10,000 times in liquid-state NMR." *Proc Natl Acad Sci U S A* 100(18): 10158-10163.

Atherton, H. J., N. J. Bailey, et al. (2006). "A combined 1H-NMR spectroscopy- and mass spectrometry-based metabolomic study of the PPAR-alpha null mutant mouse defines profound systemic changes in metabolism linked to the metabolic syndrome." *Physiol Genomics* 27(2): 178-186.

Atherton, H. J., M. A. Schroeder, et al. (2011). "Validation of the in vivo assessment of pyruvate dehydrogenase activity using hyperpolarised 13C MRS." *NMR Biomed* 24(2): 201-208.

Baracco, R., S. Mohanna, et al. (2007). "A comparison of the prevalence of metabolic syndrome and its components in high and low altitude populations in peru." *Metab Syndr Relat Disord* 5(1): 55-62.

Barger, P. M., J. M. Brandt, et al. (2000). "Deactivation of peroxisome proliferator-activated receptor-alpha during cardiac hypertrophic growth." *J Clin Invest* 105(12): 1723-1730.

Bates, J. H. and C. G. Irvin (2003). "Measuring lung function in mice: the phenotyping uncertainty principle." *J Appl Physiol* 94(4): 1297-1306.

Beall, C. M. (2007). "Two routes to functional adaptation: Tibetan and Andean high-altitude natives." *Proc Natl Acad Sci U S A* 104 Suppl 1: 8655-8660.

Beall, C. M., G. M. Brittenham, et al. (1998). "Hemoglobin concentration of high-altitude Tibetans and Bolivian Aymara." *Am J Phys Anthropol* 106(3): 385-400.

Beall, C. M., G. L. Cavalleri, et al. (2010). "Natural selection on EPAS1 (HIF2alpha) associated with low hemoglobin concentration in Tibetan highlanders." *Proc Natl Acad Sci U S A* 107(25): 11459-11464.

Beck, I., S. Ramirez, et al. (1991). "Enhancer element at the 3'-flanking region controls transcriptional response to hypoxia in the human erythropoietin gene." *J Biol Chem* 266(24): 15563-15566.

Bee, D., D. J. Pallot, et al. (1986). "Division of type I and endothelial cells in the hypoxic rat carotid body." *Acta Anat (Basel)* 126(4): 226-229.

Bekeredjian, R., C. B. Walton, et al. (2010). "Conditional HIF-1alpha expression produces a reversible cardiomyopathy." *PLoS ONE* 5(7): e11693.

Belke, D. D., T. S. Larsen, et al. (1999). "Glucose and fatty acid metabolism in the isolated working mouse heart." *Am J Physiol* 277(4 Pt 2): R1210-1217.

Benot, A. R. and J. Lopez-Barneo (1990). "Feedback Inhibition of Ca2+ Currents by Dopamine in Glomus Cells of the Carotid Body." *Eur J Neurosci* 2(9): 809-812.

Bento, M. C., K. T. Chang, et al. (2005). "Congenital polycythemia with homozygous and heterozygous mutations of von Hippel-Lindau gene: five new Caucasian patients." *Haematologica* 90(1): 128-129.

Berger, J. and D. E. Moller (2002). "The mechanisms of action of PPARs." *Annu Rev Med* 53: 409-435.

Berra, E., E. Benizri, et al. (2003). "HIF prolyl-hydroxylase 2 is the key oxygen sensor setting low steady-state levels of HIF-1alpha in normoxia." *EMBO J* 22(16): 4082-4090.

Bigham, A., M. Bauchet, et al. (2010). "Identifying signatures of natural selection in Tibetan and Andean populations using dense genome scan data." *PLoS Genet* 6(9): e1001116.

Bing, R. J., A. Siegel, et al. (1954). "Metabolism of the human heart. II. Studies on fat, ketone and amino acid metabolism." *Am J Med* 16(4): 504-515.

Bisgard, G. E. (2000). "Carotid body mechanisms in acclimatization to hypoxia." *Respir Physiol* 121(2-3): 237-246.

Bisgard, G. E., H. G. Alvarez, et al. (1969). "Decreased ventilatory response to hypoxia during acute polycythemia in the calf." *Respir Physiol* 7(3): 369-382.

Bisgard, G. E. and J. H. Vogel (1971). "Hypoventilation and pulmonary hypertension in calves after carotid body excision." *J Appl Physiol* 31(3): 431-437.

Bishop, T., D. Gallagher, et al. (2008). "Abnormal sympathoadrenal development and systemic hypotension in PHD3-/- mice." *Mol Cell Biol* 28(10): 3386-3400.

Bishop, T., N. P. Talbot, et al. (2013). "Carotid body hyperplasia and enhanced ventilatory responses to hypoxia in mice with heterozygous deficiency of PHD2." *J Physiol* 591 (14): 3565-3577.

Boudinot, E., M. J. Emery, et al. (2004). "Increased ventilation and CO2 chemosensitivity in acetylcholinesterase knockout mice." *Respir Physiol Neurobiol* 140(3): 231-241.

Bowker-Kinley, M. M., W. I. Davis, et al. (1998). "Evidence for existence of tissue-specific regulation of the mammalian pyruvate dehydrogenase complex." *Biochem J* 329 (Pt 1): 191-196.

Brandt, J. M., F. Djouadi, et al. (1998). "Fatty acids activate transcription of the muscle carnitine palmitoyltransferase I gene in cardiac myocytes via the peroxisome proliferator-activated receptor alpha." *J Biol Chem* 273(37): 23786-23792.

Bruick, R. K. and S. L. McKnight (2001). "A conserved family of prolyl-4-hydroxylases that modify HIF." *Science* 294(5545): 1337-1340.

Brunelle, J. K., E. L. Bell, et al. (2005). "Oxygen sensing requires mitochondrial ROS but not oxidative phosphorylation." *Cell Metab* 1(6): 409-414.

Brusselmans, K., V. Compernolle, et al. (2003). "Heterozygous deficiency of hypoxia-inducible factor-2alpha protects mice against pulmonary hypertension and right ventricular dysfunction during prolonged hypoxia." *J Clin Invest* 111(10): 1519-1527.

Burton, M. D. and H. Kazemi (2000). "Neurotransmitters in central respiratory control." *Respir Physiol* 122(2-3): 111-121.

Busch, M. A., G. E. Bisgard, et al. (1985). "Ventilatory acclimatization to hypoxia is not dependent on arterial hypoxemia." *J Appl Physiol* 58(6): 1874-1880.

Bushuev, V. I., G. Y. Miasnikova, et al. (2006). "Endothelin-1, vascular endothelial growth factor and systolic pulmonary artery pressure in patients with Chuvash polycythemia." *Haematologica* 91(6): 744-749.

Cario, H., K. Schwarz, et al. (2005). "Mutations in the von Hippel-Lindau (VHL) tumor suppressor gene and VHL-haplotype analysis in patients with presumable congenital erythrocytosis." *Haematologica* 90(1): 19-24.

Chan, D. A., P. D. Sutphin, et al. (2005). "Coordinate regulation of the oxygen-dependent degradation domains of hypoxia-inducible factor 1 alpha." *Mol Cell Biol* 25(15): 6415-6426.

Chan, S. Y., Y.-Y. Zhang, et al. (2009). "MicroRNA-210 Controls Mitochondrial Metabolism during Hypoxia by Repressing the Iron-Sulfur Cluster Assembly Proteins ISCU1/2." *Cell Metabolism* 10(4): 273-284.

Chen, J., L. He, et al. (2002). "Role of endothelin and endothelin A-type receptor in adaptation of the carotid body to chronic hypoxia." *Am J Physiol Lung Cell Mol Physiol* 282(6): L1314-1323.

Chen, J., L. He, et al. (2007). "Effect of the endothelin receptor antagonist bosentan on chronic hypoxia-induced morphological and physiological changes in rat carotid body." *Am J Physiol Lung Cell Mol Physiol* 292(5): L1257-1262.

Chen, R., E. M. Dioum, et al. (2011). "Hypoxia Increases Sirtuin 1 Expression in a Hypoxia-inducible Factor-dependent Manner." *Journal of Biological Chemistry* 286(16): 13869-13878.

Chiodi, H. (1957). "Respiratory Adaptations to Chronic High Altitude Hypoxia." *Journal of Applied Physiology* 10(1): 81-87.

Chun, Y. S., E. Choi, et al. (2002). "A dominant-negative isoform lacking exons 11 and 12 of the human hypoxia-inducible factor-1alpha gene." *Biochem J* 362(Pt 1): 71-79.

Chun, Y. S., E. Choi, et al. (2001). "A new HIF-1 alpha variant induced by zinc ion suppresses HIF-1-mediated hypoxic responses." *J Cell Sci* 114(Pt 22): 4051-4061.

Chun, Y. S., K. H. Lee, et al. (2003). "Phorbol ester stimulates the nonhypoxic induction of a novel hypoxia-inducible factor 1alpha isoform: implications for tumor promotion." *Cancer Res* 63(24): 8700-8707.

Clar, C., K. L. Dorrington, et al. (2001). "Effects of 8 h of isocapnic hypoxia with and without muscarinic blockade on ventilation and heart rate in humans." *Exp Physiol* 86(4): 529-538.

Compernolle, V., K. Brusselmans, et al. (2002). "Loss of HIF-2alpha and inhibition of VEGF impair fetal lung maturation, whereas treatment with VEGF prevents fatal respiratory distress in premature mice." *Nat Med* 8(7): 702-710.

Costa-Giomi, P., J. Caro, et al. (1990). "Enhancement by hypoxia of human erythropoietin gene transcription in vitro." *J Biol Chem* 265(18): 10185-10188.

Cowden Dahl, K. D., B. H. Fryer, et al. (2005). "Hypoxia-inducible factors 1alpha and 2alpha regulate trophoblast differentiation." *Mol Cell Biol* 25(23): 10479-10491.

D'Angelo, G., E. Duplan, et al. (2003). "Hypoxia up-regulates prolyl hydroxylase activity: a feedback mechanism that limits HIF-1 responses during reoxygenation." *J Biol Chem* 278(40): 38183-38187.

Dalgard, C. L., H. Lu, et al. (2004). "Endogenous 2-oxoacids differentially regulate expression of oxygen sensors." *Biochem J* 380(Pt 2): 419-424.

Dann, C. E., 3rd, R. K. Bruick, et al. (2002). "Structure of factor-inhibiting hypoxia-inducible factor 1: An asparaginyl hydroxylase involved in the hypoxic response pathway." *Proc Natl Acad Sci U S A* 99(24): 15351-15356.

Dejours, P. (1962). "Chemoreflexes in breathing." *Physiol Rev* 42: 335-358.

Dempsey, J. A. and H. V. Forster (1982). "Mediation of Ventilatory Adaptations." *Physiol Rev* 62(1): 262-346.

Dhillon, D. P., G. R. Barer, et al. (1984). "The enlarged carotid body of the chronically hypoxic and chronically hypoxic and hypercapnic rat: a morphometric analysis." *Q J Exp Physiol* 69(2): 301-317.

Di Giulio, C., P. G. Data, et al. (1991). "Chronic cobalt causes hypertrophy of glomus cells in the rat carotid body." *Am J Physiol* 261(1 Pt 1): C102-105.

Dioum, E. M., R. Chen, et al. (2009). "Regulation of hypoxia-inducible factor 2alpha signaling by the stress-responsive deacetylase sirtuin 1." *Science* 324(5932): 1289-1293.

Dioum, E. M., S. L. Clarke, et al. (2008). "HIF-2alpha-haploinsufficient mice have blunted retinal neovascularization due to impaired expression of a proangiogenic gene battery." *Invest Ophthalmol Vis Sci* 49(6): 2714-2720.

Dittrich, H. C., L. C. Chow, et al. (1989). "Early improvement in left ventricular diastolic function after relief of chronic right ventricular pressure overload." *Circulation* 80(4): 823-830.

Djouadi, F., J. M. Brandt, et al. (1999). "The role of the peroxisome proliferator-activated receptor alpha (PPAR alpha) in the control of cardiac lipid metabolism." *Prostaglandins Leukot Essent Fatty Acids* 60(5-6): 339-343.

Do, E., S. Baudet, et al. (1997). "Energy metabolism in normal and hypertrophied right ventricle of the ferret heart." *J Mol Cell Cardiol* 29(7): 1903-1913.

Dodd, M. S., V. Ball, et al. (2013). "In vivo mouse cardiac hyperpolarized magnetic resonance spectroscopy." *J Cardiovasc Magn Reson* 15: 19.

Douglas, C. G., J. S. Haldane, et al. (1913). "Physiological observations made on Pike's Peak, Colorado, with special reference to adaptation to low barometric pressure." *Philosophical Transactions of the Royal Society* B 203: 185 - 318.

Du, J., Y. Zhou, et al. (2011). "Sirt5 is a NAD-dependent protein lysine demalonylase and desuccinylase." *Science* 334(6057): 806-809.

Eckardt, K. U., P. J. Ratcliffe, et al. (1992). "Age-dependent expression of the erythropoietin gene in rat liver and kidneys." *J Clin Invest* 89(3): 753-760.

Eisele, J. H., J. Pegg, et al. (1969). "Ventilatory response to hypoxia in acutely polycythemic dogs." *J Appl Physiol* 26(6): 757-759.

Elvidge, G. P., L. Glenny, et al. (2006). "Concordant regulation of gene expression by hypoxia and 2-oxoglutarate-dependent dioxygenase inhibition: the role of HIF-1alpha, HIF-2alpha, and other pathways." *J Biol Chem* 281(22): 15215-15226.

Ema, M., S. Taya, et al. (1997). "A novel bHLH-PAS factor with close sequence similarity to hypoxia-inducible factor 1alpha regulates the VEGF expression and is potentially involved in lung and vascular development." *Proc Natl Acad Sci U S A* 94(9): 4273-4278.

Epstein, A. C., J. M. Gleadle, et al. (2001). "C. elegans EGL-9 and mammalian homologs define a family of dioxygenases that regulate HIF by prolyl hydroxylation." *Cell* 107(1): 43-54.

Epstein, M. A. and R. A. Epstein (1978). "A theoretical analysis of the barometric method for measurement of tidal volume." *Respir Physiol* 32(1): 105-120.

Essop, M. F. (2007). "Cardiac metabolic adaptations in response to chronic hypoxia." *J Physiol* 584(Pt 3): 715-726.

Eyzaguirre, C. and P. Zapata (1968). "The release of acetylcholine from carotid body tissues. Further study on the effects of acetylcholine and cholinergic blocking agents on the chemosensory discharge." *J Physiol* 195(3): 589-607.

Fell, D. A. (1998). "Increasing the flux in metabolic pathways: A metabolic control analysis perspective." *Biotechnol Bioeng* 58(2-3): 121-124.

Fell, D. A. and H. M. Sauro (1990). "Metabolic control analysis. The effects of high enzyme concentrations." *Eur J Biochem* 192(1): 183-187.

Firth, J. D., B. L. Ebert, et al. (1994). "Oxygen-regulated control elements in the phosphoglycerate kinase 1 and lactate dehydrogenase A genes: similarities with the erythropoietin 3' enhancer." *Proc Natl Acad Sci U S A* 91(14): 6496-6500.

Flamme, I., T. Frohlich, et al. (1997). "HRF, a putative basic helix-loop-helix-PAS-domain transcription factor is closely related to hypoxia-inducible factor-1 alpha and developmentally expressed in blood vessels." *Mech Dev* 63(1): 51-60.

Formenti, F., P. A. Beer, et al. (2011). "Cardiopulmonary function in two human disorders of the hypoxia-inducible factor (HIF) pathway: von Hippel-Lindau disease and HIF-2{alpha} gain-of-function mutation." *FASEB J*.

Formenti, F., D. Constantin-Teodosiu, et al. (2010). "Regulation of human metabolism by hypoxia-inducible factor." *Proceedings of the National Academy of Sciences* 107(28): 12722-12727.

Forristal, C. E., K. L. Wright, et al. (2010). "Hypoxia inducible factors regulate pluripotency and proliferation in human embryonic stem cells cultured at reduced oxygen tensions." *Reproduction* 139(1): 85-97.

Forster, H. V., G. E. Bisgard, et al. (1981). "Effect of peripheral chemoreceptor denervation on acclimatization of goats during hypoxia." *J Appl Physiol* 50(2): 392-398.

Frappell, P., C. Lanthier, et al. (1992). "Metabolism and ventilation in acute hypoxia: a comparative analysis in small mammalian species." *Am J Physiol* 262(6 Pt 2): R1040-1046.

Freedman, S. J., Z. Y. Sun, et al. (2003). "Structural basis for negative regulation of

hypoxia-inducible factor-1alpha by CITED2." *Nat Struct Biol* 10(7): 504-512.

Fukuda, R., H. Zhang, et al. (2007). "HIF-1 Regulates Cytochrome Oxidase Subunits to Optimize Efficiency of Respiration in Hypoxic Cells." *Cell* 129(1): 111-122.

Gale, D. P., S. K. Harten, et al. (2008). "Autosomal dominant erythrocytosis and pulmonary arterial hypertension associated with an activating HIF2 alpha mutation." *Blood* 112(3): 919-921.

Garland, P. B., P. J. Randle, et al. (1963). "Citrate as an Intermediary in the Inhibition of Phosphofructokinase in Rat Heart Muscle by Fatty Acids, Ketone Bodies, Pyruvate, Diabetes, and Starvation." *Nature* 200: 169-170.

Ge, R. L., T. S. Simonson, et al. (2012). "Metabolic insight into mechanisms of high-altitude adaptation in Tibetans." *Mol Genet Metab* 106(2): 244-7.

Gertz, E. W., J. A. Wisneski, et al. (1988). "Myocardial substrate utilization during exercise in humans. Dual carbon-labeled carbohydrate isotope experiments." *J Clin Invest* 82(6): 2017-2025.

Gibbs, C. L. (1978). "Cardiac energetics." *Physiol Rev* 58(1): 174-254.

Glatz, J. F., J. J. Luiken, et al. (2001). "Involvement of membrane-associated proteins in the acute regulation of cellular fatty acid uptake." *J Mol Neurosci* 16(2-3): 123-132; discussion 151-127.

Gnarra, J. R., J. M. Ward, et al. (1997). "Defective placental vasculogenesis causes embryonic lethality in VHL-deficient mice." *Proc Natl Acad Sci U S A* 94(17): 9102-9107.

Goldberg, M. A., S. P. Dunning, et al. (1988). "Regulation of the erythropoietin gene: evidence that the oxygen sensor is a heme protein." *Science* 242(4884): 1412-1415.

Goldberg, M. A., G. A. Glass, et al. (1987). "The regulated expression of erythropoietin by two human hepatoma cell lines." *Proc Natl Acad Sci U S A* 84(22): 7972-7976.

Goldwasser, E., L. O. Jacobson, et al. (1958). "Studies on erythropoiesis. V. The effect of cobalt on the production of erythropoietin." *Blood* 13(1): 55-60.

Gordeuk, V. R. (2004). "Congenital disorder of oxygen sensing: association of the homozygous Chuvash polycythemia VHL mutation with thrombosis and vascular abnormalities but not tumors." *Blood* 103(10): 3924-3932.

Gordon, C. J. and L. Fogelson (1991). "Comparative effects of hypoxia on behavioral thermoregulation in rats, hamsters, and mice." *Am J Physiol* 260(1 Pt 2): R120-125.

Gothie, E., D. E. Richard, et al. (2000). "Identification of alternative spliced variants of human hypoxia-inducible factor-1alpha." *J Biol Chem* 275(10): 6922-6927.

Griffin, J. L., H. Atherton, et al. (2011). "Metabolomics as a tool for cardiac research." *Nat Rev Cardiol* 8(11): 630-643.

Gulick, T., S. Cresci, et al. (1994). "The peroxisome proliferator-activated receptor regulates mitochondrial fatty acid oxidative enzyme gene expression." *Proc Natl Acad Sci U S A* 91(23): 11012-11016.

Guzy, R. D., B. Hoyos, et al. (2005). "Mitochondrial complex III is required for hypoxia-induced ROS production and cellular oxygen sensing." *Cell Metab* 1(6): 401-408.

Harris, R. A., B. Huang, et al. (2001). "Control of pyruvate dehydrogenase kinase gene expression." *Adv Enzyme Regul* 41: 269-288.

Henze, A. T., J. Riedel, et al. (2010). "Prolyl hydroxylases 2 and 3 act in gliomas as protective negative feedback regulators of hypoxia-inducible factors." *Cancer Res* 70(1): 357-366.

Hewitson, K. S., B. M. Lienard, et al. (2007). "Structural and mechanistic studies on the inhibition of the hypoxia-inducible transcription factor hydroxylases by tricarboxylic acid cycle intermediates." *J Biol Chem* 282(5): 3293-3301.

Hickey, M. M., J. C. Lam, et al. (2007). "von Hippel–Lindau mutation in mice recapitulates Chuvash polycythemia via hypoxia-inducible factor-2α signaling and splenic erythropoiesis." *Journal of Clinical Investigation* 117(12): 3879-89.

Hickey, M. M., T. Richardson, et al. (2010). "The von Hippel–Lindau Chuvash mutation promotes pulmonary hypertension and fibrosis

in mice." *Journal of Clinical Investigation* 120(3): 827-839.

Hochachka, P. W., C. M. Clark, et al. (1996). "31P magnetic resonance spectroscopy of the Sherpa heart: a phosphocreatine/adenosine triphosphate signature of metabolic defense against hypobaric hypoxia." *Proc Natl Acad Sci U S A* 93(3): 1215-1220.

Holden, J. E., C. K. Stone, et al. (1995). "Enhanced cardiac metabolism of plasma glucose in high-altitude natives: adaptation against chronic hypoxia." *J Appl Physiol* 79(1): 222-228.

Holloway, C., L. Cochlin, et al. (2011). "Normobaric hypoxia impairs human cardiac energetics." *The FASEB Journal* 25(9): 3130-5.

Holloway, C. J., H. E. Montgomery, et al. (2010). "Cardiac response to hypobaric hypoxia: persistent changes in cardiac mass, function, and energy metabolism after a trek to Mt. Everest Base Camp." *The FASEB Journal* 25(2): 792-796.

Holscher, M., K. Schafer, et al. (2012). "Unfavorable consequences of chronic cardiac HIF-1alpha stabilization." *Cardiovasc Res* 94(1): 77-86.

Hon, W. C., M. I. Wilson, et al. (2002). "Structural basis for the recognition of hydroxyproline in HIF-1 alpha by pVHL." *Nature* 417(6892): 975-978.

Honda, Y., S. Watanabe, et al. (1979). "Hypoxic chemosensitivity in asthmatic patients two decades after carotid body resection." *J Appl Physiol* 46(4): 632-638.

Howard, L. S. and P. A. Robbins (1995a). "Alterations in respiratory control during 8 h of isocapnic and poikilocapnic hypoxia in humans." *J Appl Physiol* 78(3): 1098-1107.

Howard, L. S. and P. A. Robbins (1995b). "Ventilatory response to 8 h of isocapnic and poikilocapnic hypoxia in humans." *J Appl Physiol* 78(3): 1092-1097.

Hu, C. J., L. Y. Wang, et al. (2003). "Differential roles of hypoxia-inducible factor 1alpha (HIF-1alpha) and HIF-2alpha in hypoxic gene regulation." *Mol Cell Biol* 23(24): 9361-9374.

Huang, B., P. Wu, et al. (2002). "Regulation of pyruvate dehydrogenase kinase expression by peroxisome proliferator-activated receptor-alpha ligands, glucocorticoids, and insulin." *Diabetes* 51(2): 276-283.

Huang, L. E., J. Gu, et al. (1998). "Regulation of hypoxia-inducible factor 1alpha is mediated by an O2-dependent degradation domain via the ubiquitin-proteasome pathway." *Proc Natl Acad Sci U S A* 95(14): 7987-7992.

Huang, Y., R. P. Hickey, et al. (2004). "Cardiac myocyte-specific HIF-1alpha deletion alters vascularization, energy availability, calcium flux, and contractility in the normoxic heart." *FASEB J* 18(10): 1138-1140.

Hue, L. and H. Taegtmeyer (2009). "The Randle cycle revisited: a new head for an old hat." *Am J Physiol Endocrinol Metab* 297(3): E578-591.

Hurford, W. E., G. Crosby, et al. (1990). "Ventricular performance and glucose uptake in rats during chronic hypobaric hypoxia." *J Nucl Med* 31(8): 1344-1351.

Huss, J. M. and D. P. Kelly (2004). "Nuclear receptor signaling and cardiac energetics." *Circ Res* 95(6): 568-578.

Hyvarinen, J., I. E. Hassinen, et al. (2010). "Hearts of hypoxia-inducible factor prolyl 4-hydroxylase-2 hypomorphic mice show protection against acute ischemia-reperfusion injury." *J Biol Chem* 285(18): 13646-13657.

Isaacs, J. S., Y. J. Jung, et al. (2005). "HIF overexpression correlates with biallelic loss of fumarate hydratase in renal cancer: novel role of fumarate in regulation of HIF stability." *Cancer Cell* 8(2): 143-153.

Ishiguro, T., M. Iwase, et al. (2006). "Impaired ventilation and metabolism response to hypoxia in histamine H1 receptor-knockout mice." *Respir Physiol Neurobiol* 154(3): 331-341.

Ivan, M., T. Haberberger, et al. (2002). "Biochemical purification and pharmacological inhibition of a mammalian prolyl hydroxylase acting on hypoxia-inducible factor." *Proc Natl Acad Sci U S A* 99(21): 13459-13464.

Ivan, M., K. Kondo, et al. (2001). "HIFalpha

targeted for VHL-mediated destruction by proline hydroxylation: implications for O2 sensing." *Science* 292(5516): 464-468.

Iyer, N. V., L. E. Kotch, et al. (1998). "Cellular and developmental control of O2 homeostasis by hypoxia-inducible factor 1 alpha." *Genes Dev* 12(2): 149-162.

Jaakkola, P., D. R. Mole, et al. (2001). "Targeting of HIF-alpha to the von Hippel-Lindau ubiquitylation complex by O2-regulated prolyl hydroxylation." *Science* 292(5516): 468-472.

Jessup, M., M. S. Sutton, et al. (1987). "The effect of chronic pulmonary hypertension on left ventricular size, function, and interventricular septal motion." *Am Heart J* 113(5): 1114-1122.

Jiang, B. H., E. Rue, et al. (1996a). "Dimerization, DNA binding, and transactivation properties of hypoxia-inducible factor 1." *J Biol Chem* 271(30): 17771-17778.

Jiang, B. H., G. L. Semenza, et al. (1996b). "Hypoxia-inducible factor 1 levels vary exponentially over a physiologically relevant range of O2 tension." *Am J Physiol* 271(4 Pt 1): C1172-1180.

Jiang, B. H., J. Z. Zheng, et al. (1997). "Transactivation and inhibitory domains of hypoxia-inducible factor 1alpha. Modulation of transcriptional activity by oxygen tension." *J Biol Chem* 272(31): 19253-19260.

Jiang, H., R. Guo, et al. (2001). "The Caenorhabditis elegans hif-1 gene encodes a bHLH-PAS protein that is required for adaptation to hypoxia." *Proc Natl Acad Sci U S A* 98(14): 7916-7921.

Joseph, V., J. Soliz, et al. (2000). "Gender differentiation of the chemoreflex during growth at high altitude: functional and neurochemical studies." *Am J Physiol Regul Integr Comp Physiol* 278(4): R806-816.

Jyung, R. W., E. E. LeClair, et al. (2000). "Expression of angiogenic growth factors in paragangliomas." *Laryngoscope* 110(1): 161-167.

Kaelin, W. G. (2007). "von Hippel-Lindau Disease." *Annual Review of Pathology: Mechanisms of Disease* 2(1): 145-173.

Kallio, P. J., W. J. Wilson, et al. (1999). "Regulation of the hypoxia-inducible transcription factor 1alpha by the ubiquitin-proteasome pathway." *J Biol Chem* 274(10): 6519-6525.

Kameda, Y., M. Miura, et al. (1998). "Different effects of prolonged isocapnic hypoxia on the carotid body and the glomus cells in the wall of the common carotid artery of the chicken." *Brain Res* 805(1-2): 191-206.

Kamura, T., S. Sato, et al. (2000). "Activation of HIF1alpha ubiquitination by a reconstituted von Hippel-Lindau (VHL) tumor suppressor complex." *Proc Natl Acad Sci U S A* 97(19): 10430-10435.

Karbowska, J., Z. Kochan, et al. (2003). "Peroxisome proliferator-activated receptor alpha is downregulated in the failing human heart." *Cell Mol Biol Lett* 8(1): 49-53.

Kerbey, A. L., P. J. Randle, et al. (1976). "Regulation of pyruvate dehydrogenase in rat heart. Mechanism of regulation of proportions of dephosphorylated and phosphorylated enzyme by oxidation of fatty acids and ketone bodies and of effects of diabetes: role of coenzyme A, acetyl-coenzyme A and reduced and oxidized nicotinamide-adenine dinucleotide." *Biochem J* 154(2): 327-348.

Kerner, J. and C. Hoppel (2000). "Fatty acid import into mitochondria." *Biochim Biophys Acta* 1486(1): 1-17.

Khamnei, S. and P. A. Robbins (1990). "Hypoxic depression of ventilation in humans: alternative models for the chemoreflexes." *Respir Physiol* 81(1): 117-134.

Kim, J.-w., I. Tchernyshyov, et al. (2006). "HIF-1-mediated expression of pyruvate dehydrogenase kinase: A metabolic switch required for cellular adaptation to hypoxia." *Cell Metabolism* 3(3): 177-185.

Kline, D. D., Y. J. Peng, et al. (2002). "Defective carotid body function and impaired ventilatory responses to chronic hypoxia in mice partially deficient for hypoxia-inducible factor 1 alpha." *Proc Natl Acad Sci U S A* 99(2): 821-826.

Koivunen, P., M. Hirsila, et al. (2004). "Catalytic properties of the asparaginyl hydroxylase (FIH) in the oxygen sensing pathway are distinct from those of its prolyl 4-hydroxylases." *J Biol Chem* 279(11): 9899-9904.

Koivunen, P., M. Hirsila, et al. (2007). "Inhibition of hypoxia-inducible factor (HIF) hydroxylases by citric acid cycle intermediates: possible links between cell metabolism and stabilization of HIF." *J Biol Chem* 282(7): 4524-4532.

Kumar, P. and N. R. Prabhakar (2012). "Peripheral Chemoreceptors: Function and Plasticity of the Carotid Body."

Kuwaki, T., W. H. Cao, et al. (1996). "Impaired ventilatory responses to hypoxia and hypercapnia in mutant mice deficient in endothelin-1." *Am J Physiol* 270(6 Pt 2): R1279-1286.

Ladroue, C., R. Carcenac, et al. (2008). "PHD2 mutation and congenital erythrocytosis with paraganglioma." *N Engl J Med* 359(25): 2685-2692.

Ladroue, C., D. Hoogewijs, et al. (2012). "Distinct deregulation of the hypoxia inducible factor by PHD2 mutants identified in germline DNA of patients with polycythemia." *Haematologica* 97(1): 9-14.

Lahiri, S., N. H. Edelman, et al. (1981). "Role of carotid chemoreflex in respiratory acclimatization to hypoxemia in goat and sheep." *Respir Physiol* 46(3): 367-382.

Laidler, P. and J. M. Kay (1975). "A quantitative morphological study of the carotid bodies of rats living at a simulated altitude of 4300 metres." *J Pathol* 117(3): 183-191.

Laidler, P. and J. M. Kay (1978). "Ultrastructure of carotid body in rats living at a simulated altitude of 4300 metres." *J Pathol* 124(1): 27-33.

Lam, S. Y., G. L. Tipoe, et al. (2008). "Differential expressions and roles of hypoxia-inducible factor-1alpha, -2alpha and -3alpha in the rat carotid body during chronic and intermittent hypoxia." *Histol Histopathol* 23(3): 271-280.

Lamb, H. J., H. P. Beyerbacht, et al. (1999). "Diastolic dysfunction in hypertensive heart disease is associated with altered myocardial metabolism." *Circulation* 99(17): 2261-2267.

Lando, D., D. J. Peet, et al. (2002a). "FIH-1 is an asparaginyl hydroxylase enzyme that regulates the transcriptional activity of hypoxia-inducible factor." *Genes Dev* 16(12): 1466-1471.

Lando, D., D. J. Peet, et al. (2002b). "Asparagine hydroxylation of the HIF transactivation domain a hypoxic switch." *Science* 295(5556): 858-861.

Latif, F., K. Tory, et al. (1993). "Identification of the von Hippel-Lindau disease tumor suppressor gene." *Science* 260(5112): 1317-1320.

Le Belle, J. E., N. G. Harris, et al. (2002). "A comparison of cell and tissue extraction techniques using high-resolution 1H-NMR spectroscopy." *NMR Biomed* 15(1): 37-44.

Lee, C., S. J. Kim, et al. (2003). "Structure of human FIH-1 reveals a unique active site pocket and interaction sites for HIF-1 and von Hippel-Lindau." *J Biol Chem* 278(9): 7558-7563.

Lee, K. H., J. W. Park, et al. (2004). "Non-hypoxic transcriptional activation of the aryl hydrocarbon receptor nuclear translocator in concert with a novel hypoxia-inducible factor-1alpha isoform." *Nucleic Acids Res* 32(18): 5499-5511.

Lei, L., S. Mason, et al. (2008). "Hypoxia-inducible factor-dependent degeneration, failure, and malignant transformation of the heart in the absence of the von Hippel-Lindau protein." *Mol Cell Biol* 28(11): 3790-3803.

Lenfant, C. and K. Sullivan (1971). "Adaptation to high altitude." *N Engl J Med* 284(23): 1298-1309.

Li, J., M. Bosch-Marce, et al. (2006). "Altered metabolic responses to intermittent hypoxia in mice with partial deficiency of hypoxia-inducible factor-1alpha." *Physiol Genomics* 25(3): 450-457.

Lieb, M. E., K. Menzies, et al. (2002). "Mammalian EGLN genes have distinct patterns of mRNA expression and regulation." *Biochem Cell Biol* 80(4): 421-426.

Lindgarde, F., M. B. Ercilla, et al. (2004). "Body adiposity, insulin, and leptin in subgroups of Peruvian Amerindians." *High Alt Med Biol* 5(1): 27-31.

Liu, E. (2004). "The worldwide distribution of the VHL 598C>T mutation indicates a single founding event." *Blood* 103(5): 1937-1940.

Loenarz, C., M. L. Coleman, et al. (2011). "The hypoxia-inducible transcription factor

pathway regulates oxygen sensing in the simplest animal, Trichoplax adhaerens." *EMBO Rep* 12(1): 63-70.

Lopaschuk, G. D. and R. L. Barr (1997). "Measurements of fatty acid and carbohydrate metabolism in the isolated working rat heart." *Mol Cell Biochem* 172(1-2): 137-147.

Lopaschuk, G. D., D. D. Belke, et al. (1994a). "Regulation of fatty acid oxidation in the mammalian heart in health and disease." *Biochim Biophys Acta* 1213(3): 263-276.

Lopaschuk, G. D., R. Collins-Nakai, et al. (1994b). "Plasma fatty acid levels in infants and adults after myocardial ischemia." *Am Heart J* 128(1): 61-67.

Lorenzo, F. R., C. Yang, et al. (2012). "A novel EPAS1/HIF2A germline mutation in a congenital polycythemia with paraganglioma." *J Mol Med (Berl)* 91(4): 507-12.

Louie, E. K., S. Rich, et al. (1986). "Doppler echocardiographic assessment of impaired left ventricular filling in patients with right ventricular pressure overload due to primary pulmonary hypertension." *J Am Coll Cardiol* 8(6): 1298-1306.

Lugliani, R., B. J. Whipp, et al. (1971). "Effect of bilateral carotid-body resection on ventilatory control at rest and during exercise in man." *N Engl J Med* 285(20): 1105-1111.

MacKenzie, E. D., M. A. Selak, et al. (2007). "Cell-permeating alpha-ketoglutarate derivatives alleviate pseudohypoxia in succinate dehydrogenase-deficient cells." *Mol Cell Biol* 27(9): 3282-3289.

Makino, Y., R. Cao, et al. (2001). "Inhibitory PAS domain protein is a negative regulator of hypoxia-inducible gene expression." *Nature* 414(6863): 550-554.

Makino, Y., A. Kanopka, et al. (2002). "Inhibitory PAS domain protein (IPAS) is a hypoxia-inducible splicing variant of the hypoxia-inducible factor-3alpha locus." *J Biol Chem* 277(36): 32405-32408.

Makino, Y., R. Uenishi, et al. (2007). "Transcriptional up-regulation of inhibitory PAS domain protein gene expression by hypoxia-inducible factor 1 (HIF-1): a negative feedback regulatory circuit in HIF-1-mediated signaling in hypoxic cells." *J Biol Chem* 282(19): 14073-14082.

Mansfield, K. D., R. D. Guzy, et al. (2005). "Mitochondrial dysfunction resulting from loss of cytochrome c impairs cellular oxygen sensing and hypoxic HIF-alpha activation." *Cell Metab* 1(6): 393-399.

Martini, M., L. Teofili, et al. (2008). "A novel heterozygous HIF2AM535I mutation reinforces the role of oxygen sensing pathway disturbances in the pathogenesis of familial erythrocytosis." *Haematologica* 93(7): 1068-1071.

Masson, N., C. Willam, et al. (2001). "Independent function of two destruction domains in hypoxia-inducible factor-alpha chains activated by prolyl hydroxylation." *EMBO J* 20(18): 5197-5206.

Maxwell, P. H., M. S. Wiesener, et al. (1999). "The tumour suppressor protein VHL targets hypoxia-inducible factors for oxygen-dependent proteolysis." *Nature* 399(6733): 271-275.

Maynard, M. A., H. Qi, et al. (2003). "Multiple splice variants of the human HIF-3 alpha locus are targets of the von Hippel-Lindau E3 ubiquitin ligase complex." *J Biol Chem* 278(13): 11032-11040.

Mazzone, M., D. Dettori, et al. (2009). "Heterozygous deficiency of PHD2 restores tumor oxygenation and inhibits metastasis via endothelial normalization." *Cell* 136(5): 839-851.

McClain, D. A., K. A. Abuelgasim, et al. (2012). "Decreased serum glucose and glycosylated hemoglobin levels in patients with Chuvash polycythemia: a role for HIF in glucose metabolism." *J Mol Med (Berl)* 91(1): 59-67.

McNeill, L. A., K. S. Hewitson, et al. (2002). "Hypoxia-inducible factor asparaginyl hydroxylase (FIH-1) catalyses hydroxylation at the beta-carbon of asparagine-803." *Biochem J* 367(Pt 3): 571-575.

Milledge, J. S. and S. Lahiri (1967). "Respiratory Control in Lowlanders and Sherpa Highlanders at Altitude." *Respiration Physiology* 2(3): 310-&.

Min, J. H., H. Yang, et al. (2002). "Structure of an HIF-1alpha -pVHL complex: hydroxyproline recognition in signaling." *Science* 296(5574): 1886-1889.

Minamishima, Y. A., J. Moslehi, et al. (2008). "Somatic inactivation of the PHD2 prolyl hydroxylase causes polycythemia and congestive heart failure." *Blood* 111(6): 3236-3244.

Minchenko, A. and J. Caro (2000). "Regulation of endothelin-1 gene expression in human microvascular endothelial cells by hypoxia and cobalt: role of hypoxia responsive element." *Mol Cell Biochem* 208(1-2): 53-62.

Mole, D. R., C. Blancher, et al. (2009). "Genome-wide association of hypoxia-inducible factor (HIF)-1alpha and HIF-2alpha DNA binding with expression profiling of hypoxia-inducible transcripts." *J Biol Chem* 284(25): 16767-16775.

Moller, M., K. Mollgard, et al. (1974). "The ultrastructure of the carotid body in chronically hypoxic rabbits." *J Physiol* 238(3): 447-453.

Moore, L. G. (2001). "Human genetic adaptation to high altitude." *High Alt Med Biol* 2(2): 257-279.

Mortola, J. P. and C. Saiki (1996). "Ventilatory response to hypoxia in rats: gender differences." *Respir Physiol* 106(1): 21-34.

Moslehi, J., Y. A. Minamishima, et al. (2010). "Loss of hypoxia-inducible factor prolyl hydroxylase activity in cardiomyocytes phenocopies ischemic cardiomyopathy." *Circulation* 122(10): 1004-1016.

Motojima, K., P. Passilly, et al. (1998). "Expression of putative fatty acid transporter genes are regulated by peroxisome proliferator-activated receptor alpha and gamma activators in a tissue- and inducer-specific manner." *J Biol Chem* 273(27): 16710-16714.

Murray, A. J., R. E. Anderson, et al. (2004). "Uncoupling proteins in human heart." *The Lancet* 364(9447): 1786-1788.

Neely, J. R., H. Liebermeister, et al. (1967). "Effect of pressure development on oxygen consumption by isolated rat heart." *Am J Physiol* 212(4): 804-814.

Neely, J. R. and H. E. Morgan (1974). "Relationship between carbohydrate and lipid metabolism and the energy balance of heart muscle." *Annu Rev Physiol* 36: 413-459.

Neubauer, S. (2007). "The failing heart--an engine out of fuel." *N Engl J Med* 356(11): 1140-1151.

Neubauer, S., M. Horn, et al. (1997). "Myocardial phosphocreatine-to-ATP ratio is a predictor of mortality in patients with dilated cardiomyopathy." *Circulation* 96(7): 2190-2196.

Neubauer, S., M. Horn, et al. (1995). "Contributions of 31P-magnetic resonance spectroscopy to the understanding of dilated heart muscle disease." *Eur Heart J* 16 Suppl O: 115-118.

Neubauer, S., T. Krahe, et al. (1992). "31P magnetic resonance spectroscopy in dilated cardiomyopathy and coronary artery disease. Altered cardiac high-energy phosphate metabolism in heart failure." *Circulation* 86(6): 1810-1818.

Newsholme, E. A. and P. J. Randle (1964). "Regulation of glucose uptake by muscle. 7. Effects of fatty acids, ketone bodies and pyruvate, and of alloxan-diabetes, starvation, hypophysectomy and adrenalectomy, on the concentrations of hexose phosphates, nucleotides and inorganic phosphate in perfused rat heart." *Biochem J* 93(3): 641-651.

Nurse, C. A. and C. Vollmer (1997). "Role of basic FGF and oxygen in control of proliferation, survival, and neuronal differentiation in carotid body chromaffin cells." *Dev Biol* 184(2): 197-206.

Oikawa, M., Y. Kagaya, et al. (2005). "Increased [18F]fluorodeoxyglucose accumulation in right ventricular free wall in patients with pulmonary hypertension and the effect of epoprostenol." *J Am Coll Cardiol* 45(11): 1849-1855.

Otonkoski, T., N. Kaminen, et al. (2003). "Physical exercise-induced hyperinsulinemic hypoglycemia is an autosomal-dominant trait characterized by abnormal pyruvate-induced insulin release." *Diabetes* 52(1): 199-204.

Paciga, M. and C. A. Nurse (2001). "Basic FGF localization in rat carotid body: paracrine role in O2 -chemoreceptor survival." *Neuroreport* 12(15): 3287-3291.

Paciga, M., C. Vollmer, et al. (1999). "Role of ET-1 in hypoxia-induced mitosis of cultured rat carotid body chemoreceptors." *Neuroreport* 10(18): 3739-3744.

Papandreou, I., R. A. Cairns, et al. (2006). "HIF-1 mediates adaptation to hypoxia by actively downregulating mitochondrial oxygen consumption." *Cell Metabolism* 3(3): 187-197.

Pardal, R., U. Ludewig, et al. (2000). "Secretory responses of intact glomus cells in thin slices of rat carotid body to hypoxia and tetraethylammonium." *Proc Natl Acad Sci U S A* 97(5): 2361-2366.

Pardal, R., P. Ortega-Sáenz, et al. (2007). "Glia-like Stem Cells Sustain Physiologic Neurogenesis in the Adult Mammalian Carotid Body." *Cell* 131(2): 364-377.

Pastore, Y., K. Jedlickova, et al. (2003a). "Mutations of von Hippel-Lindau tumor-suppressor gene and congenital polycythemia." *Am J Hum Genet* 73(2): 412-419.

Pastore, Y. D., J. Jelinek, et al. (2003b). "Mutations in the VHL gene in sporadic apparently congenital polycythemia." *Blood* 101(4): 1591-1595.

Peng, Y., Z. Yang, et al. (2011a). "Genetic variations in Tibetan populations and high-altitude adaptation at the Himalayas." *Mol Biol Evol* 28(2): 1075-1081.

Peng, Y. J., J. Nanduri, et al. (2011b). "Hypoxia-inducible factor 2alpha (HIF-2alpha) heterozygous-null mice exhibit exaggerated carotid body sensitivity to hypoxia, breathing instability, and hypertension." *Proc Natl Acad Sci U S A* 108(7): 3065-3070.

Peng, Y. J., G. Yuan, et al. (2006). "Heterozygous HIF-1alpha deficiency impairs carotid body-mediated systemic responses and reactive oxygen species generation in mice exposed to intermittent hypoxia." *J Physiol* 577(Pt 2): 705-716.

Pequignot, J. M., S. Hellstrom, et al. (1984). "Intact and sympathectomized carotid bodies of long-term hypoxic rats: a morphometric ultrastructural study." *J Neurocytol* 13(3): 481-493.

Percy, M. J., P. A. Beer, et al. (2008a). "Novel exon 12 mutations in the HIF2A gene associated with erythrocytosis." *Blood* 111(11): 5400-5402.

Percy, M. J., P. W. Furlow, et al. (2007). "A novel erythrocytosis-associated PHD2 mutation suggests the location of a HIF binding groove." *Blood* 110(6): 2193-2196.

Percy, M. J., P. W. Furlow, et al. (2008b). "A gain-of-function mutation in the HIF2A gene in familial erythrocytosis." *N Engl J Med* 358(2): 162-168.

Percy, M. J., M. F. McMullin, et al. (2003). "Chuvash-type congenital polycythemia in 4 families of Asian and Western European ancestry." *Blood* 102(3): 1097-1099.

Percy, M. J., Q. Zhao, et al. (2006). "A family with erythrocytosis establishes a role for prolyl hydroxylase domain protein 2 in oxygen homeostasis." *Proc Natl Acad Sci U S A* 103(3): 654-659.

Perrotta, S., B. Nobili, et al. (2006). "Von Hippel-Lindau-dependent polycythemia is endemic on the island of Ischia: identification of a novel cluster." *Blood* 107(2): 514-519.

Piao, L., Y.-H. Fang, et al. (2009). "The inhibition of pyruvate dehydrogenase kinase improves impaired cardiac function and electrical remodeling in two models of right ventricular hypertrophy: resuscitating the hibernating right ventricle." *Journal of Molecular Medicine* 88(1): 47-60.

Piao, L., G. Marsboom, et al. (2010). "Mitochondrial metabolic adaptation in right ventricular hypertrophy and failure." *J Mol Med (Berl)* 88(10): 1011-1020.

Pollard, P. J., J. J. Briere, et al. (2005). "Accumulation of Krebs cycle intermediates and over-expression of HIF1alpha in tumours which result from germline FH and SDH mutations." *Hum Mol Genet* 14(15): 2231-2239.

Powell, F. L., W. K. Milsom, et al. (1998). "Time domains of the hypoxic ventilatory response." *Respir Physiol* 112(2): 123-134.

Prabhakar, N. R. and F. J. Jacono (2005). "Cellular and molecular mechanisms associated with carotid body adaptations to chronic hypoxia." *High Alt Med Biol* 6(2): 112-120.

Prabhakar, N. R. and G. L. Semenza (2012). "Adaptive and maladaptive cardiorespiratory responses to continuous and intermittent hypoxia mediated by hypoxia-inducible factors 1 and 2." *Physiol Rev* 92(3): 967-1003.

Pugh, C. W., J. F. O'Rourke, et al. (1997). "Activation of hypoxia-inducible factor-1; definition of regulatory domains within the

alpha subunit." *J Biol Chem* 272(17): 11205-11214.

Pugh, C. W., C. C. Tan, et al. (1991). "Functional analysis of an oxygen-regulated transcriptional enhancer lying 3' to the mouse erythropoietin gene." *Proc Natl Acad Sci U S A* 88(23): 10553-10557.

Rahn, H. and A. B. Otis (1949). "Man's respiratory response during and after acclimatization to high altitude." *Am J Physiol* 157(3): 445-462.

Randle, P. J. (1986). "Fuel selection in animals." *Biochem Soc Trans* 14(5): 799-806.

Randle, P. J., R. M. Denton, et al. (1968). "Citrate as a metabolic regulator in muscle and adipose tissue." *Biochem Soc Symp* 27: 87-103.

Randle, P. J., P. J. England, et al. (1970). "Control of the tricarboxylate cycle and its interactions with glycolysis during acetate utilization in rat heart." *Biochem J* 117(4): 677-695.

Randle, P. J., P. B. Garland, et al. (1963). "The glucose fatty-acid cycle. Its role in insulin sensitivity and the metabolic disturbances of diabetes mellitus." *Lancet* 1(7285): 785-789.

Raval, R. R., K. W. Lau, et al. (2005). "Contrasting properties of hypoxia-inducible factor 1 (HIF-1) and HIF-2 in von Hippel-Lindau-associated renal cell carcinoma." *Mol Cell Biol* 25(13): 5675-5686.

Razeghi, P. (2001). "Hypoxia in Vivo Decreases Peroxisome Proliferator-Activated Receptor α-Regulated Gene Expression in Rat Heart." *Biochemical and Biophysical Research Communications* 287(1): 5-10.

Robbins, P. A. (1995). "Hypoxic ventilatory decline: site of action." *J Appl Physiol* 79(2): 373-374.

Rodesch, F., P. Simon, et al. (1992). "Oxygen measurements in endometrial and trophoblastic tissues during early pregnancy." *Obstet Gynecol* 80(2): 283-285.

Roux, J. C., H. Brismar, et al. (2005). "Developmental changes in HIF transcription factor in carotid body: relevance for O2 sensing by chemoreceptors." *Pediatr Res* 58(1): 53-57.

Russell, R. C., R. I. Sufan, et al. (2011). "Loss of JAK2 regulation via a heterodimeric VHL-SOCS1 E3 ubiquitin ligase underlies Chuvash polycythemia." *Nature Medicine* 17(7): 845-53.

Sable, C., Z. Aliyu, et al. (2011). "Pulmonary artery pressure and iron deficiency in patients with up-regulation of hypoxia sensing due to homozygous VHLR200W mutation (Chuvash polycythemia)." *Haematologica* 97(2): 193-200.

Sack, M. N., T. A. Rader, et al. (1996). "Fatty acid oxidation enzyme gene expression is downregulated in the failing heart." *Circulation* 94(11): 2837-2842.

Salceda, S. and J. Caro (1997). "Hypoxia-inducible factor 1alpha (HIF-1alpha) protein is rapidly degraded by the ubiquitin-proteasome system under normoxic conditions. Its stabilization by hypoxia depends on redox-induced changes." *J Biol Chem* 272(36): 22642-22647.

Salway, J. G. (2004). Metabolism at a Glance. Oxford, Blackwell Publishing Ltd. Third edition.

Sato, M., J. W. Severinghaus, et al. (1992). "Augmented hypoxic ventilatory response in men at altitude." *J Appl Physiol* 73(1): 101-107.

Schaffer, J. E. (2002). "Fatty acid transport: the roads taken." *Am J Physiol Endocrinol Metab* 282(2): E239-246.

Schoene, R. B., R. C. Roach, et al. (1990). "Operation Everest II: ventilatory adaptation during gradual decompression to extreme altitude." *Med Sci Sports Exerc* 22(6): 804-810.

Schofield, C. J. and P. J. Ratcliffe (2004). "Oxygen sensing by HIF hydroxylases." *Nature Reviews Molecular Cell Biology* 5(5): 343-354.

Schroeder, M. A., L. E. Cochlin, et al. (2008). "In vivo assessment of pyruvate dehydrogenase flux in the heart using hyperpolarized carbon-13 magnetic resonance." *Proc Natl Acad Sci U S A* 105(33): 12051-12056.

Schuster, S. J., E. V. Badiavas, et al. (1989). "Stimulation of erythropoietin gene transcription during hypoxia and cobalt

exposure." *Blood* 73(1): 13-16.

Schuster, S. J., J. H. Wilson, et al. (1987). "Physiologic regulation and tissue localization of renal erythropoietin messenger RNA." *Blood* 70(1): 316-318.

Scortegagna, M., K. Ding, et al. (2003). "Multiple organ pathology, metabolic abnormalities and impaired homeostasis of reactive oxygen species in Epas1-/- mice." *Nat Genet* 35(4): 331-340.

Scortegagna, M., K. Ding, et al. (2005). "HIF-2alpha regulates murine hematopoietic development in an erythropoietin-dependent manner." *Blood* 105(8): 3133-3140.

Seagroves, T. N., H. E. Ryan, et al. (2001). "Transcription factor HIF-1 is a necessary mediator of the pasteur effect in mammalian cells." *Mol Cell Biol* 21(10): 3436-3444.

Selak, M. A., S. M. Armour, et al. (2005). "Succinate links TCA cycle dysfunction to oncogenesis by inhibiting HIF-alpha prolyl hydroxylase." *Cancer Cell* 7(1): 77-85.

Semenza, G. L., B. H. Jiang, et al. (1996). "Hypoxia response elements in the aldolase A, enolase 1, and lactate dehydrogenase A gene promoters contain essential binding sites for hypoxia-inducible factor 1." *J Biol Chem* 271(51): 32529-32537.

Semenza, G. L., M. K. Nejfelt, et al. (1991). "Hypoxia-inducible nuclear factors bind to an enhancer element located 3' to the human erythropoietin gene." *Proc Natl Acad Sci U S A* 88(13): 5680-5684.

Semenza, G. L. and G. L. Wang (1992). "A nuclear factor induced by hypoxia via de novo protein synthesis binds to the human erythropoietin gene enhancer at a site required for transcriptional activation." *Mol Cell Biol* 12(12): 5447-5454.

Sergeyeva, A., V. R. Gordeuk, et al. (1997). "Congenital polycythemia in Chuvashia." *Blood* 89(6): 2148-2154.

Severinghaus, J. W., C. R. Bainton, et al. (1966). "Respiratory Insensitivity to Hypoxia in Chronically Hypoxic Man." *Respiration Physiology* 1(3): 308-34.

Seymour, A. M. and J. C. Chatham (1997). "The effects of hypertrophy and diabetes on cardiac pyruvate dehydrogenase activity." *J Mol Cell Cardiol* 29(10): 2771-2778.

Sharma, S. (2003). "Dynamic changes of gene expression in hypoxia-induced right ventricular hypertrophy." *AJP: Heart and Circulatory Physiology* 286(3): 1185H-1192.

Simonson, T. S., D. A. McClain, et al. (2012). "Genetic determinants of Tibetan high-altitude adaptation." *Hum Genet* 131(4): 527-533.

Simonson, T. S., Y. Yang, et al. (2010). "Genetic evidence for high-altitude adaptation in Tibet." *Science* 329(5987): 72-75.

Sivitz, W. I., D. D. Lund, et al. (1992). "Pretranslational regulation of two cardiac glucose transporters in rats exposed to hypobaric hypoxia." *Am J Physiol* 263(3 Pt 1): E562-569.

Smith, C. A., G. E. Bisgard, et al. (1986). "Carotid bodies are required for ventilatory acclimatization to chronic hypoxia." *J Appl Physiol* 60(3): 1003-1010.

Smith, T. G., J. T. Brooks, et al. (2006). "Mutation of von Hippel-Lindau tumour suppressor and human cardiopulmonary physiology." *PLoS Med* 3(7): e290.

Smith, T. G., J. T. Brooks, et al. (2008). "Mutation of the von Hippel-Lindau gene alters human cardiopulmonary physiology." *Adv Exp Med Biol* 605: 51-56.

Soliz, J., V. Joseph, et al. (2005). "Erythropoietin regulates hypoxic ventilation in mice by interacting with brainstem and carotid bodies." *J Physiol* 568(Pt 2): 559-571.

Soliz, J., C. Soulage, et al. (2007). "Acute and chronic exposure to hypoxia alters ventilatory pattern but not minute ventilation of mice overexpressing erythropoietin." *Am J Physiol Regul Integr Comp Physiol* 293(4): R1702-1710.

Sowter, H. M., R. R. Raval, et al. (2003). "Predominant role of hypoxia-inducible transcription factor (Hif)-1alpha versus Hif-2alpha in regulation of the transcriptional response to hypoxia." *Cancer Res* 63(19): 6130-6134.

Stanley, W. C., G. D. Lopaschuk, et al. (1997). "Regulation of myocardial carbohydrate metabolism under normal and ischaemic conditions. Potential for

pharmacological interventions." *Cardiovasc Res* 33(2): 243-257.

Stanley, W. C., F. A. Recchia, et al. (2005). "Myocardial substrate metabolism in the normal and failing heart." *Physiol Rev* 85(3): 1093-1129.

Stojnic, B. B., S. J. Brecker, et al. (1992). "Left ventricular filling characteristics in pulmonary hypertension: a new mode of ventricular interaction." *Br Heart J* 68(1): 16-20.

Stolle, C., G. Glenn, et al. (1998). "Improved detection of germline mutations in the von Hippel-Lindau disease tumor suppressor gene." *Hum Mutat* 12(6): 417-423.

Suga, H. (1990). "Ventricular energetics." *Physiol Rev* 70(2): 247-277.

Taegtmeyer, H. (2002). "Switching Metabolic Genes to Build a Better Heart." *Circulation* 106(16): 2043-2045.

Takeda, K., H. L. Aguila, et al. (2008). "Regulation of adult erythropoiesis by prolyl hydroxylase domain proteins." *Blood* 111(6): 3229-3235.

Takeda, K., V. C. Ho, et al. (2006). "Placental but not heart defects are associated with elevated hypoxia-inducible factor alpha levels in mice lacking prolyl hydroxylase domain protein 2." *Mol Cell Biol* 26(22): 8336-8346.

Takeyama, D., Y. Kagaya, et al. (1995). "Effects of chronic right ventricular pressure overload on myocardial glucose and free fatty acid metabolism in the conscious rat." *Cardiovasc Res* 29(6): 763-767.

Tal, R. (2012). "The role of hypoxia and hypoxia-inducible factor-1alpha in preeclampsia pathogenesis." *Biol Reprod* 87(6): 134.

Tan, Q., H. Kerestes, et al. (2013). "Erythrocytosis and Pulmonary Hypertension in a Mouse Model of Human HIF2A Gain-of-Function Mutation." *J Biol Chem* 288(24):17134-44.

Tatsumi, K., B. Hannhart, et al. (1991). "Influences of gender and sex hormones on hypoxic ventilatory response in cats." *J Appl Physiol* 71(5): 1746-1751.

Taylor, C. T. and J. C. McElwain (2010). "Ancient atmospheres and the evolution of oxygen sensing via the hypoxia-inducible factor in metazoans." *Physiology (Bethesda)* 25(5): 272-279.

Teppema, L. J. and A. Dahan (2010). "The ventilatory response to hypoxia in mammals: mechanisms, measurement, and analysis." *Physiol Rev* 90(2): 675-754.

Thrash-Bingham, C. A. and K. D. Tartof (1999). "aHIF: a natural antisense transcript overexpressed in human renal cancer and during hypoxia." *J Natl Cancer Inst* 91(2): 143-151.

Tian, H., S. L. McKnight, et al. (1997). "Endothelial PAS domain protein 1 (EPAS1), a transcription factor selectively expressed in endothelial cells." *Genes Dev* 11(1): 72-82.

Timmers, H. J., W. Wieling, et al. (2003). "Denervation of carotid baro- and chemoreceptors in humans." *J Physiol* 553(Pt 1): 3-11.

Urena, J., R. Fernandez-Chacon, et al. (1994). "Hypoxia induces voltage-dependent Ca2+ entry and quantal dopamine secretion in carotid body glomus cells." *Proc Natl Acad Sci U S A* 91(21): 10208-10211.

van Bilsen, M., G. J. van der Vusse, et al. (2002). "Peroxisome proliferator-activated receptors: lipid binding proteins controling gene expression." *Mol Cell Biochem* 239(1-2): 131-138.

van der Lee, K. A., M. M. Vork, et al. (2000). "Long-chain fatty acid-induced changes in gene expression in neonatal cardiac myocytes." *J Lipid Res* 41(1): 41-47.

van der Vusse, G. J., M. van Bilsen, et al. (2000). "Cardiac fatty acid uptake and transport in health and disease." *Cardiovasc Res* 45(2): 279-293.

van Wijk, R., S. Sutherland, et al. (2010). "Erythrocytosis associated with a novel missense mutation in the HIF2A gene." *Haematologica* 95(5): 829-832.

Wang, B., Y. B. Zhang, et al. (2011). "On the origin of Tibetans and their genetic basis in adapting high-altitude environments." *PLoS ONE* 6(2): e17002.

Wang, G. L., B. H. Jiang, et al. (1995).

"Hypoxia-inducible factor 1 is a basic-helix-loop-helix-PAS heterodimer regulated by cellular O2 tension." *Proc Natl Acad Sci U S A* 92(12): 5510-5514.

Wang, G. L. and G. L. Semenza (1995). "Purification and characterization of hypoxia-inducible factor 1." *J Biol Chem* 270(3): 1230-1237.

Wang, Z.-Y. and G. E. Bisgard (2002). "Chronic hypoxia-induced morphological and neurochemical changes in the carotid body." *Microscopy Research and Technique* 59(3): 168-177.

Wang, Z. Y., E. B. Olson, Jr., et al. (2008). "Sustained hypoxia-induced proliferation of carotid body type I cells in rats." *J Appl Physiol* 104(3): 803-808.

Wasserman, K., B. J. Whipp, et al. (1975). "Effect of carotid body resection on ventilatory and acid-base control during exercise." *J Appl Physiol* 39(3): 354-358.

Weil, J. V., Byrnequi.E, et al. (1971). "Acquired Attenuation of Chemoreceptor Function in Chronically Hypoxic Man at High Altitude." *Journal of Clinical Investigation* 50(1): 186-195.

Weil, J. V. and C. W. Zwillich (1976). "Assessment of ventilatory response to hypoxia: methods and interpretation." *Chest* 70(1 Suppl): 124-128.

Weizhen, N., M. J. Engwall, et al. (1992). "Ventilatory effects of prolonged systemic (CNS) hypoxia in awake goats." *Respir Physiol* 87(1): 37-48.

Wenger, R. H., A. Rolfs, et al. (1996). "Nucleotide sequence, chromosomal assignment and mRNA expression of mouse hypoxia-inducible factor-1 alpha." *Biochem Biophys Res Commun* 223(1): 54-59.

West, J. B., R. B. Schoene, et al. (2007). High Altitude Medicine and Physiology, Hodder Education. Fourth edition.

White, C. R. and R. S. Seymour (2003). "Mammalian basal metabolic rate is proportional to body mass2/3." *Proc Natl Acad Sci U S A* 100(7): 4046-4049.

Whitehouse, S., R. H. Cooper, et al. (1974). "Mechanism of activation of pyruvate dehydrogenase by dichloroacetate and other halogenated carboxylic acids." *Biochem J* 141(3): 761-774.

Wieland, O., E. Siess, et al. (1971). "Active and inactive forms of pyruvate dehydrogenase in rat heart and kidney: effect of diabetes, fasting, and refeeding on pyruvate dehydrogenase interconversion." *Arch Biochem Biophys* 143(2): 593-601.

Wiener, C. M., G. Booth, et al. (1996). "In vivo expression of mRNAs encoding hypoxia-inducible factor 1." *Biochem Biophys Res Commun* 225(2): 485-488.

Wiesener, M. S., J. S. Jurgensen, et al. (2003). "Widespread hypoxia-inducible expression of HIF-2alpha in distinct cell populations of different organs." *FASEB J* 17(2): 271-273.

Wisneski, J. A., E. W. Gertz, et al. (1985a). "Dual carbon-labeled isotope experiments using D-[6-14C] glucose and L-[1,2,3-13C3] lactate: a new approach for investigating human myocardial metabolism during ischemia." *J Am Coll Cardiol* 5(5): 1138-1146.

Wisneski, J. A., E. W. Gertz, et al. (1985b). "Metabolic fate of extracted glucose in normal human myocardium." *J Clin Invest* 76(5): 1819-1827.

Wisneski, J. A., E. W. Gertz, et al. (1987). "Myocardial metabolism of free fatty acids. Studies with 14C-labeled substrates in humans." *J Clin Invest* 79(2): 359-366.

Wisneski, J. A., W. C. Stanley, et al. (1990). "Effects of acute hyperglycemia on myocardial glycolytic activity in humans." *J Clin Invest* 85(5): 1648-1656.

Wood, S. C. (1991). "Interactions between hypoxia and hypothermia." *Annu Rev Physiol* 53: 71-85.

Wu, P., J. M. Peters, et al. (2001). "Adaptive increase in pyruvate dehydrogenase kinase 4 during starvation is mediated by peroxisome proliferator-activated receptor alpha." *Biochem Biophys Res Commun* 287(2): 391-396.

Wu, T., X. Wang, et al. (2005). "Hemoglobin levels in Qinghai-Tibet: different effects of gender for Tibetans vs. Han." *J Appl Physiol* 98(2): 598-604.

Wyatt, C. N. and C. Peers (1995). "Ca(2+)-activated K+ channels in isolated type I cells

of the neonatal rat carotid body." *J Physiol* 483 (Pt 3): 559-565.

Xu, S., S. Li, et al. (2011). "A genome-wide search for signals of high-altitude adaptation in Tibetans." *Mol Biol Evol* 28(2): 1003-1011.

Xu, W., T. Koeck, et al. (2007). "Alterations of cellular bioenergetics in pulmonary artery endothelial cells." *Proceedings of the National Academy of Sciences* 104(4): 1342-1347.

Xue, W., L. Cai, et al. (2010). "Cardiac-specific overexpression of HIF-1{alpha} prevents deterioration of glycolytic pathway and cardiac remodeling in streptozotocin-induced diabetic mice." *Am J Pathol* 177(1): 97-105.

Yang, C., M. G. Sun, et al. (2013). "Novel HIF2A mutations disrupt oxygen sensing leading to polycythemia, paragangliomas and somatostatinomas." *Blood*.

Yi, X., Y. Liang, et al. (2010). "Sequencing of 50 human exomes reveals adaptation to high altitude." *Science* 329(5987): 75-78.

Yoon, D., D. V. Okhotin, et al. (2010). "Increased size of solid organs in patients with Chuvash polycythemia and in mice with altered expression of HIF-1α and HIF-2α." *Journal of Molecular Medicine* 88(5): 523-530.

Young, L. H., D. L. Coven, et al. (2000). "Cellular and molecular regulation of cardiac glucose transport." *J Nucl Cardiol* 7(3): 267-276.

Young, L. H., Y. Renfu, et al. (1997). "Low-flow ischemia leads to translocation of canine heart GLUT-4 and GLUT-1 glucose transporters to the sarcolemma in vivo." *Circulation* 95(2): 415-422.

Young, M. E., S. Patil, et al. (2001). "Uncoupling protein 3 transcription is regulated by peroxisome proliferator-activated receptor (alpha) in the adult rodent heart." *FASEB J* 15(3): 833-845.

Yu, A. Y., M. G. Frid, et al. (1998). "Temporal, spatial, and oxygen-regulated expression of hypoxia-inducible factor-1 in the lung." *Am J Physiol* 275(4 Pt 1): L818-826.

Yu, A. Y., L. A. Shimoda, et al. (1999). "Impaired physiological responses to chronic hypoxia in mice partially deficient for hypoxia-inducible factor 1alpha." *J Clin Invest* 103(5): 691-696.

Yuan, G., Y. J. Peng, et al. (2013). "Mutual antagonism between hypoxia-inducible factors 1alpha and 2alpha regulates oxygen sensing and cardio-respiratory homeostasis." *Proc Natl Acad Sci U S A* 110(19): E1788-96.

Yuan, Y., G. Hilliard, et al. (2003). "Cobalt inhibits the interaction between hypoxia-inducible factor-alpha and von Hippel-Lindau protein by direct binding to hypoxia-inducible factor-alpha." *J Biol Chem* 278(18): 15911-15916.

Zhang, H., M. Bosch-Marce, et al. (2008). "Mitochondrial Autophagy Is an HIF-1-dependent Adaptive Metabolic Response to Hypoxia." *Journal of Biological Chemistry* 283(16): 10892-10903.

Zhang, M., H. Zhong, et al. (2000). "Co-release of ATP and ACh mediates hypoxic signalling at rat carotid body chemoreceptors." *J Physiol* 525 Pt 1: 143-158.

Zhang, N., Z. Fu, et al. (2010). "The Asparaginyl Hydroxylase Factor Inhibiting HIF-1α Is an Essential Regulator of Metabolism." *Cell Metabolism* 11(5): 364-378.

Zhang, Z., J. Ren, et al. (2002). "Crystal structure of a clavaminate synthase-Fe(II)-2-oxoglutarate-substrate-NO complex: evidence for metal centered rearrangements." *FEBS Lett* 517(1-3): 7-12.

Zhang, Z., M. Tan, et al. (2011). "Identification of lysine succinylation as a new post-translational modification." *Nat Chem Biol* 7(1): 58-63.

Zhuang, Z., C. Yang, et al. (2012). "Somatic HIF2A gain-of-function mutations in paraganglioma with polycythemia." *N Engl J Med* 367(10): 922-930.

Zierhut, M. L., Y. F. Yen, et al. (2010). "Kinetic modeling of hyperpolarized 13C1-pyruvate metabolism in normal rats and TRAMP mice." *J Magn Reson* 202(1): 85-92.

Appendices

7.1 MOUSE BREEDING

Figure 7.1: The Chuvash breeding spreadsheet

Over the course of this thesis 1129 mice were bred (for experiments, breeding and backcrossing). The final spreadsheet was printed on 20 A4 pages, font size 10 pt. Pikes Peak is pictured above.

7.2 FULL METABOLOMICS DATASET

Table 7.1: Summary of metabolomics using NMR

Concentration is mM per gram of dry tissue.

Metabolite	Wild type	Chuvash	*p* value
Acetate	3.9 ± 0.9	4.1 ± 0.6	0.858
AMP/ADP/ATP	18.6 ± 0.9	24.8 ± 0.9	**0.001**
Alanine	20.1 ± 2.0	20.7 ± 2.5	0.846
Aspartate	36.6 ± 9.2	32.7 ± 6.0	0.73
Creatine/phosphocreatine	90.1 ± 10.3	90.2 ± 11.5	0.998
Glucose	22.0 ± 3.9	18.1 ± 2.6	0.427
Glutamate	43.5 ± 3.5	48.3 ± 6.1	0.513
Glutamine	55.9 ± 8.6	62.5 ± 8.1	0.585
Glycine	4.5 ± 0.5	4.5 ± 0.4	0.985
Glycolate/unknown	17.0 ± 4.1	33.3 ± 3.7	**0.014**
Lactate	20.7 ± 4.0	17.3 ± 2.7	0.503
NAD+	9.2 ± 1.2	9.3 ± 0.8	0.961
Succinate	1.6 ± 0.3	1.9 ± 0.4	0.469
Taurine	237.4 ± 22.7	301.8 ± 36.1	0.162

Table 7.2: Summary of metabolomics using targeted LCMS

Concentration is μM per gram of dry tissue. CDP choline (cytidine diphosphate-choline); CMP (cytidine monophosphate); FAD (flavin adenine dinucleotide); GSSG (glutathione disulphide).

Metabolite	Wild type	Chuvash	*p* value
Acetoacetyl CoA	2.7 ± 0.5	4.3 ± 1.0	0.157
Acetyl CoA	4.8 ± 3.9	0.9 ± 0.5	0.335
Adenine	614 ± 94	516 ± 52	0.384
Adenosine	6067 ± 1274	8009 ± 3647	0.626
ADP	20 656 ± 2506	20 233 ± 3131	0.918
AMP	22 289 ± 2870	19 242 ± 882	0.334
ATP	3333 ± 507	3650 ± 417	0.639
cAMP	71 ± 8	72 ± 10	0.921
CDP choline	880 ± 104	756 ± 68	0.343
cGMP	5.4 ± 0.4	7.1 ± 0.7	0.065
CMP	412 ± 46	443 ± 49	0.658
Cytidine	188 ± 34	217 ± 29	0.528
Cytosine	158 ± 53	122 ± 21	0.547
FAD	883 ± 63	783 ± 69	0.308
GDP	6.2 ± 2.9	10.1 ± 4.3	0.473
Glutathione	201 ± 28	219 ± 26	0.661
GMP	309 ± 45	300 ± 25	0.869
GSSG	1500 ± 232	1376 ± 313	0.756
GTP	6.1 ± 2.3	8.2 ± 2.5	0.571
Guanine	12 ± 1	15 ± 4	0.472
Guanosine	50 ± 10	341 ± 285	0.332
Malonyl CoA	2.8 ± 1.0	1.2 ± 0.2	0.167
Methylcytosine	6.4 ± 1.4	4.4 ± 0.8	0.263
NAD	9523 ± 523	7864 ± 671	0.08
Oxoguanine	32 ± 7	13 ± 2	**0.029**
Oxomethionine	251 ± 31	233 ± 37	0.722
Phosphoenolpyruvate	433 ± 36	418 ± 38	0.791
Phosphoglycerate	2415 ± 481	2291 ± 380	0.844
S-adenosyl-L-homocysteine	73 ± 8	71 ± 9	0.892
S-adenosyl-L-methionine	158 ± 34	134 ± 29	0.616
Succinyl CoA	1.2 ± 0.3	2.7 ± 0.4	**0.012**
UMP	292 ± 40	277 ± 48	0.816
Uracil	8.7 ± 2.7	5.4 ± 1.5	0.305

Table 7.3: Summary of metabolomics using GCMS

Metabolites are expressed as a percentage of the total metabolites detected using this technique. There were several 'unidentified' metabolites, hence the total for wild type or Chuvash in this table isn't 100 %.

Metabolite	Wild type	Chuvash	*p* value
Acetate	0.51 ± 0.03	0.47 ± 0.09	0.644
Acetylglutamine	0.64 ± 0.09	0.71 ± 0.11	0.599
Adenylic acid	0.93 ± 0.09	0.86 ± 0.26	0.817
Alanine	1.58 ± 0.16	1.53 ± 0.09	0.820
Aspartate	6.05 ± 0.44	5.87 ± 0.73	0.835
Butanoic acid	0.14 ± 0.04	0.13 ± 0.03	0.726
Creatinine enol	0.37 ± 0.01	0.31 ± 0.01	**0.007**
D-Galactopyranoside/galactose	0.13 ± 0.01	0.09 ± 0.005	**0.039**
D-glucopyranose	0.40 ± 0.04	0.52 ± 0.04	0.068
Fumarate	0.45 ± 0.17	0.29 ± 0.08	0.405
Galactose	1.47 ± 0.17	1.27 ± 0.15	0.384
Glutamate	0.39 ± 0.06	0.38 ± 0.04	0.951
Glutamine	4.31 ± 0.32	4.32 ± 0.18	0.980
Glycerophosphate	0.17 ± 0.05	0.13 ± 0.01	0.454
Glycine	0.45 ± 0.05	0.48 ± 0.02	0.517
Hexadecanoic acid	1.22 ± 0.16	1.14 ± 0.19	0.765
Isocitric acid	1.00 ± 0.14	0.97 ± 0.08	0.884
Lysine	0.49 ± 0.09	0.46 ± 0.03	0.731
Malate	1.63 ± 0.16	1.61 ± 0.12	0.902
Myo-inositol	1.35 ± 0.09	1.03 ± 0.07	**0.016**
Octadecanoic acid	2.25 ± 0.27	2.24 ± 0.39	0.981
Phosphate	9.53 ± 0.90	7.57 ± 0.54	0.077
Propanoic acid	2.02 ± 0.34	1.51 ± 0.16	0.203
Pyrophosphate	0.42 ± 0.11	0.47 ± 0.06	0.683
Serine	0.26 ± 0.03	0.35 ± 0.02	**0.035**
Succinate	0.31 ± 0.03	0.22 ± 0.02	0.064
Threonine	0.20 ± 0.02	0.24 ± 0.01	0.148
Urea	2.72 ± 0.25	2.99 ± 0.23	0.444
Valine	0.14 ± 0.01	0.15 ± 0.02	0.702

7.3 ADDITIONAL MICROARRAY DATASETS

Table 7.4: Summary of microarray data using first alternative analysis

Analysis performed using RMA normalisation and unpaired T test to compare groups. (* = chemokine (C-C motif) ligand 21A (serine) /// predicted gene 1987 /// chemokine (C-C motif) ligand 21C (leucine) /// c-C motif chemokine 21c-like /// chemokine (C-C motif) ligand 21B (leucine) /// predicted gene 10591 /// predicted gene 13304 /// c-C motif chemokine 21c-like)

Gene name	Fold change	Direction	*p* value
myosin, light polypeptide 7, regulatory	2.6	down	0.004
alpha-2-macroglobulin	2.4	up	2.5E-05
myosin, light polypeptide 4	2.3	down	0.005
synuclein, alpha	2.3	up	0.05
nuclear receptor subfamily 4, group A, member 3	1.7	down	0.05
nebulin	1.7	up	7.3E-05
arachidonate 5-lipoxygenase	1.7	down	9.6E-05
myosin, light polypeptide 1	1.7	up	0.002
interferon activated gene 205	1.6	down	0.03
myosin binding protein H-like /// predicted gene 12522	1.6	down	0.02
dopachrome tautomerase	1.6	up	0.005
EF hand domain containing 1	1.5	up	0.003
SH3-domain GRB2-like 2	1.4	up	0.003
serine (or cysteine) peptidase inhibitor, clade A, member 1E/C/A	1.4	up	3.5E-04
lectin, galactoside-binding, soluble, 3 binding protein	1.4	down	0.03
nephrocan	1.4	up	0.03
indolethylamine N-methyltransferase	1.4	down	0.005
sarcolipin	1.4	down	0.004
actin, alpha 2, smooth muscle, aorta	1.4	up	0.01
---	1.4	up	0.004
ganglioside-induced differentiation-associated-protein 10	1.4	down	0.01
chemokine (C-C motif) ligand 11	1.4	down	0.02
solute carrier family 24 (sodium/potassium/calcium exchanger), member 2	1.4	up	0.02
insulin-like growth factor binding protein 3	1.4	down	0.02
---	1.4	up	0.02
cell death-inducing DNA fragmentation factor, alpha subunit-like effector B	1.3	up	0.01
---	1.3	up	0.04
predicted gene 13152 /// predicted gene 13212 /// predicted gene 13154	1.3	up	0.02
6-phosphofructo-2-kinase/fructose-2,6-biphosphatase 1	1.3	down	0.02

neuropeptide Y receptor Y1	1.3	down	0.01
G protein-coupled receptor 126	1.3	down	0.01
apolipoprotein B mRNA editing enzyme, catalytic polypeptide 1	1.3	down	0.04
Plasmalemma vesicle associated protein	1.3	down	0.001
cadherin 11	1.3	down	0.004
*	1.3	down	0.01
*	1.3	down	0.01
*	1.3	down	0.01
*	1.3	down	0.01
regulator of G-protein signaling 5	1.3	up	0.01
predicted gene 1078	1.3	down	0.02
lectin, galactose binding, soluble 6 /// lectin, galactose binding, soluble 4	1.3	down	0.01

Table 7.5: Summary of microarray data using second alternative analysis

Analysis performed using Plier normalisation and unpaired T test to compare groups. (* = chemokine (C-C motif) ligand 21A (serine) /// predicted gene 1987 /// chemokine (C-C motif) ligand 21C (leucine) /// c-C motif chemokine 21c-like /// chemokine (C-C motif) ligand 21B (leucine) /// predicted gene 10591 /// predicted gene 13304 /// c-C motif chemokine 21c-like)

Gene name	Fold change	Direction	*p* value
synuclein, alpha	3.4	up	0.05
alpha-2-macroglobulin	3.1	up	4.9E-05
myosin, light polypeptide 7, regulatory	2.8	down	0.004
myosin, light polypeptide 4	2.5	down	0.004
sarcolipin	2.0	down	0.03
nuclear receptor subfamily 4, group A, member 3	2.0	down	0.04
myosin binding protein H-like /// predicted gene 12522	1.9	down	0.02
myosin, light polypeptide 1	1.9	up	7.9E-04
nebulin	1.8	up	1.0E-04
arachidonate 5-lipoxygenase	1.8	down	1.8E-04
nephrocan	1.7	up	0.02
EF hand domain containing 1	1.7	up	0.002
serine (or cysteine) peptidase inhibitor, clade A, member 1E/C/A	1.6	up	1.1E-04
dopachrome tautomerase	1.6	up	0.007
---	1.5	up	0.03
interferon activated gene 205	1.5	down	0.03
serine (or cysteine) peptidase inhibitor, clade A, member 1C /// serine (or cysteine) peptidase inhibitor, clade A, member 1A	1.5	up	1.8E-04
SH3-domain GRB2-like 2	1.5	up	0.003
---	1.5	up	0.002
---	1.5	up	0.04
predicted gene 13152 /// predicted gene 13212 /// predicted gene 13154	1.5	up	0.03
---	1.5	up	0.01
chemokine (C-C motif) ligand 11	1.5	down	0.02
centromere protein F	1.5	up	0.03
---	1.4	up	0.02
solute carrier family 24 (sodium/potassium/calcium exchanger), member 2	1.4	up	0.03
indolethylamine N-methyltransferase	1.4	down	0.006
---	1.4	up	0.04
neuropeptide Y receptor Y1	1.4	down	0.006
---	1.4	up	0.02
---	1.4	up	0.004
zinc finger, CCHC domain containing 5	1.4	up	0.008

ubiquitin carboxy-terminal hydrolase L1	1.4	up	0.006
lectin, galactose binding, soluble 6 /// lectin, galactose binding, soluble 4	1.4	down	0.007
lectin, galactoside-binding, soluble, 3 binding protein	1.4	down	0.04
insulin-like growth factor binding protein 3	1.4	down	0.01
actin, alpha 2, smooth muscle, aorta	1.4	up	0.02
plasmalemma vesicle associated protein	1.4	down	7.5E-04
cell death-inducing DNA fragmentation factor, alpha subunit-like effector B	1.4	up	0.008
expressed sequence AI593442	1.4	up	0.04
dipeptidylpeptidase 6	1.4	up	0.01
predicted gene 13154	1.4	up	0.006
aspartate-beta-hydroxylase /// clavesin 1	1.4	up	0.02
apolipoprotein B mRNA editing enzyme, catalytic polypeptide 1	1.4	down	0.05
XIAP associated factor 1	1.4	down	0.05
cystatin A	1.4	up	0.009
ganglioside-induced differentiation-associated-protein 10	1.4	down	0.02
cadherin 11	1.4	down	0.003
mucin 16	1.4	down	0.03
*	1.4	down	0.01
*	1.4	down	0.01
*	1.4	down	0.01
*	1.4	down	0.01
CUB and zona pellucida-like domains 1	1.3	up	0.008
---	1.3	up	0.03
cysteine dioxygenase 1, cytosolic	1.3	up	0.04
aquaporin 4	1.3	up	0.01
6-phosphofructo-2-kinase/fructose-2,6-biphosphatase 1	1.3	down	0.02
CUB and Sushi multiple domains 3	1.3	up	0.009
G protein-coupled receptor 126	1.3	down	0.02
---	1.3	up	0.02
---	1.3	up	0.05
---	1.3	up	0.008
---	1.3	up	0.004
---	1.3	up	0.009
predicted gene 1078	1.3	down	0.05
solute carrier family 12, member 5	1.3	up	0.002
immunoglobulin superfamily, member 1	1.3	up	0.005
beta-site APP-cleaving enzyme 2	1.3	down	0.001
RIKEN cDNA 4930534B04 gene	1.3	up	0.01
---	1.3	up	0.02

receptor (calcitonin) activity modifying protein 1	1.3	down	0.002
slit homolog 2 (Drosophila)	1.3	down	0.01
PHD finger protein 11	1.3	down	0.01
a disintegrin and metallopeptidase domain 34 /// predicted gene 5347	1.3	up	0.005
regulator of G-protein signaling 5	1.3	up	0.01
integrin alpha L	1.3	down	0.05
UBX domain protein 10 /// phospholipase A2, group IIC	1.3	up	0.006
transmembrane protein 196	1.3	up	0.04
fibrinogen-like protein 2	1.3	up	0.02
pleckstrin homology domain containing, family H (with MyTH4 domain) member 1	1.3	up	0.003
KAT8 regulatory NSL complex subunit 1	1.3	down	0.04
sodium channel, voltage-gated, type IX, alpha /// predicted gene 13629	1.3	up	0.04
aldehyde dehydrogenase 1 family, member L1	1.3	up	0.003
gap junction protein, alpha 5	1.3	down	0.002
nephroblastoma overexpressed gene	1.3	down	0.02
dickkopf homolog 3 (Xenopus laevis)	1.3	down	0.04
---	1.3	up	0.03
PDZ domain containing RING finger 4	1.3	up	0.02
acyl-coenzyme A amino acid N-acyltransferase 2	1.3	up	0.02
---	1.3	down	0.02